London South Bank
University

The study, development and experimental investigation of a novel, solar powered refrigeration system based on the jet-pump cycle

by

R.L.Fenton, BSc

A Thesis Submitted in partial fulfillment of the requirements for the Degree of Doctor of Philosophy

June 2015

School of the Built Environment and Architecture
London South Bank University

Supervisors
Prof Graeme Maidment, Prof Ian Eames and Prof John Missenden

Abstract

Every year, millions of people die from diseases that are preventable by vaccination. The lack of an effective cold-chain in developing countries means that many of the vaccinations intended for administration are spoiled and wasted. Poor energy infrastructure in these countries is often coupled with high solar irradiance values, providing a compelling reason for research into effective solar powered refrigeration systems.

A number of studies have shown that a refrigeration system, thermally powered via a jet-pump circuit, as an alternative to an electrically driven compressor, could provide a working solution. Such a system could be powered largely by heat (i.e. solar energy) and would find application in developing countries with high solar availability. A comparative review of prior research into small scale jet-pump refrigeration systems highlighted a gap in existing knowledge as the performance of small scale units (<500W) has not previously been investigated.

A system specification was defined, based on current World Health Organisation (WHO) standards for solar-powered vaccine refrigerators. A jet-pump, rated to deliver 100 W

evaporator cooling capacity using R134a as a working fluid, was developed and tested at the defined operating conditions (T_e=6°C, T_g=90°C and T_c=42°C). The experimental study focused on the need for technology that is suited to off-grid applications and the use of secondary heat sinks (i.e. cooling water circuits) was avoided. Alternatives to an electrically powered refrigerant feed pump were investigated and a novel reservoir transfer system is presented and experimentally evaluated. In order to minimise moving parts, the use of natural convection heat transfer (i.e no fans) was also investigated for both the evaporator and condenser heat exchangers. Automated systems were used to control the apparatus and experimental data collected to evaluate the systems thermal coefficient of performance (COP).

Experimental results showed that the system could achieve COPs of 0.06 - 0.12 and demonstrates the potential for small capacity jet-pump cooling systems using less than 50 W electrical power.

DECLARATION

The research described in this thesis is the original work of the author except where otherwise specified, or acknowledgement is made by reference.

It was carried out at the Faculty of Engineering, Science and the Built Environment, London South Bank University and under the supervision of Prof.G.G. Maidment, Prof.I.W.Eames and Prof.J.F. Missenden.

The work has not been submitted for another degree or award of another academic or professional institution during the research program.

Ryan L Fenton

Acknowledgements

I wish to express my grateful thanks to Prof. G.G. Maidment, Prof. I.W.Eames and Prof. J.F.Missenden. You have all provided me with invaluable support, guidance and expertise throughout this research project.

On Prof.Maidment's approval, my application to join IDC (the company I still work for today) was successful and I was recruited as a KTP associate in September 2006. From that day forward, I have been able to count on Prof.Maidment's support, including through times of personal difficulties, and for that I am truly thankful.

When I began the KTP programme, I had only a rudimentary understanding of the traditional vapour compression refrigeration cycle. Over the coming months, I attended a thermodynamics lecture programme at LSBU, and with the help of Prof.Missenden (whose lecture notes I still use today) the subject of thermodynamics was elucidated

Prof. Eames, whose previous research was the inspiration for this experimental study, provided my introduction to jet-pump theory. As the research programme became more defined and my knowledge grew, he provided crucial expertise and advised on the direction and focus of my research. I am forever indebted for the support he provided in

helping me make the transition from student to researcher; developing skills that would prove invaluable later in my career.

I also wish to give special thanks to Dr. S.Knowles (MD) and the rest of the staff at IDC Ltd for their continued support throughout my doctoral studies. In particular, I would like to extend my thanks to Mr. O.Morris for his invaluable help in the manufacture of all three versions of the experimental prototype system and Mr B.Gough for his ongoing encouragement and counsel.

It is important also to thank the team behind the Knowledge Transfer Partnership (KTP) that made this research programme possible. Those who helped facilitate the KTP project during the first two years deserve a special mention, namely Mrs. J.Dobson (KTP), Mr. Chung Lam (LSBU) and Ms. Louise Campbell (LSBU).

In addition, I would like to recognise the important contribution of Dr. A.Ablwaifa, a University of Nottingham researcher, who provided the key-geometries for the jet pump design used in this experimental study, supported by CFD analysis.

Finally, I would like to thank my friends and family, who have provided unflagging support and encouragement throughout my doctoral studies. Thanks to Ms.R.Jansen (my ex wife) who helped me navigate the highs and lows of my research during the early years. Thanks to Ms E.Wessels for her relentless optimism when the mountain seemed too high. Thanks to my friend Dr.R.Hughes Jones for his help and advice in setting up my software systems. A very special thanks to my partner, Dr E.Yates, for her love and ongoing support; without you I don't think I would have ever completed this thesis. You provided me with the time and opportunity to complete my final write-up, despite this

coinciding with the purchase of our first home. You often shouldered the weight of renovations alone and I am eternally grateful for your patience and altruistic support. Thank you Crispin, my wonderful cat, for all your contributions. I have not cited you in the references, but without the "jjjjjjjjjkkkkkkkkkkkkkkkkkkkkkkk" and the ppppppppppppp————" paw on keyboard contributions, I would never have made it through the tough times. I would also like to thank my late grandmother, Mrs Rachel Taylor, who taught me the value of hard-work and determination. She also taught me how to see the funny side, when things don't go quite as planned.

And last, but certainly not least, thanks to my mother, Mrs.R.Fenton - without you, none of this would have been possible. Had it not been for your tireless efforts to provide me with the best in education and opportunities, I would never have been able to reach this point in my career. Your continued faith in my abilities and potential has been instrumental in helping me to realise my dreams.

Contents

Abstract **iii**

Declaration **v**

Acknowledgements **vi**

List of Figures **xix**

List of Tables **xxvi**

Nomenclature **xxix**

Glossary **xxxv**

1 Introduction **1**

1.1 Background 1

1.2 Scope and structure of thesis 3

1.2.1 Scope 3

1.2.2 Structure 4

2 Literature Review **8**

2.1 Introduction to Chapter 8
2.1.1 Description of Literature Review 8
2.1.2 Sources Searched 9
2.2 Identification of Research Need 10
2.2.1 The Importance of Vaccines 11
2.2.2 Consequences of an Interrupted Cold Chain 13
2.3 Solar Powered Cooling 16
2.3.1 Solar Powered Cooling Cycles 17
2.3.2 Solar Energy Conversion Technology 18
2.3.3 Solar Cooling Performance Metrics 22
2.3.4 Solar Electric Cooling Technology 25
2.3.5 Solar Thermal Cooling Technology 27
2.3.6 Solar Cooling Technology Comparison 32
2.4 Jet Pump Cooling Cycle 35
2.4.1 Jet Pump History 35
2.4.2 Jet Pump Operating Principles 36
2.4.3 Jet Pump Performance Characteristics 38
2.4.4 Jet Pump Cooling Cycle Configurations 40
2.4.5 Jet-pump Cycle Enhancements 43
2.4.6 Jet-pump Cycle Working Fluids 46
2.4.7 Comparative Review of Jet-Pump Research 49
2.5 Chapter Conclusions 52
2.5.1 Summary of Literature Review 52

2.5.2 Specific Research Opportunities 52

2.5.3 Conclusion 54

3 Proposition **56**

4 Feasibility, Concept Design and Methodology **60**

4.1 Introduction to Chapter 60

4.2 Methodology and Assumptions 63

4.2.1 Key Assumptions 63

4.2.2 Natural Convection : Theory and Approximations 64

4.3 Refrigerant Selection 65

4.3.1 Refrigerant Selection Criteria 65

4.3.2 R134a - Justification and Limitations 66

4.4 Jet Pump Cooling Cycle Sub-Circuits 68

4.5 Evaporator Requirement Specification 70

4.5.1 Relevant Standards 70

4.5.2 Evaporator Temperature 72

4.5.3 Evaporator Storage Volume and Cooling Capacity 72

4.6 Generator Requirement Specification 74

4.7 Condenser Requirement Specification 75

4.8 Initial System Condition and Performance Specification 77

4.9 Jet Pump Theoretical Design 78

4.9.1 First Principles 79

4.9.2 Computational Fluid Dynamics (CFD) 80

4.10 Final System Condition and Performance Specification 86
4.11 Basic Prototyping Strategy 87
4.11.1 Generator 87
4.11.2 Condenser 89
4.11.3 Evaporator 89
4.12 Product Design Specification 90
4.13 Chapter Conclusion 93

5 Experimental Investigation of the Concept (EP1 & EP2) 95

5.1 Introduction 95
5.1.1 EP1 and EP2 Development and Analysis Scope 97
5.2 Experimental Prototyping Methods and Apparatus 99
5.2.1 Data-logging 100
5.2.2 Basic Construction Of Prototype 101
5.2.3 Custom Made Items 101
5.3 Condenser Sub-system 105
5.3.1 Condenser Heat Exchanger : Theory and Experimental Methods . . 106
5.3.2 Heat Exchanger Test Results 112
5.3.3 Heat Exchanger Selection 123
5.3.4 Auxiliary Condenser Components 124
5.3.5 Condenser Sub-System Construction 124
5.4 Evaporator Sub-system 125
5.4.1 Evaporator Sub-system Specification 126

5.4.2 Evaporator Heat Exchanger 127
5.4.3 Cool-box Construction 127
5.4.4 Theoretical Performance 129
5.4.5 Experimental Validation 131
5.4.6 Evaporator Feed 139
5.4.7 Auxiliary Evaporator Components 141
5.5 Generator Sub-system 142
5.5.1 Generator Sub-system Specification 143
5.5.2 Generator Heat Exchanger 144
5.5.3 Generator Oil Circuit 145
5.5.4 Heat Input: Calculations and Assumptions 145
5.5.5 Generator Refrigerant Feed 148
5.5.6 Theoretical Energy Balance of Generator Feed 153
5.5.7 Jet Pump Feed 155
5.6 Jet Pump Design and Optimisation 157
5.6.1 Jet Pump Design 157
5.6.2 Jet-pump nozzle: Mechanical Stress 162
5.6.3 Jet Pump Optimisation 162
5.7 Integrated System Design 166
5.7.1 EP1 - Initial Test System 166
5.7.2 EP2 - Development System 169
5.7.3 Integrated System Testing and Characterisation 172
5.7.4 Commissioning the Prototypes 177

5.8 Chapter Discussion 180

6 Automated Experimental Prototype (EP3) 182

6.1 Introduction 182

6.2 Generator Development Studies (EP2) 183

6.2.1 Simulation Tests 185

6.2.2 Reservoir Transfer Concepts 188

6.2.3 Selection and Validation of Concept 194

6.2.4 Discussion of Generator Development Studies 195

6.3 Generator Sub-system EP3 197

6.3.1 Generator Feed System 199

6.3.2 Generator Heat Exchanger and Phase Separator 202

6.3.3 Collector Circuit 203

6.3.4 Other Generator Enhancements 205

6.4 Condenser Sub-system EP3 208

6.4.1 Condenser Capacity 208

6.4.2 Condenser inlet : Vapour Bleed Line 208

6.5 Evaporator Sub-system EP3 211

6.5.1 Evaporator Flow Control 212

6.5.2 Other Evaporator Enhancements 214

6.6 Integrated System Design EP3 217

6.7 Automated Control Hardware Specification 220

6.7.1 Electrically Actuated Valves 221

6.7.2 Input Transducers . . . 225
6.7.3 Safety Considerations . . . 227
6.7.4 Programmable Logic Controller . . . 230
6.7.5 Power Supply . . . 232
6.7.6 Control Circuit Design . . . 233
6.7.7 Control Box Hardware . . . 233
6.8 Control Logic . . . 238
6.8.1 High-pressure Safety Logic . . . 238
6.8.2 Generator Pressure Management . . . 238
6.8.3 Fluid Transfer Cycling . . . 240
6.9 Commissioning EP3 . . . 241
6.9.1 Refrigerant Charging . . . 243
6.9.2 Programming the PLC . . . 243
6.10 Chapter Discussion . . . 247

7 Testing and Analysis of Results 249

7.1 Introduction . . . 249
7.2 Review of Experimental Procedure . . . 250
7.3 Typical Behaviour . . . 252
7.3.1 Typical Temperature Plot (EP2) . . . 252
7.3.2 Typical Pressure Plot (EP3) . . . 253
7.3.3 Typical COP Plot (EP3) . . . 254
7.3.4 Typical Experimental Issues . . . 255

7.4 EP2: Operational Test Data . . . 257
7.4.1 EP2: Scope of Collected Data . . . 257
7.4.2 EP2: Selected Operational Test Data . . . 258
7.4.3 EP2: Results Discussion . . . 260
7.5 EP3: Operational Test Data . . . 260
7.5.1 EP3: Scope of Collected Data . . . 262
7.5.2 EP3: Selected Operational Test Data . . . 263
7.6 Chapter Conclusion . . . 272
7.6.1 EP3: Results Discussion . . . 272
7.6.2 Effects of Thermal Energy Losses Due to RTS . . . 272

8 Technology Limitations and Applications Research 274

8.1 Introduction . . . 274
8.2 Production Design Concept for Solar Powered Jet-Pump Vaccine Refrigerator 275
8.3 Technology Limitations . . . 279
8.3.1 Production Cost Estimates . . . 281
8.4 Other Applications for the Jet-Pump Cooling Cycle . . . 282
8.4.1 Air-conditioning . . . 283
8.4.2 Dual Mode AC and Space Heater System . . . 286
8.4.3 Industrial Applications . . . 289
8.4.4 Concept Applications . . . 289
8.5 Funding Models . . . 291
8.6 Chapter Conclusions . . . 292

9 Conclusions **293**

9.1 Introduction . . . 293

9.2 Experimental Results . . . 294

9.2.1 Experimental Difficulties . . . 294

9.2.2 Key Performance Data . . . 295

9.3 Evaluation of Prototype Against PDS . . . 296

9.4 Research Outcomes . . . 298

9.5 Contributions to Knowledge . . . 301

9.6 Future Work . . . 302

9.6.1 Recommendations for Future Experimental Studies . . . 302

9.6.2 Commercial Development Opportunities . . . 303

9.6.3 Scope for Further Research . . . 304

9.7 Conclusion . . . 307

References **309**

Appendices **320**

A R134a Refrigerant Data **321**

B Estimation of Natural Convection Surface Heat Transfer Coefficient **322**

C Transient Cooling Model **324**

D Jet-pump Throat Area Calculation Proof **325**

E Computational Fluid Dynamics: Method and Assumptions **329**

E.1 CFD Simulation Criteria 330
E.1.1 Turbulence Model and Boundary Conditions 330
E.1.2 Grid Size and Type 330
E.2 CFD Assumptions 331

F Jet-pump Dimensioned Drawings 332

G PLC Specification 336

H Control electronics : Supporting calculations 338

H.1 Input Transducers 338
H.1.1 Temperature Transducers 339
H.1.2 Pressure Transducers 339
H.2 Analogue to Digital Conversion 340
H.3 Oil Pump Speed Control 342

I Experimental Uncertainty and Error Analysis 343

I.1 Error Approximation Method 344
I.2 Experimental Error Evaluation 345
I.2.1 Systematic Errors 345
I.3 Other Errors 349

List of Figures

2.1 Developing country population percentages without access to electricity, 2010, adapted from World Energy Outlook 2012 [13] 14

2.2 World map showing annual irradiance values kWh/m^2 - adapted from Jakob 2009 [16] 17

2.3 Diagram of solar cooling paths (Adapted from [21], [19] and [1]) 18

2.4 Diagram of heat balance for refrigeration cycle 23

2.5 Heat powered refrigeration cycle schematic (adapted from [23]) 24

2.6 Schematic diagram of PV powered vapour compressions system 25

2.7 Simplified Schematic of Adsorption Cooling Cycle 28

2.8 Simplified Schematic of Jet-Pump Cooling Cycle 31

2.9 Jet-pump illustrative diagram showing flow velocity and pressure plots adapted from [28] 37

2.10 Critical pressure plot (Illustrative) 39

2.11 Multi Stage Jet Pump Cooling Cycle (Adapted from [21]) 41

2.12 Hybrid Jet-Pump Absorption Cooling Cycle (Adapted from [35]) 43

2.13 Illustration of automatic float-type feed mechanism - Petrenko 2011 [42] . . 45

2.14 Comparative plot of prior jet-pump refrigeration research
Extracted from [50],[51],[40], [52], [32],[39],[53] and [48]. 50

4.1 System Design Methodology Flowchart 62

4.2 R134a p-h plot and schematic diagram of proposed cycle
adapted from Yapichi 2005 [58] 67

4.3 Simplified Schematic of Jet-Pump Cooling Cycle 69

4.4 Graph showing ideal Carnot perfromance at T_g = 90 °C, T_c = 40 °C 76

4.5 Diagram showing geometries for steam jet-pump (Eames et al 1999 [63]) . . 79

4.6 Diagram showing geometries for R141b jet-pump (Huang et al 2001 [64]) . . 79

4.7 Diagram of jet-pump nozzle with key dimensions 81

4.8 Diagram of jet-pump diffuser with key dimensions 81

4.9 Sonic velocity plots showing the effect of increasing condenser temperature
(back pressure) at T_g = +90°C and T_e = +6°C [55] 82

4.10 Mach number contours at T_g = +90 °C, T_c = +42 °C and T_e = +6 °C [55] 83

4.11 Theoretical optimisation of jet-pump nozzle spacing [55] 84

4.12 Graph showing critical condenser pressures at T_e 4-8°C and T_g = 90 °C [55] 84

4.13 CFD predicted entrainment ratios and critical condenser temperatures [55] 85

5.1 Photograph of EP2 102

5.2 Photograph showing thermocouple locations 112

5.3 Photograph of three finned pipe samples 113

5.4 Dimensioned details of TB-Condenser units 117

5.5 Condenser static temperature decay - Natural convection
Vertical configuration 118

5.6 Condenser static temperature decay - Forced convection Vertical configuration 118

5.7 Condenser single phase flow temperature losses Horizontal Configuration 121

5.8 Photograph of EP1/EP2 condenser bank 125

5.9 Diagram showing inner dimensions of cool-box 128

5.10 Photo - Cool box interior 128

5.11 Temperature in cool-box containing 92.7 W heater over 8 hr period. 133

5.12 Temperature in cool-box containing 36.1 W heater over 8 hr period. 135

5.13 Transient model - illustration of terms 136

5.14 Graph showing temperature decay in cool-box over 10 hr period 137

5.15 Graph showing $ln(\frac{\Delta T}{\Delta T^1})$ against time 137

5.16 Graph showing evaporator power distribution with 24L water load, working 20 °C below ambient 138

5.17 Diagram showing pipe dimensions of evaporator transfer feed 141

5.18 Photograph of generator heat exchanger EP1 - Version 1 144

5.19 Graph showing oil flow rate against temperature *(Mocal pump)* 146

5.20 Graph showing Mocal vegetable oil flow rate against pump supply voltage . 147

5.21 Graph showing mass of one litre of vegetable oil at various temperatures . . 147

5.22 Schematic of EP1 generator refrigerant feed system 149

5.23 Schematic of EP2 generator refrigerant feed system 152

5.24 Schematic diagram of reservoir transfer energy balance 154

5.25 Illustrative diagram of cyclonic vapour separator concept 156

5.26 Jet-pump assembly drawing 158

5.27 Isometric view of CAD assembly . . . 159
5.28 Photograph of jet-pump assembly . . . 160
5.29 Graph showing suction pressure against relative position of jet-pump . . . 164
5.30 Potential cooling temperatures against the relative position of the nozzle . . 165
5.31 Dimensioned drawing of optimum nozzle insertion . . . 165
5.32 2D Schematic of EP1 . . . 167
5.33 Hand drawn manufacturing concept sketch for EP1 . . . 168
5.34 2D Schematic of EP2 . . . 170
5.35 Isometric Schematic of EP2 . . . 171
5.36 Graph showing jet pump suction pressure against condenser back pressure . 174
5.37 Graph showing jet pump suction pressure against generator pressure . . . 176
5.38 Illustration of hydrostatic pressure test rig . . . 179

6.1 Schematic of generator sub-system (EP2) . . . 183
6.2 Simplified schematic to illustrate simulation valving . . . 185
6.3 Reservoir Transfer Concept 1 . . . 189
6.4 Reservoir Transfer Concept 2 . . . 190
6.5 Reservoir Transfer Concept 3 . . . 191
6.6 Reservoir Transfer Concept 4 . . . 192
6.7 Reservoir Transfer Concept 5 . . . 193
6.8 Schematic diagram of generator fluid delivery system (EP3) . . . 200
6.9 Specific heat capacity against temperature for NoTox HT Fluid 32 . . . 203
6.10 Graph showing Micropump (GJ-N27) flow calibration at 3450 RPM . . . 205

6.11 Extrapolated capillary data from ASHRAE 2006 210
6.12 Illustration of condenser reservoir capillary bleed line 211
6.13 Photo - Manufacture of directional T-junction 211
6.14 ASHRAE 2006 Extract- Capillary tables 213
6.15 Illustration showing implementation of evaporator buffer zone 214
6.16 Illustration of evaporator feed pipe-work 216
6.17 Photo - NRV compact strainer solution 216
6.18 2D Schematic of EP3 218
6.19 Schematic of "T" port valve operation 224
6.20 PLC Input Wiring Summary 226
6.21 Safety circuit schematic 229
6.22 Main control box schematic 234
6.23 Manual / automatic switching circuit 235
6.24 Photo of control box 236
6.25 Control box layout 237
6.26 Control logic flow diagram 239
6.27 Photograph of EP3 248

7.1 Typical evaporator behaviour (DLC 65 extract) 252
7.2 Typical systems pressures plot (DLC 119 Extract) 254
7.3 Typical systems pressures and temperatures (DLC 103 Extract) 255
7.4 Q/COP against time showing various cycle counts (DLC 113 Extract) . . . 256
7.5 Temperature against time plot(DLC 53-54) 258

7.6 Cooling chamber air temperature against time (DLC 65) 259
7.7 Cool box temperatures against time plot (DLC 113) 265
7.8 Q/COP against time (DLC 113) 266
7.9 Temp 24 l/COP water against time (DLC 113) 267
7.10 Q/COP against time (DLC 119) 269
7.11 T/COP against time (DLC-119) 269
7.12 Water temperature and COP against time (DLC-124) 271
7.13 Synchronised Pressure Plot : DLC 119 and DLC 124 271
7.14 DLC 119 Pressure Plot Extract 273

8.1 Illustration of proposed control interface 276
8.2 Illustration of jet-pump powered vaccination station 278
8.3 Summary of prototype and estimated production costs 282
8.4 Illustration of solar powered mobile hospital - reproduced from [73] 283
8.5 Predictions of AC performance 285
8.6 Theoretical performance data for combined AC and heating 287
8.7 Illustration showing dual function system installed in house 287
8.8 Schematic layout of proposed system in heating and cooling mode 288
8.9 Approximate Volume Ratio of System 289
8.10 Selection of concepts from Kingston University design student project . . . 290

A.1 R134a (CH_2F-CF_3)- Highlighted extract from Rogers and Mayhew [62] . . . 321

D.1 Schematic diagram of jet-pump 325

E.1 Example of mesh grid adaptation[33] 331

F.1 Dimensioned drawing of the jet-pump body 333

F.2 Dimensioned drawing of the jet-pump diffuser 334

F.3 Dimensioned drawing of the jet-pump nozzle 335

G.1 PLC market research table 336

H.1 Pressure transducer to PLC potential divider circuit 340

H.2 0-5V Speed control signal circuit 342

I.1 TC-08 Thermocouple calibration test 347

List of Tables

2.1 List of academic sources searched 9

2.2 List of literature review search terms 10

2.3 Disease eradication and control by vaccination, in terms of annual life years saved (LYS) and disability adjusted life years (DALYs) saved. Adapted from Ehreth 2003 [6] 12

2.4 Estimated Number of Deaths in the Absence of Vaccination, Deaths from Vaccine-preventable Diseases, and Deaths Averted by Vaccination, All Ages, by Region and Vaccine, 2001 (thousands) [12] 15

2.5 Comparative evaluation of existing solar powered cooling technologies . . . 33

2.6 Advantages and disadvantages of current solar powered cooling technologies 34

4.1 Initial Design Point Operating Conditions 77

4.2 Final System Conditions and Performance Specification - Full List 88

4.3 Product Design Specification 92

4.4 Summary of final design point operating specification 94

5.1 Condenser Test Rig - Thermocouple Locations 111

5.2 Static Temperature Decay Experiment - Assumptions 113

5.3 Table showing results of finned pipe tests 114

5.4 Pressed Static Temperature Decay Test Results - Vertical 119

5.5 Condenser Test Results - Horizontal 121

5.6 Cool box - Construction Material Thermal Conductivity 130

5.7 Cool box conductance values 130

5.8 Cool box contents : Mass and specific heat values 132

5.9 Sources of specific heat vales of vegetable oil from the web 145

5.10 Jet-pump nozzle spacing combinations 161

5.11 Jet-pump nozzle shim washer labels 161

5.12 EP2 Operating Procedure - Version 1 173

6.1 Summary of reservoir transfer concept details 194

6.2 EP2 Operating Procedure - Version 2
With reference to figure 6.2 196

6.3 EP3 Generator Reservoir Transfer System Specification 198

6.4 EP3 Heat Exchanger Specification 202

6.5 Mesh sizes and open area 217

6.6 Boolean logic for relays 1 and 2 228

6.7 PLC inputs and outputs 231

6.8 List of electrical outputs and their power requirements 232

6.9 Table showing basic fluid transfer operating procedure (EP3) 242

6.10 Table showing liquid volume measurements 244

6.11 Boolean table for ABV4 close command signal (ABV4 C-CS) 246

6.12 Boolean table for ABV4 open command signal (ABV4 O-CS) 246

7.1 DLC References for three experimental prototype (EP) versions 250

8.1 Assumptions for energy saving calculation 288

I.1 Summary of propagated errors (EP3 - 5 cycle) 350

NOMENCLATURE

Symbols

Symbol	Stands For	Units
A	Area	m^2
a	Sonic velocity	m/s
c	Specific Heat Capacity (mass)	kJ/kg·K
C_p	Constant pressure heat capacity	J/kg·K
C_v	Constant temperature heat capacity	J/kg·K
COP	Coefficient of Performance	-
$\varnothing$ (or D)	Diameter	mm
E	Energy	kJ
ξ	Minor Loss Coefficient	-
g	Strength of gravitational field (9.81)	m/s^2
Gr	Grashof number	-
h	Enthalpy	kJ/kg
H	Heat Transfer Coefficient	W/m^2·K

I	Irradiance (Solar)	W/m^2
k	Thermal Conductivity	W/m·K
L_f	Heat of Fusion	kJ/kg
M	Mach number	-
m	Mass	kg
$\dot{m}$	Mass Flow	kg/s
η	Efficiency	-
p	Pressure (absolute)	bar
ϕ	Flow Correction Factor	-
Pr	Prandtl number	-
Q	Heat Gain	J
$\dot{Q}$	Heat Transfer Rate	W
R	Resistance (or impedance)	Ω
Ra	Rayleigh number	-
R_m	Entrainment Ratio	-
R^o	Universal Gas Constant	J/kg·K
ρ	Density	kg/m^3
S	Entropy	kJ/kg·K
t	Time	s
T	Temperature	°C

ΔT	Temperature Difference	K
τ	Static Temperature	K
μ	Dynamic Viscosity	Pa·s
Nu	Nusselt Number	-
U	Overall Heat Transfer Coefficient	$W/m^2 \cdot K$
v	velocity	m/s
$\mathcal{V}$	Voltage	V
V	Volume	m^3
$\dot{V}$	Volume Flow Rate	m^3/s
γ	Heat capacity ratio	-
W_p	Work (pump)	W
X	Nominal value	-

Subscripts

If a combination of subscripts is required the sections are strung together using an underscore to show a new section is included. For example if the average ambient temperature was required the symbol would therefore be t_{avg_amb}.

Subscript	Stands For
amb	Ambient
atm	Atmospheric
avg	Average
car	Carnot
c (or con)	Condenser
cap	Capacity
comb	Combined
conv	Convection
cool	Cooling
cycle	Cooling cycle
e (or evp)	Evaporator
elec	Electrical
eng	Engine
eq	Equalised
ex	Experimental
g (or gen)	Generator
HT	High Temperature

hx	Heat Exchanger
i	Inner
init	Initial
lat	Latent
liq	Liquid
LT	Low Temperature
min	Minimum
max	Maximum
o	Total (or stagnation) condition
O	Outer
ovrl	Overall
p	Pump
panel	Solar collector panel
pri	Primary
ref	Refrigerator
rel	Relative
req	Required
res	Reservoir
sec	Secondary
s (or suc)	Suction
surf	Surface

th or therm	Thermal
theo	Theoretical
thr	Throat
vap	Vapour

Glossary of Abbreviations

Acronymn	Stands For
ABV	Actuated Ball Valve
AC	Air-Conditioning
ac	Alternating current
ADC	Analogue to Digital Converter
BS	British Standard
BV	Ball Valve
C-CS	Close - Command Signal
C-MS	Close - Microswitch
CAD	Computer Aided Design
CD	Charge/Discharge (generator operational ratio)
CFC	Chlorofluorocarbon
CFD	Computational Fluid Dynamics
CO_2	Carbon Dioxide
COM	Communication Signal

COP	Coefficient of Performance
CSA	Cross Sectional Area
DALY	Disability Adjusted Life Year
dc	Direct Current
DFM	Design For Manufacture (analysis)
DIN	Deutches Institut für Normung
DIY	Do-It-Yourself
DLC	Data Log Capture (datasets)
EMF	Electromotive Force
EMR	European Metal Recycling
EP#	Experimental Prototype Number (e.g. EP3)
FBD	Function Block Diagram
FEA	Finite Element Analysis
GND	Ground (Electrical)
GTD	Greater Temperature Difference
GUI	Graphical User Interface
GWP	Global Warming Potential
HC	Hydrocarbon
HCFC	Hydrochlorofluorocarbon
HDP	Heat Driven Pump
HFC	Hydrofluorocarbon

HFO	Hydrofluoroolefin
HIPS	High-Impact Polystyrene
HP	High Pressure
hr(s)	Hour(s)
HT	Heat Transfer
HX	Heat Exchanger
ID	Internal Diameter
IDC	Industrial Design Consultancy
IEC	International Electrotechnical Commission
IIR	International Institute of Refrigeration
JP	Jet-pump
LCD	Liquid Crystal Display
LED	Light Emitting Diode
LiBr	Lithium Bromide
LLS	Liquid Level Switch
LMTD	Logarithmic Mean Temperature Difference
ln	Natural logarithm
LP	Low Pressure
LSBU	London South Bank University
LTD	Lesser Temperature Difference
LYS	Life Years Saved

MCV	Manual Control Valve (Ball Valve)
MDF	Medium-Density Fibreboard
MFG	Multi-function Generator
min(s)	Minute (s)
MOPD	Maximum Operational Pressure Differential
MWP	Maximum Working Pressure
NC	Normally Closed
NCHTC	Natural Convection Surface Heat Transfer Coefficient
NEMA	National Electrical Manufacturers Association
NO	Normally Open
NRV	Non Return Valve
NXP	Nozzle Exit Position
O-CS	Open - Command Signal
O-MS	Open - Microswitch
OD	Outside diameter
ODP	Ozone Depleting Potential
OEM	Original Equipment Manufacturer
OPD	Operating Pressure Differential
PCB	Printed Circuit Board
PCM	Phase Change Material
PEEK	Polyether Ether Ketone

PID	Proportional Integral Derivative
PLC	Programmable Logic Controller
PRV	Pressure Relief Valve
PSU	Power Supply Unit
PT	Pressure Transducer
PTFE	Polytetrafluoroethylene
PV	Photovoltaic
R#	Reservoir number (e.g R3)
RES	Reservoir
RMS	Root Mean Squared
RPM	Revolutions Per Minute
RTC	Reservoir Transfer System (Concept)
RTS	Reservoir Transfer System (Validated)
SCH	Schrader Valve
SFEE	Steady Flow Energy Equation
SI	Système International (standard notation)
SIG	Signal
SOL	Solenoid
TB	Tricity Bendix (OEM condenser pipe-work)
TC	Thermocouple
TEV	Thermostatic Expansion Valve

TS	Temperature Sensor
US	United States of America
USB	Universal Serial Bus
USD	US Dollars (currency)
WEEE	Waste Electrical and Electronic Equipment recycling (EU legislation)
WGF	Workless Generator Feed
WHO	World Health Organisation
1D/2D/3D	1/2/3 dimensional
V#	Valve number (e.g. V3)

Chapter 1

Introduction

1.1 Background

Reliance on refrigeration poses numerous opportunities and challenges worldwide. It is estimated that cooling equipment accounts for 15-20% of world energy demand, contributing significantly to the problem of global warming [1]. Perhaps a more imminent issue however is the lack of reliable refrigeration in the developing world. Currently over $1\frac{1}{2}$billion people do not have access to electricity [2] and this makes the safe storage of foodstuffs and vaccines an ongoing challenge. The World Health Organisation (WHO) reports that in some areas, vaccine wastage is as high as 50% [3].

Solar powered refrigeration systems can provide a compelling and cost effective solution to this challenge. The higher the ambient temperature, the higher the cooling demand and with solar irradiance values approaching their maximum around the less developed equatorial regions of the globe, such systems have the potential to provide cooling

performance that is well matched to demand.

Such systems have already been developed and implemented, including traditional vapour compression systems (powered via photovoltaic panels) and heat powered systems (e.g sorption cycles) however the capital cost still represents a significant barrier to uptake. This initial cost is often coupled with ongoing maintenance costs.

A less well known thermally powered cycle, the jet-pump cycle, has the potential to deliver solar powered refrigeration at lower costs. With no moving parts, the jet-pump replaces the compressor found in conventional electric refrigerators. Although such systems have been developed for large air conditioning (AC) applications, the viability of the cycle at lower temperatures and lower cooling capacities has not been fully explored. This forms the basis of the proposition for this study.

Building on the work of others in this area of research, this study describes the experimental development of three iterative prototype systems to provide ≈100W cooling via the jet pump cycle, powered using a thermal energy source (hot oil circuit).

The challenges of this study were principally related to the relatively small system capacity. The volumetric flow of refrigerant (R134a in this study) for a 100W system is much less than the flow for larger AC systems and therefore the jet-pump has to be much smaller. Investigation and development of a jet-pump at this scale represented the first key challenge.

The second key challenge for this study, again related to the relatively small system capacity, was the investigation of an energy efficient mechanism to transfer refrigerant between the primary cooling circuit and the secondary jet-pump circuit.

The third key challenge of this study was to investigate a system that can run

autonomously. Automating the experimental prototype required real-time monitoring of system conditions and feedback loops that controlled refrigerant flow and thermal input management.

The objective of the work is to evaluate the practical limitations of jet-pump technology in providing low capacity (≈100W) refrigeration through the experimental investigation of a prototype system. Iterative development and automation of the prototype system provides performance data that can be used to asses the jet-pump cooling cycle against other comparable technologies.

Providing reliable autonomous refrigeration in off grid locations is important for numerous reasons. Meats and dairy products can be stored safely for longer durations, helping to prevent food waste in areas where malnutrition is prevalent. Maintaining low temperatures for harvested food stock also allows farmers to be part of the cold chain which can provide valuable income for rural communities. But perhaps most importantly, refrigeration in off grid locations is used to store temperature sensitive medicines and vaccines which have the potential to save millions of live. This study further advances the state of the art knowledge in jet-pump cycle refrigeration, providing an important step towards solving some of the problems mentioned above.

1.2 Scope and structure of thesis

1.2.1 Scope

The scope of this thesis, outside the breadth of the literature review, covers the design, development and experimental study of a low capacity jet pump refrigeration system.

Following the identification of a gap in existing knowledge, an experimental study is proposed. The study has been structured to assess the performance, limitations and viability of a single, fixed geometry jet-pump in providing small capacity (≈100W) cooling equipment for off grid applications.

The thesis is intended to provide future readers with the knowledge necessary to advance the research into the jet-pump cooling cycle. Concept designs are explored, details of system evaluation techniques are discussed and the results generated from experimental tests are presented and reviewed.

1.2.2 Structure

The thesis begins with a literature review which, following a contextual introduction, provides information on appropriate performance metrics and thermodynamic limitations for solar powered cooling systems.

A critical review of the pertinent academic literature is presented, summarising the existing solar powered cooling technologies and focussing on previous work concerning jet-pump refrigeration cycles. Various working fluids for the jet-pump cycle are also examined and discussed.

A gap in existing knowledge is identified and a research proposition is defined in Chapter 3

Chapter 4 investigates the feasibility of the study, specifying the performance requirements and critical assumptions. The jet pump capacity and consequent sub-system capacities are presented along with supporting calculations. A basic outline of methodologies and techniques used is also described as part of this chapter. This

chapter provides a specification framework for the subsequent research and investigative work.

In order to refine and evaluate the performance of the jet-pump fully, a series of three experimental prototype systems (EP1, EP2 and EP3) were developed and tested during this research study. A short description of each prototype and its functionality is given below.

- **EP1:** The first prototype system was used as a test platform on which to confirm operation of the jet-pump and evaluate different mechanical methods of delivering refrigerant fluid from the cooling circuit to jet-pump vapour generator circuit.
- **EP2:** The second prototype employed a system of valves and reservoirs to transfer the fluid to the generator circuit.
- **EP3:** The final, fully automated prototype system included a novel, four reservoir, generator feed sub-system and vapour superheater.

The development of the first two experimental systems (EP1 & EP2) is described in Chapter 5, beginning with a specification of the test equipment and experimental apparatus.

The investigation and development of each subsystem (the condenser, the evaporator and the generator) is presented in sequence. The theoretical performance and experimental validation of each subsystem, in isolation, is described.

The manufacturing development for the system jet pump is then presented and the experimental optimisation process discussed.The experimental performance is compared against the theoretical.

The integrated system designs and operating procedures for EP1 and EP2 are then presented. This chapter also includes information on the complex commissioning process. The chapter concludes with a discussion of the findings from experimental testing of the first two prototype systems (EP1 & EP2).

Chapter 6 describes the development and subsequent automation of the final experimental prototype (EP3).

The chapter begins with a section detailing the experimental development of the EP3 secondary generator circuit. Achieving low electrical power consumption for the generator refrigerant feed mechanism was of key interest to this study. Various generator feed concept systems were devised and theoretically evaluated using experimental data obtained from simulation tests conducted on EP2. The final generator subsystem is presented, followed by updated versions of both the condenser and evaporator sub-systems.

The EP3 system schematic of is presented along with the operating procedure. Considerations for automation are discussed and the associated components specified. The investigation of the control box, to allow manual and automated operation, is detailed followed by an examination of the required control logic.

Chapter 7 summarises the key experimental results obtained from testing of EP2 and EP3. The chapter begins with an introduction to the typical performance cycle of the system, including common features which can be seen in all of the plots. Following a selection of individual test results, characterisation of the system is revisited before the chapter concludes with a discussion on system performance.

Chapter 8 provides a concept vision for a solar powered vaccine refrigerator and reviews

the limitations of the jet-pump cooling cycle, including the capital cost. A number of alternate applications (e.g. air-conditioning) are also appraised.

The final chapter of the thesis defines the key research outcomes and discusses the merits and limitations of this study, highlighting the contributions to knowledge. The chapter concludes with a section that suggests avenues for future work.

Chapter 2

Literature Review

2.1 Introduction to Chapter

2.1.1 Description of Literature Review

This literature review uses evidence from various sources to validate the experimental development study of a small capacity, thermally powered, jet-pump refrigeration system.

Firstly, the need for effective low energy refrigeration solutions is demonstrated. These solutions are needed to overcome the challenges associated with the temperature-controlled supply chain (cold-chain) of consumables, in particular vaccines, in off-grid countries.

The state of the art of solar powered cooling systems is then presented, including an introduction to the various cycles and collector technologies. A summary of the key metrics used in the evaluation of solar powered cooling devices is also presented. This

section concludes with an analysis of the benefits and drawbacks of each system.

It then focusses specifically on state of the art of the jet-pump cooling cycle. This includes an introduction to the operating principles of the jet-pump, cooling cycle configurations and jet-pump performance characteristics. The section concludes with a review of the previous research on jet-pump cooling systems, both theoretical and experimental, with particular attention given to the choice of working fluids (refrigerant).

The chapter concludes with a summary of the previous research on jet-pump cooling cycles in order to provide a reference framework for this study.

2.1.2 Sources Searched

The sources searched for relevant literature are listed in table 2.1. These sources were searched using a combination of the terms listed in table 2.2 (a minimum of two terms, though not from the same column).These terms were also used to perform Google searches of the internet.

Academic Onefile	IngentaConnect
ANTE database	London South Bank University Library
ASHRAE	GreenFile
ASME	Journal Citation Reports
British Standards Online	Sage Journals Online
Emerald research database	Science Direct
Index to Theses	SCOPUS Research database

Table 2.1: List of academic sources searched

Search Term 1	Search Term 2	Search Term 3
Solar	Refrigeration	Jet Pump
Solar Powered	Refrigerator	Ejector
Solar Thermal	Air conditioning	Injector
Thermally Powered	Air Conditioner	Eductor
Thermally Activated	Cooling	Thermocompressor
Heat Powered	Cooler	R134a
Heat Activated	Chiller	
	Freezer	
	Cold Store	

Table 2.2: List of literature review search terms

Source papers were initially evaluated by the abstract and conclusion. Over 150 journal and conference papers were reviewed in full, and then were catalogued into a database. Each paper was assigned a research category (Background, Parallel, Jet-pump Theoretical or Jet-pump Experimental)

2.2 Identification of Research Need

Although global warming provides a compelling argument for research into solar powered cooling systems, the consequences of an interrupted cold chain in the delivery of vaccines poses an ongoing threat to human life, particularly in developing countries.

2.2.1 The Importance of Vaccines

Historically, second only to the supply of clean water, vaccination has had the greatest impact on mortality reduction and population growth [4] and there is a clear correlation between incidence of vaccine preventable disease and global vaccination coverage [5]. Although vaccination is one of the most cost effective public health measures [6], the World Health Organisation (WHO) estimates that 21.8 million children, worldwide, miss out on basic vaccines, including diphtheria, measles, pertussis, pneumonia, polio, rotavirus diarrhoea, rubella and tetanus that otherwise prevent the deaths of 2 to 3 million people a year [7].

The highest child mortality rates for vaccine-preventable disease are seen with pneumococcal disease (716,000 deaths in under fives), rotavirus (402,000 deaths in under fives) and Hib infection (386,000 deaths in under fives) [8]. Incomplete vaccination coverage, not only leads to large numbers of avoidable deaths but also a high social and economic burden associated with disability, cost of treatment/care and lost work/school days. Those children who survive may suffer severe disability due to complications such as bacterial meningitis (caused by Hib and pneumococcal disease) which in turn can cause deafness, blindness and cognitive impairment. The malnutrition associated with rotavirus, can not only result in developmental and physical growth impairments but can leave the child susceptible to other mortality associated diseases such as lower respiratory tract infections.

Effective eradication of disease (e.g. smallpox) by vaccination is possible, and although initial investment is high, the long term cost savings are considerable. It is estimated that $300 million in direct cost savings has resulted from the smallpox vaccination program [6]. When considering polio, it is estimated that a $13.6 billion will have been

saved by the vaccination programme by the year 2040 [6]. The impact of smallpox, polio and measles vaccination in terms of annual life years saved (LYS) and disability adjusted life years (DALYs) in shown in table 2.3.

Disease	Africa		Global	
	LYS	DALYs	LYS	DALYs
Smallpox	933,065	NA	5,000,000	NA
Polio	484,230	279,000	33,750,000	1,725,000
Measles	2,125,500	17,463,000	71,500,000	29,838,000

NA = Not available

Table 2.3: Disease eradication and control by vaccination, in terms of annual life years saved (LYS) and disability adjusted life years (DALYs) saved.
Adapted from Ehreth 2003 [6]

When considering measles (one of the most contagious diseases known to man); a vaccination initiative targeting 82.1 million children across 12 African countries between 2000 and 2003, demonstrated an average decline in the number of reported cases of 91%. This equated to an estimated 90,000 averted deaths in the year 2003. [9]. It is estimated that one case of measles costs 23 times as much as the cost of vaccinating a child against the disease [6]. The cost of measles vaccination is $0.14 vaccine, however measles vaccination coverage in Sub-Saharan Africa is still poor [10]

When considering the benefit of vaccination it is important to factor in not only mortality and health benefits but broader societal factors. For example, vaccination can lead to better productivity outcomes due to ability of children to reach their full cognitive potential which in turn leads to healthier, more educated adults.

The role of vaccination is set to gain even further prominence in the era of antibiotic resistance. The potential inability to treat infection increases the need for a "prevention, rather than cure" mentality and vaccination is integral to the 2015 WHO Antimicrobial Resistance Action Plan (*Objective 3: Reduce the incidence of infection through effective sanitation, hygiene and infection prevention measures*) [11].

2.2.2 Consequences of an Interrupted Cold Chain

Currently over $1\frac{1}{2}$ billion people do not have access to electricity [2] and this makes the safe storage of medicines and vaccines one of the critical applications for solar powered cooling systems. Immunisation programmes are one of the most cost effective public health interventions available [12] and yet the effective transportation and distribution of these temperature sensitive vaccinations continues to present an ongoing challenge.

The resultant morbidity and mortality arising from immunisation preventable diseases places an additional burden on the social and economic structure of low-income nations. Of the immunisable diseases, measles is by far the most devastating in terms of global mortality and Sub-Saharan Africa accounts for over half of the total worldwide deaths (348k out of 676k)[12].

Compounding the issues of accessibility is the issue of vaccine wastage. Open vial wastage occurs due to the use of large vials containing multiple dosage units as a low-cost alternative to the inefficiencies in transportation and storage costs of single dose vials [12]. In some areas of the developing world, estimates suggest vaccine wastage is as high as 50% [3].

In many cases, there is a correlation between countries with a low vaccination coverage

rate and those with high radiant heat. For example, Sub-Saharan Africa has one of the worst vaccination coverage rates; table 2.4 compares the number incidences of certain diseases averted by vaccination in high income countries compared to lower income countries. Due to its poor vaccination coverage rates, Sub-Saharan Africa has the greatest global burden of disease, accounting for 58% of pertussis deaths, 41% of tetanus deaths and 51% of measles deaths[12]. It also has the highest percentage of population without access to electricity (figure 2.1). However, when located on an irradiation map (figure 2.2), Sub-Sahara boasts over 2300 kWh / m^2 of radiant solar energy compared with the UK which has 900 kWh / m^2 typically. With such an abundant source of energy it is logical that solar powered cooling devices would be a sensible and appropriate solution for the transport and storage of much needed vaccinations to the these areas.

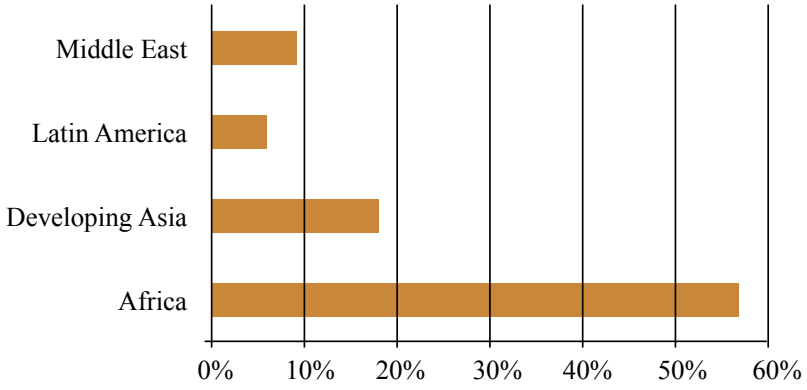

Figure 2.1: Developing country population percentages without access to electricity, 2010, adapted from World Energy Outlook 2012 [13]

Utilising solar powered refrigerators to transport and store vaccines in remote regions is not a new idea and the World Health Organisation (WHO) have produced requirement specifications for solar powered vaccine refrigerators. These specifications provide full

Disease		Total	High income	East Asia and the Pacific	Europe and Central Asia	Latin America and the Caribbean	Middle East and North Africa	South Asia	Sub-Saharan Africa
Diphtheria									
	If no vaccination	78	3	28	4	8	5	21	10
	Estimated deaths	5	<1	1	<1	<1	<1	3	1
	Deaths averted	73	3	27	4	8	5	18	9
Pertussis									
	If no vaccination	1,343	7	377	4	138	93	428	296
	Estimated deaths	301	<1	3	<1	6	8	108	176
	Deaths averted	1,042	7	374	4	132	85	320	120
Tetanus									
	If no vaccination	936	<1	110	<1	20	23	543	239
	Estimated deaths	293	<1	27	<1	1	4	140	121
	Deaths averted	643	<1	83	<1	19	19	403	118
Measles									
	If no vaccination	2,000	6	301	36	6	55	567	1,025
	Estimated deaths	676	<1	77	4	<1	7	239	348
	Deaths averted	1,237	5	229	28	6	40	351	578
Hib									
	If no vaccination	468	<1	28	2	9	14	199	216
	Estimated deaths	463	<1	28	2	5	14	199	215
	Deaths averted	5	<1	<1	<1	4	<1	<1	1
Hepatitis B									
	If no vaccination	600	34	370	36	11	17	75	58
	Estimated deaths	600	34	370	36	11	17	75	58
	Deaths averted	<1	<1	<1	<1	<1	<1	<1	<1

Excerpt from Brenzel 2006 [12]Disease Control in Developing Countries, Chapter 20, Vaccine-preventable Diseases

Table 2.4: Estimated Number of Deaths in the Absence of Vaccination, Deaths from Vaccine-preventable Diseases, and Deaths Averted by Vaccination, All Ages, by Region and Vaccine, 2001 (thousands) [12]

details for the range of permissible ambient temperatures, required holdover time (during periods of no sunshine), cooling performance and most critically, the temperature range (including transient excursions) within which the vaccines must be stored (+2°C - +8°C) [14]. In this application, solar powered cooling devices not only save energy, but save lives.

2.3 Solar Powered Cooling

Cooling demand increases with a rise in ambient temperatures, hence using solar energy to power cooling devices provides a synergistic solution to meeting this demand. Average annual irradiance values are shown on a map view in figure 2.2. Considering central air conditioning (AC) systems, one estimate shows that between 1980 and 2000 the European demand increased by approximately 300% [15]. Considering Europe alone, a 100% growth in the AC market was been observed in the 4 years following 2005 [16]. With the industrialisation of developing nations , it is likely that a world-wide increase in such cooling requirements with an associated rise in energy costs will be seen. Studies estimate between 40-60% of world energy demand is required for heating and cooling duties [17, 18]. Presently, only 2-3% of this demand is met using renewable energy technologies [17]. Considering refrigeration and air-conditioning duties specifically, the International Institute of Refrigeration in Paris (IIR) has estimated that this accounts for 15% of the electricity produced worldwide [1].

The sun provides 1.366 kW/m^2 (solar constant) however this is typically approximated as 1 kW/m^2 ,when the sun is directly overhead, due to atmospheric variations [19, 20]. This means that every minute, the sun provides the earth with as much energy as the world consumes in an entire year [18]). Applied to the problem of interrupted cold

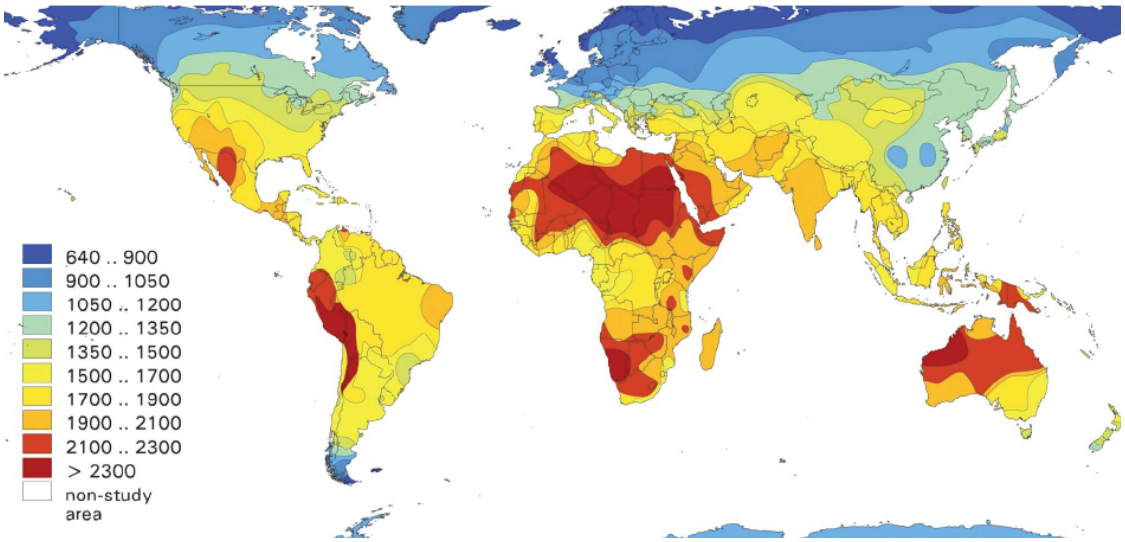

Figure 2.2: World map showing annual irradiance values kWh/m^2 - adapted from Jakob 2009 [16]

chains, efficient, low-cost and low-maintenance solar powered cooling devices have the potential not only to save energy, but also to save lives.

2.3.1 Solar Powered Cooling Cycles

A number of different technologies have been developed that utilise solar energy in order to provide cooling and they can be broadly divided into two categories, solar electric and solar thermal, based on the type of solar collector employed. This review examines both types of system, with particular reference to the system's cost and efficiency.

Figure 2.3 illustrates the range of solar cooling systems examined as part of this review, differentiating between solar thermal and solar electric driven systems. Typical applications for each technology are given on the right hand side of the diagram using a colour key to indicate the cooling load temperature.

For solar thermal systems, the temperature required to drive each cycle is also provided via a colour key (see left hand side of diagram), which determines the type of collector required (see section 2.3.2 for more details).

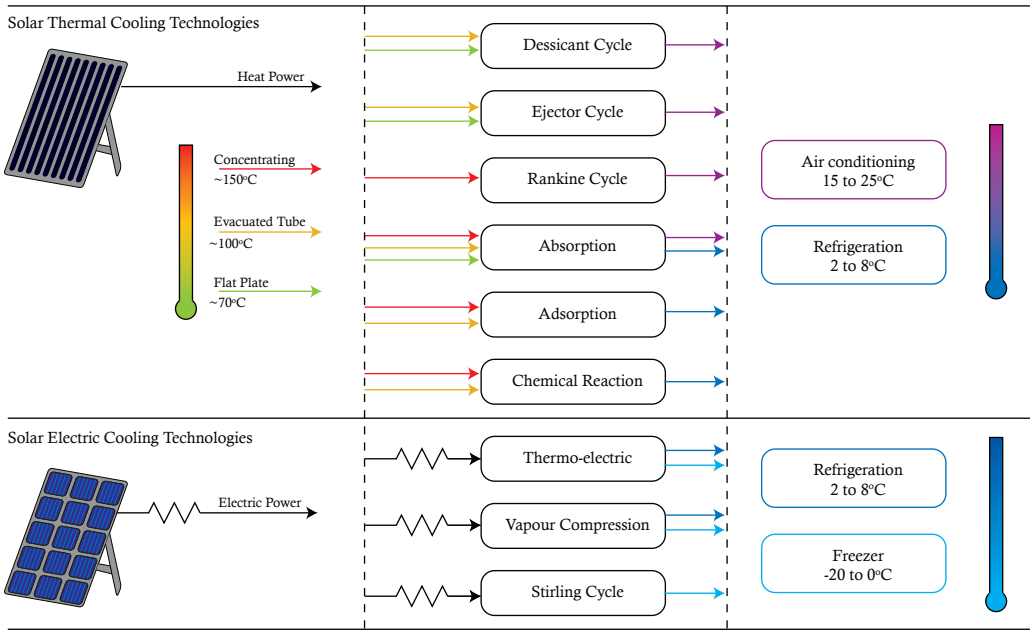

Figure 2.3: Diagram of solar cooling paths (Adapted from [21], [19] and [1])

2.3.2 Solar Energy Conversion Technology

Solar energy conversion, particularly solar electric, has been the focus of research and development for many years and these technologies have now become part of everyday life; powering portable devices, remote systems and on a larger scale, an important part of the energy supply chain. Access to these technologies is available to everyone: from

large scale industry to the individual consumer. The cost of solar energy conversion systems continues to fall but long payback periods still mean other incentives are required when comparing directly against systems using traditional fossil fuel derived energy.

Solar Electric Conversion

Solar electric cells, otherwise known as photovoltaic (PV) cells, convert the energy of the sun into electrical energy using semiconductor technology. They can be used in a wide-variety of applications to either reduce or replace the requirement for mains electricity. The cells primarily make use of crystalline silicon to convert solar radiation into electrical energy. Current high performance solar panels have efficiencies, under optimum conditions, of around 15% [19]; hence a $1m^2$ panel can provide around 150W of electricity under direct sunlight.

In some applications, optical lenses are used to concentrate the sunlight and generate more electricity. Although this strategy helps reduce the need for expensive semi-conductor material, it requires a higher specification for other panel materials and a tracking system to follow the path of the sun.

Traditionally, a photovoltaic system requires additional components including a batteries, chargers and charge controllers (potentially installed alongside a backup generator). The combined expense of a photovoltaic panel and associated electrical energy storage components can lead to a prohibitively high cost for solar electric systems. In addition, when considering the use of PV systems in developing countries, the relative complexity of such systems and the technical knowledge required to maintain/repair them should not be overlooked.

During recent times, increased research funding has led to the development of alternative photovoltaic solutions including thin film technologies, such as amorphous silicone. Thin films help to reduce the cost of solar cells as they use less semiconductor material and can be manufactured as one complete cell, rather than an array of connected cells.

Solar Thermal Conversion

Solar thermal systems collect and directly employ the heat of the solar radiation. The panels are constructed in one of two ways. Flat plate collectors, the type most widely used, pass the working fluid through pipes that are attached to metal backing plate. As flat plate collector temperature rises, their efficiency decreases. Evacuated glass tube collectors offer higher efficiencies with a higher associated cost. When higher temperatures are required, lens systems can be used to concentrate the radiation onto the collector.

Solar Collector Technology Comparison

Solar thermal collectors offer several benefits over a photovoltaic system. The primary advantage lies in the manufacturing cost. A solar thermal collector is very simple in construction and panels can even be made by the DIY enthusiast using copper pipes painted black [22].

The technology has obvious benefits in augmenting or replacing water heating for domestic and commercial purposes, however the thermal energy can also be used in other applications such as the generation of high pressure steam with which to drive turbines. One such system was constructed in the Mojave desert during the 1980s that

provides a reliable supply of 350MW [20].

Solar thermal panels can also provide higher collector efficiencies than PV panels. Flat plate thermal collectors can provide efficiencies of 50% while evacuated tube collectors can achieve efficiencies in excess of 65% [19]. In comparing the relative efficiencies of solar electric versus solar thermal panels in this way, it is important to note that the overall performance evaluation of solar powered cooling systems must also consider the efficiency of the cooling cycle (i.e. vapour compression cycle, absorption cycle, jet-pump cycle etc). This distinction is discussed further in section 2.3.3

When considering the use of panels for applications when the option to power the system from an auxiliary source may be of benefit; although PV driven systems can also be powered from a mains electricity supply, a thermally powered cooling system offers much greater flexibility. The use of stove power (fire) can be considered as an alternate thermal energy source. In larger scale installations, the possibility of using waste heat from industrial processes provides further opportunities for thermally powered systems.

The complex manufacturing method of PV cells, and embedded carbon content of the silicon leads to higher economic and environmental costs. Considering all of the factors mentioned above, thermal panels provide a promising alternative to PV for solar energy conversion.

2.3.3 Solar Cooling Performance Metrics

Coefficient of Performance

Coefficient of performance (COP) is widely used as a measure of efficiency for refrigeration systems and is one of the key evaluation metrics used in this study. When evaluating the overall performance of a solar powered cooling system, both the collector efficiency (η_{panel}) and cooling cycle efficiency (COP_{cycle}) must be considered as shown in equation 2.1.

$$COP_{ovrl} = \eta_{panel} * COP_{cycle} \tag{2.1}$$

A brief review of solar panels efficiency (η_{panel}) has already been presented, however as the energy available from solar collectors is dependant on many external factors (e.g. geographic location, seasonal variance, relative capital cost of panels etc), it is often useful to consider the COP of the refrigeration cycle independently. Subsequent use of the term COP in this thesis refers specifically to the refrigerator cycle performance (COP_{cycle}). Figure 2.4 shows the energy balance for electrically and thermally powered refrigeration cycles.

For a traditional, electrically driven vapour compression type refrigerator the COP can be defined as;

$$COP_{elec} = \frac{Q_e}{W_p} \tag{2.2}$$

Where Q_e, is the cooling power of the evaporator and W_p is electrical work input of the compressor.

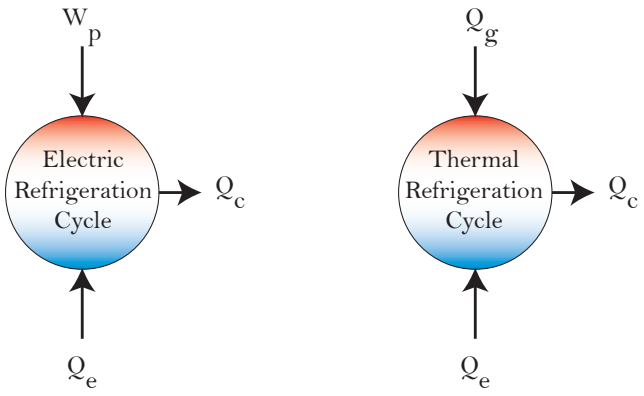

Figure 2.4: Diagram of heat balance for refrigeration cycle

For a thermally driven cooling system it can be defined as;

$$COP_{therm} = \frac{Q_e}{Q_g} \tag{2.3}$$

Where Q_e, is the cooling power of the evaporator and Q_g is the vapour generator heat input. It should be noted that COP_{therm} does not take into account any feed pump electrical requirement. Equation 2.3 can be extended to include this.

$$COP_{comb} = \frac{Q_e}{Q_g + W_p} \tag{2.4}$$

The work of the liquid feed pump (W_p) in thermally powered refrigeration cycles is often considered negligible (in comparison to the heat work) and outside the research framework, however this study draws particular attention to the need for a low power feed system.

Carnot Efficiency

Thermally powered systems compress the refrigerant in its liquid state, as opposed to traditional electrically driven vapour compression systems, therefore the work required to drive the cycle is only a small fraction of the total [19] [23]. Figure 2.5 shows a schematic representation of a thermally powered refrigeration cycle.

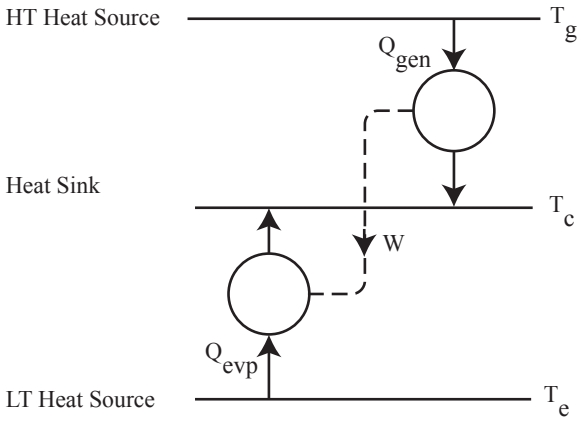

Figure 2.5: Heat powered refrigeration cycle schematic (adapted from [23])

In this system, generator heat (Q_g) at T_g is absorbed into the heat engine to produce work (W). Heat is also rejected via the condenser at T_c. Driven by the work, the refrigerator absorbs heat (Q_e) from the evaporator at T_e, again rejecting heat to the condenser at T_c [23].

In application, the maximum thermodynamic efficiencies of both the heat engine and refrigerator are limited by those of the Carnot cycle working at the same temperatures [19]. The product of these two Carnot efficiencies (η_{eng} = heat engine efficiency and η_{ref} = refrigerator efficiency) is the COP_{car} as shown in equation 2.5. Comparing the actual COP of a system against the ideal COP_{car} provides a particularly useful metric when

comparing thermally powered refrigeration cycles against electrically driven cycles.

$$\begin{aligned} COP_{car} &= \eta_{eng} * \eta_{ref} \\ &= \frac{Q_e}{Q_g} \\ &= (\frac{T_g - T_c}{T_c - T_e})(\frac{T_e}{T_g}) \end{aligned} \tag{2.5}$$

2.3.4 Solar Electric Cooling Technology

Despite the high costs, various photovoltaic refrigeration systems have been developed and taken to market [24]. These units can provide crucial refrigeration in applications such as vaccine storage in the developing world. The units are normally of the vapour compression type as illustrated in figure 2.6

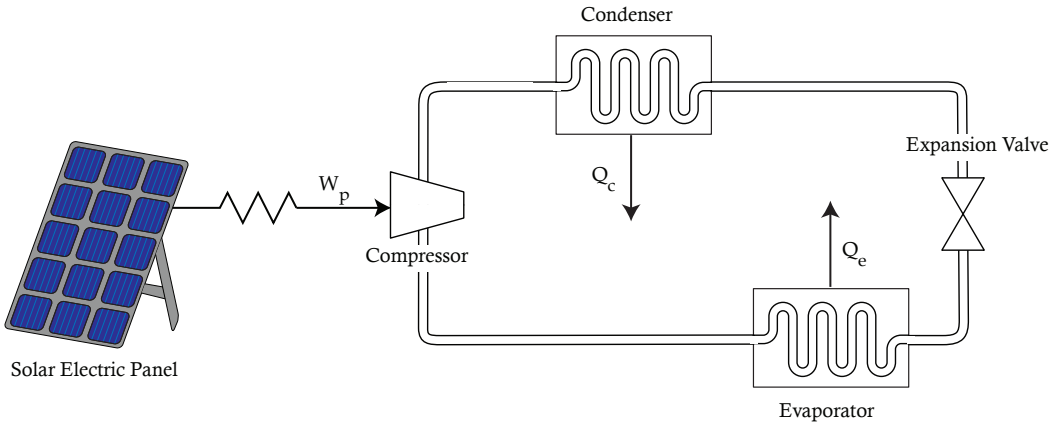

Figure 2.6: Schematic diagram of PV powered vapour compressions system

One 2008 study [19] estimates PV refrigeration systems of this type cost around €4,200 per kW [19] (based on a panel efficiency of 10% and COP of 3.0). In recent times the

falling cost of photovoltaics ($4.76 per watt for systems $\leq$ 2 kW: 2013 median cost [25])has provided opportunities for electrically powered systems to become more cost effective. In order to reduce the costs of photovoltaic refrigeration various companies (e.g. Dulas, Sure Chill, SolarChill) have developed systems that employ solar direct drive (SDD)[26]. SDD systems use the electricity generated from the PV panels to drive the compressor directly and no batteries or charge controllers are needed. A chamber of water surrounds the refrigerated compartment and during active cooling periods, ice forms. When no electricity is available (e.g. during cloudy periods or outside daylight hours) the ice melts and maintains the temperature within the refrigerated compartment. This strategy also prevents the compartment temperature reaching freezing temperature.

Only a limited number of these companies have met the WHO performance regulations for vaccine storage. Dulas produce the largest (132 litre storage capacity) WHO pre-qualified, solar vaccine refrigerator currently available (VC200SDD). Despite the cost savings offered by PV SDD refrigerators, a 2015 quotation from Dulas revealed the initial capital costs are still relatively high (£3,473). Another WHO approved solar powered refrigerator manufacturer (SureChill) have developed a similar system costing £3,450 at 2015 prices (BLF100DC).

Although PV refrigeration devices are normally of the vapour compression (VC) type, research into other technologies has also been conducted. Thermoelectric (peltier) technology offers an alternative to VC, using semiconductor technology, to convert heat into electrical energy. The benefits of thermoelectric over PV are in the simplicity of construction, containing no moving parts (nor refrigerant), however the COP of such systems is very low (0.16) in relation to a high cost [27].

Using electricity from PVs to drive a Stirling cycle refrigerator is another possible

option, however the research conducted so far has shown that this provides a low COP 1.7 in relation to cost €6,700 per kW ([19] 2008). Thermo-acoustic system (suitable for small capacity systems only) and magnetic cooling (used in cryogenic cooling) are two other options however applications are limited as the COP of traditional vapour compression systems are higher [19] leading to higher relative costs.

2.3.5 Solar Thermal Cooling Technology

Providing cooling using the heat of the sun is logical due to the increased thermal energy input during warmer periods, will match the required cooling load. In addition, thermally driven systems have the advantage of being able to use a variety of energy sources including solar, biomass, geothermal or waste heat. This would also allow for the relatively simple integration of an auxiliary power supply.

There are a variety of methods that can be used to provide refrigeration using a thermal energy source, including sorption systems (absorption,adsorption and dessicant), rankine cycle and jet-pump cycle, and these are described in more detail below.

Sorption Technologies

One of the most common approaches to solar thermal cooling is to use sorption technologies, including absorption, adsorption and desiccant systems. The basic operating principles of all three sorption systems are similar and the simplified schematic of the adsorption cycle shown in figure 2.7 can be used as reference. These systems use two substances, a sorbent and a sorbate to produce a cooling effect. The sorbent substance absorbs or attracts the sorbate, which acts as the refrigerant, within the

absorber pulling the temperature of the evaporator down. The heat collected from solar thermal panels is used to regenerate the sorbent sending the refrigerant back to the condenser, and then on to the evaporator via an expansion valve. Absorption systems chemically absorb the refrigerant whereas adsorption systems attract the sorbate to the surface of the solid sorbent. Desiccant systems are used in AC applications and combine dehumidification with evaporative cooling processes to provide a cooling effect. All three systems require the use of a high temperature generator ($> 80°C$) to regenerate / desaturate the sorbent.

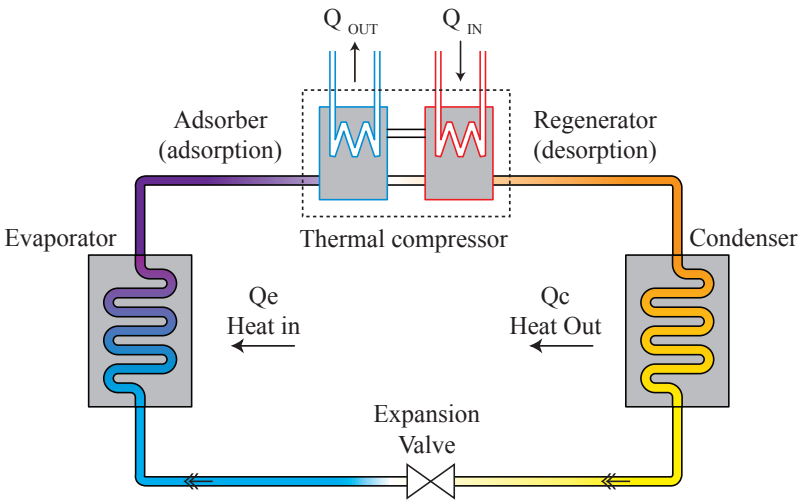

Figure 2.7: Simplified Schematic of Adsorption Cooling Cycle

Absorption systems have proven to be the most popular choice for solar cooling and are available as single effect or double effect units. In a single effect unit, the condenser functions as above, whereas in a double effect machine, some of the waste heat from the first generator is used to drive a secondary generator. Single effect units provide the lowest capital cost solution, operating at COPs of around 0.7 to provide cooling from a 80-90°C thermal energy source [18, 19, 23]. The units are around twice the price of a

traditional vapour compression refrigerator, giving a cost performance of approximately €1,000/kW (2008 estimate) [19, 23].

Double effect absorption refrigerators provide higher COPs, 1.1-1.2, however they require higher regeneration temperatures, 120-150°C resulting in a higher capital cost of around €1,200/kW (2008 estimate) [19, 23]. Triple effect machines have also been developed, however the capital cost of such systems is even higher [18].

Lithium bromide/water and water/ammonia are common working pairs for absorption systems, however these present potential drawbacks. Using water as a refrigerant limits the low temperature side of the system to above 0°C, and the benefits of using ammonia as a sorbent are offset by the associated health and safety risk [28]. Another drawback, specific to LiBr/water systems, is that they must be held at vacuum pressure [28]. Both LiBr and ammonia are corrosive to ferrous metal, causing both a reduction of the internal vacuum and generation of debris that can block system orifices. In addition the cost implication of a regeneration heat exchanger should not be understated.

There is significant commercial interest in the field of thermally powered cooling. SolarNext (Germany), ClimateWell (Finland) and Yazaki (Japan) all provide thermally powered absorption systems for industrial applications. The use of parabolic collectors, and vacuum tube collectors have allowed large scale absorption systems to be employed in industrial applications, however flat plate collectors continue to provide a cost effective alternative for systems with a lower T_g.

Other sorption systems, (i.e. adsorption), have also been developed for solar-thermal cooling application. The simplified schematic in figure 2.7 shows the operating cycle of the adsorption system. Various COP values have been achieved using adsorption systems ranging from 0.1-0.6 however the cooling power densities of such systems are low, making

them unsuitable for small scale applications [19] such as vaccine storage.

Jet Pump Cooling

The jet-pump can be used to replace the electrically powered compressor found in traditional vapour compression refrigeration circuits as shown in figure 2.8. Thermal energy, which can be collected from solar panels, is used to provide heat to a vapour generator. This vapour is then used as the primary flow to entrain fluid from the evaporator and generate the cooling effect. The jet-pump therefore acts as a thermally powered compressor.

Numerous configurations of the jet-pump cycle have previously been considered including multi-stage systems, hybrid systems and adjustable geometry jet-pumps however this additional complexity comes at additional cost, making these systems unsuitable for low-cost vaccine storage applications. Experimental studies into the more simple single stage, fixed geometry jet-pump systems have reported COPs in excess of 0.8 [29] for AC applications and cost estimates suggests the relative cost of jet-pump systems to be €2,300 per kW cooling [19].

Other Solar Thermal Cooling Technologies

Rankine cycle generators and Stirling cycle engines have previously been considered as thermo-mechanical solutions for solar refrigeration. The Rankine cycle uses a high pressure working fluid to drive a turbine/generator and produce the mechanical work to drive the compressor. A Stirling engine also uses heat to produce mechanical work, however the temperature difference of the working fluid is used to drive a piston. In both

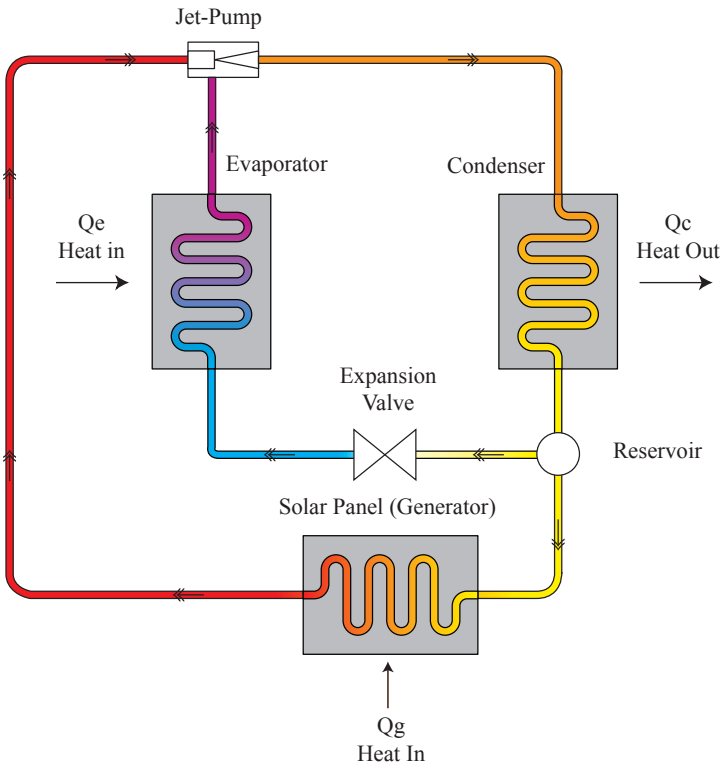

Figure 2.8: Simplified Schematic of Jet-Pump Cooling Cycle

instances a relatively high generator temperature is required and the conversion from thermal energy to mechanical energy is only around 20% efficient leading to higher capital energy costs for such systems [19].

Electrochemical refrigeration is a relatively new concept based around a reversible chemical reaction that can absorb heat. The technology is still in its infancy and data on performance is limited.

2.3.6 Solar Cooling Technology Comparison

Table 2.5 shows a comparative summary of the existing solar powered cooling technologies along with notes on achievable COP values, relative cost per kW_{cool} and relative mechanical complexity. Table 2.6 lists some of the corresponding advantages, disadvantages and current applications for these technologies. Exotic technologies such as thermo-acoustic and magnetic refrigeration are not included in this comparison.

Of particular interest to this study are the cycles which are suitable for small scale refrigeration applications, specifically vaccine storage. In this area, PV driven vapour compression systems dominate the commercial landscape.

Vapour compression is a well understood refrigeration technology and therefore these systems required less innovation in order to realise market-ready products. The required capital investment for such systems should not be understated however, and the initial cost of WHO accredited vaccine refrigerators ranges from 2K-5K USD [21].

The other main technology which has had some success in this area is thermoelectric (peltier) refrigerators however the cost per kW_{cool} is around five times that of a similar capacity solar powered vapour compression system[19]

Solar thermal powered refrigerators are less common however both absorption and adsorption systems have been trialled and approved by the WHO. Although the initial costs are favourable when compared against PV powered vapour compression systems, the technical complexity makes servicing and maintenance an ongoing challenge for this emerging technology.

Previously, jet-pump systems have primarily been used in air-conditioning applications

Cooling Cycle	Minimum T_g (°C)	COP_{cycle}	Relative Cost	Mechanical Complexity
Solar Electric				
Vapour Compression	*PV*	3-5	***	***
Thermoelectric	*PV*	0.5	*******	*
Stirling	*PV*	1.7-3	****	*****
Solar Thermal				
Absorption Single Effect	80	0.6-0.8	*	****
Absorption Double Effect	150	1.2	**	*****
Adsorption Single Effect	80	0.3-0.8	**	****
Chemical Reaction	80	0.1-0.2	**?**	*****
Duplex Rankine	120	0.3-0.5	***	***
Dessicant Cooling	40	0.5-1.5	**	**
Jet Pump	80	0.3-0.8	**	*

* Primary sources [19],[21]

Table 2.5: Comparative evaluation of existing solar powered cooling technologies

Cooling Cycle	Advantages	Disadvantages	Current Uses
Vapour Compression	High COP, Commercially mature, Scaleable	High cost	Ref/Frz
Thermoelectric	No refrigerant or moving parts	Low COP = high cost Limited to small scale, Thermal short circuit when not powered	Ref/Frz
Stirling (El)	High COP, Low temperatures possible	High cost and complex design	Frz
Absorption Single Effect	Low Tg, No moving parts	Complex, Limited to 0°C when using LiBr/H2O	AC/Ref
Absorption Double Effect	Higher COP,	Suitable for large systems, Complex, Higher generator temps required.	AC/Ref
Adsorption Single Effect	Low Tg, No moving parts, Low temperatures possible	Limited to small scale, Low pressures challenging, Cycllic system	Ref
Chemical Reaction	Low temperatures possible, No moving parts	Low COP, Limited to small scale, Low pressures challenging, Complex	Ref
Duplex Rankine	Suitable for large scale, Poly generation	High cost, Large system, Lots of maintenance	AC
Dessicant Cooling	Low Tg, Environmentally friendly, Good for AC	Humidity affects performance	AC
Jet Pump	Low Tg required, Low cost and low maintenace, No moving parts,	Low COP, Works best at specific temperatures	AC

KEY :Frz = Freezing, Ref = Refrigeration and AC = Air-conditioning (Primary sources [19] and [21])

Table 2.6: Advantages and disadvantages of current solar powered cooling technologies

due; in part to the manufacturing limitations of small scale jet-pumps, and secondly to the difficulty in maintaining continuous performance at varying system conditions. In addition, lower evaporator temperatures result in lower entrainment ratios for the jet-pump therefore working at air-conditioning temperatures provides the best opportunity to increase the system COP.

The mechanical simplicity of the jet-pump cycle however, and low manufacturing cost, does have the potential to make it a good candidate for solar powered refrigeration. In addition, the low generator temperatures required allow flat plate collectors to be employed, further serving to reduce the cost of the entire system. For these reasons, consideration of the technology as a vehicle to providing low-cost refrigeration of vaccines in off-grid locations is valid.

2.4 Jet Pump Cooling Cycle

The following section examines the jet-pump cycle in more technical detail - reviewing cycle specific performance metrics and behaviours. A summary of the previous research into single stage, multiple stage and variable geometry jet-pumps is presented and discussed.

2.4.1 Jet Pump History

Records show that utilising the power of a discharging jet for the purposes of pumping was considered as early as 1570, however it was not until 1858, when Henri Jaques Giffard patented *"L' Injecteur Automoteur"* that the scientific study of jet-pumps (otherwise known as injectors, ejectors, eductors or thermocompressors) began in

earnest[30]. The Giffard injector used high pressure steam to pump water to the boiler in steam engines. Later, in 1901, LeBlanc and Parsons applied the technology to the refrigeration cycle, and developed the first steam jet refrigerator[31]. Although large air-conditioning (AC) systems using jet-pumps were developed during the 1930's the technology has received relatively little development attention since [28] and it is only during recent times that the potential benefits of the technology have been revisited.

2.4.2 Jet Pump Operating Principles

Jet pump technology provides a simple and reliable alternative to provide cooling from a thermal energy source. A jet-pump uses a high-pressure source, known as the primary flow, to create suction and entrain vapour or fluid, known as the secondary flow. The primary flow enters the jet-pump via a convergent-divergent (De Laval) nozzle and is accelerated to supersonic speeds, as shown in fig 2.9. As the flow exits the nozzle, an area of low pressure is formed within the mixing chamber and secondary flow is entrained and carried into the diffuser section of the jet-pump.

Referring to the pressure plot in figure 2.9, the back pressure from the condenser induces a shock wave in the supersonic flow within the constant area section, (throat) causing the flow to choke, and pressure recovery to occur

There are two methods of solving the momentum equations used in the design of jet-pumps; the constant pressure mixing assumption and the constant area mixing assumption. Experimental evidence has shown that jet-pumps designed using the constant pressure mixing assumption outperform those which are designed using the constant area assumption [28].

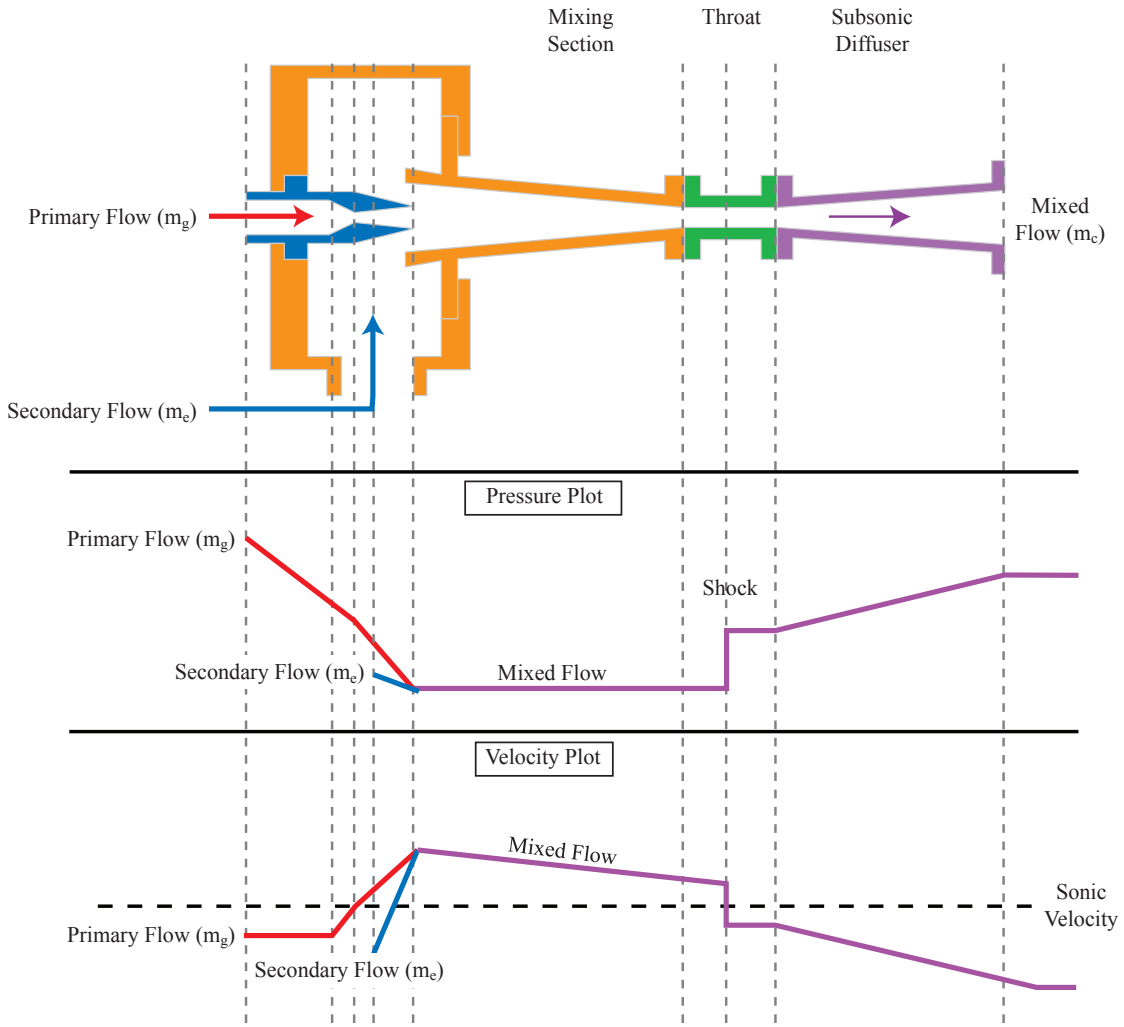

Figure 2.9: Jet-pump illustrative diagram showing flow velocity and pressure plots adapted from [28]

2.4.3 Jet Pump Performance Characteristics

Numerous factors have an impact on jet-pump performance, particularly system pressures (p_e, p_g and p_c). Several metrics, specific to jet-pumps have been defined by previous research (entrainment ratio and critical condenser pressure)and these are now presented.

Entrainment Ratio

The entrainment ratio (R_m) is one of the key performance characteristics of any jet-pump and is obtained, with reference to figure 2.9, via the equation 2.6

$$\begin{aligned} R_m &= \frac{\dot{m}_{sec}}{\dot{m}_{pri}} \\ R_m &= \frac{\dot{m}_{evp}}{\dot{m}_{gen}} \end{aligned} \tag{2.6}$$

The evaporator mass flow (also known as the secondary mass flow) determines the cooling capacity of the system and hence the COP_{cycle} of a jet-pump refrigerator system is closely related to the entrainment ratio (R_m).

Several factors affect the entrainment ratio, including the system pressures and jet-pump geometry. With a fixed jet-pump geometry, varying system temperatures also affects the entrainment ratio of the jet-pump.

An increase in evaporator temperature increases the entrainment ratio, as does a decrease in the generator temperature however the latter also requires a decrease in the

temperature of the condenser [23].

Critical Condenser Value

Under normal operation, the supersonic flow is choked within the constant area section of the diffuser. The position of this effect is governed by the pressure at the outlet of the diffuser section (p_c). As the outlet pressure increases, the choking location moves backwards into the mixing section and the entrainment ratio decreases rapidly. The outlet pressure at which this occurs is known as the critical value [31]. Operating close to the critical condenser pressure ensures that the jet pump is performing at an optimum level [28].

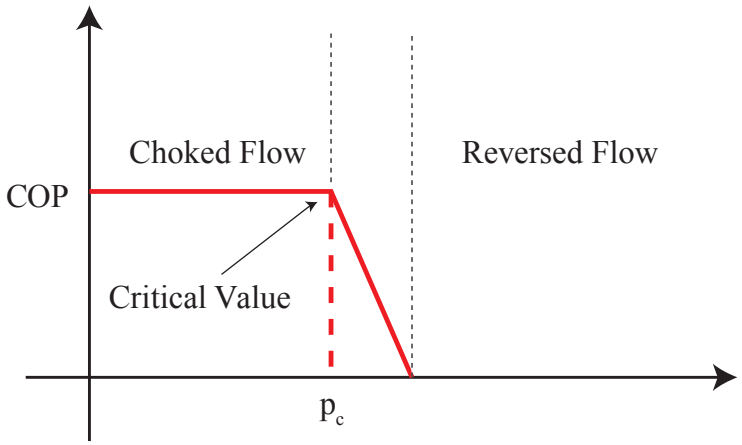

Figure 2.10: Critical pressure plot (Illustrative)

The only way to increase the critical condenser value, for a fixed jet-pump geometry, is to increase the pressure of either the generator or the evaporator. This requires either more heat input or a higher minimum cooling temperature respectively.

Studies have also shown that the position of the nozzle exit (NXP) is critical to the operating performance of the jet pump cooling cycle [32]. Retracting the nozzle out of the mixing section of diffuser generates a higher entrainment ratio, and higher COP, however reduces the critical condenser pressure. Conversely, higher condenser pressures can be achieved by inserting the nozzle further inside the mixing section of the diffuser however this results in a lower entrainment ratio due to the reduced CSA (annular area outside supersonic jet core) available for entrained secondary flow [33].

Working close to the critical value helps to achieve the best possible performance and therefore an optimum nozzle position can be found experimentally for each system based on fixed operating conditions [31].

2.4.4 Jet Pump Cooling Cycle Configurations

Single Stage Jet-pump Cooling Cycle

The schematic in figure 2.8 shows how the jet-pump can be used to replace the electrically powered compressor within a traditional vapour compression refrigeration circuit.

Thermal energy is used to provide heat to a vapour generator. This vapour is then used as the motive force to entrain fluid from the evaporator and generate the cooling effect.

Single stage ejector circuits typically have lower COP's than sorption systems, however higher COP values are attainable. One study reports on a system that has achieved COP's in excess of 0.8 however generator temperatures of 200°C were required [29].

Multi Stage Jet-pump Cooling Cycles

One of the key restrictions for the jet-pump cooling circuit is the sensitivity to changes in system temperatures/pressures. This is particularly problematic when ambient temperatures are considered as increases in the condenser pressure, beyond the critical pressure, dramatically affect the performance of the jet-pump.

One potential solution is to couple several jet-pumps in parallel, providing the flexibility to operate across a range of condenser pressures. The system schematic for a multi-stage jet-pump cooling circuit is shown in figure 2.11. Although the entrainment ratio (R_m) does fall at higher condenser pressure, secondary jet-pumps provide the capacity to continue effective operation [21].

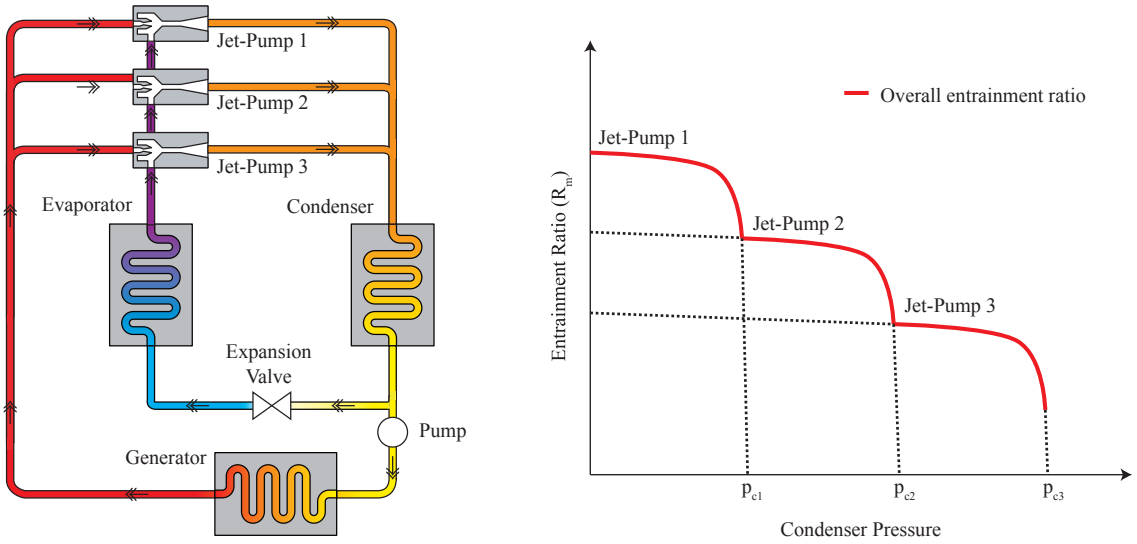

Figure 2.11: Multi Stage Jet Pump Cooling Cycle (Adapted from [21])

Another option is to operate two jet-pumps in series, which has been reported to provide

a 15% improvement in efficiency however higher generator temperatures are required for this strategy [34]. Although multi-stage ejector systems provide the flexibility to work with a wider range of system conditions, the relative complexity of such systems detract from the low costs associated with singe stage ejector circuits[28].

Hybrid jet-pump cooling cycles

Various hybrid systems have previously been considered, using jet-pumps to augment other refrigeration circuits. In particular hybrid adsorption systems and hybrid vapour compression systems are of interest. A schematic illustration of a hybrid jet-pump absorption cooling cycle is shown in figure 2.12

COPs of 1.04 have been reported in one study of a hybrid jet-pump absorption system, however high generator temperatures (190-210°C) were required [35]. Another study of jet-pump/adsorption integration shows that the addition of a jet-pump can increase the COP of an absorption system from 0.6 to 0.9 however. Again higher generator temperatures (160°C) are required [23].

Considering jet-pump augmented vapour compression cycles, one study reports on a system that saw a 50% efficiency increase following the addition of a jet-pump sub-cycle [36].

Although hybrid systems have the potential to provide higher efficiencies, the benefit in a cold-chain vaccine storage scenario is offset by the additional cost and complexity.

One suitable application for hybrid technologies is in the provision of air-conditioning for vehicles using the waste heat (20-400kW) from the engine as a thermal energy source [37]. It is estimated that 42-53 billion litres of petrol are used to provide air-conditioning

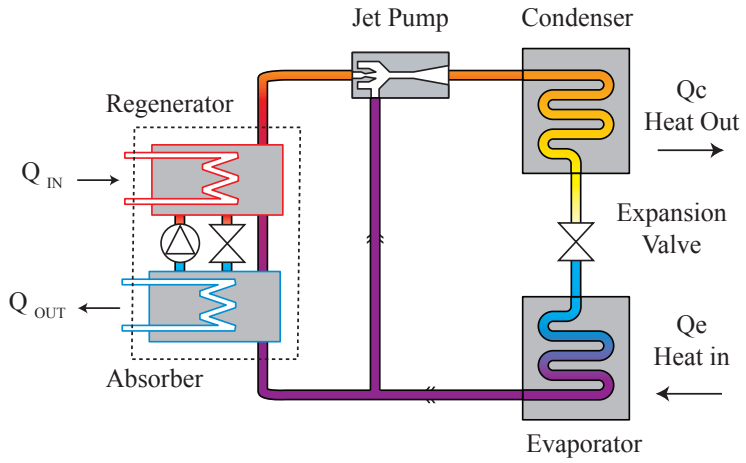

Figure 2.12: Hybrid Jet-Pump Absorption Cooling Cycle (Adapted from [35])

in vehicles each year in the US [37]. Toyota are currently developing a hybrid air-conditioning system that uses an additional jet-pump circuit to provide cooling for a chilled drinks compartment [38].

2.4.5 Jet-pump Cycle Enhancements

This sub-section of the literature review is used to investigate the potential benefits of enhancements to the single stage jet-pump cooling cycle.

Generator Refrigerant Circulation

Although the jet-pump itself has no moving parts, there is a requirement to deliver liquid refrigerant from the condenser circuit to the generator circuit and an electrically powered circulation pump is often incorporated into jet-pump cooling systems. Despite

the low power requirement of the circulating pump, the required electrical energy could prove a disadvantage for off-grid applications. A pump would require supplementary electricity supplied from PV panels. In addition, the increased complexity of service and maintenance should not be overlooked when evaluating the technology as a solution to vaccine storage in developing countries.

Various strategies have been explored to provide thermal pumping including gravity based systems and additional generators. One experimental study (Srisastra 2008 [39]) , using R141b, investigates the use of feed tanks and gravity to provide a *workless generator feed* (WGF). Although only minimal electrical power was required to operate the valving sequence of the system, an additional 10-15% thermal power input was required from the generator to operate the system. COPs ranging from (0.12-0.13) were reported at T_g = 110°C and T_e = 5°C. The experimental apparatus was designed to allow both parallel and series operation of two identical WGF systems, however this study focusses on parallel operation. It is suggested that series operation could provide more stability in generator temperature and uninterrupted vapour supply to the jet-pump. Practical evaluation of this study is difficult as the experimental set-up uses cooling water circuits and an auxiliary condenser.

Another R141b experimental study, which reports a COP of 0.218 (at T_g = 90°C and T_e = 8.2°C), proposes the use a multi function generators (MFG) which serves as both vapour generator and pump [40]. The concept relies on cooling jackets to remove unwanted heat from the generator feed chambers following refrigerant charging. In this study, the use of the MFG system reduces the COP by approximately 18%. Wang et al (2009) further developed the concept to achieve continuous operation with the use of two MFGs working in tandem. This study achieved experimental COPs of 0.225 (at T_g = 90°C, T_c = 37.5 and and T_e = 8.5°C). Practical evaluation of both systems is difficult

due to the requirement for cooling jackets (supplied with chilled water). All three of the above studies identify the need to minimise the frequency of generator cycles [39] [40][41].

Wang et al (2009)[41] also reports on the work of other in developing heat-driven pumps (HDP), however concludes that the use of HDPs in jet-pump cooling systems is problematic due to low efficiencies and complex parts.

Fully autonomous liquid feed systems have also been proposed for this application. The use of a float has been considered to actuate valve switch over, from condenser to generator circuits (see figure 2.13) however the practical implementation of this approach was not verified[42].

Nguyen et al (2001) proposed and constructed an jet-pump cooling system [43] that used potential energy (i.e. gravitational head) as the motive force to transfer refrigerant (water) from the condenser to the generator. Although the system achieved a COP of 0.32 (Q_e = 5.09 kW and T_e = 1.5°C) the required vertical separation between the condenser and generator was 7 m which limits the practical application of this approach.

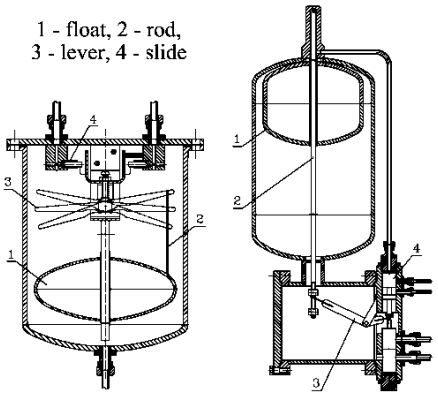

Figure 2.13: Illustration of automatic float-type feed mechanism - Petrenko 2011 [42]

Heat Recovery

One strategy used to improve the efficiency of jet-pump refrigeration systems, is the installation of pre-heater / pre-cooler heat exchangers. A pre-cooling heat exchanger can be installed on the suction line from the evaporator. As recently condensed fluid travels to the expansion valve, it is cooled by the vapour returning from the evaporator. A pre-heater works in a similar way, heating the fluid travelling to the generator using the waste heat at the condenser input. These methods help to improve the performance of the system via heat recovery [28][40][44][45].

Variable Geometry Jet-pumps

Research work has been conducted on variable geometry jet-pump systems that provide more flexibility in the operating conditions of any given system [44]. The increased cost and complexities of these systems detract from the simplicity offered by a fixed geometry jet-pump system.

2.4.6 Jet-pump Cycle Working Fluids

Another key factor that affects the operating performance of the jet-pump system is the fluid chosen as the refrigerant. The thermodynamic properties of the fluid determine the potential cooling capacity of the evaporator and the performance of the jet-pump. Further details on the specific criteria used to select a refrigerant for this particular study are discussed in more detail in section 4.3.1.

Water

Various working fluids have been trialled for jet-pump systems and in particular the use of water has been widely researched [23, 28, 31, 45]. Using water as a refrigerant provides several key advantages. From an environmental perspective, water has zero ozone depleting potential (ODP) and zero global warming potential (GWP). Water also has a high heat of vaporization, allowing low circulation rates in the system. For experimental studies, water has the benefit of requiring a comparatively large jet-pump due to the molecular size [45].

There are however drawbacks to using water as a working fluid. The main drawback is the limited range of operating temperatures. A steam jet-pump system requires comparatively high generator temperatures (120-160°C) to achieve low COP's (0.1-0.4) when compared against other refrigerants.[28, 31, 32, 45]

Another key consideration is that water freezes at 0°C and therefore this represents the minimum temperature achievable in the evaporator (unless anti-freeze is added).Water systems provide low entrainment and COP values when compared against hydrocarbon refrigerants [28, 45]. Additionally, it is necessary to hold vacuum pressures in a water system which can be prove practically challenging, particularly for smaller systems.

Chlorofluorocarbons (CFCs)

A simulation study that compares jet-pump performance for 11 different refrigerants shows that R12 has the highest entrainment ratio, however production and import of CFCs has been prohibited, under the Montreal Protocol, since 1995 [45].

Hydrofluorocarbons (HFCs)

Amongst the HFCs evaluated, R134a was shown to be a promising working fluid, achieving a theoretical COP of 0.46, given a generator temperature of 90°C, with corresponding evaporator and condenser temperatures of 5°C and 25°C respectively [45].

Various theoretical and experimental studies of jet-pump driven refrigeration systems that use R134a have been evaluated as part of this review. One of the benefits offered by an R134a system is the potential for comparatively low generator temperatures required (70-85°C) [28]. One theoretical study, that uses jet-pump theory originally proposed by Keenan et al [46], provides estimates of COPs ranging from 0.035-0.199 for a solar system operated in the Athens area with generator temperatures of 82-92°C [47].

Another experimental study shows that it is possible to realise COPs above 0.2 when using R134a as a refrigerant. This system is based on the opertaing conditions; T_e = 5°C, T_c = 27°C and T_g = 85°C [32].

Hydrocarbons (HCs)

Hydrocarbons can provide good system efficiency and one theoretical study [48], that uses R600a (iso-butane) as a refrigerant suggests a COP of 0.48 can be achieved for evaporator temperatures of 15°C (3.5 kW capacity). The study notes that the system can only be effective in an area with high solar radiant heat and where a low condenser temperature (5°C above ambient) can be maintained.

The development practicalities of working with a hydrocarbon refrigerant should not be understated and the risk of explosion or fire during commissioning is of key concern.

Ammonia

Using ammonia (R717) as a working fluid has several key benefits, not least of which is the zero ozone depleting potential (ODP) and zero global warming potential (GWP), however there are also limitations. As ammonia is not compatible with copper, steel pipework is required leading to higher costs. In addition ammonia is poisonous in high concentrations. A 2004 theoretical comparison study of the jet-pump working with various refrigerants [49], showed that ammonia achieved the lowest COP ($COP_{R717} \approx 0.14$) when $T_g = 3 \cdot Tc$ and $T_e = 5°C$. The same study reported favourable results for R134a at the same operating conditions ($COP_{R134a} \approx 0.37$).

2.4.7 Comparative Review of Jet-Pump Research

Previous research on the jet-pump cooling cycle has primarily been focussed on systems with larger evaporator cooling capacities (>4 kW), often implemented in AC applications.

Prior work in assessing systems with a smaller cooling capacity is limited and a comparative summary research into jet-pump cooling systems where $Q_e < 4$ kW is shown in figure 2.14

The vertical red line shows the cooling capacity of the proposed system (0.1 kW), highlighting the lack of prior research into jet-pump systems of this scale.

Of particular interest are three studies experimental studies, [52], [32] and [40] that tested systems with cooling capacities below 1 kW and these are discussed in more detail below.

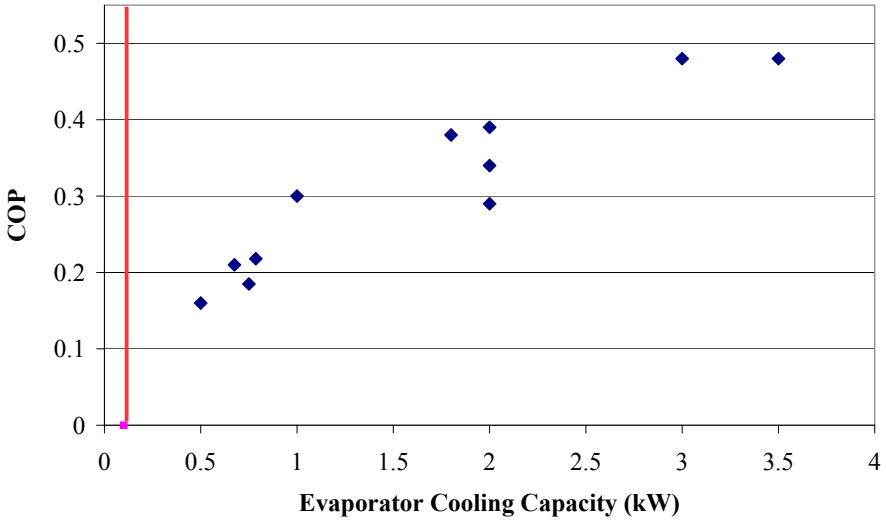

Figure 2.14: Comparative plot of prior jet-pump refrigeration research Extracted from [50],[51],[40], [52], [32],[39],[53] and [48].

Murthy et al - 1991 [52]: This study makes use of R11 as refrigerant, at generator temperatures of 75 to 85°C, evaporator temperatures of -3 to 18°C and a fixed condenser temperature of 33°C. Cooling water circuits are used to control the temperature of both the evaporator and condenser and achieve steady state operation however this makes the practical evaluation of the system difficult as the operating temperatures are fixed. The study provides a useful comparative evaluation of eight jet-pumps (configurations derived from a selection of 5 nozzles and 7 diffusers) and characterises the performance across a range of different evaporator and generator temperatures. COPs ranging from 0.08 - 0.33 are reported with the highest performing jet-pump configuration *(N3-D5)*at $T_e = 6°C$) provides a COP of 0.21 ($Q_e \approx 650$ W)

Selvaraju and Mani - 2006 [32]: This study shows that it is experimentally possible to realise COPs above 0.2 for a cooling capacity of 500 W using R134a as a working

fluid. The study reports experimental results with generator, condenser and evaporator temperatures of 65-90°C, 26-37°C, and 2-12°C respectively. Working at this lower capacity provides several key challenges, not least of which the manufacture of a miniature jet-pump.

Once again, the experimental set-up of the study is geared toward proving the performance of the jet-pump alone, rather than the entire system. The experimental set up employs both a diaphragm pump for refrigerant circulation and a water-cooled condenser. In addition, chilled water is circulated through the evaporator to help remove initial evaporator refrigeration load. This lab-based set-up does not provide the opportunity to evaluate the potential of the refrigerator as an autonomous, solar-powered system.

Huang et all - 2006 [40]: This study uses R141b as a working fluid, and realises experimental COP values of 0.22 at 0.79 kW evaporator cooling capacity (T_g =90°C, T_e = 8.2 T_c = 32.4°C). This study draws particular attention to the potential of a the jet-pump cycle in providing cooling without the need for any (or very little) electrical energy. A multi-function generator is described that, at a cost of $\approx$ 15% thermal energy input, transfers refrigerant from the condenser to the generator. Although the primary motive force is pressure differential, the study also describes the vertical arrangement of system components necessary for gravity to assist the fluid transfer. A dual-generator system is proposed that would allow continuous jet-pump operation, with the performance estimated via a single generator prototype. Once again, the experimental study employs of cooling water circuits to attain steady state operation, thereby preventing evaluation of the system under *"real world"* conditions.

2.5 Chapter Conclusions

2.5.1 Summary of Literature Review

The literature began by establishing a need for solar powered refrigerator to transport and store vaccines in the developing world.

A broad review of solar cooling technologies was then presented and evaluation metrics discussed. Prior research into both solar electric systems and solar thermal systems has been presented and comparatively reviewed.

After evaluating the currently available technology, the jet-pump cooling system has been identified as a mechanically simple, and potentially lower cost, alternative to more commercially mature technologies (e.g. photovoltaic driven vapour compression systems).

Prior research which defines jet pump operating principles, relevant performance metrics and experimentally characterised behaviour has been presented and discussed. The various configurations of the jet-pump cooling system have been reviewed and both theoretical and experimental studies of the jet-pump cycle, using a variety of different working fluids have been examined. A comparative review of previous research into small capacity (< 4 kW) jet-pump cooling systems has also been presented.

2.5.2 Specific Research Opportunities

Following the literature review this section identifies the research opportunities, based on the lack of published work in specific areas.

Evaporator Cooling Capacity

Previous research on the jet-pump cooling cycle has primarily been focussed on systems with larger evaporator cooling capacities, often implemented in AC applications.

As illustrated in figure 2.14, prior research in assessing jet-pump systems with smaller cooling capacities (<4 kW) is limited.

Use of Appropriate Technologies

The literature review revealed that little consideration has previously been given to the use of appropriate technologies in prior studies of solar powered jet-pump cooling systems. When evaluating the system as a potential technology for the provision of solar-powered vaccine refrigeration, many factors other that efficiency should be considered.

The core components of a jet-pump cooling systems are relatively simple to both manufacture and maintain. This simplicity provides a compelling argument for the application of the technology in remote, off-grid locations where spare parts and competent service engineers are limited in availability. The simplicity of the system also has the potential to provide off-grid refrigeration at a reduced cost: another important benefit when comparing against the considerable initial capital investment required for existing solar powered vaccine refrigerators (e.g. photovoltaic driven systems).

Minimising the electrical requirements of any off-grid, solar-powered system reduces the requirement for expensive photovoltaic panels. Some prior research (Srisastra 2008 ([39] and Huang 2006 [40])has reported experimental studies into the benefits of replacing the

electrical pump, conventionally used to transfer refrigerant from the refrigerant circuits (condenser) to the jet-pump circuit (generator), with a reservoir transfer mechanism that employs a combination of potential (gravity) and thermal energy (lost) to transfer refrigerant between the two circuits. These previous studies are difficult to appraise as *real-world* solutions as they have both used secondary water circuits (e.g. cooling jackets).

The practicality, serviceability and initial capital investment should all be included in the appraisal of jet-pump technology for solar powered vaccine refrigerators.

Autonomy and Repeatability

The reviewed experimental research studies do not provide sufficient detail of automated control systems or control procedures. Understanding the characterised performance of the system (including outside design point operating conditions) is important when evaluating the practical benefits of system in providing autonomous cooling.

2.5.3 Conclusion

The current technologies used in the provision of solar powered refrigeration (primarily PV driven) present challenges for use in developing countries due to the complexity of such systems, the relative cost and the technical knowledge required to maintain and repair them.

After evaluation of the literature on existing solar powered cooling technologies, a requirement for low cost, solar powered refrigeration systems has been identified. Not only can they provide refrigeration for off-grid applications such as vaccine storage, but

they also have the potential to reduce carbon emissions on a wider scale. The correlation between higher levels of solar irradiance and higher cooling requirements provides a compelling benefit for such systems, however existing technologies (e.g. PV vapour compression refrigerators), have a significant cost attached (≈€4,200 per kW cooling [19]). In recent times the falling cost of photovoltaics ($4.76 per watt for systems $\leq$ 2 kW: 2013 median cost [25])has led to a decrease in the prices of PV powered VC refrigerators, however the cost of WHO approved vaccine refrigerators is still relatively high (≈£3,450).

Although research has previously been conducted on jet-pump refrigeration systems, the work in evaluating these systems at a smaller scale (≈ 100 W), has been overlooked. Such a system could potentially be suitable for the transport and storage of temperature sensitive medicines such as vaccines. Evaluation of such a system requires "real world" constraints to also be considered such as the availability of cold water circuits or electrical power requirements. Relatively few experimental studies have attempted to appraise the system with this practical rigour.

Jet-pumps cooling systems offer low capital cost (≈€1,700 per kW cooling [19]) with potentially higher reliability that adsorption or absorption, therefore research in this area is justified and relevant.

In order to analyse the potential of jet-pump refrigeration fully the complete system must be experimentally tested and optimised. If adequate COP values can be attained, at reasonable cost, it is hoped that jet-pump technology can provide a viable solution to the challenge of off-grid transport and storage of temperature sensitive vaccines.

Chapter 3

Proposition

Every year, millions of people die from diseases that are preventable by vaccination. The lack of an effective cold-chain in developing countries means that many of the vaccinations intended for administration are spoiled and wasted. Poor energy infrastructure in these countries is often coupled with high solar irradiance values, providing a compelling reason for research into effective solar powered refrigeration systems. Photovoltaic driven vapour compression systems have been developed to meet this requirement however the relative complexity of these systems provide challenges in terms of capital cost, reliability and the technical knowledge required to maintain and repair them.

A number of studies have shown that a refrigeration system, thermally powered via a jet-pump circuit as an alternative to an electrically driven compressor, could provide a working solution. Such a system could be powered largely by heat (i.e. solar energy) and would find application in developing countries with high solar availability. These studies (described previously in chapter 2) identified the need to optimise the geometry of the

jet-pump for the specific applications (i.e choices of refrigerant and working pressures) Previous research has also characterised the performance of jet-pump systems working above and below design point conditions however relatively few studies have investigated automated control systems that adjust generator temperature to match demand.

Several studies have identified the potential benefits associated with minimising the (already small) electrical requirements of the jet pump cooling cycle. The primary electrical requirement of the system is the pump required to transfer liquid refrigerant from the condenser to the vapour generator. Replacing this pump with a thermally powered mechanism would significantly reduce the electrical requirements of the system and various alternative methods have previously been proposed and experimentally evaluated, however these studies rely on the availability of a secondary heat sink (i.e. cold water circuit).

A comparative review of prior research into small scale (<4 kW) jet-pump refrigeration systems (see figure 2.14) highlighted a gap in existing knowledge as the performance of small scale units (<500 W) has not previously been investigated either for performance, component/system design or optimisation.

Accordingly, it was proposed to investigate the design of a small, ($\approx$ 100 W) cooling duty solar powered refrigeration system.

The method used was to investigate discreet elements of the system using a combination of theoretical design and experimental component performance observations, leading to an automated experimental prototype unit which was investigated in respect to its overall performance.

The three main investigations were:

- Experimental investigation, optimisation and evaluation of a 100 W jet-pump cycle refrigerator.
- Experimental, investigation of novel, low power alternatives to an electrically powered generator feed pump.
- Experimental evaluation of a complete system using appropriate supporting technologies (i.e. no use of secondary heat sinks and minimal use of electrical power/moving parts).

The outcomes of this research were:

- Experimental data showing the characterised performance of the optimised jet-pump for comparison against theoretical performance data.
- Experimentally validated performance data for individual sub-systems (e.g. evaporator).
- Experimental data showing the operation of a novel, low power generator feed system.
- Experimental data showing the performance of a complete system, automatically controlled using technology appropriate for off-grid vaccine storage.
- Evaluations of the systems limitations including cost estimates of the new system for comparison against competing technologies.

The original contributions to knowledge are;

- Experimental data from a small capacity (≈100 W) jet pump refrigeration system.
- Experimental investigation of a novel generator refrigerant feed system that minimises the electrical power requirements of the system (i.e an alternative to an electrically powered, high pressure differential pump)
- Experimental investigation of the jet-pump refrigerator using technologies appropriate for the application (i.e. off-grid vaccine transport and storage) including;
  - Avoidance of cooling water circuits (i.e. no secondary heat sinks).
  - Minimal use of moving parts, (e.g. natural convection heat transfer, rather than fan driven forced convection, used at evaporator and condenser).
  - Adaptive, automated control systems to provide effective performance outside of design point operating conditions

Chapter 4

Feasibility, Concept Design and Methodology

4.1 Introduction to Chapter

The literature review identified a research opportunity in the area of low capacity, solar powered jet- pump refrigeration. This chapter describes the initial concept design of the prototype system. Building on the existing knowledge (Chapter 2), the research proposition (Chapter 3) and existing WHO standards for solar powered vaccine storage refrigerators [54], the system specifications are defined in this chapter and the feasibility evaluated.

The chapter begins with a summary of the key thermodynamic formulae used to calculate system conditions. A review of the assumptions made to facilitate subsequent calculations is then presented and an introduction to natural (free) convection heat

transfer theory and the estimates used in this study is also provided.

The choice of working fluid, refrigerant R134a, is justified with particular reference to previous research and approximate system conditions.

The basic operation on the jet-pump cooling cycle is then revisited, to provide context specific information to the reader. A specification for the refrigerated compartment design temperature, volumetric capacity and evaporator heat transfer rate is then defined, based upon the relevant WHO standards for solar powered vaccine refrigerators. The required evaporator flow rate is then calculated.

A generator temperature range is set, based upon the performance of flat panel collectors currently available. The entrainment ratio of the jet-pump is calculated (based on previous research) and the generator flow rate is estimated. This provides an initial estimate for the heat transfer rate of the generator.

With the combined totals of generator and evaporator flow rates estimated, the condenser flow rate can now be estimated. The same is also true for the combined heat transfer rates of the evaporator and generator. A maximum condenser temperature is then defined, based the the ambient temperatures provided in WHO guidelines. At this stage, an initial performance specification for the experimental prototype is defined.

The jet-pump specification is then considered. Based on the estimated generator mass flow and operating temperature, an approximation of the nozzle throat area is then calculated. The computational fluid dynamics (CFD) study [55] is then introduced. Geometric design data for the jet-pump is presented and the final design point operating conditions of the system are calculated. The system design method is summarised in flow chart format in figure 4.1.

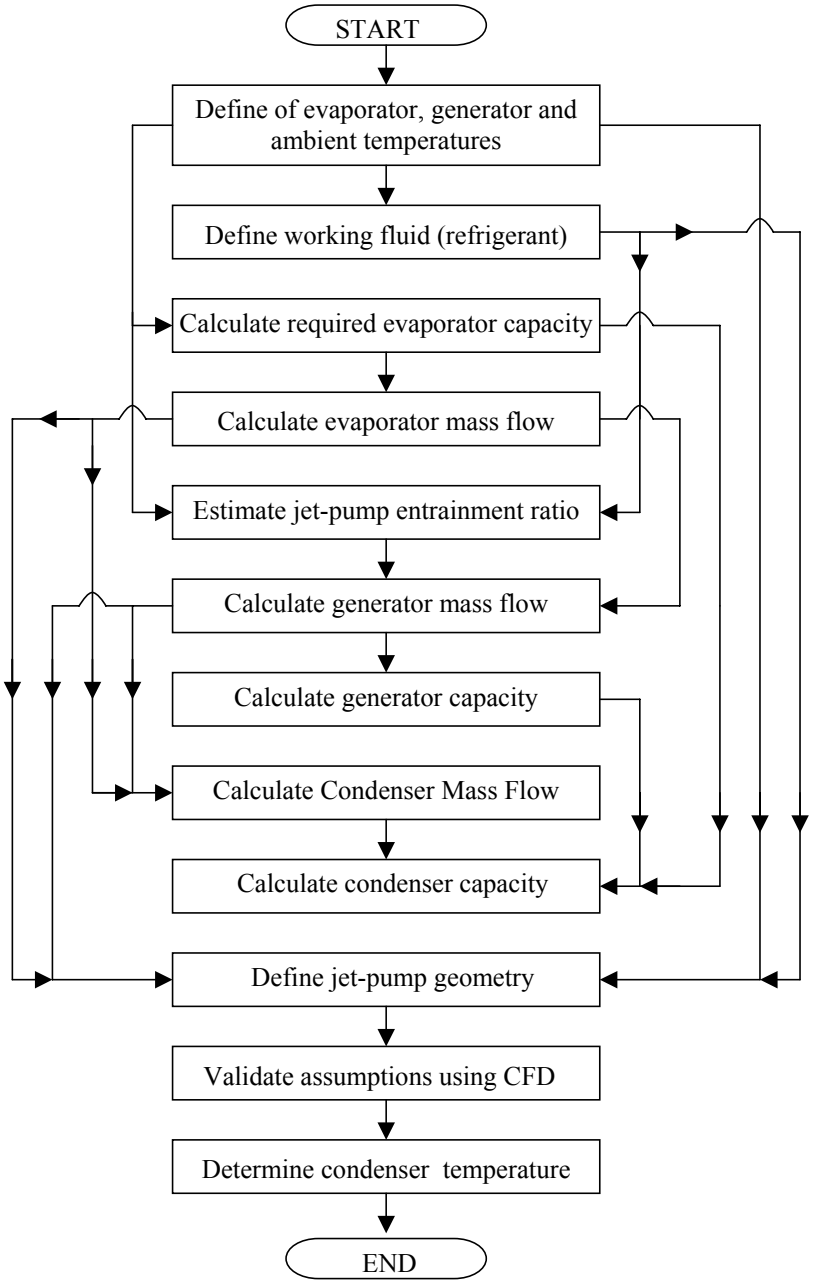

Figure 4.1: System Design Methodology Flowchart

An outline of the design strategy for each sub-system is provided, drawing specific attention to the target operating power of the generator refrigerator feed system. The chapter concludes with a product design specification (PDS) for a solar powered vaccine refrigerator, based on WHO guidelines, which can be used later for evaluation of the prototype system.

4.2 Methodology and Assumptions

The key formulae used in the design calculations are presented in this section along with the critical assumptions made to facilitate an initial feasibility evaluation.The section concludes with a review of natural convection heat transfer theory.

4.2.1 Key Assumptions

- **Specification**

  The system will operate as a refrigerator (0-10°C) and will be powered using low cost flat plate thermal collectors at vapour generator temperatures below 100°C.

- **Environmental Assumptions**

  This research aims to develop a prototype system capable of active cooling during sunny periods. The jet-pump will operate most effectively during times of peak irradiance and an assumption of 1 $kW \cdot m^{-2}$ is made for most calculations. The apparatus will be tested in ambient conditions ranging from 20 - 27°C. The normal temperature of the laboratory where this research was conducted was 22°C however air-heaters could be used to simulate higher ambient temperatures.

- **Collector Efficiency Assumptions**

A collector panel efficiency of 50% was assumed which is in-line with current mid-range solar thermal collectors. Given a collector area of 2 m^2 and an irradiance value of 1 kW/m^2, up to 1kW thermal energy would be available from the generator sub-circuit.

- **Initial Entrainment Ratio Assumptions**

  Based on previous experimental studies of jet-pumps ([32]) an entrainment ratio of 0.15 has been assumed for initial sizing estimates prior to the computational fluid dynamics study.

4.2.2 Natural Convection : Theory and Approximations

Both the evaporator and condenser sub-systems make use of natural (free) convection heat exchangers. In order to theoretically evaluate the performance of a heat exchangers in this operating mode, the surface heat transfer coefficient (H_{conv}) must be estimated. Appendix B shows the theoretical method used to calculate a surface to air convective heat transfer coefficient of 7.5 $W/m^2 \cdot K$. Newtons law of cooling (equation(4.1)) can then be applied using the temperature difference (ΔT) to find the heat transfer rate (Q)

$$Q_c = H_{conv} \cdot A \cdot \Delta T \tag{4.1}$$

The equation can be further refined by taking account of fin efficiency (η_{fin}) as shown in equation 4.2. Calculation of theoretical fin efficiency can be complex, however it has been shown that aluminium fins with a height of less than ≈34 mm yield efficiencies of 90% or above ([56]). This calculation is based on a uniform heat transfer coefficient (7.5 $W/m^2 \cdot K$) across the entire fin and a rectangular fin profile of 1 mm width. As all of the finned tube samples, evaluated later in chapter 5, have fin heights below 34 mm fin

efficiency is assumed to be 100%.

$$Q_{hx-th} = H_{conv} \cdot A \cdot \Delta T * \eta_{fin} \tag{4.2}$$

4.3 Refrigerant Selection

The selection of a suitable working fluid is one of the critical design options for a jet-pump cooling cycle. This section describes the selection criteria and justifies the choice of R134a.

4.3.1 Refrigerant Selection Criteria

A number of refrigerants were considered for this study and evaluated against the following criteria.

- The fluid should be well matched to the cooling cycle specification ; i.e a positive pressure at the minimum evaporator temperature and the lowest possible pressure at maximum generator temperatures.
- The fluid should have a high latent heat of vaporisation in order to minimise the work required per unit of cooling capacity [1].
- Due to the small capacity of the system and the manufacturing limitations for the nozzle/diffuser, a working fluid with a smaller molecular mass is preferred as this will require a comparatively larger ejector [45].
- The fluid should be non-toxic, non-flammable and non-corrosive. Selecting a fluid

that is safe to work with will help to accelerate research and reduce the cost of manufacturing and maintenance.

- The fluid should be low cost and readily available, as this will help to accelerate research and reduce the cost of manufacturing and maintenance.
- The fluid should be environmentally friendly (e.g. no CFCs as per the Montreal Protocol)
- The fluid should have favourable thermodynamic qualities, e.g. low viscosity and high thermal conductivity [1].

4.3.2 R134a - Justification and Limitations

R134a was selected as the working fluid for the system for several reasons. The literature review provides a good foundation on which to build [32, 45, 47, 57]. Another key reason for selecting R134a is that the refrigerant has suitable thermodynamic properties for the proposed system temperatures. Even at 0°C, R134a is still a liquid at positive pressures of 3 bar. At the higher end of the temperature scale the p-h diagram for R134a shows that even at temperatures of 100°C, the saturation pressure is below 40 bar absolute.

R134a is a well understood and readily available refrigerant; the availability of standard OEM components (e.g. TEV) also make this working fluid an attractive choice.

For development, manufacturing and maintenance purposes, R134a is also a prudent choice, achieving the safest rating, A1, for flammability and toxicity (BS EN 378 [59]).

In comparison to other refrigerants (R11,R12,R113, R123, R141b) R134a has a relatively low molecular mass meaning the ejector can be a comparably larger ejector which is a

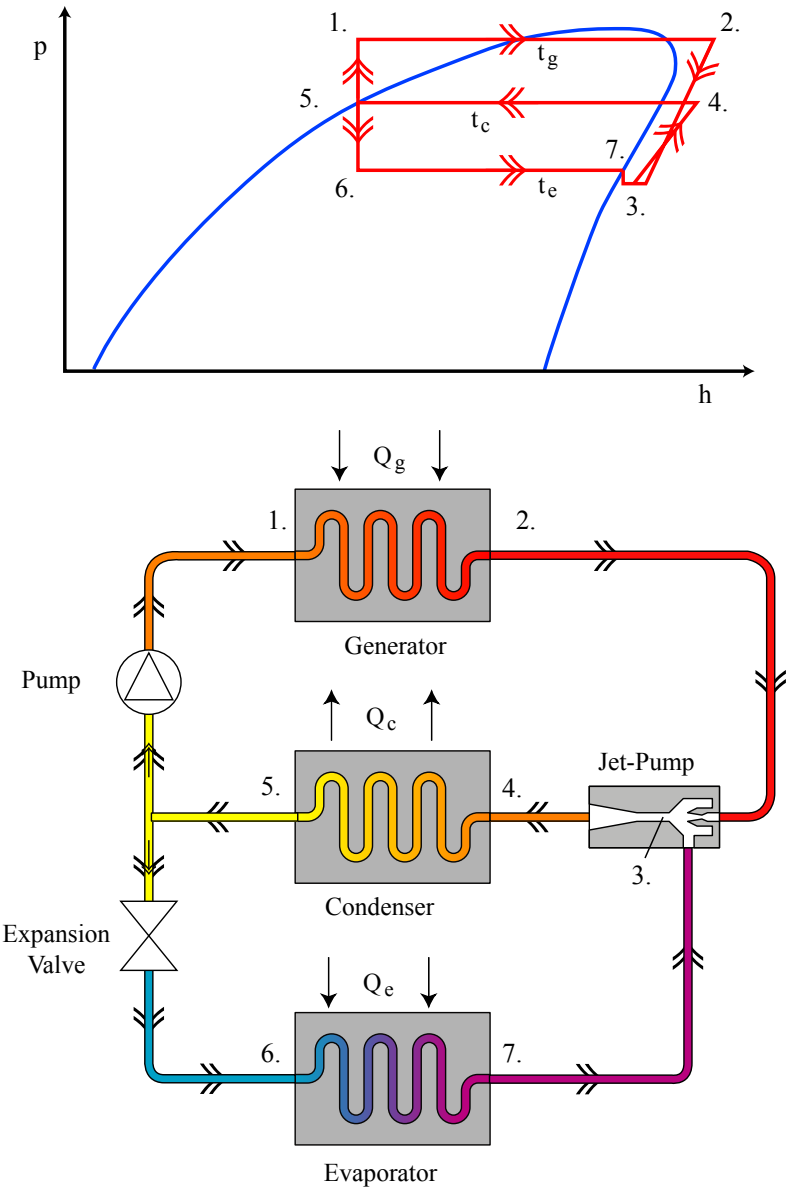

Figure 4.2: R134a p-h plot and schematic diagram of proposed cycle adapted from Yapichi 2005 [58]

benefit when working at lower capacities. [45][1]

One drawback of using R134a is that it is has a negative gradient on the vapour side of the T-s diagram, meaning that that the refrigerant will undergo a phase change during the expansion process through the primary nozzle. This means that small droplets of liquid could form, restricting flow and potentially damaging the nozzle tip and interrupting normal flow [60]. This difficulty however can be overcome by super-heating the vapour that is supplied to the jet-pump.

4.4 Jet Pump Cooling Cycle Sub-Circuits

As presented in the literature review, chapter 2, the simplified schematic of a solar-powered jet-pump refrigeration cycle (Figure 4.3), illustrates the key refrigerant flow circuits. The compressor found in a traditional vapour-compression refrigeration cycle is replaced by a jet-pump, which is powered by a solar thermal panel on a secondary circuit.

A description of the three sub-circuits and their function is provided below.

The Generator Sub-circuit

Fed from the condenser reservoir, the generator sub-circuit is used to generate a supply of high-pressure refrigerant vapour, necessary to power the jet-pump which is used to entrain flow from the evaporator. The thermal energy source for the generator is the energy collected from the solar panels.

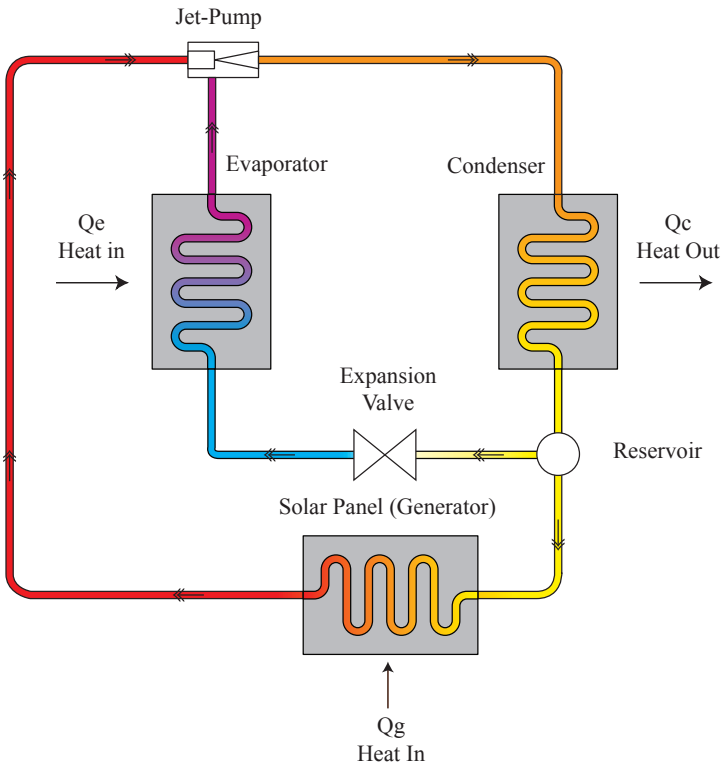

Figure 4.3: Simplified Schematic of Jet-Pump Cooling Cycle

The Condenser Sub-circuit

The mixed flow exiting the jet-pump then continues to the condenser where it loses thermal energy to the surroundings and re-liquefies before collecting in the condenser reservoir. The reservoir also supplies refrigerant to the evaporator cooling circuit.

The Evaporator Sub-circuit

Liquid refrigerant undergoes a sudden pressure drop upon passing through the expansion valve at the inlet of the evaporator. This causes the liquid to vaporize and, under low pressure, boil, drawing thermal energy from the cool box via the evaporator coils. The flow is entrained by the jet-pump completing the circuit.

4.5 Evaporator Requirement Specification

This section of the chapter sets out a specification for the prototype system, drawing particular attention to standards for vaccine storage.

4.5.1 Relevant Standards

The World Health Organisation published a number of specification standards for solar powered vaccine refrigerator in 2007 which were subsequently revised in 2010 [54]. These standards primarily focus on the traditional vapour compression cycles (e.g. [61]) however specification for absorption cycle refrigerators have also been issued [14]. A review of all the pertinent WHO standards revealed some common specifications which

are relevant to this study.

- **Temperature Range**[54]

  The acceptable temperature range for storing vaccines is +2 °C to +8 °C. However transient excursions outside this range will be tolerated, within the following limits. No excursion must exceed +20 °C. No excursion must reach 0 °C. The mean kinetic temperature (MKT) over a five day test must fall within the primary temperature range.

- **Temperature Zones**[54]

  Hot Zone : Hot zone units must operate at a steady +43 °C ambient temperature and over a +43 °C / +25 °C day/night cycling range

  Temperate Zone : Temperate zone units must operate at a steady +32 °C ambient temperature and over a +32 °C / +15 °C day/night cycling range

  Moderate Zone : Moderate zone units must operate at a steady +27 °C ambient temperature and over a +27 °C / +10 °C day/night cycling range

- **Water-pack freezing**[54]

  In combined units with a freezer compartment, a minimum of 1.6 kg and not less than 2.4kg per 50 litres of gross freezer volume must be frozen per 24hrs. Some overnight ice loss is acceptable

- **Montreal Protocol**[54]

  The refrigerant should not be banned under the Montreal Protocol which legislates against substances that deplete the ozone layer

4.5.2 Evaporator Temperature

The WHO guidelines for vaccine storage refrigerator were used to generate an initial specification for the experimental system. An evaporator temperature range of +4°C to +8 °C was selected (based on the range given in the WHO standards (+2 °C to +8 °C) As lower temperatures are a challenge for jet-pump systems, maintaining an evaporator temperature below 4 °C is likely to be difficult.

4.5.3 Evaporator Storage Volume and Cooling Capacity

Based on a mean target evaporator temperature of +6 °C, and the selected volumetric size of the refrigerated compartment, the required heat transfer rate (cooling capacity) of the evaporator can be calculated, using the WHO standards as a guide.

Refrigerator Volumetric Capacity (Storage Volume)

Although the liquid volume per vaccine is relatively small (5-10 ml), allowing water to be stored alongside the vaccines provides a useful thermal damping effect that will mitigate against temporary fluctuations in air temperature when new stock is being added to the cool-box. In addition, due to the the large latent heat released from water prior to freezing, the risk of dropping the temperature of the cool box below 0 °C is greatly reduced. In addition to the required volume for the water load, a large evaporator surface area would allow for a lower ΔT between the evaporator pipework and cool-box air temperature. The prototype evaporator pipework was estimated to occupy 120 L of the total cool-box volume. Allowing for an air-gap below the water load and the height/volume of the evaporator pipework, a volumetric capacity of 300 L was specified

for the refrigerated compartment.

Evaporator Heat Transfer Capacity

Using the WHO specifications as a guide [54][14][61], a target evaporator heat transfer rate (Q_e) was calculated. For combined units with a freezer compartment, the WHO guidelines provide a specification for the amount of ice which must be produced in a 24hr period (2.4kg per 50 lites of gross freezer volume). Although the experimental system in this study will not be acting as an ice freezer, it is possible to use this specified performance as a metric to calculate the required Q_e. Taking the worst case WHO specified environmental conditions (ambient of +43 °C), the required heat transfer rate can be calculated thus.

$$
\begin{aligned}
&\textit{Given...} \\
\textit{Specific heat capacity of water } (C_{p-water}) &= 4.186\ kJ/kg \cdot K \\
\textit{Heat of fusion of ice } (L_{f-ice}) &= 334\ kJ/kg \\
\textit{Mass of ice required in 24 hrs } (m) &= 14.4\ kg \\
\textit{Initial temperature of water} &= 43°C \\
\textit{Energy to reduce water temperature to } 0°C (E_1) &= m \cdot C_p \cdot (t_2 - t_1) \\
&= 2,983\ kJ \\
\textit{Energy to freeze water } (E_2) &= m \cdot L_{f-ice} \\
&= 4,810\ kJ \\
E_{total} &= E_1 + E_2 \\
&= 7,792\ kJ
\end{aligned}
\tag{4.3}
$$

To remove this much energy in 24hrs, Q_e a heat transfer rate of 90 W. This was rounded up to 100 W. Although hot zone ambient temperatures (+43°C) have been used to calculate the required cooling capacity, the ambient temperature will also act as a limitation when considering the required condenser capacity.

The use of phase change materials (PCMs) is discussed later in the thesis as a mechanism of providing a thermal damping effect similar to that which ice packs would offer.

Evaporator Mass Flow Rate

Given a cooling capacity of 100 W, equation 4.4 can be re-arranged to find the evaporator mass flow ($\dot{m}_e$) using the latent enthalpy (h_{lat} = $h_{vap-evap}$ - $h_{liq-cond}$) of R134a at 6 °C

$$\begin{aligned} \dot{Q}_e &= \dot{m}_e \cdot h_{lat} \\ \dot{m}_e &= \frac{\dot{Q}_e}{h_{lat}} \\ &= 0.7 g/s \end{aligned} \tag{4.4}$$

4.6 Generator Requirement Specification

Generator temperatures as low as +85 °C have previously been used to power jet-pump cycles [28] however lower generator temperatures also limit the COP of the system via maximum Carnot efficiency. Current mid-range flat plate collectors operate in the region of +80 °C to +100 °C, with efficiency dropping off above these temperatures. A median value of +90 °C is used for these initial specification calculations.

Previous studies have reported entrainment ratios for low capacity jet-pump cycles operating anywhere in the range of 0.1. to 0.2 [32]. A median value of 0.15 is used for these initial specification calculations.

Given the previously estimated evaporator mass flow (m_e) of 0.7 g/s and an entrainment ratio of 0.15, the generator mass flow (m_g) can estimated at 4.7 g/s using equation 2.6.

Equation 4.4 is adapted (as shown in equation 4.5) to calculate a generator heat transfer rate of 788 W. This result provides a COP_{theo} of 0.13. As the generator is required to raise the temperature of the refrigerant fluid arriving from the condenser , an initial estimate of the condenser temperature was required to in order to calculate Q_g. As described in section 4.7 a condenser temperature, of 40 °C is used in this initial specification estimate.

$$\dot{Q}_g = \dot{m}_g \cdot (h_{vap\_gen} - h_{liq\_cond}) \tag{4.5}$$

4.7 Condenser Requirement Specification

With the combined estimated mass flow rates of the evaporator and generator the condenser mass flow rate can now be derived via equation 4.6

$$\begin{aligned} \dot{m}_c &= \dot{m}_e + \dot{m}_g \\ &= 5.4 g/s \end{aligned} \tag{4.6}$$

Similarly, the combined heat transfer rates of the evaporator and generator provide an initial estimated heat transfer rate for the condenser via equation 4.7

$$\begin{aligned} \dot{Q}_c &= \dot{Q}_e + \dot{Q}_g \\ &= 888W \end{aligned} \tag{4.7}$$

Considering the ideal Carnot cycle, as described by equation (2.5) , a condenser temperature of +40°C (with $T_g = 90$°C and $T_e = 6$°C) provides a theoretical COP_{carnot} of 1.13 as illustrated by figure 4.4. It is important to note that this ideal performance takes no account of any additional mechanical/thermal energy used in the transfer of refrigerant from the condenser sub-circuit to the generator sub-circuit.

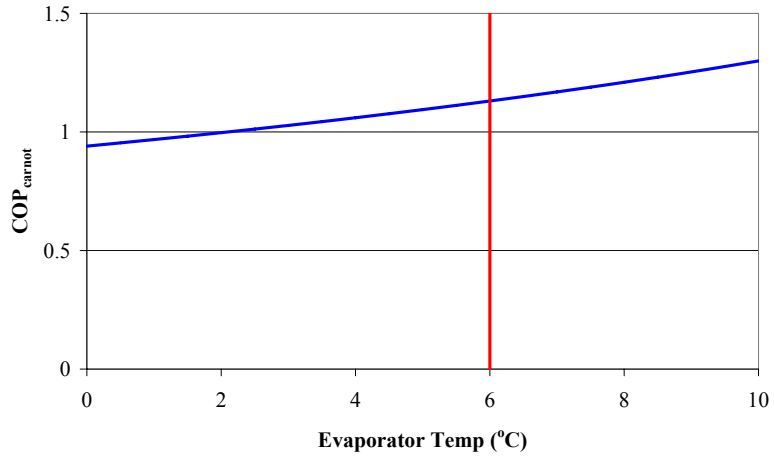

Figure 4.4: Graph showing ideal Carnot perfromance at $T_g = 90$ °C, $T_c = 40$ °C

4.8 Initial System Condition and Performance Specification

This section provides a specification for the system temperatures based on initial performance estimates. With design temperatures of the three sub-circuits specified, the other properties of the refrigerant could be sourced from data tables. [62]. These tables provide data on refrigerant properties at intervals of 5°C. Where the value required (X_{req}) fell between two of the values provided (e.g. +6 °C falls between 5 °C and 10°C), equation 4.8, based on a constant gradient, can be rearranged (equation 4.9) to interpolate the required value. Via this method, a range of thermodynamic properties, at the given operating temperatures, were interpolated and compiled into table 4.1.

$$\frac{X_2 - X_1}{T_2 - T_1} = \frac{X_{req} - X_1}{T_{req} - T_1} \tag{4.8}$$

$$X_{req} = X_1 + \frac{(T_{req} - T_1) * (X_2 - X_1)}{T_2 - T_1} \tag{4.9}$$

Evaporator		Condenser		Generator	
T_{evp}	$\Rightarrow$ 6°C	T_{con}	$\Rightarrow$ 40 °C	T_g	$\Rightarrow$ 90 °C
p_{evp}	$\Rightarrow$ 362.64 kPa	p_c	$\Rightarrow$ 1016.3 kPa	p_g	$\Rightarrow$ 3243.3 kPa
ρ_{g_evp}	$\Rightarrow$ 17.68 kg/m^3	ρ_{g_con}	$\Rightarrow$ 50.05 kg/m^3	ρ_{g_gen}	$\Rightarrow$ 216.45 kg/m^3
h_{f_evp}	$\Rightarrow$ 208.11 kJ/kg	h_{f_con}	$\Rightarrow$ 256.38 kJ/kg	h_{f_gen}	$\Rightarrow$ 342.79 kJ/kg
h_{g_evp}	$\Rightarrow$ 401.9 kJ/kg	h_{g_con}	$\Rightarrow$ 419.41 kJ/kg	h_{g_gen}	$\Rightarrow$ 425.4 kJ/kg
h_{fg_evp}	$\Rightarrow$ 193.79 kJ/kg	h_{fg_con}	$\Rightarrow$ 163.03 kJ/kg	h_{fg_gen}	$\Rightarrow$ 82.61 kJ/kg

Table 4.1: Initial Design Point Operating Conditions

4.9 Jet Pump Theoretical Design

This section presents the theoretical design of the system jet-pump, and is largely focussed on output from a computational fluid dynamics (CFD) study [55] provided by Dr.Ablwaifa, a Nottingham University researcher, in 2007.

Guided by Prof I.W. Eames, Dr Ali Ablwaifa modelled a jet-pump in ANSYS Fluent software, suited to operate using R134a at the approximate operating conditions of the system [55]. The basic geometry of the jet-pump is adapted from the prior work of others in this field with particular reference to the theoretical work of Keenan et al in 1950 [46] and experimental designs presented by Eames et al in 1999 [63] and Huang et al in 2001 [64] (see figures 4.5 and4.6).The jet-pump in figure 4.5 used steam as a refrigerant however the jet-pump in figure 4.6 employed R141b which has a similar molecular mass (116.95 kg/kmol) to R134a (102.03 kg/kmol) therefore the geometry ratios are more comparable to the final jet-pump geometries trialled in this study. The CFD model used for analysis had previously been verified against these two experimental jet-pump studies [33] and is further detailed in appendix E.

The section begins with a first principles calculation of the nozzle throat diameter, used to initially verify the scale of a $\approx$ 100 W jet-pump system using R134a. This calculation is based on a generator temperature of 90°C and estimated mass flow rate of 4.7 g/s.

The output from Dr.Ablwaifa's CFD study is then presented, showing the theoretical characterised performance. This informs minor revisions to the specified operating temperatures for the condenser. The experimental work of others [65] confirms that a suitable area ratio (diffuser/nozzle) for a jet-pump operating with R134a was achieved.

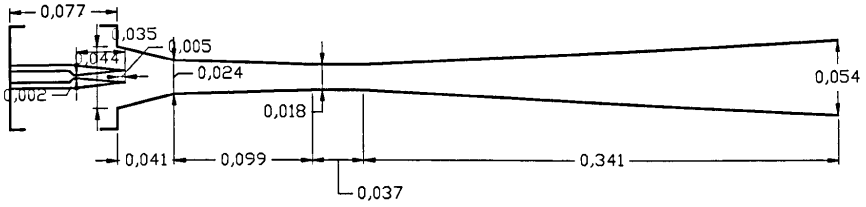

Figure 4.5: Diagram showing geometries for steam jet-pump (Eames et al 1999 [63])

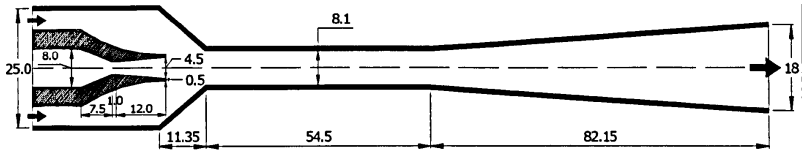

Figure 4.6: Diagram showing geometries for R141b jet-pump (Huang et al 2001 [64])

4.9.1 First Principles

Using the steady flow energy equation (SFEE) for isentropic flow and applying accepted thermodynamic identities (e.g. $\gamma = \frac{C_p}{C_v}$) the jet-pump throat area, at sonic flow velocity (M=1), can be calculated via equation (4.10). The full proof of this equation can be found in appendix D.

Given a generator operating temperature of 90 °C (pressure 32.4 bar), equation (4.10) can be used to calculate the throat area of the jet-pump nozzle as 0.282 mm^2. This provides an estimate for diameter of the jet pump nozzle throat to be 0.623 mm.

$$\frac{\dot{m}}{A_{throat}} = \sqrt{\gamma \cdot \left(\frac{2}{1+\gamma}\right)^{\frac{\gamma+1}{\gamma-1}} \cdot \left(\frac{P_o}{V_o}\right)} \tag{4.10}$$

4.9.2 Computational Fluid Dynamics (CFD)

Computational fluid dynamics (CFD) is an important and increasingly accurate computational tool used to evaluate fluid motion, mass and thermal interactions. It can be used to support the development of thermo-fluid system systems prior to experimental studies, thereby saving time and money. The CFD computational engine is based on the Navier-Stokes equations for compressible and viscous flow.

The key geometry of the jet-pump was initially determined by Prof. I.W.Eames, based on a one-dimensional analysis originally proposed by Keenan et al in 1950 [46] and using the initial system specifications (estimated operating temperatures and chosen refrigerant). In collaboration, Dr. Ablwaifa modelled this geometry (axisymmetric 2D) to produce a CFD study [55] of the jet pump using *ANSYS Fluent* software. CFD allowed the estimated jet-pump performance to be evaluated before experimental work began. Further details on the method and assumptions used in the CFD study can be found in appendix E.

Final Jet-pump Geometry

The CFD model was used to iteratively evaluate the geometry of the jet-pump, with particular attention given to the nozzle exit position [55]. The final critical geometry of the experimental jet-pump nozzle is shown in figure 4.7 and the diffuser in figure 4.8. As previously mentioned, the ratio of diffuser to nozzle throat area (3.7:1) is supported by previous experimental research of an R134a jet-pump [65].

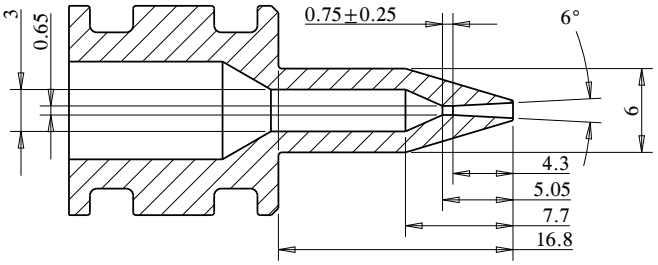

Figure 4.7: Diagram of jet-pump nozzle with key dimensions

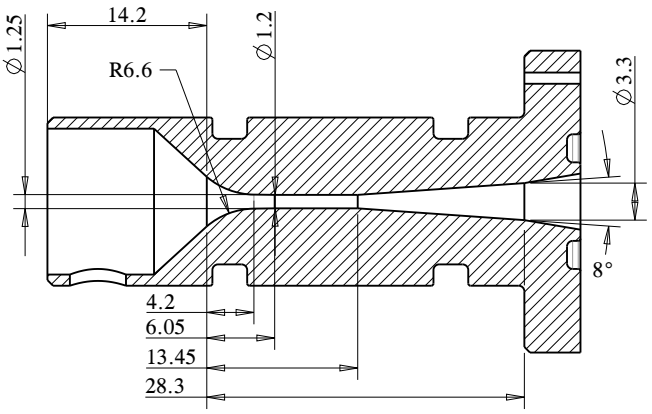

Figure 4.8: Diagram of jet-pump diffuser with key dimensions

Theoretical Performance

With the final 2D geometry of the jet-pump modelled in CFD [55], flow simulations could be computed for various system conditions. Figure 4.9 shows the supersonic velocity plots for the jet-pump at varying condenser temperatures for T_g = 90°C and T_e = 6°C. It is illustrated that as the condenser back pressure increases, the supersonic region decreases as the transverse shock wave moves back towards the nozzle.

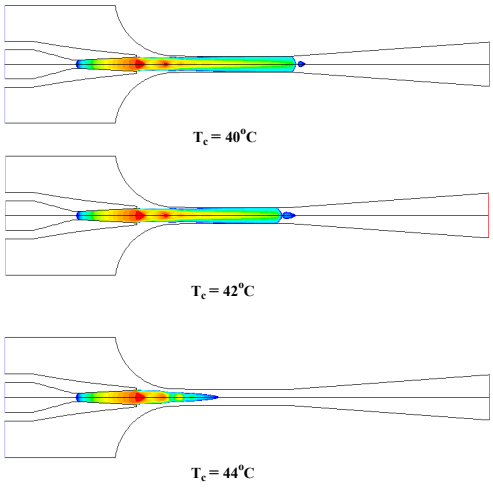

Figure 4.9: Sonic velocity plots showing the effect of increasing condenser temperature (back pressure) at T_g = +90°C and T_e = +6°C [55]

Figure 4.10 shows a flow speed mach contour plot for the jet-pump at T_e = +6°C, T_c =

+42°C and T_g = +90°C. The upper plot in figure 4.10 illustrates the decelerating behaviour of the mixed flow, downstream from the point of sonic shock when pressure recovery occurs. The lower plot in figure 4.10 illustrates the regions where the flow is at supersonic velocities.

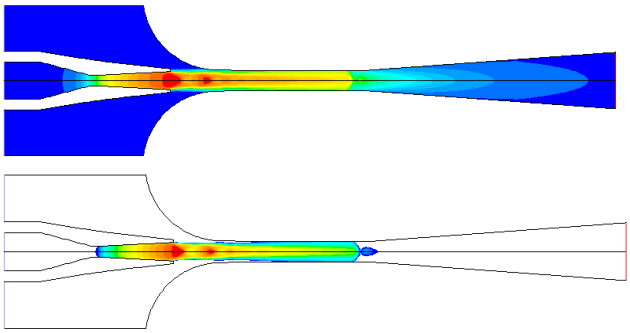

Figure 4.10: Mach number contours at T_g = +90 °C, T_c = +42 °C and T_e = +6 °C [55]

The spacing between the nozzle exit and the start of the converging section of the diffuser (NXP) was also varied as part of the CFD study. A theoretical optimal nozzle spacing of 1.6 mm was iteratively determined by the CFD study [55] (see figure 4.11).

Figure 4.12, shows the predicted effects of increased evaporator temperatures on both critical condenser pressure and entrainment ratio of the jet-pump at a fixed generator temperature of 90 °C [55].

CFD simulations were computed for conditions both above and below design point [55]. Evaporator and generator temperatures were both varied (3x3 array) to show the combined effect on critical condenser pressure. The characterised performance is illustrated in the graph of entrainment ratio against condenser temperature in figure 4.13. As predicted by jet-pump theory [23] higher generator pressures allow for higher condenser pressures, but sacrifice jet-pump performance via lower entrainment ratios

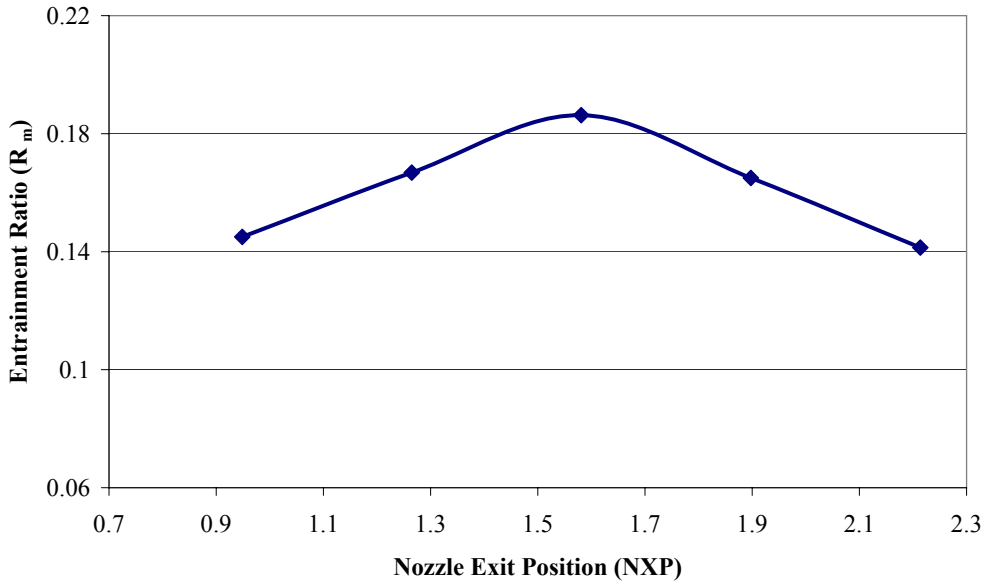

Figure 4.11: Theoretical optimisation of jet-pump nozzle spacing [55]

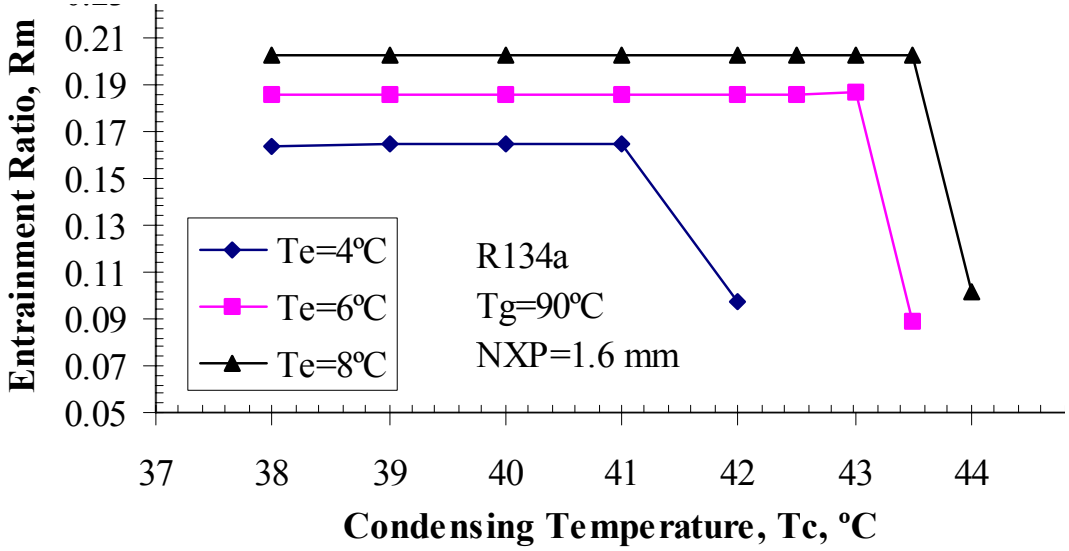

Figure 4.12: Graph showing critical condenser pressures at T_e 4-8°C and T_g = 90 °C [55]

(R_m). Although increasing the primary mass flow increases the velocity and momentum, due to the expanded supersonic region, less effective area is available for secondary flow [33]. The combined effect leads to a decrease in the entrainment ratio. Figure 4.13 also highlights the effect of increasing the evaporator temperature (secondary flow). Higher evaporator pressures lead to higher entrainment ratios. Although benefiting performance, the evaporator temperature should be matched to the application. As previously discussed, operating close to the critical condenser pressure helps to achieve maximum performance from the jet-pump [28].

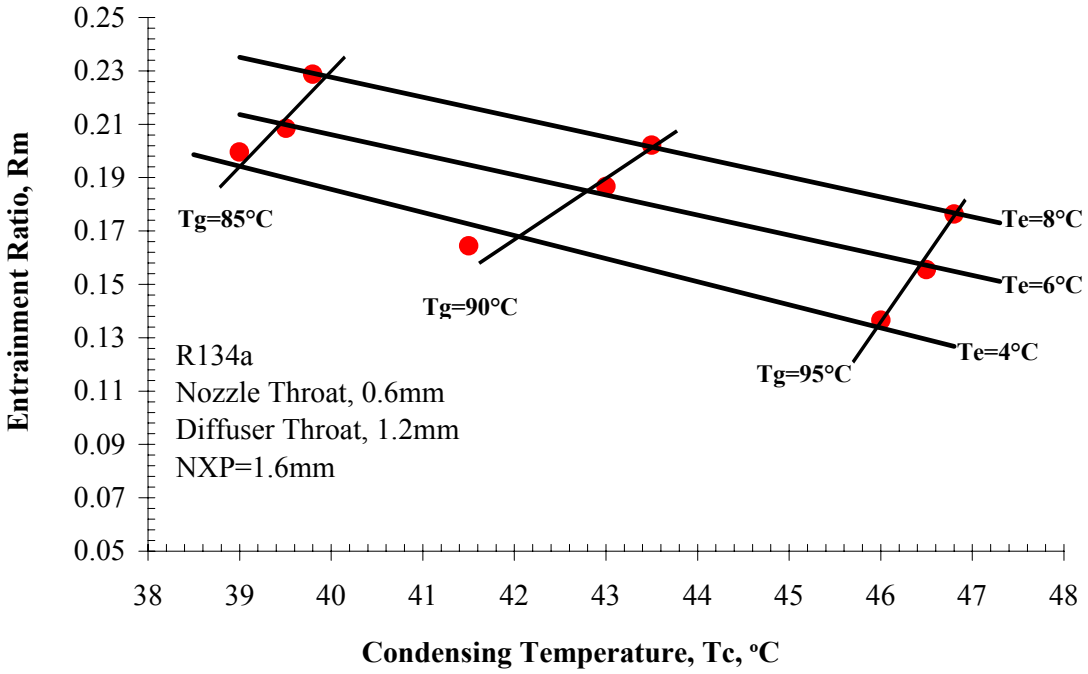

Figure 4.13: CFD predicted entrainment ratios and critical condenser temperatures [55]

4.10 Final System Condition and Performance Specification

The CFD study [55] of the jet-pump system showed that for an evaporator temperature of 6 °C and a generator temperature of 90 °C, the critical condenser temperature is 43.5°C. As discussed in section 2.4.3, operating close to this critical condenser temperature value allows the jet-pump to work most effectively. At temperatures above the critical value, reverse flow will occur and therefore a temperature of 42°C was chosen to provide a 1.5°C margin for error. This temperature is 10°C above WHO temperate zone ambient (32°C) and 1°C under the WHO hot zone ambient (43°C)

This revision to the working temperature of the condenser has knock-on effects to the specification of the heat transfer rate for both the generator (see equation 4.5) and the condenser (see equation 4.7). In addition, the CFD study [55] offered a more accurate theoretical value for the design point entrainment ratio of the jet-pump (0.186), which affected the estimated mass flow of the generator via equation 2.6 and subsequently the mass flow of the condenser via equation 4.6. The effects of these revisions to the initial specification are captured in the more comprehensive, final design point system condition values listed in table 4.2). Additional values (enthaply density, viscosity etc) were interpolated from R134a data tables using equation 4.9.

Although the CFD study suggested that a COP of 0.16 could theoretically be achieved, the design capacity for the heat transfer rates of both the condenser and generator sub-circuits assumed a more conservative COP of 0.1, (Q_{gen_max} = 1,000 W, Q_{con_max} = 1,100 W) providing extra capacity for the system to work outside of design point values. Over-sizing both the generator (1kW) and condenser (1.1kW) would allow the system to

be powered effectively outside of peak solar irradiance hours.

4.11 Basic Prototyping Strategy

4.11.1 Generator

In order to complete the experimental study within a controlled indoor environment, the energy available from 2 m^2 solar thermal collectors (1 kW) was simulated and maintained using an oil heater. This energy will be delivered to the refrigerant via a secondary oil circuit and a heat exchanger. The thermal input to the generator circuit will be monitored and controlled using real-time temperature measurement of the oil inlet/outlet.

Generator Vapour Separation

For EP1 & EP2, passive methods of vapour separation were employed to ensure the primary inlet of the jet-pump is fed with dry saturated vapour.

EP3 made use of a a second heat exchanger, connected in series, to act as a superheater. This proved to be an effective and reliable solution during experimental trials and the specification is discussed in more detail in chapter 6

Generator Fluid Delivery

As previously discussed, reliance on photovoltaics was avoided to help minimise the final unit's complexity and cost. The main electrical demand of the system is the pumping

	Evaporator		Condenser		Generator	
Heat Rate (design)	Q_{evp}	100 W	Q_{con}	724.73 W	Q_{gen}	624.73 W
Heat Rate (capacity)	$Q_{cap-evp}$	>100 W	$Q_{cap-con}$	1100 W	$Q_{cap-gen}$	1000 W
Mass Flow Rate	$\dot{m}_{evp}$	0.7 g/s	$\dot{m}_{con}$	4.46 g/s	$\dot{m}_{gen}$	3.76 g/s
Temperature	T_{evp}	6°C	T_{con}	42°C	T_{gen}	90°C
Pressure	p_{evp}	362.64 kPa	p_{con}	1073.58 kPa	p_{gen}	3243.3 kPa
Density Liquid *	ρ_{f_evp}	1274.68 kg/m^3	ρ_{f_con}	1138.16 kg/m^3	ρ_{f_gen}	837.25 kg/m^3
Density Vapour	ρ_{g_evp}	17.68 kg/mm^3	ρ_{g_con}	52.83 kg/m^3	ρ_{g_gen}	216.45 kg/m^3
Enthalpy Liquid	h_{f_evp}	208.11 kJ/kg	h_{f_con}	259.4 kJ/kg	h_{f_gen}	342.79 kJ/kg
Enthalpy Vapour	h_{g_evp}	401.9 kJ/kg	h_{g_con}	420.26 kJ/kg	h_{g_gen}	425.4 kJ/kg
Latent Enthalpy	h_{fg_evp}	193.79 kJ/kg	h_{fg_con}	160.86 kJ/kg	h_{fg_gen}	82.61 kJ/kg
Viscosity Liquid *	μ_{f_evp}	0.251 x 10^{-3} Pa·s	μ_{f_con}	0.159 x 10^{-3} Pa·s	μ_{f_gen}	0.0702 x 10^{-3} Pa·s
Viscosity Vapour *	μ_{g_evp}	0.011 x 10^{-3} Pa·s	μ_{g_con}	0.0126 x 10^{-3} Pa·s	μ_{g_gen}	0.0178 x 10^{-3} Pa·s
Thermal Conductivity Liquid *	k_{f_evp}	0.0894 W/m·K	k_{f_con}	0.0739 W/m·K	k_{f_gen}	0.0529 W/m·K
Thermal Conductivity Vapour *	k_{g_evp}	0.012 W/m·K	k_{g_con}	0.0157 W/m·K	k_{g_gen}	0.03 W/m·K
Specific Heat Liquid *	$c_{p\_f\_evp}$	1.353 kJ/kg·K	$c_{p\_f\_con}$	1.513 kJ/kg·K	$c_{p\_f\_gen}$	2.766 kJ/kg·K
Specific Heat Vapour *	$c_{p\_g\_evp}$	0.91 kJ/kg·K	$c_{p\_g\_con}$	1.138 kJ/kg·K	$c_{p\_g\_gen}$	3.064 kJ/kg·K

* Denotes that values for these variables were sourced from the ASHRAE Handbook [66]

Table 4.2: Final System Conditions and Performance Specification - Full List

duty required to deliver refrigerant condensate to the generator. This research study investigates various pumping methods, including gravity feed systems that sacrifice thermal power in order to minimise the electromechanical requirement.

4.11.2 Condenser

Given a maximum generator thermal transfer of 1000W and an evaporator developed to remove 100W, a 1100W capacity condenser was required. With a view to minimising any electrical power requirement a natural convection condenser was specified, developed to operate at refrigerant pressures up to 12 bar (≈ 45°C), and ambient temperatures of up to 32°C (WHO specified temperate zone) [54].

4.11.3 Evaporator

A flooded evaporator design will be used to increase the capacity of the cool-box and eliminate hot-spots caused by poor refrigerant distribution. This design is advantageous for the cyclic operation of the proposed jet-pump circuit as it provides more reliable evaporator behaviour. A large evaporator surface area will allow a lower temperature difference between the pipes and the cool-box air; the evaporator pressure can therefore be higher, resulting in a higher jet-pump entrainment ratio and higher COP. A chest style cool-box will be employed to help minimise the conductive losses when the cooling load stock is removed or added.

4.12 Product Design Specification

This section of the chapter provides a product design specification (PDS) for a mass-manufactured version of the solar powered jet-pump vaccine refrigerator. This specification is primarily derived from the existing WHO standards for such devices [14] [54][61]. Although the three experimental prototypes (EP1,EP2 and EP3) were designed to simulate the performance characteristics of a mass manufactured products, some of the methodologies employed did not fully replicate production standard equivalents. A good example of this is the cool-box which would be mass-manufactured using a press formed aluminium shell with vacuum-formed acrylic interior and expanded polyurethane insulation. For the prototype system the cool-box was produced using an MDF shell with Styrofoam insulation and a HIPS lining. Although this prototyping approach allowed modifications to be made easily during development and provided reasonable thermal performance, the weight of the cool-box was comparably heavier.

Due consideration to the intended use environment (not required for the prototype) would also be required for a production system including corrosion resistance and ingress protection. Although not specified in the WHO standards, IP64 (no ingress of dust and protected against water splashes from all directions) was deemed as an appropriate rating for the this PDS.

The intended users for the refrigerator are health care professionals (HCPs) however the WHO standards state that the device *"must be usable by the widest practicable range of active health workers regardless of age, gender, size or minor disability, including colour blind users and long-sighted people without glasses, in accordance with the general principles laid out in ISO 20282-1: 2006"* [14]. Furthermore, the WHO standard states that *"the thermostat, thermometer and other visual displays may be positioned on the*

front of the unit; preferably as close to eye level as possible. Alternatively they may be mounted on top of the unit at a height not exceeding 1.3 metres." [14]. Although not directly relevant for prototype evaluation, these are important factors when considering the final use scenario.

In addition to the more general requirements for solar powered vaccine refrigerators provided in table 4.3, a number of requirements specific to thermally powered jet-pump driven refrigerators have also been identified, namely;

- Phase separation at generator to ensure dry vapour supply received at primary inlet of jet-pump.
- Minimal reliance on solar electric collectors to reduce overall cost and complexity of system (target value of 50 W; equivalent to $0.3m^2$ photovoltaics). The development of a low-power generator feed system is of key importance in this respect.
- Minimal reliance on moving parts due to the risk of mechanical failure during the lifetime of the product. The use of natural convection at both evaporator and condenser heat exchangers is proposed and evaluated.
- The use of a flooded evaporator to suit the cyclic operation of the system and eliminate hot-spots in the cool-box caused by poor refrigerant distribution.
- The use of a chest style refrigerated compartment to minimise convective losses during stock loading/removal.
- No reliance on secondary heat sinks (i.e. cooling water circuits) that would limit the practical installation of the system in remote regions.
- Adjustable position of the jet-pump nozzle to allow the system to be configured for various ambient conditions.

	Item	Specification
	Intended Use	Solar powered vaccine refrigerator
	Intended Market	Governments, NGOs and charities
	Intended Territories	Africa, SE Asia and Latin America
*	Intended User	HCPs (ISO 20282-1: 2006)
*	Refrigerator Temperature (MKT)	+2°C to +8°C
*	Refrigerator Temperature (Transient)	+0°C to +20°C
*	Ambient Temperature	+32°C day, +15°C night
*	Cooling Capacity	100 W
*	Holdover Period	1.5 hrs
*	User Requirements	Autonomous : no training required
*	Electrical Requirements	12-24V DC to suit photovoltaic output
*	Product Lifecycle (MTBF)	10 years
*	Maintenance or Repair	Maintenance free
*	Size	710 x 710 x 1700 mm
*	Weight	100 kg (4 men)
*	Corrosion Resistance	DIN 8985
*	Electrical Safety	IEC 60335-1 and IEC60335-2-24
*	Refrigerant	Montreal Protocol Compliant
	Ingress Protection	IP54
	Target Production Quantities	10,000
	Target Manufacturing Cost	£500

* Specifications sourced from WHO vaccine refrigerator guidelines [14] [54][61]

Table 4.3: Product Design Specification

- The use of conventional manufacturing technologies to ensure low cost production costs remain possible.

4.13 Chapter Conclusion

This chapter has defined the initial concept design of the prototype system and evaluated the theoretical feasibility.

As discussed in section 4.3, R134a was selected as a working fluid for this study based on several criteria. One important benefit of using R134a is that it has a relatively low molecular mass which allows for a comparatively larger ejector; an advantage when considering the manufacturing limitations imposed by the small capacity of the system.

Using existing WHO standards for solar powered vaccine storage refrigerators [54], a specification for the evaporator was first defined in order to estimate both generator and condenser requirements.

- Evaporator temperature = 6°C
- Evaporator heat transfer capacity = 100 W
- Evaporator mass flow = 0.7 g/s

Using the evaporator specification above and and an estimated jet-pump entrainment ratio (0.15 [32]), mass flow rates and heat transfer rates for both the generator and condenser could be calculated to provide an initial system specification and confirm the feasibility of the proposition.

The jet-pump design was then considered in detail. The jet-pump throat orifice area was initially calculated (equivalent to a diameter of 0.623 mm) from first principles based on the estimated generator mass flow and operating temperature. The CFD work of Dr A. Ablwaifa [55] was then presented and the final jet-pump nozzle and diffuser geometries were provided (shown in figures 4.7 and 4.8).

The final design point operating conditions were then defined as summarised in table 4.4. It is important to note that although the CFD suggests a COP of 0.16 could theoretically be achieved, a COP of 0.1 was assumed to provide a safety margin when sizing both the generator and condenser heat exchangers (Q_{gen_max} = 1,000 W, Q_{con_max} = 1,100 W). This approach helped to ensure that neither the generator or condenser sub-systems were undersized and also provided extra capacity for the system to work outside of design point values.

An outline of the design strategy for each sub-system, drawing specific attention to both the evaporator (flooded to minimise the effects of cyclic operation) and generator (refrigerator feed system designed to minimise the use of electrical energy). The chapter concluded with a product design specification for a solar powered vaccine refrigerator, based on WHO guidelines, which can be used later for evaluation of the prototype.

Evaporator		Condenser		Generator	
T_{evap}	$\Rightarrow$ 6°C	T_{con}	$\Rightarrow$ 42 °C	T_{gen}	$\Rightarrow$ 90 °C
p_{evap}	$\Rightarrow$ 362.64 kPa	p_{con}	$\Rightarrow$ 1073.58 kPa	p_{gen}	$\Rightarrow$ 3243.3 kPa
Q_{evap}	$\Rightarrow$ 100 W	Q_{con_max}	$\Rightarrow$ 1,000 W	Q_{gen_max}	$\Rightarrow$ 1,000 W

Table 4.4: Summary of final design point operating specification

Chapter 5

Experimental Investigation of the Concept (EP1 & EP2)

5.1 Introduction

In order to refine and evaluate the performance of the jet-pump fully, a series of three experimental prototype systems (EP1, EP2 and EP3) were developed and tested during this research study. This chapter of the thesis details the iterative development of the first two versions of the experimental prototype apparatus (EP1 and EP2).

The first prototype system (EP1) was used as an initial test platform on which to confirm operation of the jet-pump and validate the performance of individual sub-systems. Several methods of delivering refrigerant fluid from the cooling circuit (condenser outlet) to the jet-pump circuit (generator inlet) were explored using the EP1 apparatus, leading to the reservoir transfer system which was designed, installed and

tested on the second experimental prototype rig (EP2). This generator fluid delivery system is the primary difference between EP1 and EP2 and represented a significant development milestone, allowing the vapour fed jet-pump to generate useful cooling ($\approx$ 100 W) at the evaporator for the first time.

Following definition of the development scope, this chapter begins with a description of the data-collection and prototyping methods, including an overview of the requirement for custom made items and manufacturing techniques.

The following three sections of this chapter provide a description of the investigation and development of each subsystem (the condenser, the evaporator and the generator) in series. The theoretical performance and experimental validation of each subsystem, in isolation, is described.

The manufacturing design for the jet-pump is presented in section 5.6, along with details of the experimental optimisation process and subsequent system performance characterisation.

In section 5.7, two development versions of the experimental prototypes (i.e. the entire system) are presented (EP1 and EP2) and design iterations are discussed. The commissioning of the systems is also presented in this section. EP1, the initial prototype, is briefly introduced, however the focus of this section is EP2. The operating procedure for EP2 is examined and refined. The development and experimental testing of EP2, discussed in the conclusion to this chapter, provided the foundation to execute the final development prototype, EP3, which is presented subsequently in chapter 6.

5.1.1 EP1 and EP2 Development and Analysis Scope

The overall scope of this chapter is to provide detail of the design, development and performance of the first two versions of the experimental prototype apparatus (EP1 and EP2). The sub-systems are trialled first in isolation, then in combination to provide performance characterisation.

Test data has been collected throughout the development process to validate improvements and optimise operational procedure. With the jet-pump providing the necessary work, three principle sub-systems were defined (the generator, the evaporator and the condenser). During the early stages of prototype development, a modular approach to testing and validation was adopted. Theoretical values were compared against experimental data collected on each sub-system. By limiting the initial scope in this way, and testing each sub-systems in isolation, development activities could be independent and specifically targeted, avoiding potential problems in identifying the cause of poor system performance at a later stage. An overview of the design and testing of these three sub-systems, each containing a heat exchanger, is described below. The jet-pump performance optimisation and characterisation is also described. Finally, the evaluation method for the integrated prototype systems is outlined.

Condenser Sub-system

The mixed refrigerant flow (generator plus evaporator) from the jet-pump passes to the condenser heat exchanger where the waste heat is expelled to the local environment. Two types of test (static temperature decay and single phase flow) were used to experimentally evaluate a selection of condenser heat exchangers in order to specify a

low cost, custom made condenser for the prototype. The function of the condenser reservoir is also discussed in this section.

Evaporator Sub-system

The jet-pump entrains flow from the evaporator heat exchanger, thereby producing the desired cooling effect. The evaporator heat exchanger, fed from the condenser sub-system, is located within the cool box (refrigerated compartment). The manufacturing design of the evaporator and cool box is presented and theoretical estimations for conductive losses and thermal mass are calculated. The estimations are then validated via experimental testing.

Generator Sub-system

The generator heat exchanger, fed from the condenser sub-system, is used to produce a supply of high-pressure refrigerant vapour at the primary inlet of the jet-pump . As low electrical power consumption is one of key aims of this research, minimising the power requirement of the generator feed is given particular attention. EP2 employed a novel reservoir transfer system to periodically deliver refrigerant fluid from the condenser to the generator sub-system. This reservoir transfer approach is further refined to provide the final generator feed mechanism which is dicussed later in chapter 6. The flow rate of the oil circulation pump, used to deliver heat to the generator, is calibrated to allow real time calculation of the generator heat transfer rate. Various methods of phase separation are also discussed in this section.

Jet-pump Optimisation and Characterisation

The manufacturing design of the system jet-pump (presented in section 5.6.1) provides functionality to adjust the lateral position of the nozzle, at 0.25mm increments, within the diffuser section. This distance has previously been shown to have a dramatic effect on jet-pump performance [32]. The optimised jet-pump is subsequently used in EP2 to experimentally produce system characterisation metrics.

Integrated Systems (EP1 and EP2)

Specifications for the entire system are presented in schematic form in section 5.7. Focussing on EP2, the operating procedure is defined and discussed. Refinements to the operating procedure, in order to reduce the cycle charge / discharge ratio are also presented.

5.2 Experimental Prototyping Methods and Apparatus

Construction of an experimental prototype system was necessary to collect performance data, develop the system architecture and evaluate the practical implementation of a jet-pump refrigerator. Although solar thermal input is simulated using an oil heater, all other components were specified to represent the likely manufacturing design.

Both EP1 and EP2 are manually controlled systems. Although this presents some difficulties in achieving consistent performance, it allowed for the operating procedure to be adjusted easily in real-time. In order to provide consistent results over longer test periods, EP3 (presented in chapter 6) was controlled automatically.

This section describes the experimental apparatus and begins with a specification of the data-collection equipment. An overview of the basic construction materials and prototyping methods is presented, followed by a list of the custom made items.

5.2.1 Data-logging

Throughout the development of all three prototype systems (EP1, EP2 and EP3), a Pico Technology TC-08 (8 channel) thermocouple data-logger has been used to capture temperature data at various locations both within and out-with the system (i.e. ambient). A summary of the experimental uncertainty and error approximation is provided in appendix I. Type K thermocouples were used. When thermocouples needed to be located on the surface of the pipework, silicone thermal transfer paste was used to ensure a good thermal contact and the sensor was fixed to the surface using heat compliant tape. EP3 also employed a Pico Technology ADC-11 (11-channel analogue to digital) data-logger which was used to monitor pressures and flow-rates.

Temperature data was collected at 100mm height intervals within the cool-box, across the evaporator pipe-work i.e. evaporator level 1 is 100mm from the cool box internal floor and evaporator level 5 is 100mm from the internal surface of the cool box lid. In addition, the cooling chamber air temperature is measured using a thermocouple located at the approximate centre of the the cool-box.

Relevant calibration procedures and error approximation for temperature, pressure and flowrate measurement equipment is provided in appendix I.

5.2.2 Basic Construction Of Prototype

This section contains an introduction to the basic tools, materials and processes used in the manufacture of the development prototypes.

A combination of OEM components, heat exchangers and custom manufactured parts were used in the development of the prototype. The refrigerant circuit was piped using refrigeration grade copper, ranging in diameters from $\frac{1}{2}$" down to capillary. A combination of brazing and compression fittings were used in the construction. The generator heat transfer circuit was piped using 12mm stainless steel pipes and compression fittings.

Polymer tubing (i.e. PTFE or PEEK) was considered as a possible alternative to piping the refrigerant circuit to help minimise development costs, however a suitable grade (temperatures of -20 °C to 140 °C at pressures of 0-35 bara) could not easily be sourced. In addition, the labour time involved when making modifications to the pipe-work may have been considerable.

All of the pipe-work and components were fitted to a mobile wooden base. This enabled modifications to the system to be made easily. A photo of the experimental apparatus (EP2) is shown in figure 5.1. The schematic for EP2 is presented later in this chapter (figure 5.34)

5.2.3 Custom Made Items

A number of *bespoke* items were needed to suit the specific requirements of the prototype system. Of key importance, and not available as a stock item, the system jet-pump was

Figure 5.1: Photograph of EP2

custom manufactured. In addition, both the condenser and evaporator heat exchanger arrays were custom made to suit the the study requirements. A number of other components, including the cool box (refrigerated compartment) were also constructed using basic manufacturing techniques to allow easy modifications during development. A description of the custom made items and the basic manufacturing methods is presented below.

Jet-pump

Due to the relatively high working pressures and thermo-mechanical stresses, the prototype jet-pump was machined from solid metal (brass) rather than plastic. Dimensioned drawings of the jet-pump can be found in appendix F. Silicon o-rings were employed to prevent internal pressure leakage. A number of design features are implemented to allow easy adjustment and optimization of the nozzle position within the diffuser. In production, it is anticipated that detailed finite element analysis (FEA) could allow for a mass manufactured injection moulded jet-pump to be realised.

Heat Exchangers

Three heat exchangers (condenser, evaporator and generator), are used in the jet-pump cooling cycle. The generator heat exchanger (heat transfer oil to refrigerant liquid) is relatively simple to specify as the heat input on the prototype can be controlled via pump speed however both the evaporator (air to mixed phase refrigerant)and condenser (mixed phase refrigerant to air) employ heat transfer via natural convection. In order to meet the requirements set out in chapter 4, it was necessary to specify a custom made condenser and evaporator. This allowed the specific requirements to met, both in terms

of operation and ease of modification during development.

Several possible methods of constructing both the condenser and evaporator were investigated. A number of aluminium finned copper pipe samples were obtained and evaluated from a specialist manufacturer in short lengths. In addition, a number of used OEM condensers and evaporators were sourced (serpentine pipe arrays with press formed finning). Following implementation of the European WEEE directive in 2006 various companies have emerged to deal with the responsible disposable of consumer/commercial refrigeration equipment. One such company was used to source a range of OEM heat exchangers (condenser and evaporator pipe-work arrays).

Cool-box

A custom made cool box (refrigerated compartment) was manufactured to house the evaporator sub-system. Contained within an (medium density fibreboard (MDF) shell, a chest style refrigerated compartment was lined with high-impact polystyrene (HIPS) and insulated using polystyrene foam. Although prototyping the refrigerated compartment in this manner probably compromised its thermal efficiency, it allowed easy access for component adjustment, temperature measurement and other sub-system modifications during development.

Other Items

A number of other *bespoke* items were manufactured for the prototype systems. Of particular note are the feed pipes to both the condenser and the evaporator. The use of capillary diameter copper tubing is used in both instances to restrict flow and decrease

pressure, as described later in this chapter.

Passive methods of generator vapour separation were explored during the development of EP1 and EP2, and this item is described further in section 5.5.7. Other minor components, such as *bespoke* filters, were also custom made for the development prototypes.

5.3 Condenser Sub-system

This section describes the specification, experimental validation and design of the condenser sub-system. Of specific interest is the selection and testing of a heat exchanger, suitable for 1.1 kW natural convective cooling as defined in chapter 4.

With the specified cooling rate (1.1kW), and assuming a convective (free convection) heat transfer coefficient of 7.5 W/m^2 K (see section 4.2.2), it was possible to estimate the required condenser surface area using Newtons law of cooling (equation 4.1).

Given a condenser temperature of 42 °C (as specified in chapter 4) and an ambient temperatures 32 °C (WHO temperate zone maximum) the required surface area was calculated to be 14.7 m^2. If $\frac{1}{4}$" copper piping was used, a length in excess of 735 m would be required. In order to decrease the physical volume of the condenser, a finned pipe heat exchanger was required.

A range of prototyping methods were considered for this custom made heat exchanger, including both new (aluminium finned copper pipe) and used (press form finned steel pipe) samples. Aluminium finned copper pipe is shown to offer high efficiency however is burdened by a high initial cost.

Two experimental tests were devised to assess the heat exchanger pipe samples. For the short sample lengths of aluminium finned pipe, a static, single phase temperature decay experiment was used to determine the approximate heat transfer coefficient. The theoretical values for a number of finned pipe heat exchangers were compared against experimental values for this single phase experiment. For the press form steel finned serpentine pipe arrays, a single phase flow experiment was used.

The results of these tests led to a design specification for the prototype condenser. A final pipe specification, orientation and array size is presented along with prototype construction details. Later in this chapter, (section 5.7.3), the performance characteristics of the condenser at various generator pressures is analysed and discussed.

5.3.1 Condenser Heat Exchanger : Theory and Experimental Methods

This subsection details the theoretical and experimental method of determining the heat transfer rate of the various finned pipe samples.

The static temperature decay experiment provided an approximation of the heat transfer rate for short lengths of aluminium finned copper pipe. Although this method was easy to implement for short lengths of pipe, maintaining a constant temperature across larger pipe arrays proved difficult. As presented and discussed in the upcoming section, the experimental results from the static temperature decay experiments diverged from the theoretical values when fin height was increased.

Single phase flow experiments proved more practical for longer samples of heat exchanger, and provided a better simulation of the actual use scenario (mixed phase flow of refrigerant). For this second set of experiments, the logarithmic mean temperature

difference was used to provide a more accurate estimate of the heat transfer rate.

Static Temperature Decay Experiment

As mentioned above, a static temperature decay experiment was devised to assess the shorter length samples of finned pipe heat exchangers. Although this does not represent the normal use scenario of the heat exchanger, a flow based experiment was not practically appropriate for some of the shorter pipe samples. When the pipe samples were short in length ($<$ 300 mm) only small temperature differences, from inlet to outlet, could be observed under flow conditions therefore measurement error had a proportionately larger effect.

Theoretical: The theoretical heat transfer rate (Q_{hx-th}) of various samples was calculated using equation (4.2). A convective heat transfer coefficient of 7.5 $W/m^2 \cdot K$ was applied and a fin efficiency of 100% was assumed (see section 4.2.2). The external surface area of the finned pipe was calculated using pipe diameter, fin spacing and fin height (assumes zero fin width). A continuous temperature difference of 10 K was used in the calculation.

Experimental: After first measuring the liquid volume capacity and the mass of the pipe itself (approximating the mass of fins and pipe separately where necessary), the experimental method involved filling the pipe with water at a given temperature, and recording how long it took for the heat to be dissipated. The pipe-work was filled with water at a approximately 50 °C above the ambient temperature.

Given a fixed volume of water, within the pipe-work, the temperature decay, of both the water and pipe, can be used to determine the experimental heat transfer rate (Q_{hx-ex})

via the transient cooling model (see appendix C). Given a known value for $\Sigma\,(m \cdot C_p)$, equation 5.1 shows that plotting the natural log of $\frac{\Delta T}{\Delta T_{init}}$ against time will yield an experimental value for U·A. Note: In most cases, measuring the temperature across different radii of the heat exchanger fins was impractical and so the temperature of the pipe has been assumed to be at the same temperature as the water.

$$ln\left(\frac{\Delta T}{\Delta T_{init}}\right) = -\frac{U \cdot A}{\Sigma\,(m \cdot C_p)} \cdot t \tag{5.1}$$

The heat loss rate of the pipe samples ($\dot{Q}_{hx}$) is directly proportional to the temperature difference between the fluid and the ambient environment ($Q = U \cdot A \cdot \Delta T$) and hence decreases as the condenser approaches room temperature. The relative heat loss rate ($\dot{Q}_{rel}$) in W/K can be described as shown in equation 5.2

$$\dot{Q}_{rel} = \frac{\dot{Q}_{hx}}{\Delta T} \tag{5.2}$$

The experimental U·A values can therefore be used determine the condenser suitability across any temperature range. Assuming a condenser temperature of 42 °C and and ambient temperature of 32 °C (WHO temperate zone ambient maximum) a ΔT of 10 K is used in this evaluation.

The results can then be factored using the length of the sample pipe to calculate the total length of pipe work required to achieve design point condenser performance.

Although this experiment was specifically devised for short pipe samples, the static temperature decay experiment was also conducted on some of the larger pipe array samples, however this presented experimental difficulties. In order to maintain a uniform temperature across the entire length of the pipe, water had to delivered at a high flow

rate as the outlet temperature was always lower than the inlet temperature. For larger heat exchangers, a pump was used to help obtain an outlet temperature that was reduced to within 10% of the inlet temperature. In addition, during the filling procedure, insulation (bubble-wrap) was used to temporarily limit the heat transfer potential of the pipe work.

Single Phase Flow Experiment

A second experiment was then devised to test pipe work samples under single phase (liquid) flow conditions. This experiment was only suitable for longer lengths of heat exchanger pipe-work as the ΔT_{water} across inlet and outlet temperatures was too small (difficult to measure) in shorter pipe lengths. This mode of testing was much more representative of normal condenser operating conditions, however in practical application, the overall heat transfer coefficient will be under mixed flow (condensing) conditions, rather than single phase conditions. The heat exchanger is therefore still tested out of context however the effect of this experimental difference is negligible: as the air side heat transfer rate (under free convection conditions) is much lower than the internal heat transfer, and the air side area is relatively low (when compared against radially finned pipe) the air side heat transfer rate will heavily influence the overall heat transfer rate. Improving the internal heat transfer rate (i.e. single phase) will therefore have a positive but comparatively small effect on the overall heat transfer rate. It is also important to note that these calculations will only be used to estimate the heat transfer area required for the prototype system and a factor of safety has already been applied during the initial specification (see chapter 4)

Theoretical: The theoretical heat transfer of larger, pressed fin pipe arrays was

estimated using equation 4.2. Following the analysis of the theoretical versus experimental figures from the static temperature decay data, a fin efficiency of 1 was assumed based on the relatively shallow fin height.

Experimental: The flow-rate and temperatures are measured experimentally and the heat transfer rate is calculated using equation 5.3.

$$\begin{aligned} \textit{For an ideal gas} \qquad \dot{Q} + \dot{W} &= \dot{m}.C_p(T_2 - T_1) \\ \textit{As no work is done} \qquad \dot{Q} &= \dot{m}.C_p(T_2 - T_1) \end{aligned} \tag{5.3}$$

In this instance, as the mass and temperature of the pipework remain constant ($\dot{m}_{pipe}$= 0, $\Delta T_{pipe} = 0$), it is only the mass flow of the water ($\dot{m}_{water}$) and temperature difference (ΔT_{water}) of the water (across inlet to outlet) that determines the experimental heat transfer rate (Q_{hx-ex}) of the pipe-work. For this single phase flow experiment, the equation used to calculate the relative heat transfer rate (equation 5.2) is refined, replacing ΔT with the logarithmic mean temperature difference (LMTD). The LMTD is caculated as shown in equation 5.4

$$LMTD = \frac{GTD - LTD}{ln(GTD/LTD)} \tag{5.4}$$

The average input, output and ambient temperatures are recorded experimentally and are used to calculate the LMTD between inlet and outlet. GTD is the greatest temperature difference, which in this case is the inlet temperature above ambient, and LTD is the least temperature difference, or outlet temperature above ambient. The

relative heat loss rate (Q_{rel}) can now be calculated as shown in equation 5.5.

$$Q_{rel} = \frac{Q_{hx}}{LMTD} \tag{5.5}$$

The reclaimed heat exchangers were mounted onto a free-standing frame. This arrangement allowed air to pass freely through the frame and across the fins/pipes. An 8-channel thermocouple data-logger was used to capture temperature data from various points on the system as outlined in table 5.1. Positions for the thermocouples are shown on the photograph of an example condenser in figure 5.2.

Channel	Location Name
1	Reservoir
2	Inlet Pipe Lower
3	Inlet Pipe Outer
4	Approx' Mid High Outer
5	Approx' Mid Low Outer
6	Outlet Pipe Outer
7	Ambient Far
8	Ambient Near

Table 5.1: Condenser Test Rig - Thermocouple Locations

Initial experiments were performed to measure the difference between the internal liquid and external surface of the pipes. As this difference was negligible, all subsequent temperature data was collected from the outside surface of the pipe-work.

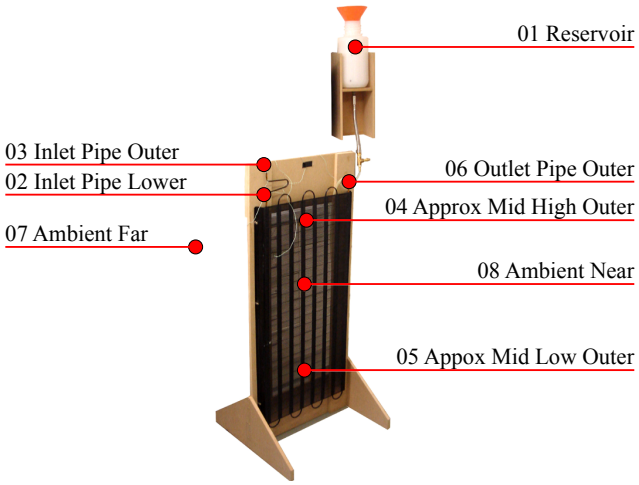

Figure 5.2: Photograph showing thermocouple locations

5.3.2 Heat Exchanger Test Results

Static Temperature Decay Results

Experimental data was collected from a wide range of heat-exchanger pipe types including short samples of aluminium finned copper pipe and reclaimed steel pipe-work arrays (with press-formed finning).

Theoretical values were estimated using equation 4.2 based on the assumptions listed in table 5.2 and the total surface area (calculated from pipe diameter, fin geometry and fin distribution).

The samples were then experimentally evaluated using the test method described in section 5.3.1. The experimental heat rate was calculated using equation 5.1 taking account of the different materials and relative masses used in each heat exchanger sample (i.e. C_{p_hx} and m_{hx})

Figure 5.3 shows a photograph of three samples of aluminium finned, copper pipe (complete with resin bungs).

Table 5.3 shows a comparison between the relative theoretical and experimental heat transfer rates per metre length of pipe.

Property	Symbol	Assumed value	Units
Surface heat transfer coefficient	H_{conv}	7.5	$W/m^2 \cdot K$
Initial estimate of fin efficiency	η_{fin}	100	%
Density of water	ρ_{water}	1	kg/l
Specific heat capacity of water	C_{p_water}	4,200	J/kg·K
Specific heat capacity of steel	C_{p_steel}	466	J/kg·K
Specific heat capacity of copper	C_{p_copper}	385	J/kg·K
Specific heat capacity of aluminium	$C_{p\_aluminium}$	897	J/kg·K

Table 5.2: Static Temperature Decay Experiment - Assumptions

Figure 5.3: Photograph of three finned pipe samples

The results in table 5.3 show that the fin efficiency assumption may be invalid when the ratio between fin height and pipe diameter exceeds 1:1 Reviewing the experimental/theoretical data of pipe sample "A", the limitations of the initial assumptions (i.e. temperature remains constant in water, pipe and across all fin heights) are apparent. Sample "X" however (a plain copper pipe) shows the theory and experimental equipment are well matched when the effects of fin efficiency are not relevant. The reasons for the discrepancy between theoretical and experimental results could be attributed to a number of causes;

Pipe	Pipe OD (m)	Fin Height (m)	Fins per metre	Theoretical (W/m)	Experimental (W/m)
A	0.0254	0.044	622	160.36	27.23
B	0.0191	0.025	433	45.09	22.10
C	0.0254	0.006	6	*Wire wound*	18.62
D	0.0191	0.011	315	13.94	17.79
E	0.0170	0.027	394	41.73	27.12
F	0.0254	0.025	472	56.87	28.71
G	0.0170	0.002	787	6.79	8.18
H	0.0130	0.002	787	5.23	5.89
X	0.0125	0.000	0	5.30	5.07

Table 5.3: Table showing results of finned pipe tests

- The theoretical model assumes a constant Δ T of 10 K, however Δ T in the experimental method varied from $\approx$ 7-40 K
- A theoretical fin efficiency (η_{fin}) of 100% was assumed
- A uniform temperature (T) and uniform heat transfer coefficient (H) was assumed across the entire fin for the purposes of theoretical evaluation
- The boundary conditions of the theoretical evaluations did not take account of the varying heat loss rates at the ends of the pipe samples (i.e. resin bungs and un-finned lengths at pipe ends

The experimental data in table 5.3 can be used to calculate the length of finned pipe required to provide 1.1 kW heat rejection via natural convection. Based on an ambient temperature difference of 10 K the estimated manufacturing costs, at low volume, would be approximately £700-1,200.

Although aluminium finned pipe would provide the most compact pipe array, the low manufacturing costs offered by conventional manufacturing techniques is of particular interest to this study. In order to produce a prototype system that simulated these manufacturing techniques, a series of OEM refrigerator condensers (steel pipework with pressed fins) could be connected in parallel to provide the required duty.

The WEEE directive aims to minimise the effect of electrical and electronic goods on the environment and requires the manufacturers to ensure proper treatment and disposal of certain key products, including refrigerators, at the end of the product life. Following the introduction of this legislation in 2005, several large firms have emerged to meet this requirement. Sims (of Newport, UK) and EMR (of London, UK) are two of the larger companies who deal with refrigerator recycling in the South of the UK. Several site visits

to EMR's facility in Willesden, London, resulted in a numerous condenser/evaporators pipe arrays being supplied free of charge for testing and development. Initial temperature decay tests over 2 min periods, revealed that these units (of approximate surface areas ranging from 0.5 - 1 m^2) could dissipate between 50-150 W heat when operating at 10 K above ambient. This is in line with the theoretical estimate that a 1 m^2 area would produce 75 W heat transfer (assuming a free convection heat transfer coefficient of 7.5 $W/m^2 \cdot K$). This initial test run assumed a linear heat transfer rate and further tests (of longer duration) were conducted on samples of particular interest.

Tricity Bendix (TB) Condenser

Among the reclaimed pipe-work samples obtained, a condenser unit installed on several models of Tricity Bendix refrigerators (hereafter referred to as TB condensers), showed promising results. The physical properties and pipe arrangement of the TB condenser, are shown in figure 5.4. The internal volume of the pipe array was measured as 67ml and the external surface area estimated to be 0.9 m^2. The material, including sheet pressed finning, was all made of steel (excluding black paint) and weighed 2.9 kg.

The static temperature decay test data collected on this sample is presented and discussed below. The assumed values the relevant specific heat capacities have previously been provided in table 5.2. It is also assumed that the temperature across fins, pipe and water was uniform.

Following analysis of the results collected on shorter length of aluminium finned tube, due to the shallow height of the finning, a fin efficiency of 100% was used in calculating the theoretical heat transfer rate. Equation 4.2 is used to provide a theoretical heat transfer rate of 67.5 W.

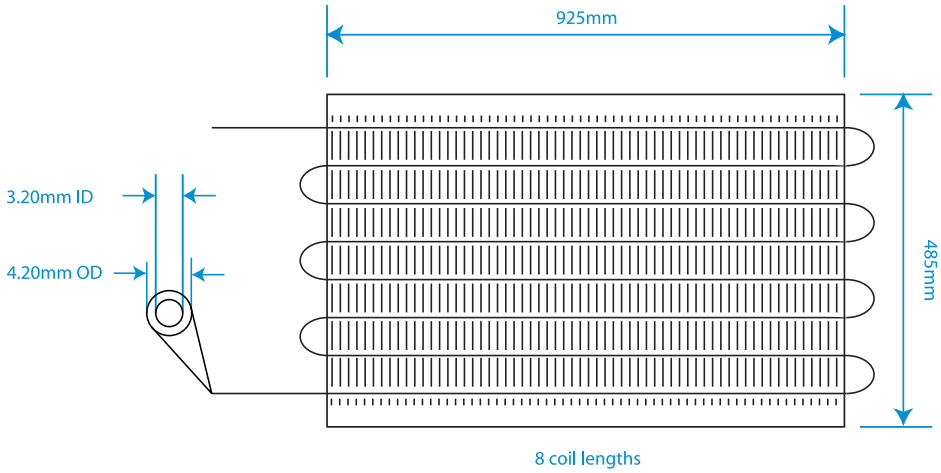

Figure 5.4: Dimensioned details of TB-Condenser units

As previously mentioned, bubble wrap sheeting was used to temporarily insulate the pipework during the fill procedure. A pump was also used to drive hot water through the pipes and get the assembly close to a uniform temperature before the experiment began.

The graph in figure 5.5 shows the inlet, outlet and ambient temperatures of the system when heated to an approximately uniform temperature of 75°C and left to dissipate heat via natural convection.

In order to asses the potential improvement in using forced convection the experiment was repeated using a fan to apply forced convection. The fan helps to disturb the boundary layer of air that has collected on the surface of the condenser and therefore facilitates a higher cooling rate. In light of the proposed application (solar powered refrigeration using minimal PV) a small DC fan was used for this experiment (4 W). The results are graphed in figure 5.6.

The experimental heat loss rate was calculated using the transient cooling model (see appendix C and the results are shown in table 5.4. Although a low power (4 W) fan can

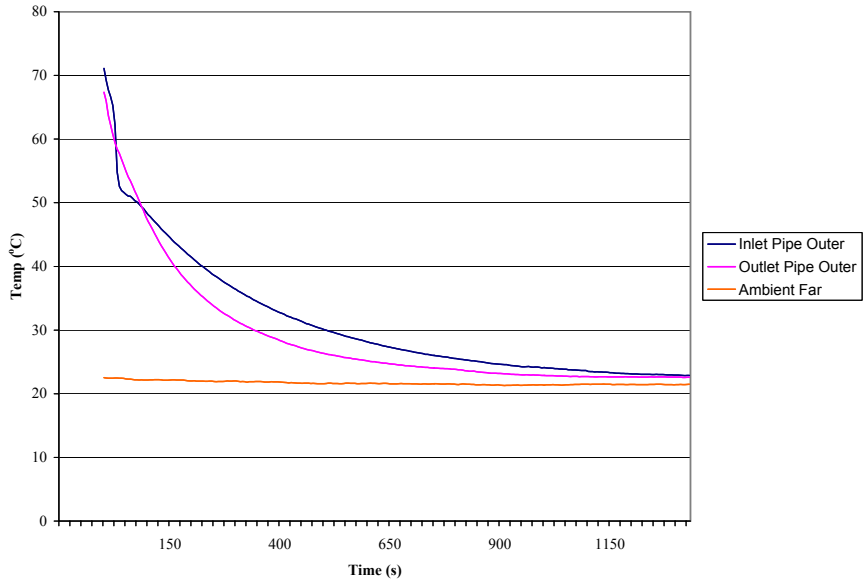

Figure 5.5: Condenser static temperature decay - Natural convection Vertical configuration

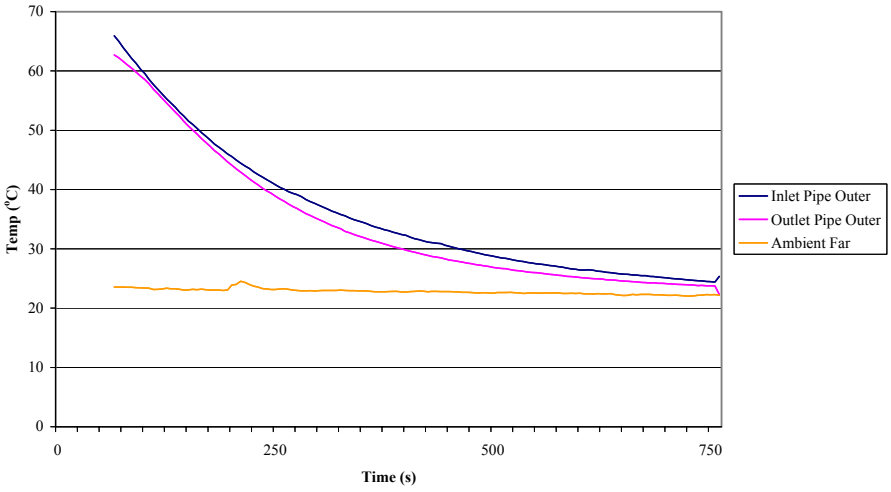

Figure 5.6: Condenser static temperature decay - Forced convection Vertical configuration

Natural Convection	
Average Cooling Rate (at 10 K above ambient)	62.8 W
Forced Convection	
Average Cooling Rate (at 10 K above ambient)	85.2 W

Table 5.4: Pressed Static Temperature Decay Test Results - Vertical

increase the performance by over 50%, the lack of moving parts within a jet-pump system was considered a significant benefit of the technology, and therefore reliance of forced convection was undesirable. This factor is reconsidered in the conclusion to the thesis. The performance of the condenser under natural convection (62.8 W) compares favourably with the predicted value (67.5 W) The small discrepancy could be caused by the approximation of either the fin efficiency or surface heat transfer coefficient.

Using natural convection alone, a bank of approximately 18 TB condenser pipe arrays would be required to meet the 1.1 kW maximum load. This pipe array was retested under single phase flow conditions to further validate the assumptions and performance. As described later, the orientation of the pipe-array was also changed to improve performance.

Single Phase Flow Results

As previously discussed, conducting static temperature decay experiments on larger pipe samples meant, despite employing pumps and insulation during the fill procedure, a difference between inlet and outlet temperatures was inevitable.

A single phase (water) flow experiment was devised for larger pipe arrays which more

closely simulated the traditional condenser use scenario (i.e. mixed phase refrigerant). Water was delivered, via a hot reservoir, using a peristaltic pump as explained earlier in this chapter. A flow rate in line with design specification(<5 g/s) was used.

The use of multi-parallel serpentine pipework, with press formed steel surface finning, was preferred for this study as it employed low cost manufacturing techniques which were well suited to the intended research application area (*low cost* solar powered cooling for medicine storage in the developing world).

It had previously been noted that the flow routing of the TB condenser was a vertical array meaning that the refrigerant had to repeatedly lose and gain potential energy when passing through the heat exchanger. This orientation also meant that liquid condensate could impeded the flow of refrigerant vapour. A series of experiments were conducted on the condenser in a horizontal orientation. The results presented in this section are based on the condenser in horizontal configuration. This would allow the refrigerant to lose (and not gain) potential energy gradually across the heat exchanger and, in operation, avoid the potential liquid problem mentioned above. The results of the single phase flow experiment (TB condenser in horizontal configuration) are shown in figure 5.7.

The red/yellow lines of the graph in figure 5.7 plots the temperature measured at the inlet pipe and the green line represents the temperature measured at the outlet. The lower blue/pink lines show the ambient temperature. Maintaining a continuous temperature of water at the inlet proved challenging because of the relatively small hot water reservoir size. Fluctuations in the inlet temperature can be seen in the results however the deviation is normally less than +/- 5 °C. From the data collected, the average temperature values at the TB condenser inlet, outlet and ambient points were obtained and these are presented in table 5.5.

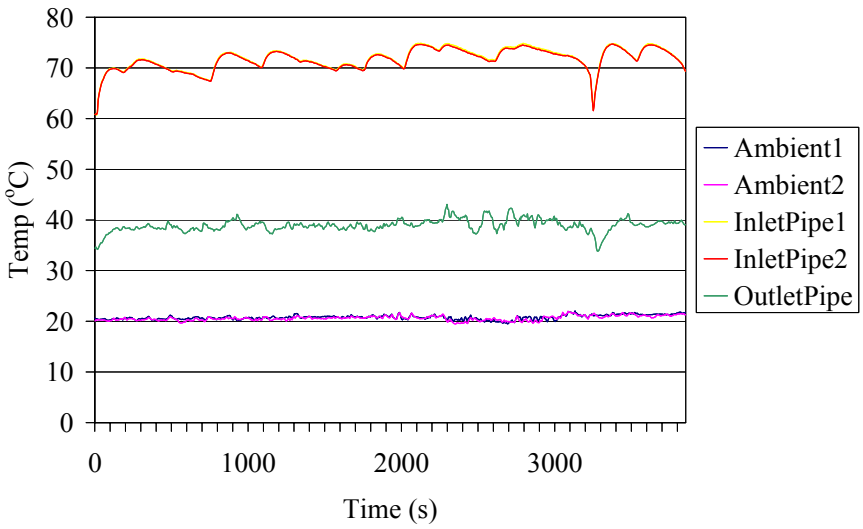

Figure 5.7: Condenser single phase flow temperature losses Horizontal Configuration

Location	Avg Temp (°C)
Inlet	71.7
Outlet	38.9
Ambient	20.7

Table 5.5: Condenser Test Results - Horizontal

With reference to equation 5.4 the GTD is 51 K the and LTD is 18.2 K. The logarithmic mean temperature difference can therefore be calculated as 31.8 K.

The actual flow-rate through the TB condenser was measured and found to be 3.3 ml/s ($\dot{m}$= 3.3g/s) Using the formulae 5.5, the relative heat loss rate has been calculated to be 14.4 W/K meaning that each TB condenser would provide approximately 144 W of cooling power if operated at 10K above ambient. This result indicates that only 8 of the condensers connected in parallel are required to achieve the 1.1 kW design specification condensing duty.

There is a marked improvement in the experimental performance of the TB condenser from the static temperature decay experiment. One factor which may affect this is the horizontal orientation however it was concluded that the primary reason for the difference is measurement error in the static decay experiment.

The theoretical performance of this condenser had previously been estimated at 6.75 W/K, however this was based on several assumptions, including a natural convection heat transfer coefficient of 7.5 W/m$^2\cdot$ K. The results from the single phase flow experiment indicates that a higher heat transfer coefficient is actually being achieved (maximum 16 W/m$^2\cdot$). The other possible explanation of the difference between theoretical and experimental values in this instance is the measured surface area of the heat exchanger. The overall footprint of the array is 0.9 m^2 however this approximation takes no account of the additional surface area provided by the swaged fins. The difference between theoretical and experimental cooling rates is thought to be caused by a combination of both of these factors.

5.3.3 Heat Exchanger Selection

Various condenser types and configurations were experimentally evaluated via both the static temperature decay and single phase flow experiments described previously. This experimental evaluation provided a mechanism to evaluate the relative cost of each design. Although aluminium finned copper pipe provided the highest cooling power per unit area, the cost of such a condenser would be prohibitively high for low volume manufacture. The data in 5.3 was used to estimate costs of £700 - 1,200 for an array sized to meet the required 1.1 kW condenser duty. The multi-parallel serpentine pipe array, with finned surface features (typically used in home refrigerators) provided a much lower production cost estimate of $<$ £100.

A specific OEM condenser pipe-work array (TB condenser) was chosen based on both the experimental performance and wide-spread manufacturing tooling availability. The results previously presented in section 5.3.2 highlight the experimental performance of this unit.

It was observed that the layout of the cooling pipes/fins on this particular condenser was unconventional and it was also tested in a horizontal orientation. This configuration yielded improved cooling performance. Data from the tests on the chosen OEM condenser unit (in horizontal configuration) have already been presented in figure 5.7.

The experimental results show this OEM unit can deliver 144 W of heat dissipation in ambient conditions which are 10 K below the condenser temperature.

5.3.4 Auxiliary Condenser Components

Condenser Reservoir

Based upon a condenser mass flow rate of 4.5 g/s and a refrigerant density (at 42 °C) of 1,138 kg/m^3 a condenser reservoir (2.8 l) was installed on EP2 to provide the condenser with the capacity to operate for periods of up to 1 minute whilst the generator sub system completed refrigerant charging cycles.

Moisture Filter

The refrigerant flow from both the generator and evaporator must pass through the condenser in order to recirculate around the system, making it the ideal location to collect residual water. A filter/drier ($\frac{3}{8}$" *ADK 53*), containing silica gel crystals, was installed on the condenser liquid line to absorb water from the refrigerant.

5.3.5 Condenser Sub-System Construction

The condenser was constructed using a bank of 10 TB condenser units, coupled in parallel to deliver up to 1,440 W. This arrangement provided the flexibility to easily increase the capacity if necessary. A photograph, taken during the prototype construction phase, of the TB condenser array used in the testing and development of EP1/EP2 is shown in figure 5.8.

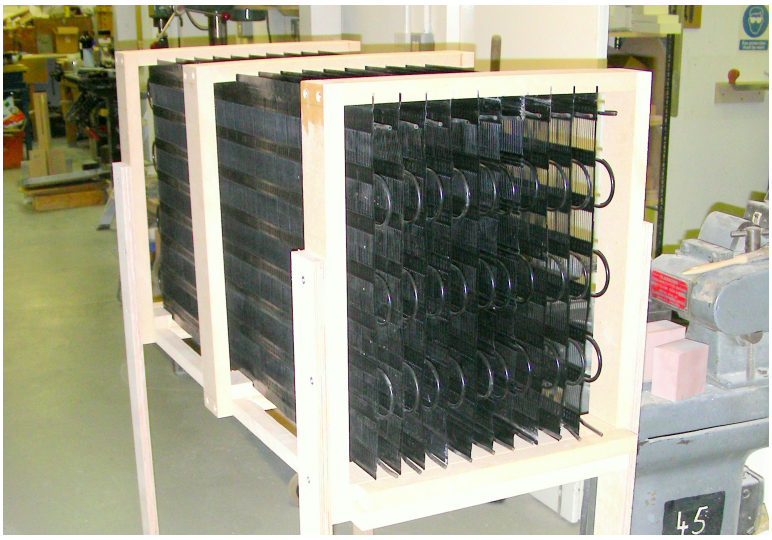

Figure 5.8: Photograph of EP1/EP2 condenser bank

5.4 Evaporator Sub-system

This section describes the theoretical design, specification, manufacture and subsequent testing of the evaporator sub-system. The primary heat exchanger, hereafter referred to as the *evaporator HX*, is specified and the construction of the refrigerated compartment, hereafter referred to as the *cool box*, is described.

Theoretical values for thermal mass and thermal losses were calculated and the results subsequently compared against experimental data. The section concludes with a discussion of the initial and final development evaporator feed methods.

5.4.1 Evaporator Sub-system Specification

The evaporator sub-system comprises the evaporator feed, cool-box, evaporator HX and jet-pump feed. During later developments, heat recovery sub-circuits provided added efficiency.

A flooded evaporator was specified for the cool-box as this offered more stable performance during the charge-discharge cycling of the generator sub-system. Equation 4.2 was used to estimate the theoretically required surface area (3.3 m^2) for 100W cooling duty. The estimation was based upon a fin efficiency of 1.0, a surface heat transfer coefficient of 7.5 $W/m^2 \cdot K$ (see section 4.2.2 and a ΔT_{air} of 4°C).

The selection of a suitable heat exchanger was also influenced by the results collected in section 5.3 and a four sided press finned heat exchanger array was chosen to provide maximum heat transfer.

Various methods of passive liquid level control (evaporator feed) were investigated during the development process and the iterations and outcomes are described in the final subsection. The chosen method must deliver refrigerant flow of approximately 0.7 g/s to provide the 100 W cooling duty. In addition, the liquid level with the evaporator would ideally be maintained at 75% full to maximise the heat transfer area whilst retaining an error margin for system fluctuations.

A simple insulated cool-box chamber was designed and manufactured to contain the evaporator HX and associated valves. Theoretical values for both thermal mass and heat losses were calculated. These theoretical estimates were subsequently validated by experiment and the results compared.

5.4.2 Evaporator Heat Exchanger

The OEM pipe-work (TB Condenser) used for the construction of the prototype condenser (serpentine pipe with punched plate finning) proved to be a good alternative to the flat plate type of evaporator traditionally found within refrigerators, offering 14.4 $W/m^2 \cdot K$ versus 3.9 $W/m^2 \cdot K$. Although flat plate evaporators are traditionally used in refrigeration for hygiene and durability reasons, higher efficiency finned pipes can be used in specialist applications. Four TB condenser units were bent and coupled in parallel to fit the four internal walls of an insulated chamber (the cool-box). The large evaporator surface area will allow design point cooling to be achieved with a smaller difference between the heat exchanger and the air temperature within the cool-box. Given the experimentally validated performance of 14.4 W/K per unit (57.6 W/K total) the evaporator HX could still deliver design point cooling at $\Delta T_{air} = 2$ °C.

5.4.3 Cool-box Construction

The insulated compartment that houses the evaporator HX, known as the cool-box, was sized to allow a wide range of duty loads to be refrigerated. The cool box, with internal surface area of 2.7 m^2, could easily hold the 24 L water duty load that was used in later performance evaluation experiments. The approximate dimensions of the cool-box are shown in figure 5.9 and a photo of the prototype cool box, containing an experimental cooling load of 24 litres of water (16 x 1.5 L bottles) is shown in figure 5.10.

A chest style cool-box was specified to minimise the convective losses that occur during loading/unloading of the cool-box contents. The cool-box was constructed within a 12 mm MDF outer shell. The internals walls of the cool-box were lined with 1.6 mm thick

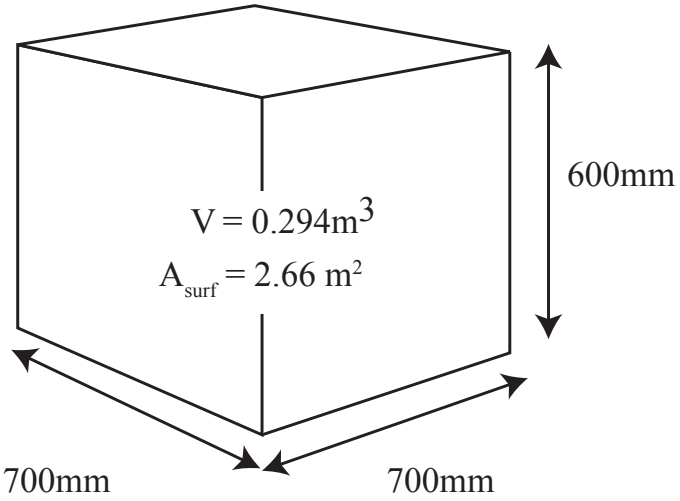

Figure 5.9: Diagram showing inner dimensions of cool-box

Figure 5.10: Photo - Cool box interior

polystyrene sheet and insulated using a 70 mm layer of Styrofoam 1B.

5.4.4 Theoretical Performance

The design and manufacture of a bespoke cool-box, not only allowed easy modifications to be made to the evaporator sub-system, but also allowed for the insulation materials to be specified with known thickness and thermal properties. This data allowed theoretical approximations for losses and thermal mass to be estimated with reasonable confidence.

Details of the insulation materials and thickness allows the conductive losses (measured in W/K) to be approximated using thermal series conductance formulae. Theoretical conduction losses of approximately 1.1 W/K are estimated in the upcoming section.

The thermal mass (measured in J/K) of the cool-box and cool-box contents, is another important metric that is used to define the total cooling load. From the theoretical calculations that follow it is determined that it would take approximately 18.4 kJ to bring the temperature down by 1 K. It is important to note that this approximation takes no account of the losses that would also contribute to overall performance. For the purposes of theoretical examination, the effects of boundary layer resistance are considered negligible in this approximation and are therefore ignored. Details of the error analysis are provided in appendix I.

Conductive Losses

Thermal losses from the refrigeration chamber were originally calculated using conduction theory. The material properties in table 5.6 were used to calculate the thermal losses. A natural convective heat transfer on both the inner and outer surfaces

of 7.5 W/m·K was also assumed, as detailed in table 5.7.

Material	k value	Source
Polystyrene (HIPS)	0.141 W/m·K	www.matweb.com
Styrofoam 1B	0.033 W/m·K	www.dow.com
MDF	0.135 W/m·K	www.woodpanels.org.au

Table 5.6: Cool box - Construction Material Thermal Conductivity

Item	Material	Thickness x (m)	Thermal Conductivity k (W/m·K)	Conductance U ($W/m^2 \cdot K$)
Chamber Lining	Polystyrene (HIPS)	0.0016	0.141	88.13
Insulation	Styrofoam (1B)	0.07	0.033	0.47
Box Structure	MDF Board	0.012	0.135	11.25
Inner Surface	↼ Natural Convective Heat Transfer ⇁			7.50
Outer Surface	↼ Natural Convective Heat Transfer ⇁			7.50

Table 5.7: Cool box conductance values

Using the standard method of calculating total conductance shown in equation 5.6...

$$\frac{1}{U_{total}} = \frac{1}{U_1} + \frac{1}{U_2} + \frac{1}{U_3} + ... \tag{5.6}$$

A total conductance of 2.49 $W/m^2 \cdot$ K was calculated. The internal surface area of the cool box box was 2.66m^2, and therefore Fouriers equation ($\dot{Q} = U \cdot A \cdot (-\Delta T)$) could be used to provide a theoretical estimate for losses at 1.07 W/K. If the refrigeration

chamber was 20°C below ambient (i.e. prototype test environment), the estimate suggests that the cooling power should include losses of around 21 W. This theoretical estimate however, does not take into account the infiltration losses through the gaps in the box where the evaporator pipe-work enters/exits.

Thermal Mass

Initial consideration of an empty cool-box provides 0.354 kg as the mass of air within the box. To understand the relevance of thermal mass, consider the power required to bring the temperature of this air down by 1 K in 1 minute; 5.9 W of cooling power would be required. The cool-box also contains numerous other components including the steel body of the heat exchangers themselves. A full list of the cool-box contents and their relative masses and specific heat values is presented in table 5.8. One litre of water has been included as a duty load. In later tests, a 24 litre load was used to increase the overall thermal mass of the experiment and allow more accurate performance data to be collected. Allowance is also provided for the thermal mass of the insulation material. In this instance, a linear temperature gradient (box to ambient) has been assumed and the mass of the insulation reduced by 50% accordingly. As shown in table 5.8, the estimated thermal mass suggests that 18.35 kJ would be required to pull down the temperature of the box contents by 1 K.

5.4.5 Experimental Validation

This subsection describes the experimental evaluation of cool-box losses (conductive heat gain through walls) and thermal mass. One possible experimental method of determining conductive losses is to refrigerate the cool-box down to operating

Material	Item	m (kg)	Cp (J/kg.K)	m.Cp (kJ/K)
Water	Duty load (1 litre)	1.00	4186	4.19
Styrofoam 1B	Insulation (50% thickness)	5.05	1200	6.06
Steel	Evaporator HX and supports	13.53	511	6.91
Copper	Interconnecting pipework	1.21	386	0.47
Brass	Ball valve / TEV	0.67	380	0.25
Aluminium	HX mounting brackets	0.24	500	0.12
Air	Cool box volume	0.35	1003.5	0.36
	Total			18.35

Table 5.8: Cool box contents : Mass and specific heat values

temperature and record the time taken (and rate of change) for the contents to raise to ambient temperature (i.e. measuring the heat gain from the local environment). Installing temporary refrigeration equipment within the cool box was not practically viable, and therefore a decision was taken to measure the flow of heat in the opposite direction, by heating the contents of the box.

A bulb socket fixture was installed within the cool box and incandescent bulbs were used to heat the inside of the box via natural convection. Less than 10% of the power consumed by incandescent bulbs is converted to light with the remainder being rejected as heat [67]. The actual efficiency of both 40 W bulbs and 100 W can be as low as 1.86% and 2.6% respectively[68]. Some studies report higher experimental efficiencies [69], however adopting the more conservative estimate was considered prudent as a lux-meter was not available.

After allowing the bulb to reach working temperature, the power was measured (RMS voltage and current draw) and the efficiency estimates applied to calculate the heat input.

The heat input of the "40 W" and the "100 W" bulb were calculated as 36.1 W and 92.7 W respectively.

Conductive Losses

During initial experiments the 100 W bulb (92.7 W heater) was placed inside the box and the lid closed. The temperature inside the box increased until the losses balanced the thermal input provided by the bulb. A set of these preliminary results is shown in figure 5.11.

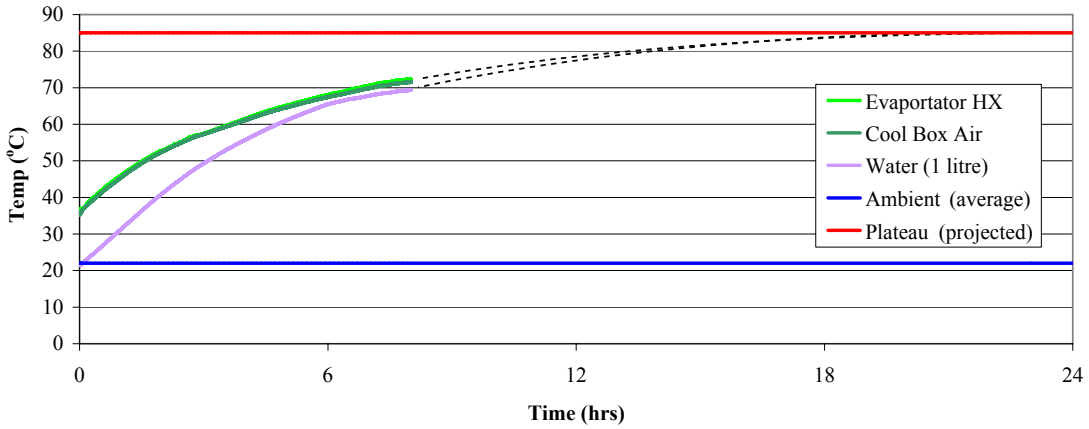

Figure 5.11: Temperature in cool-box containing 92.7 W heater over 8 hr period.

Figure 5.11 shows 8 hrs of experimental data. This is further extrapolated (24 hrs) with the use of 2 polynomial curves to approximate an asymptote at 85°C, 62.7°C above the mean ambient temperature (T_{amb} = 22.3°C).

Given the estimated 92.7 W heat input rate, Fouriers equation ($\dot{Q} = U \cdot A \cdot [-\Delta T]$) can be rearranged to calculate U·A as 1.48 W/K as shown in equation 5.7. This initial approximation shows that the losses may be more than 30% higher than the theoretical estimate. Giving context to this heat loss rate, if the cool-box was 20°C below ambient this figure would suggest that the cooling performance should include losses of around 29.5 W.

$$U \cdot A = \frac{\dot{Q}}{-\Delta T} \tag{5.7}$$

The experiment was repeated, however the 100 W bulb was replaced with a 40 W bulb (36.1 W heater) part-way through (t=12,200 s) the experiment to allow the temperature to reach an asymptote within a shorter time-frame. The temperature of the water was also increased artificially at t=12,200 s in order to reach an asymptote more quickly. The results of this experiment are plotted in figure 5.12. The air and steel temperature drops and reaches the same plateau temperature as the water (53.1°C), 25.6 K above the mean ambient. Using equation 5.7 the estimate for the relative conductive losses (U·A) can be refined to 1.41 W/K.

Thermal Mass

Temperature decay data was collected following an earlier experiment (previously plotted in figure 5.11), where a 100 W bulb was used to bring the box temperature up to approximately 75°C. The temperature of the cool-box (and cool-box contents) rises towards the external (ambient) temperature. The transient model of cooling (see appendix C can be used to experimentally infer the thermal mass via the previously calculated thermal losses (U·A). An illustration of the relevant terms applied to the

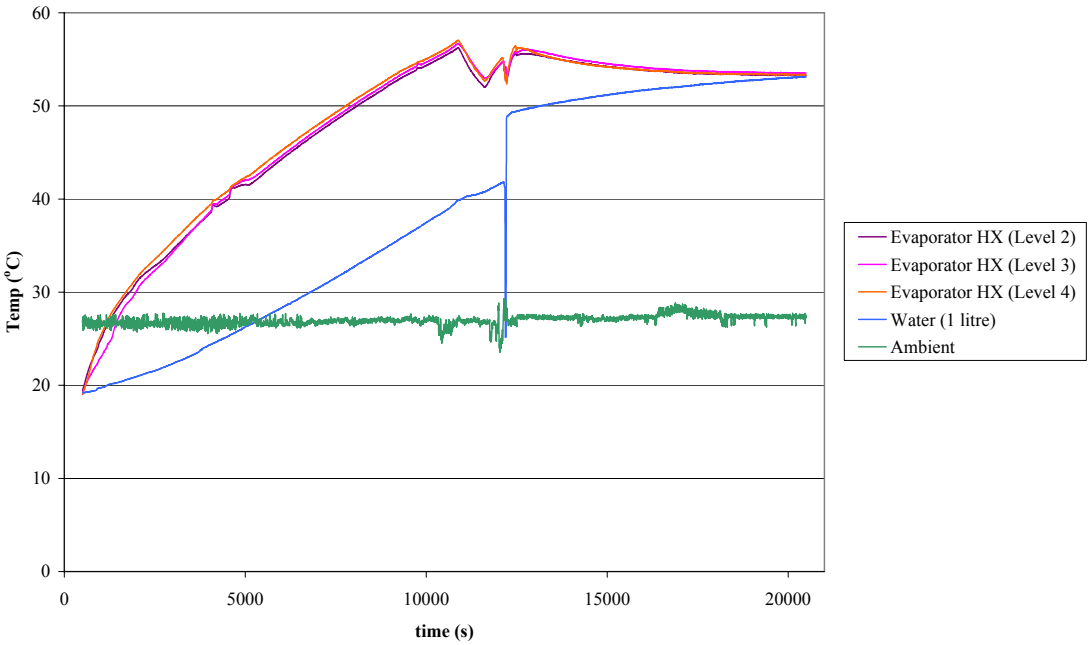

Figure 5.12: Temperature in cool-box containing 36.1 W heater over 8 hr period.

transient cooling model is shown in figure 5.13

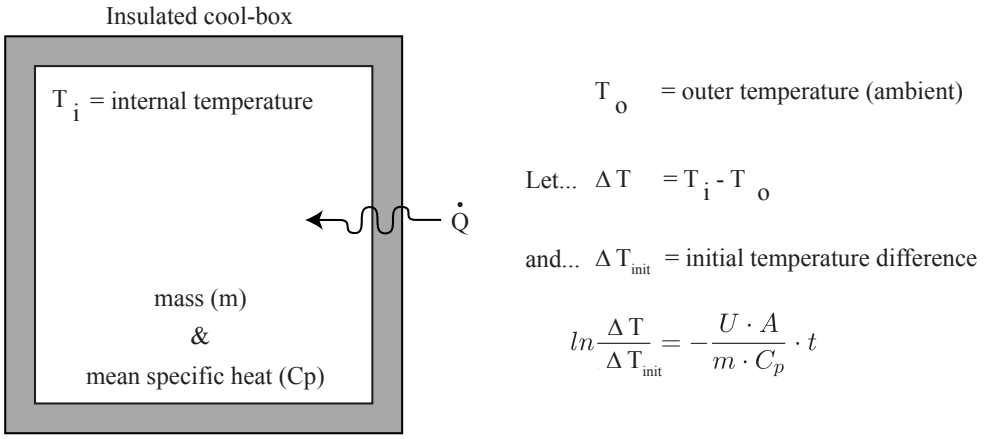

Figure 5.13: Transient model - illustration of terms

The temperature decay data collected is plotted in figure 5.14. By plotting the natural log of $\frac{\Delta T}{\Delta T_{init}}$ against time (t) as illustrated in figure 5.15 it is possible to determine the gradient of $\frac{U \cdot A}{m \cdot C_p}$. It has previously been experimentally derived that the thermal losses (U·A) are 1.41 W/K. After approximately 16,600 seconds ($ln(\frac{\Delta T}{\Delta T_{init}}) = 1.41$, therefore the thermal mass (m·C_p) can be approximated as 16.6 kJ/ K. This is lower than the 18.35 kJ/K theoretical estimate. It is thought that this difference could be explained by the lack of full temperature data across all components (i.e. the box insulation and heat exchanger framework temperatures were not recorded and assumed to be identical to the air temperature throughout the experiment).

Experimental Performance Implications

Figure 5.16 shows the percentage split of cooling load required to bring the entire cool-box and contents (including 24 l water) down by 1 K at the design point cooling rate (100 W). Of key interest are the losses, which at cool box temperatures of only 20 K

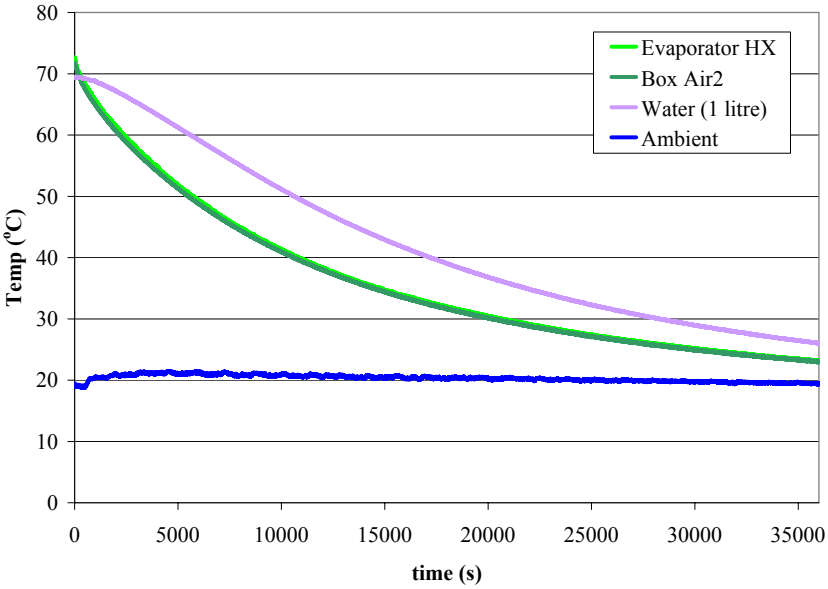

Figure 5.14: Graph showing temperature decay in cool-box over 10 hr period

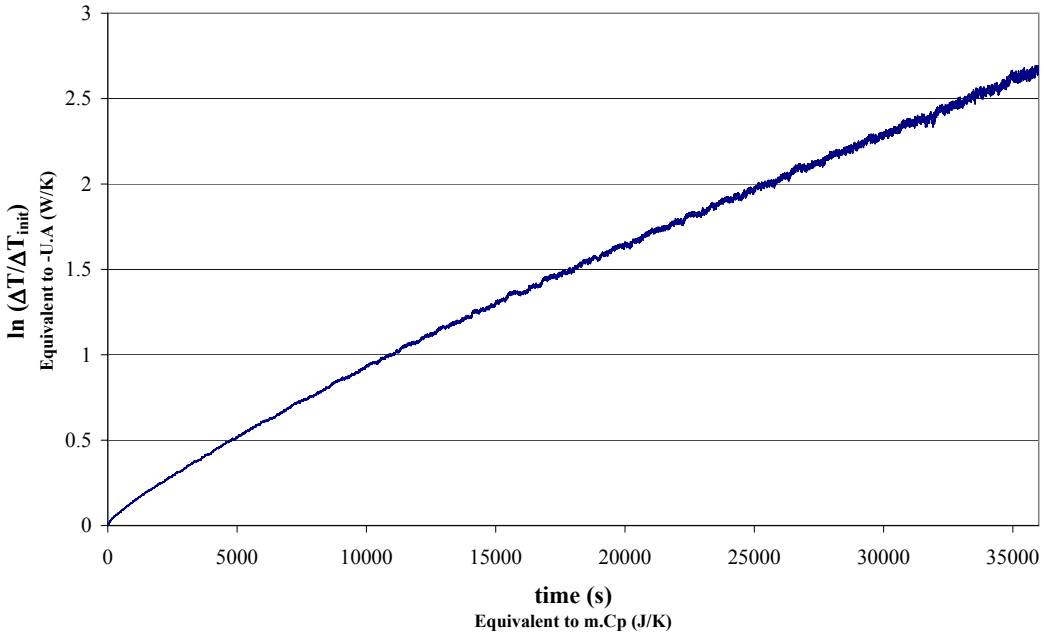

Figure 5.15: Graph showing $ln(\frac{\Delta T}{\Delta T^1})$ against time

below ambient, contribute significantly to the overall cooling load. At Δ T = 36 K (i.e maximum design point cooling load), the percentage of cooling duty lost to the local environment rises to 50%)

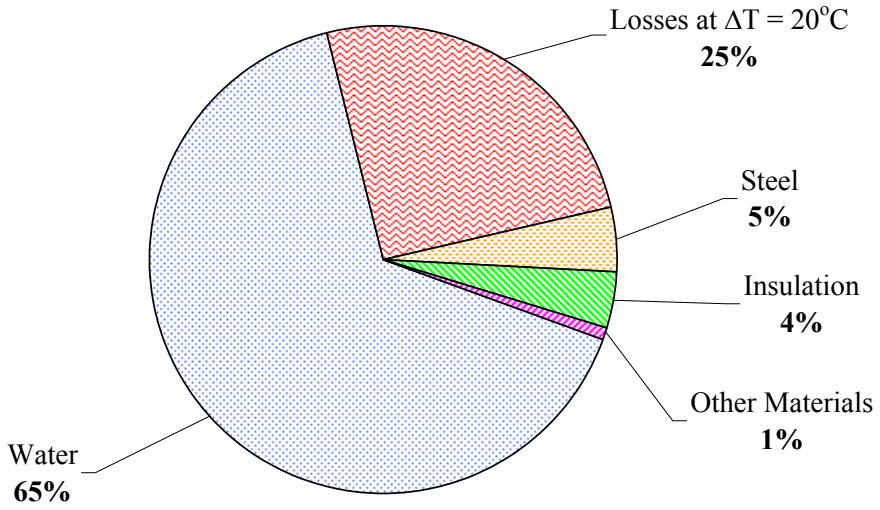

Figure 5.16: Graph showing evaporator power distribution with 24L water load, working 20 °C below ambient

Convective Cool-box Losses

In addition to the conductive losses discussed previously, the cool-box will also incur convective losses when the compartment is opened to load/unload the contents. The prototype has been specified to have a chest style, refrigerated compartment to minimise the effects of these losses however in a conventional, door-opening, home fridge, the convective losses are considerably higher. When the door of a home fridge is opened, the cold air flows downwards, out of the fridge compartment, and is replaced by warm ambient temperature air from the surrounding environment. This is the reason why most fridges contain plastic drawers for fresh produce (i.e. fruit and vegetable) at the bottom

of the fridge which retain some of the cold air when the door is opened.

For a 300L refrigerated compartment and assuming 20 door openings per day, a refrigerator temperature of 6°C, an ambient temperature of 32°C and with the worst case scenario (100% air exchange during each opening), equation 5.3 can be used to calculate the total convective energy loss as 192 kJ per day.

In order to limit these potential losses, a chest style refrigerated compartment was specified for the prototype which reduces these losses by approximately 90% [70]. In section 8.2 of this thesis, a production design concept for a solar powered vaccine refrigerator is presented which includes a smaller, secondary refrigerated compartment to limit the number of times the main compartments is opened to twice daily. Applying both of these loss reduction techniques (chest style compartment which is opened less frequently) reduces the convective energy loss to 1.92 kJ per day. Assuming that the 300 L air volume must be reduced from 32°C ambient to 6°C temperature within ten minutes of the door closing, this is equivalent to an additional 1.6 W load on the evaporator. This is less than 2% of the prototype evaporator cooling capacity and is not considered further in the evaluation of the prototype system.

5.4.6 Evaporator Feed

A flooded evaporator was used to help reduce fluctuations in temperature during generator charge/discharge cycles. Flooded evaporators are traditionally used in larger scale applications where a ball float valve is used to control the liquid level however this was considered to be impractical for the smaller capacity of this system.

Initially, capillary feed and variable orifice metering solutions were experimentally

trialled as passive evaporator feed devices however the fluctuating system pressures made it difficult to define fixed delivery rates. In order to progress the development of the other sub-systems, and better understand the evaporator flow requirements, control valves were installed to allow the evaporator flow rate to be metered manually.

Given sufficient flow from the condenser, a fixed volume of liquid refrigerant in the pipework between the ball valve (installed downstream of the condenser reservoir) and the needle valve (installed inside the cool-box, upstream of the evaporator heat exchanger) could be accurately calculated. Using the pipe dimensions in figure 5.17, the total liquid volume can be calculated as 5.9×10^{-3} m^3.

Table 4.2 provides a design point evaporator mass flow of 0.7 g/s. Given a design point evaporator temperature of 6°C, R134a thermodynamic property tables [62] were used to determine the relative liquid density ($\rho_{liq\_R134a} = 1274.7$ kg/m^3) . Given the fixed pipework transfer volume illustrated in figure 5.17 a cycle duration of approximately 108 seconds was calculated based on design point mass flow.

This method (fixed transfer volume) allowed a degree of experimental repeatability to be achieved by manually controlled valve sequencing.

The temperature of the evaporator pipe-work was collected at 200 mm height intervals to allow the liquid level to be detected via superheat. Monitoring the evaporator in this way allowed the theoretical charge cycle duration to be experimentally verified. The needle valve opening could be adjusted to control the fluid delivery rate and the ball valve could be used to increase or decrease the frequency of charge cycles.

The manually controlled operating method described above was used as the evaporator feed system on EP1 and EP2. In the final prototype version (see EP3, chapter 6) a

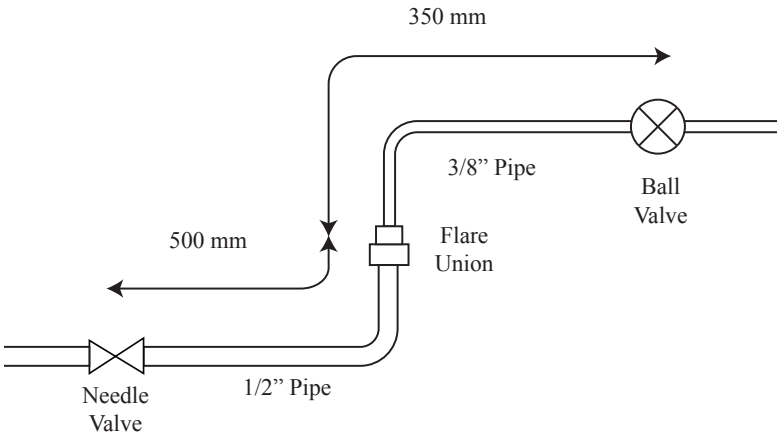

Figure 5.17: Diagram showing pipe dimensions of evaporator transfer feed

thermostatic expansion valve was employed to actively meter the evaporator flow rate and provide more repeatable results.

5.4.7 Auxiliary Evaporator Components

Evaporator Outlet (Jet-pump feed)

A non-return valve (NRV) was installed on the outlet of the evaporator, en route to the secondary inlet of the jet-pump. This prevented high pressure refrigerant from flowing back down into the evaporator during generator charge cycles (or in the event of the condenser back pressure exceeding the critical point).

Evaporator Heat Recovery

A heat exchanger was installed on the evaporator suction line, fed from the condenser outlet, to provide heat recovery and improve system efficiency. This enhancement was implemented on EP3 which is described in more detail in chapter 6

5.5 Generator Sub-system

Fed from the condenser reservoir, refrigerant is transferred to the generator sub-system, where heat input, via an oil fed heat exchanger, is used to produce a supply of high pressure vapour for jet-pump. As solar thermal collectors would have limited the scope of experimental testing, the energy available from $2m^2$ thermal panels was simulated using an oil heater. This heat input is transferred to the refrigerant that passes through the generator via a low pressure oil circuit. This thermal energy generates high pressure refrigerant vapour ($\approx$ 30 bar) which is fed to the primary inlet of jet-pump, thereby creating the motive forced used to entrain flow from the evaporator.

The generator sub-system comprises the generator feed, the oil circuit (including the generator heat exchanger), the vapour separator and the jet-pump feed line. The generator feed is of key interest to this study as it represents the largest of the requirements for electro-mechanical power. Minimising the reliance on costly photovoltaic panels would therefore principally be achieved by minimising the electrical demand of the generator feed system. Vegetable oil was used as the heat transfer medium for EP1 and EP2 however a more specific grade, with better heat transfer characteristics, was specified for EP3.

This section begins with a short description of the options explored in the specification of the oil circuit heat exchangers. A description of the oil circuit is then presented including details of calibration and experimental validation.

Various methods of mechanically delivering refrigerant fluid from the condenser reservoir, at 10 bar, to the generator heat exchanger, at 30 bar, were explored. Subsection 5.5.5 describes the methods that were experimentally trialled.

The jet-pump feed is then discussed, including passive methods of vapour separation. This phase separation is necessary, as wet vapour has been shown to negatively impact both the longevity and performance of the jet-pump nozzle.

Generator performance characterisation is discussed later in this chapter, in section 5.7.3.

5.5.1 Generator Sub-system Specification

The generator subsystem operates at high pressure ($\approx$ 30 bar) and provides the thermal power source necessary to drive the jet-pump cycle. The oil circuit, powered by an oil heater, and delivered via a small DC pump *(Mocal)*, is used to simulate the power available from 2m^2 of thermal collectors. The experimental calibration of the oil circuit is discussed in section 5.5.3.

As previously discussed, refrigerant delivery, from the condenser to the generator, represents the primary demand for electrical power within this experimental study. Section 5.5.5 discusses the options that were experimentally trialled to achieve low power refrigerant feed to the generator.

To ensure the jet-pump receives a supply of dry vapour, phase separation of the flow

exiting the generator heat exchanger was necessary. This requirement is discussed in more detail in section 5.5.7.

5.5.2 Generator Heat Exchanger

Initially, (on EP1), a bespoke pipe array, shown in figure 5.18, was manufactured to fit inside the oil heater bath. This approach was experimentally trialled, however failed to deliver sufficient heat to the refrigerant due to poor heat distribution.

Figure 5.18: Photograph of generator heat exchanger EP1 - Version 1

On EP2, an OEM (*SWEP*) brazed plate heat exchanger was specified and installed to provide better heat transfer. The thermal energy input of the oil was continuously evaluated by measuring the oil flow rate and monitoring the temperature of both the heat exchanger oil inlet and outlet pipes.

5.5.3 Generator Oil Circuit

5.5.4 Heat Input: Calculations and Assumptions

The heat input (Q_{oil}) provided by the oil circuit at any given time, was calculated, via equation 5.8, using a combination of experimental data ($\dot{V}_{oil}$ and Δ T_{oil} across the heat exchanger), relative density, and an assumed specific heat value for the oil.

$$\dot{Q} = \dot{m} \cdot C_p \cdot (T_2 - T_1) \tag{5.8}$$

A range of sources were queried to obtain a specific heat capacity for the vegetable oil and these are listed in table 5.9. Taking a rounded average from the sourced data, a value of 1850 J/kg·K was assumed for the EP2 generator heat input calculations.

BTU/(lb·°F)	J/kg·K	Source
0.43	1800	www.hotwatt.com/table3.htm
0.47	1970	www.olivesource.com/olivechemistry.htm
0.43	1800	www.thermalink.com/math/liquid.htm

Table 5.9: Sources of specific heat vales of vegetable oil from the web

Prototype sytstems EP1 and EP2 employed a low power ($\approx$ 20W) positive displacement pump (Mocal) to pump the oil around the circuit. The volumetric flow rate, at varying temperatures, was experimentally verified by measuring the time taken to pump a fixed volume (3 litres) of vegetable oil and characterize the pump performance. An extract of these results is shown in figure 5.19. Note, the range of possible error is from the linear trend line is almost $\pm$ 20%

During the tests, the oil pump was connected to a regulated power supply allowing both

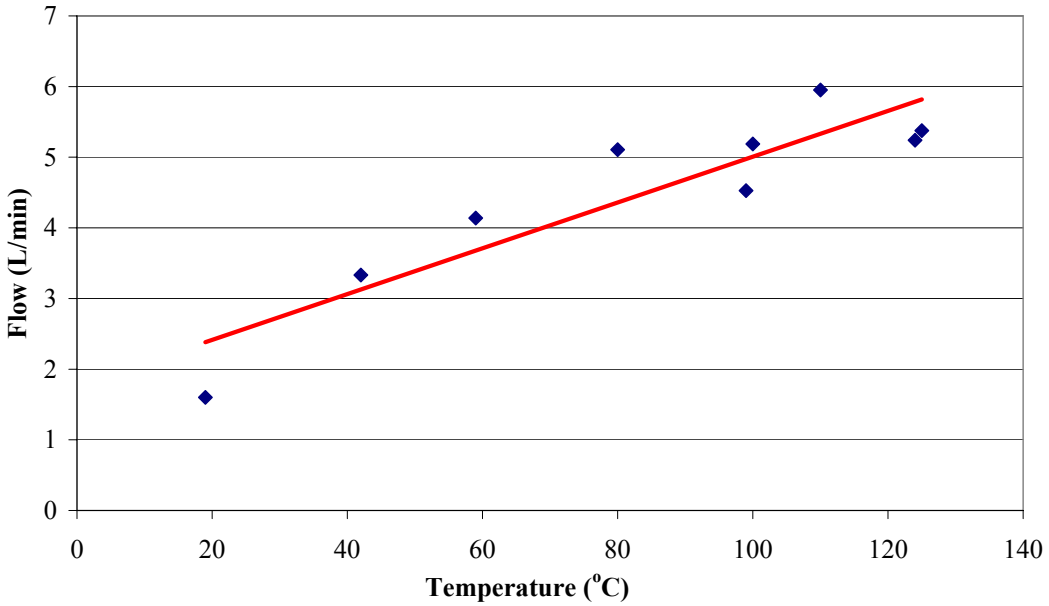

Figure 5.19: Graph showing oil flow rate against temperature *(Mocal pump)*

current and voltage to be measured. A close correlation existed between the voltage supplied and the volumetric flow rate as illustrated in figure 5.20. As voltage is directly linked to pump speed the change in viscosity of the oil at higher temperatures does not appear to affect the measurement of flow-rate via pump voltage input power. The range of possible error from the linear trend line is now reduced to less than ± 10%.

In order to calculate the heat input (Q), the volumetric flow rate ($\dot{V}_{oil}$)rate had to be translated to a mass flow rate($\dot{m}_{oil}$). In order to determine the relative density of the oil, the weight was plotted against the temperature (figure 5.21) and a linear trend line extrapolated.

With the necessary data obtained, it was now possible to estimate the thermal power input to the heat exchanger at any given time by measuring the temperature difference across the oil inlet and oil outlet to the heat exchanger and observing the supply voltage

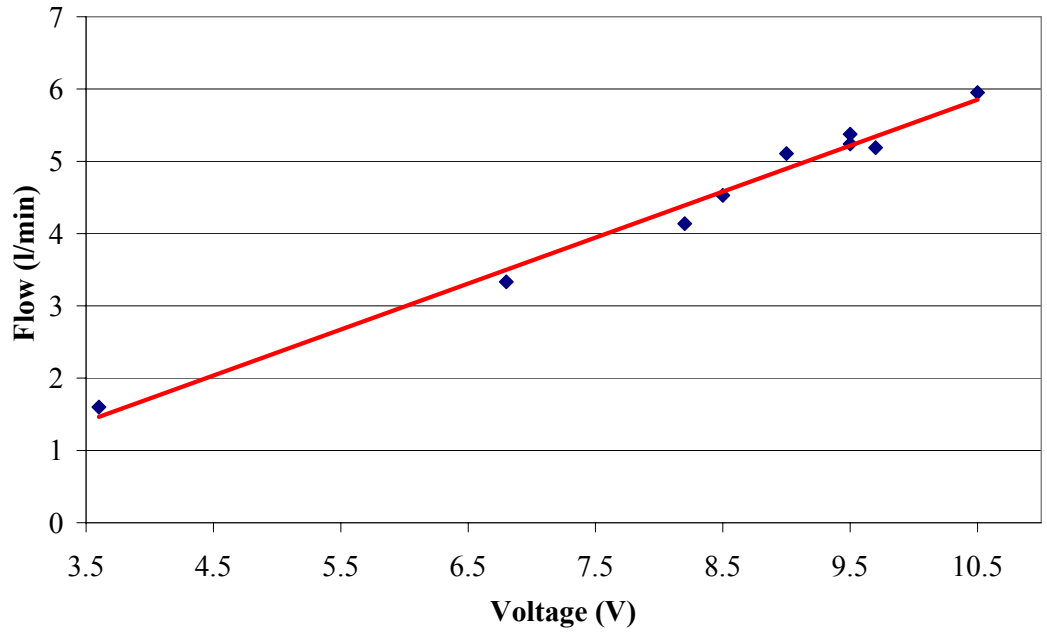

Figure 5.20: Graph showing Mocal vegetable oil flow rate against pump supply voltage

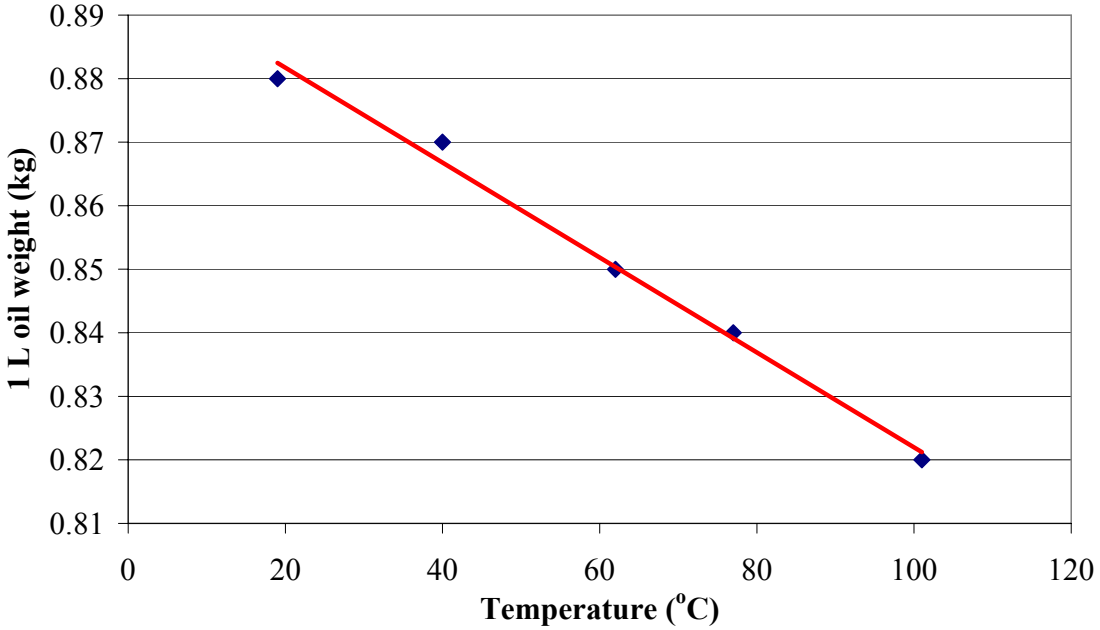

Figure 5.21: Graph showing mass of one litre of vegetable oil at various temperatures

to the oil pump.

5.5.5 Generator Refrigerant Feed

EP1 Generator Feed

Minimising the electrical demand of the generator feed sub-system is of key concern when considering the total electrical duty of the system. A gravity assisted, transfer volume was originally envisaged that utilised a vertical length of pipe which could be isolated from either the condenser or generator. The premise invloved allowing the volume to fill with refrigerant fluid from the condenser outlet and then isolating this volume before opening the lower valve allowing the fluid to flow downward into the generator. In practise, the relatively small volume of the transfer volume pipe initially trialled proved to be ineffective.

Research was conducted to try and source a conventional positive displacement pump. The requirement specification was to pump R134A at 600ml/min with a 21.7 bar pressure rise (From 10.7 to 32.4 bara). A gear pump was subsequently trialled however cavitation of the recently condensed fluid caused poor efficiency. A booster pump (impeller pump) was installed on the inlet to the gear pump to increase the feed pressure and the EP1 pumping solution is shown in figure 5.22. Although this did improve the performance, cavitation was still a problem. In one test, pumping R134a at a condenser temperature of 25°C ($\approx$ 6.6 bara), with the booster pump pre-pressurizing the refrigerant to 7.3 bara, the gear pump could only achieve generator pressures of 21 bara before cavitation began to occur and the performance rapidly declined. In addition to poor performance, the electrical demand of this pumping method (350-400 W) was also a

significant drawback. The required duty of the pumping system (low flow, high pressure differential) is unusual and very few parallel applications exist. Diesel fuel injectors were explored as one possible technology however the fluid was not compatible with OEM diesel pumps. Dosing pumps are another possible solution however the cost for this technology was too high ($\backsim$£900).

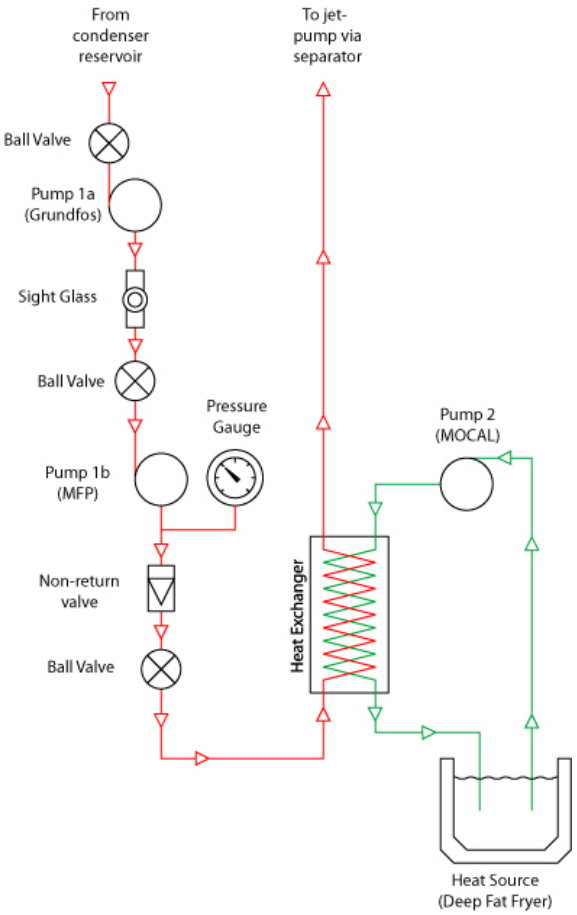

Figure 5.22: Schematic of EP1 generator refrigerant feed system

EP2 Generator Feed

Figure 5.23 shows the construction schematic for the components that relate to the generator sub-system in EP2. Following the problems that were experienced with the booster pump and gear-pump in EP1, a decision was taken to return to the gravity-feed solution previously considered. The premise is similar to the initial EP1 *transfer volume* solution described above, however rather than continuously transferring small amounts of refrigerant by gravity feed, a reservoir was installed on the high-pressure (generator) side of the system. Once filled and isolated, the thermal energy contained in the vegetable oil is transferred to the fluid using a heat exchanger. Based on the theoretical flow rate of the generator, this reservoir will then be able to supply high-pressure refrigerant vapour to the jet-pump for periods of approximately 500 seconds.

This system has several advantages over previous solutions. By raising the temperature of a fluid reservoir to the saturation point, it will be able to vaporise fluid continuously for fixed discharge periods. Although this means that the jet-pump will only operate intermittently, the nozzle performance, and consequently the entrainment from the evaporator, should be consistent during these discharge periods.

There is also a distinct advantage in the reduction of electrical components. The jet-pump itself only needs thermal energy, therefore ideally no electricity would be used in the refrigeration circuit. This would mean that no photovoltaic panels (in addition to the one required for the oil circulation pump) would be re required and hence the system would be cheaper to manufacture and more reliable. In practise, a small photovoltaic will be needed to power the control electronics and electrically actuated valves, but this requirement is small in comparison to the power needed to operate two pumps.

For safety reasons, the pressure reservoir was sized to accommodate the full volume of the condenser reservoir, allowing for the expansion of the liquid at a maximum generator temperature of 95°C. Equation 5.9 shows how the required generator reservoir volume was calculated at 4.57 L. Note: The closest off-the-shelf pressure vessel available was 4.6 litres.

$$\begin{aligned} R134a\ \rho_f\ at\ 42°C &= 1138.16\ kg/m^3 \\ R134a\ \rho_f\ at\ 95°C &= 837.25\ kg/m^3 \\ Liquid\ expansion\ ratio &= 1.36 \\ Factor\ of\ Safety &= 1.2 \\ Condenser\ reservoir\ volume &= 2.8\ L \\ \therefore Required\ generator\ reservoir\ volume &= 4.57\ L \end{aligned} \tag{5.9}$$

A schematic illustration of the EP2 reservoir circuit is shown in figure 5.23. The small stars indicate where flare unions were included to allow for servicing. An isometric diagram contained later in this chapter(figure 5.35) shows the layout of the EP2 generator sub-system in situ.

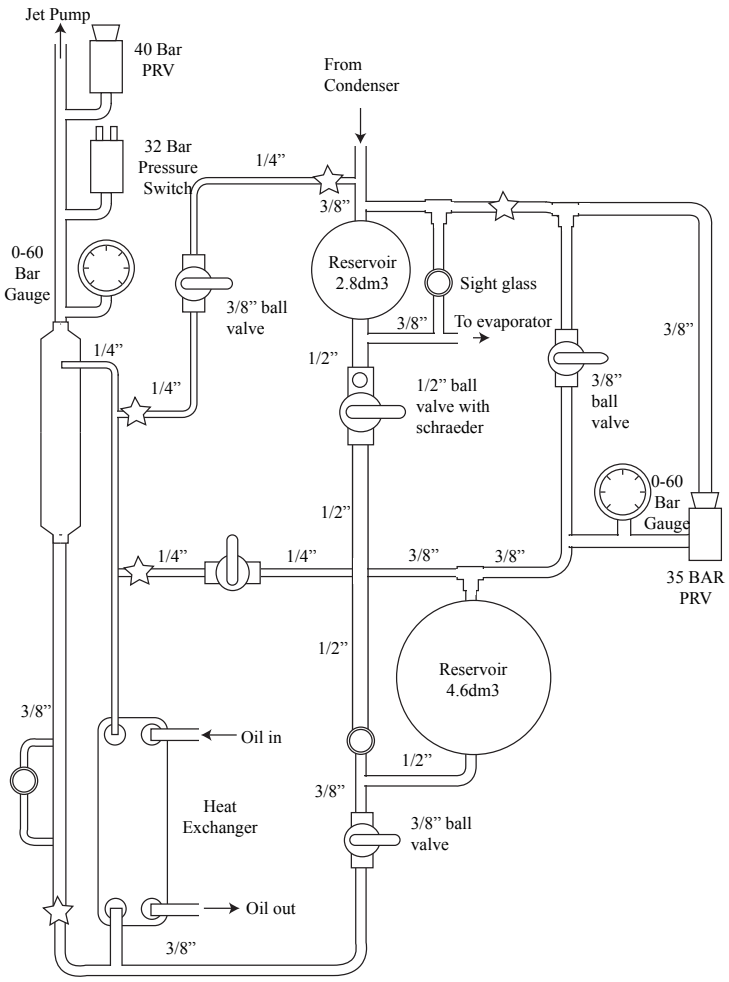

Figure 5.23: Schematic of EP2 generator refrigerant feed system

5.5.6 Theoretical Energy Balance of Generator Feed

As it was not possible to verify the relative effect of the reservoir transfer system on overall COP experimentally (i.e by direct comparison with the same system using an electrically powered pump), a theoretical estimate of the additional thermal energy requirement (Q_{RTS}) was calculated. The reservoir transfer system operates on a charge discharge (CD)cycle. With reference to figure 5.24 the following assumptions were made in order to estimate Q_{RTS};

- Prior to charge cycling, the condenser reservoir (2.8 L) is entirely full of saturated R134a liquid at p_1 (T =42°C)
- Prior to charge cycling, the generator reservoir (4.6 L) is entirely full of saturated R134a vapour at p_2 (T = 90°C)
- When the isolated reservoirs are connected, and the refrigerant fluid is transferred (equalised at p_{eq}), the process is assumed to be adiabatic and the new liquid/vapour mass ratio determined based on no change in the total energy or total refrigerant mass.
- The energy required to bring the equalised liquid/vapour mass back to pre-charge conditions (i.e. p_1 and p_2) is used to calculate the total energy requirement of the cycle (i.e. $Q_{RTS} = E_{Tot-Post}$ - $E_{Tot-Pre}$).

When switched back to normal operation (i.e. discharge mode) the thermal energy consumption of the CD cycle is calculated as the sum of the heat required to bring the transferred fluid up to generator pressure and the waste heat rejected to the condenser.

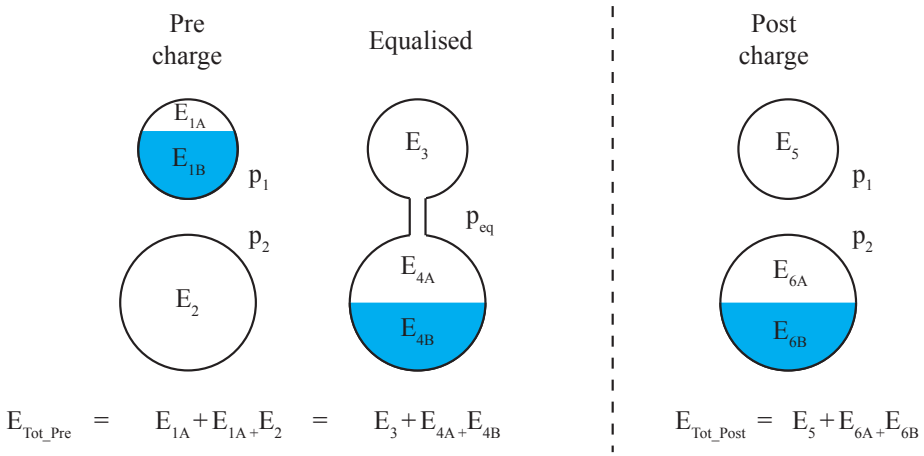

Figure 5.24: Schematic diagram of reservoir transfer energy balance

The initial energy, based on the conditions listed above, of the two isolated reservoirs is 1,251 kJ. Following liquid refrigerant transfer, an equalisation pressure of 17.2 bar provides the new relative liquid and vapour masses with no change in overall mass or total energy. The reservoirs are then isolated once again before being reintroduced to the primary condenser and generator circuits.

Excess energy contained in the condenser reservoir (1.7 kJ) must be rejected back to the condenser and a further 203.7 kJ energy is required to increase the contents of the generator reservoir up to operating temperature.

The total thermal energy requirement to operate one CD cycle is therefore ≈207.3 kJ.

Based upon a total cycle duration of 750 s (250 charge plus 500 discharge) the thermal power requirement of the transfer cycle ($\dot{Q}_{RTS}$) is estimated at 276 W. At Q_g = 1,000 W, the additional thermal energy demand of the CD cycle is 27.6% of total generator input. This is higher that the figure reported by others operating similar experimental studies (10-20% [39][40]) however this calculation is revisited in section 7.6.2 with

reference to EP3 experimental results and the additional load on the generator is found to be significantly lower (15.6%).

Despite the need for additional thermal energy, this system uses less electrical energy than the equivalent mechanical pump. As stated in the research proposition, this investigation is focussed on reducing the electrical energy requirements of the system. As only minimal electrical energy is required, reliance on photovoltaic panels is reduced and therefore the initial capital outlay for this system would likely be less.

5.5.7 Jet Pump Feed

The jet-pump feed line from the generator supplies the jet-pump with high pressure vapour. A non-return valve was installed on the jet-pump feed line to prevent reverse flow entering the evaporator when generator pressures dropped below this operating level.

Phase Separation

In order for the jet-pump to function effectively is supply should be dry-superheated vapour. Upon exit from the generator heat exchanger, some residual liquid is still present, therefore passive methods of phase separation were explored.

To ensure the jet-pump receives a supply of dry vapour, a phase separator is required on the outlet of the generator. A pipe in pipe cyclonic separator was installed on EP1 and EP2 (see figure 5.25).

Although this method proved broadly effective, it did not perform well under flooded

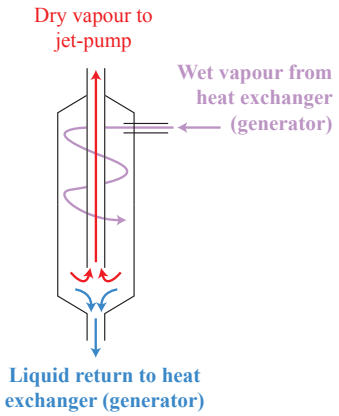

Figure 5.25: Illustrative diagram of cyclonic vapour separator concept

generator conditions. Experimental tests on EP3 confirmed that a second heat exchanger, installed in series above the generator, was more reliable in providing the jet pump with a dry, super-heated vapour source. This solution is described in more detail in chapter 6

5.6 Jet Pump Design and Optimisation

This section describes the manufacturing design of the system jet-pump and subsequent experimental optimisation of the nozzle position.

The section begins with a presentation of the manufacturing design for the jet-pump, based on the 2D CFD study cited earlier in this thesis [55]. Details of the incremental geometry adjustment features are illustrated and the adjustment range and resolution is specified.

The section also includes experimental data, which is used to define the optimal position of the jet-pump nozzle.

5.6.1 Jet Pump Design

Based on the results obtained from the CFD [55], the critical dimensions for jet-pump nozzle and diffuser were defined. A full set of these dimensions are supplied in appendix F.

A manufacturing and assembly design of the jet-pump was created using ProEngineer CAD software. Figure 5.27 shows an sectioned isometric view of the CAD model and figure 5.26 shows a side elevation drawing. The design incorporates a central bore, into which both the nozzle and diffuser are inserted. Silicon o-rings fitted on both the nozzle and diffuser prevent leakage paths being formed around the components. Three spacer washers allow adjustment to the nozzle position. Flanged pipe fittings, which are sealed to the valve body using capping nuts, allow $\frac{1}{2}$" copper pipe to be connected.
Conventional machining techniques (milling and turning) were used to produce all of the

parts in brass (excluding the silicone o rings).

The simple design would provides the potential of in-field user servicing of the equipment: a useful benefit of the jet-pump cooling system in the provision of vaccine refrigeration.

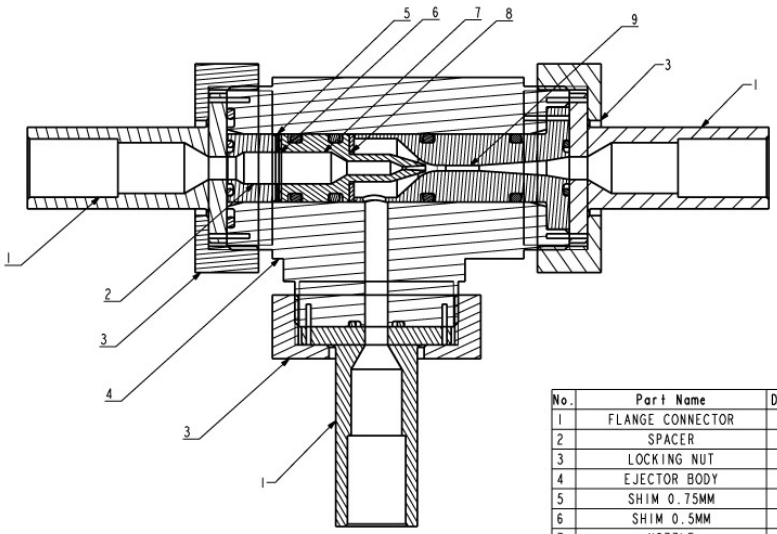

No.	Part Name	Drawing No.	Qty.
1	FLANGE CONNECTOR	21260	3
2	SPACER	21259	1
3	LOCKING NUT	21261	3
4	EJECTOR BODY	21256	1
5	SHIM 0.75MM	21263	1
6	SHIM 0.5MM	21264	1
7	NOZZLE	21258	1
8	SHIM 1MM	21262	1
9	DIFFUSER	21257	1

Figure 5.26: Jet-pump assembly drawing

Practical Limitations

The small bore size of both the nozzle (0.65 mm) and diffuser (1.2 mm) represent the practical limitations in manufacturing jet-pumps at this scale using conventional metal machining techniques.

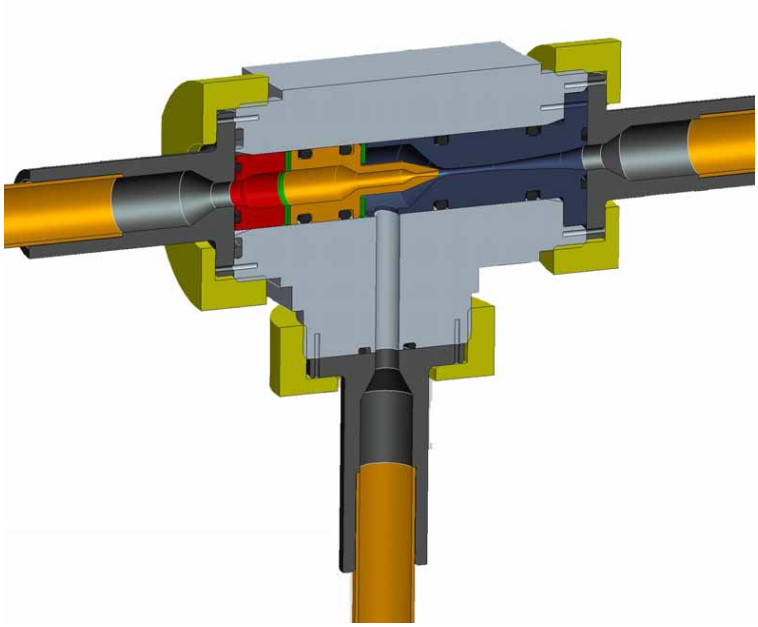

Figure 5.27: Isometric view of CAD assembly

Geometry Adjustment

The multi-part design provides the ability to incrementally adjust the position of the nozzle within the mixing section of the diffuser, using shim washers inserted either behind or in front of the nozzle body. Optimisation of this positioning is described in more detail in subsection 5.6.3. Figure 5.26 shows a 2D assembly drawing of the final jet-pump design.

Three shim washers form part of the jet-pump assembly allowing the nozzle to be spaced at varying distances from the diffuser throat. This arrangement is more clearly illustrated in figure 5.31. These washers have three different thicknesses (0.5, 0.75 and 1 mm) By using various combinations either behind or in front of the nozzle, it is possible

Figure 5.28: Photograph of jet-pump assembly

to obtain eight different nozzle positions, which are listed in table 5.10. The labelling convention for the three washers is presented in table 5.11. The nozzle exit position (NXP), has previously been mentioned in chapter 4 and is defined as the distance between the nozzle tip and the start of the radius at the convergent inlet of the diffuser. For reference, the CFD study, [55], predicts an optimum NXP of 1.6 mm.

Combination			NXP (mm)
-	▷	ABC	2.85
A	▷	BC	2.35
B	▷	AC	2.1
C	▷	AB	1.85
AB	▷	C	1.6
AC	▷	B	1.35
BC	▷	A	1.1
ABC	▷	-	0.6

Table 5.10: Jet-pump nozzle spacing combinations

Washer	Thickness (mm)
A	0.5
B	0.75
C	1

Table 5.11: Jet-pump nozzle shim washer labels

5.6.2 Jet-pump nozzle: Mechanical Stress

As the radius / wall thickness ratio of the jet pump (3mm/1.5mm) is less than 20, it is considered as at thick walled vessel [71]. Derivatives of Lame's equations were used to calculate both the radial and hoop stress within the jet-pump nozzle. Given the design dimensions for the convergent section of the nozzle (ID 3mm, OD 6mm), and assuming an internal pressure of 32.43 bara (p_{gen}) and external pressure (p_{evap}) of 3.6 bara, both the hoop stress (2.31 MPa) and radial stress (1.11 Mpa) fall well below the yield stress of brass ($\approx$ 200 MPa).

5.6.3 Jet Pump Optimisation

Once a system capable of maintaining sufficient generator pressure had been developed (EP2), work could begin on characterisation and optimisation of the jet-pump. Studies have shown that the position of the nozzle tip within the diffuser can be used to increase either the entrainment ratio or critical condenser pressure. As described previously, the multi-part jet-pump design includes the ability to adjust the position of the nozzle position in 0.25mm increments. Operational tests were carried out at various nozzle positions to find the optimum position for maximum entrainment. To find the optimum nozzle position, these test were initially carried out at $\pm$ 5% design point conditions (i.e Generator = 30.8-34 bar, Condenser = 10.2-11.2 bar) and then later across a wider range of lower system pressures (Generator = 21.5-34 bar, Condenser = 6.8-11.2 bar). Optimising the position of the jet-pump nozzle ensures that maximum suction is achieved on the evaporator, when both generator and condenser are at design point conditions. Later in this chapter, in section 5.7.3, the experimental results collected across the wider range of generator and condenser pressures are presented to help

characterise system performance.

Optimisation Method

Tests were conducted to find the optimum position for the jet pump. The experiments conducted measured the suction pressure on the secondary inlet of the jet-pump, whilst the evaporator remained isolated. This method meant only two variables (p_g and p_c) would affect the result

Various measures were introduced to allow the jet-pump nozzle to be repositioned during tests without the need to de-gas the entire system. Ball valves were installed on the three pipes that lead from the jet-pump, (see figure 5.34: V7, V9 and V10) allowing the jet-pump to be isolated. A schrader charging connection forms part of the pump body and following each nozzle repositioning operation, this allowed a vacuum to be drawn across the jet-pump before opening any of the ball valves and re-completing the refrigeration circuit. For testing purposes the evaporator line ball valve, V9, was closed and a service gauge attached, via a Schrader valve, to the secondary inlet in order to measure the suction pressures.

Optimisation Results

A summary of the experimental optimisation results is shown in figure 5.29. These results show the performance of the jet-pump at design point conditions, however as demonstrated later in section 5.7.3, lower suction pressures could be achieved when operating at lower condenser pressures.

Using the property tables for R134a in the Rogers and Mayhew steam tables [62], it was

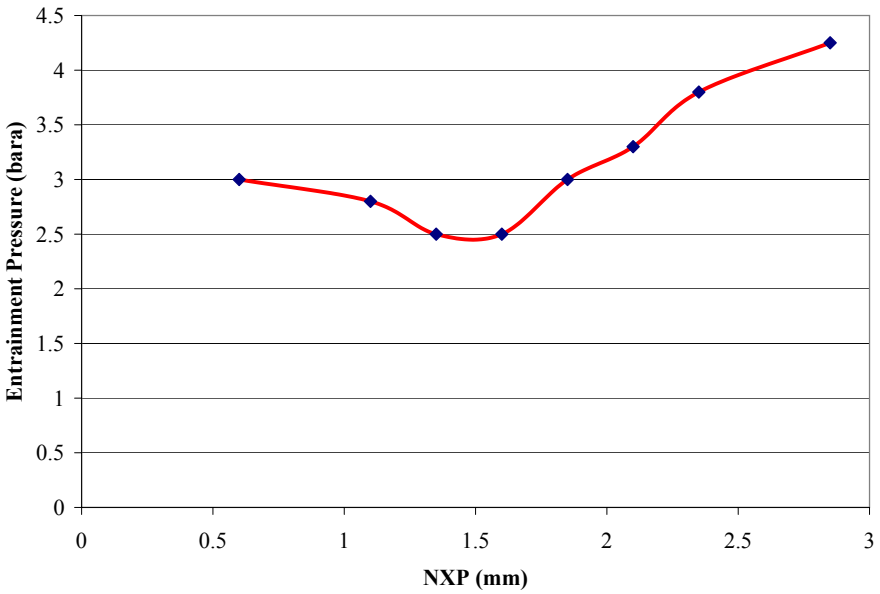

Figure 5.29: Graph showing suction pressure against relative position of jet-pump

then possible to convert this data to illustrate the potential cooling capabilities of the jet pump. The corresponding temperature data is shown in figure 5.30.

Optimisation Discussion

The optimum nozzle exit position (NXP) provided by the CFD data [55] for a 100W R134a jet pump is 1.6 mm. The results presented in figure 5.30 confirm that the CFD predictions are closely matched by the experimental results. Figure 5.31 shows the adjustable jet-pump assembly with a 1.00 mm shim washer sitting ahead of the nozzle, providing a 1.60 mm displacement between the tip of the nozzle and the start of the radius on the convergent section of the diffuser (NXP).

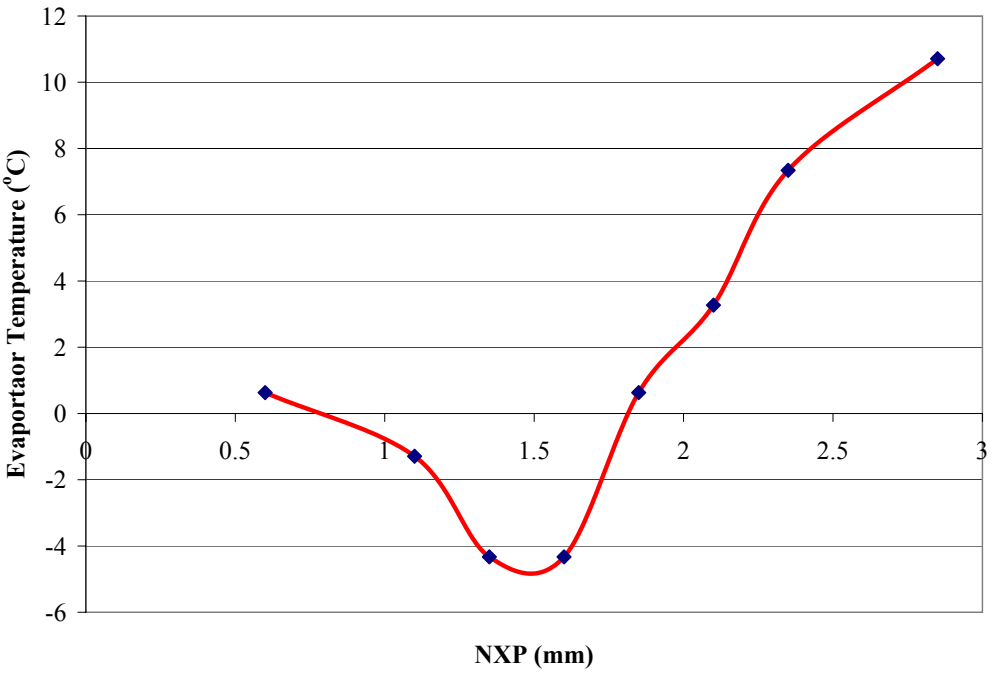

Figure 5.30: Potential cooling temperatures against the relative position of the nozzle

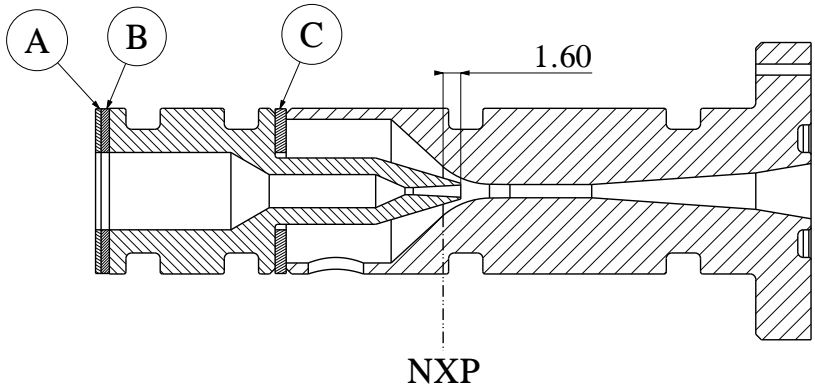

Figure 5.31: Dimensioned drawing of optimum nozzle insertion

5.7 Integrated System Design

This section of the chapter provides information on the first two development versions of the integrated system including schematic layouts and operating procedures. This section focusses primarily on EP2, as EP1 was primarily a development exercise, used to better understand the characteristics and requirements of the integrated system

Version 1 of the integrated system (EP1) was used to initially validate the cooling cycle and jet-pump operation. Various mechanical pumping systems were trialled for the generator feed, with only limited success. EP1 did allow for the sub-systems to be tested in series however cooling performance was hindered by the lack of a fully functional generator feed system.

Version 2 of the integrated system (EP2) employed two fluid reservoirs in order to maintain generator pressure for longer periods and further characterise system performance. This allowed for the jet-pump nozzle position to be optimised.

5.7.1 EP1 - Initial Test System

Figure 5.32 shows the schematic layout of EP1. In this diagram, the generator feed has been illustrated showing the *transfer volume* however as previously discussed section 5.5.5, a conventional pumping solution was also trialled on EP1.

EP1 - Operating Procedure and System Schematic

In the EP1 schematic configuration illustrated (figure 5.32), V11 and V12, were opened and closed in sequence to transport small volumes of refrigerant liquid from the

condenser to the generator, whilst never allowing the two sub-systems to be connected directly. V20 was used to allow the generator to build up sufficient pressure before opening the vapour flow line to the jet-pump. As previously discussed in 5.5.5 the volume of liquid transferred each time was not sufficient to maintain design point generator pressures and so further development was necessary.

An initial manufacturing concept sketch, including OEM part numbers and pipe diameters, for EP1 is shown in 5.33.

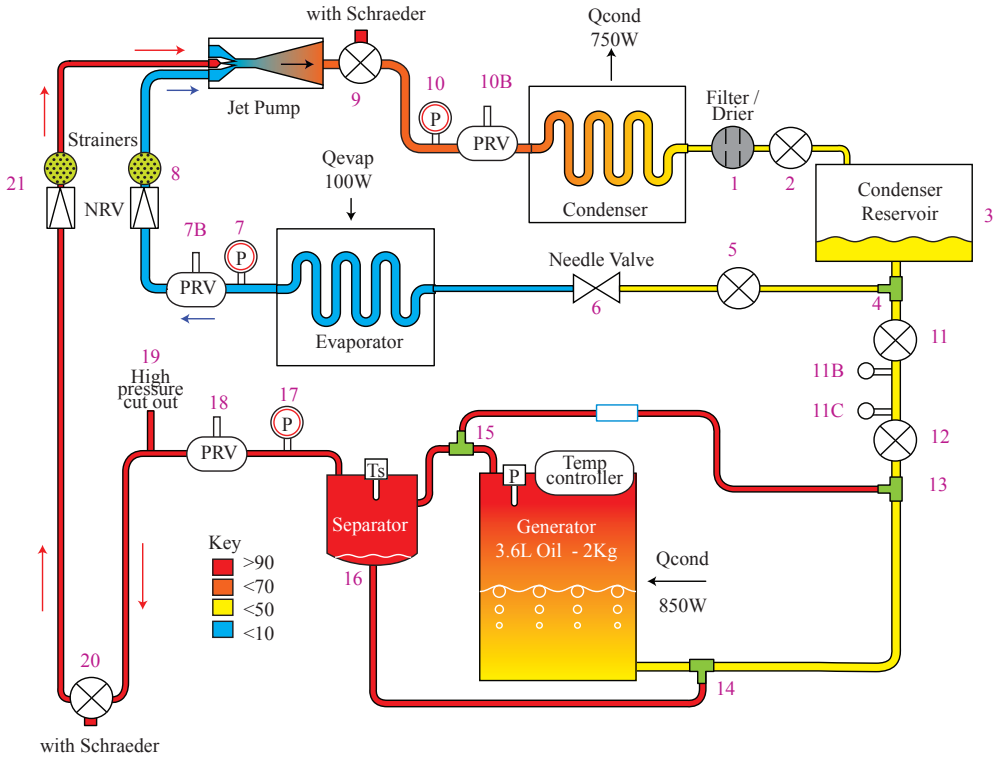

Figure 5.32: 2D Schematic of EP1

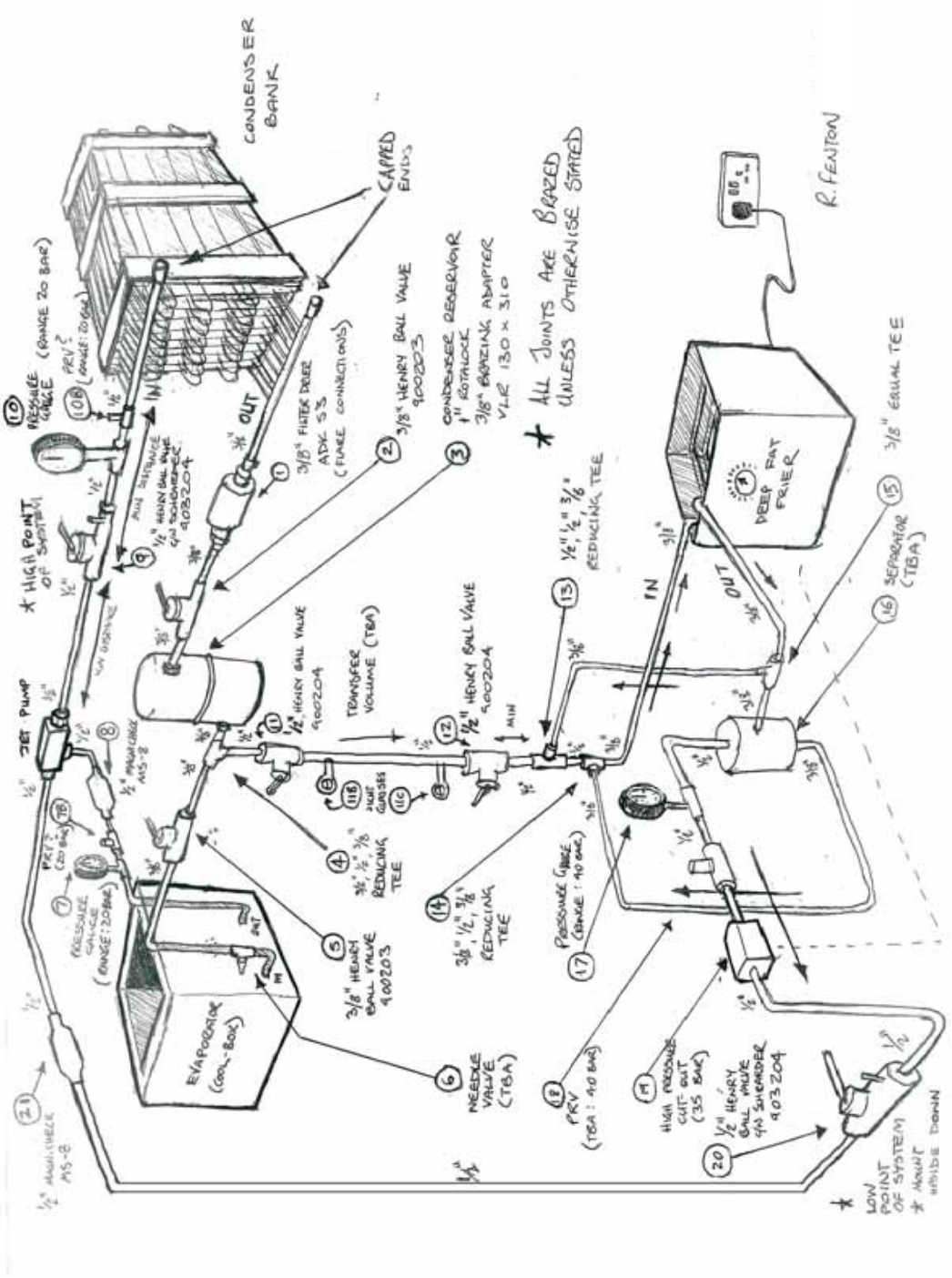

Figure 5.33: Hand drawn manufacturing concept sketch for EP1

5.7.2 EP2 - Development System

This section details the design, operating procedure, and experimental evaluation of EP2. The first version of the prototype system (EP1) provided several key learning outcomes, and was a useful foundation on which to build. One of the key failings of EP1, was the lack of a satisfactory generator feed system. Building on the idea of using gravity, heat and appropriate valving to transfer refrigerant from the condenser to the generator, a scheme which employed two reservoirs was conceived. These reservoirs provided the capacity for a charge / discharge (CD) strategy to be implemented, allowing the generator to supply the the jet-pump with high pressure vapour for periods of up to 500 seconds, without any additional refrigerant being delivered from the condenser. In turn, the condenser needed to have a reservoir to collect a volume (2.8 L) of refrigerant in preparation for the next charge cycle. A schematic of the EP2 generator reservoir delivery system has already been presented in figure 5.23.

Figure 5.34 shows a schematic layout of EP2, including the new reservoirs, passive vapour separation device and oil fed brazed plate heat exchanger. As isometric schematic is also provided in figure 5.35 which shows the three-dimensional layout of EP2. It is important to note the relative heights of the reservoirs in relation to both the condenser and the generator. In order for the new generator feed system to operate effectively, the jet-pump must feed into the condenser at the highest point in the system. The condensed refrigerant fluid then collects in the condenser reservoir, which in turn sits above the generator reservoir. The generator reservoir sits above the generator heat exchanger, but below the separator, providing basic generator liquid level management. EP2 allowed the system to run effectively for the first time, producing significant cooling at design point conditions. Some of the experimental data collected from EP2 is presented in chapter 7.

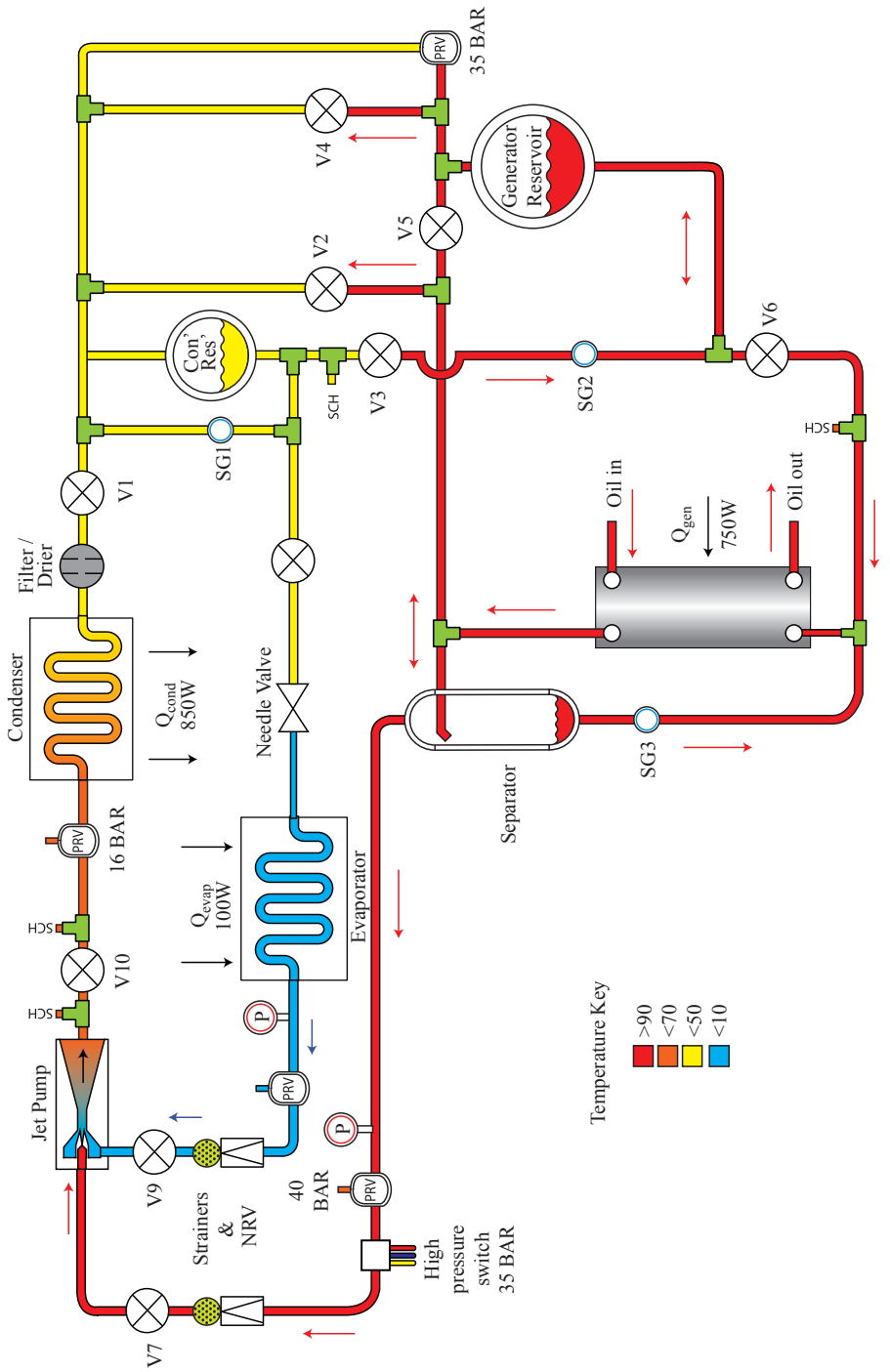

Figure 5.34: 2D Schematic of EP2

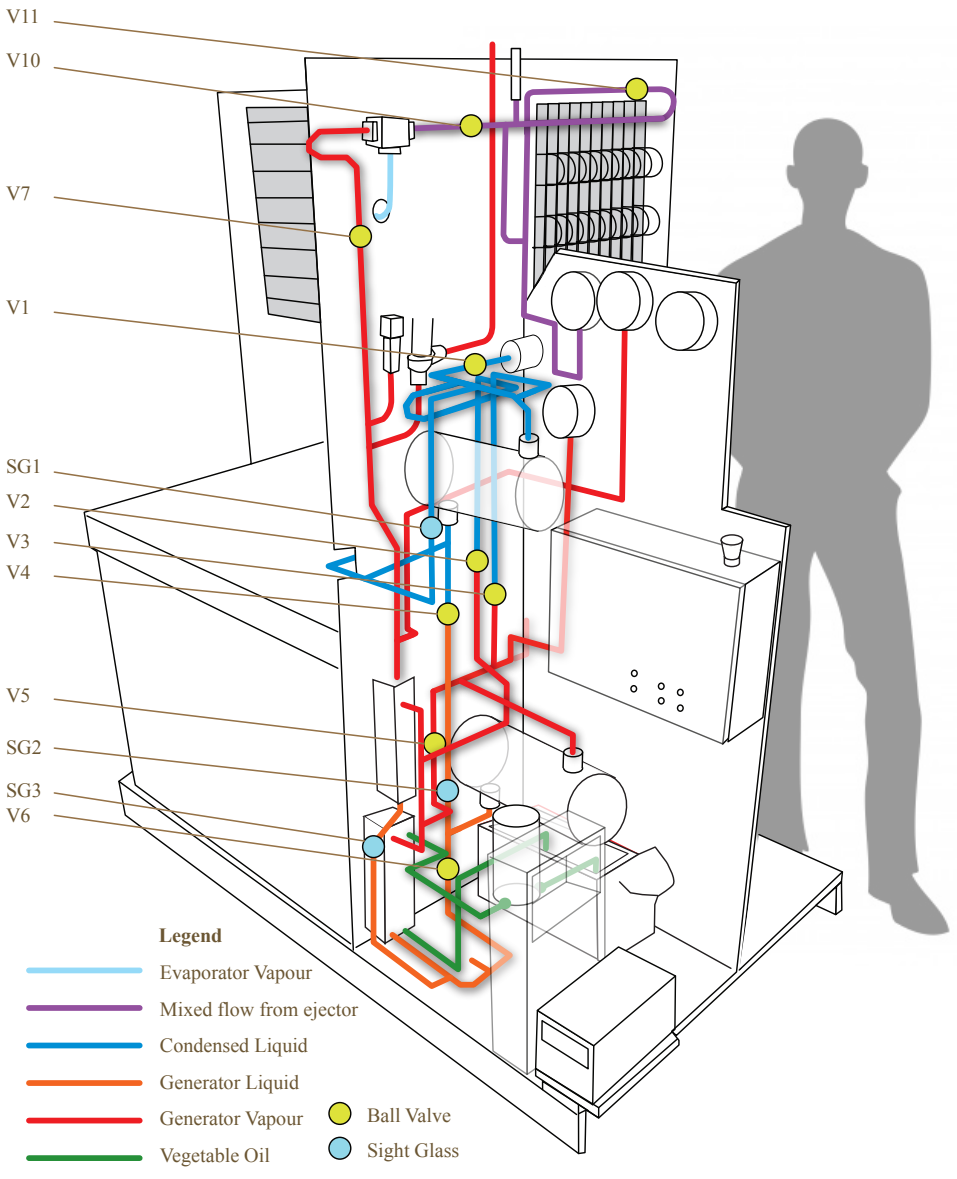

Figure 5.35: Isometric Schematic of EP2

EP2 Operating Procedure

The procedure begins from the point directly after the generator reservoir has been completely vented. (i.e. V7 open and $p_{gen} < 20$ bara) Referring to the system schematic in figure 5.34, the operating procedure is described in table 5.12.

Once sufficient pressure can no longer be provided from the generator, it is isolated from the generator reservoir. Before a transfer procedure begins, a fixed volume of refrigerant is delivered to the evaporator via a needle valve. It is important to note, that in this operation sequence, the condenser is not isolated from the condenser reservoir, which allows refrigerant vapour, during reservoir equalisation, to flow upstream, and into the condenser. After equalisation has finished (approximately 45 seconds) and the generator reservoir has received a fresh supply of refrigerant liquid, it is once again isolated from the condenser reservoir before being reintroduced to the generator circuit. The fill level of the generator is manually moderated, using sight glasses to determine when the generator heat exchanger is $\approx \frac{2}{3}$ full. Once the vapour line to the jet pump has been opened, the liquid level within the generator heat exchanger is monitored and the generator pressure controlled via the delivery of additional liquid from the reservoir. This continues, until the reservoir is empty and the cycle begins again. Due to the manually controlled nature of operation, the cycle durations are difficult to specify accurately however the ratio between charge and discharge is approximately 1:2

5.7.3 Integrated System Testing and Characterisation

This sub-section describes the experimental characterisation of both the condenser and generator. These results help to validate and define the optimum system operating

Step	Description	Action
1	Isolate HP Side from LP side	Close V7, Close V5, Close V6
2	Deliver transfer volume to evaporator	Close V8, Open NV,
3	Wait for volume to transfer (approx 10 seconds)	n/a
4	Fill Transfer Volume	Close NV, Open V8
5	Fill R_{gen}	Open V3, Open V4
6	Wait for R_{con} to equalise with R_{gen} and fluid to transfer (approx 45 secs)	n/a
7	Isolate HP reservoir	Close V3, Close V4
8	Initially fill heat exchanger	Open V5, Open V6
9	Moderate V6 and try to balance circuit so that HE is 2/3 full, close when generator pressure is 32 bara	n/a
10	Supply jet-pump	Open V7
11	Repeat fill heat exchanger	Open V6, Close V6
12	Maintain a generator pressure between 24-28 bara by opening and closing V6 as necessary	n/a
13	Cycle ends when reservoir has run dry and generator pressure drops below 20 bara	n/a

Table 5.12: EP2 Operating Procedure - Version 1

conditions. These tests were operated with the ejector nozzle in the optimum position (NXP = 1.6mm) and the secondary inlet to the jet-pump closed to remove any effect of evaporator load. It is important to note that the data to characterise both condenser and generator performance was collected simultaneously as maintaining a constant pressure on either sub-system proved impractical. This approach allowed twice the number of data-points to be plotted on each scatter diagram.

Condenser Performance Validation and Characterisation

With the ejector nozzle in the optimum position (NXP = 1.6 mm), the refrigeration cycle was operated 91 times with the evaporator closed and the suction pressures logged manually. The condenser pressure was also logged and results plotted in figure 5.36.

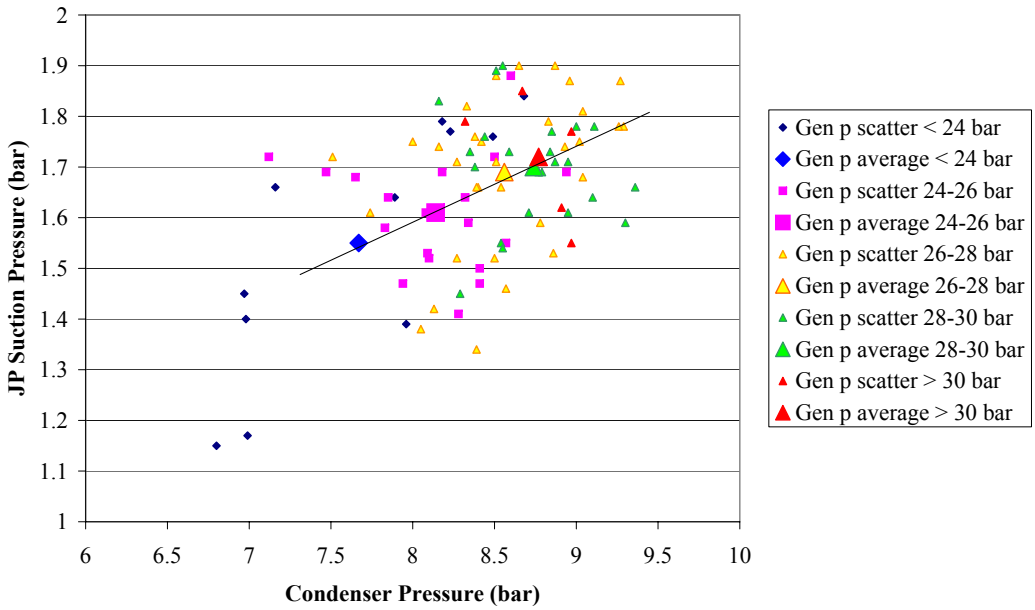

Figure 5.36: Graph showing jet pump suction pressure against condenser back pressure

The lowest suction pressures were achieved at condenser pressures around 6.8 bar

however effective entrainment was recorded up until 9.4 bar. After this point, the performance dropped off rapidly. This is below the predicted performance previously presented in section 4.9 which predicted a critical condenser pressure of 10.73 bar when operating at design point generator/evaporator pressures. Operating close to this critical condenser pressure helps to achieve maximum entrainment. The main reason for the large scatter in this plot, is because the system was operating at varying generator pressures during these tests (22-32 bar) What is apparent when reviewing the data is a general trend between lower condenser pressures and lower evaporator pressures. This effect has already been predicted by the theoretical performance discussed in chapters 2 and 4. The colour coded categorisation of generator pressures also illustrates the inter-relationship between the primary inlet and outlet pressures of the jet-pump. In order to achieve the lowest suction pressures (p_e), the condenser pressure should be as low as possible.

Later, in chapter 7, the results of operational tests are presented. A condenser pressure of 8-9 bar is maintained under normal operation in order to achieve lower evaporator pressures.

Generator Performance Validation and Characterisation

As mentioned in the introduction to this section, data on both the condenser and generator was collected simultaneously during these characterisation tests.

With the ejector nozzle in the optimised position, the cooling cycle was operated 91 times. With the evaporator closed, the suction pressure on the secondary inlet of the jet-pump was recorded manually. The maximum suction pressure and corresponding generator pressures are shown in a scatter plot - figure 5.37.

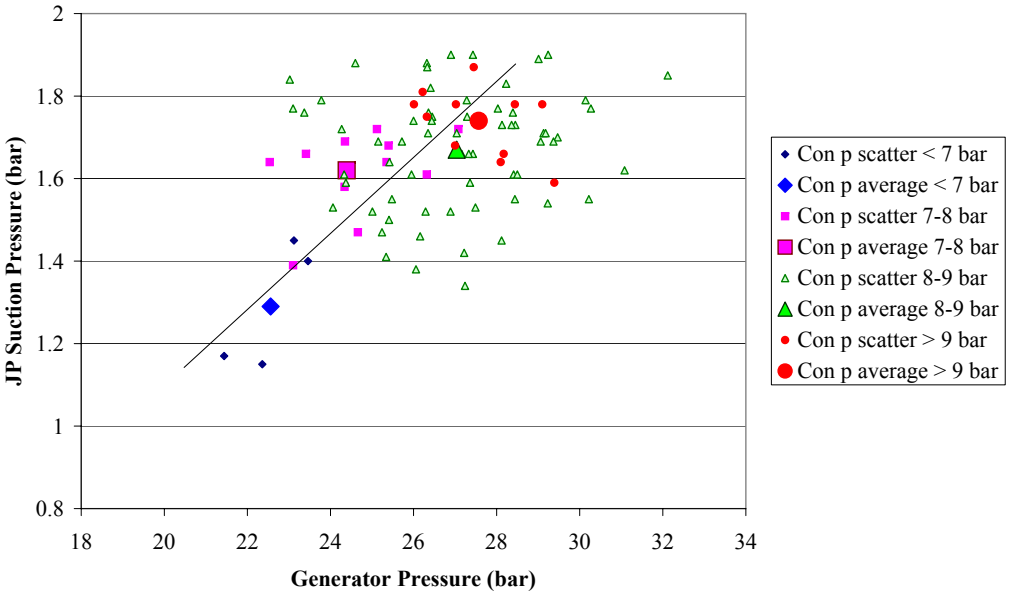

Figure 5.37: Graph showing jet pump suction pressure against generator pressure

Once again, the main reason for the size of the scatter range in figure 5.37 is that the condenser pressure is not constant throughout each of the tests. The data does show however that the lowest suction pressure was achieved at 22.5 bar. Although this is significantly lower than the 32.4 bar design point generator pressure predicted in section 4.9, the condenser pressure was also significantly lower during this particular test. At design point generator pressure, and condenser pressure of 8.7 bar, the suction pressure was 1.8 bar which is below the design point pressure of the evaporator (3.6 bar).

When reviewing the colour coded categorisation of associated condenser pressures, the inter-relationship between jet-pump primary inlet and outlet pressures is apparent. The scatter plot indicates that working at lower condenser pressures will deliver the lowest evaporator pressures/temperatures.

It is also important to note that there is no fixed optimum pressure for the generator as

this is dependant on the back-pressure from the condenser. Higher condenser pressures will require higher generator pressures to prevent the location of the shock wave within the diffuser from moving back into the jet-pump mixing chamber.

5.7.4 Commissioning the Prototypes

This sub-section describes the commissioning process for the prototype systems. The information contained here is relevant to all three prototype systems (EP1, EP2 and EP3).

Insulation and Loss Minimisation

Isotherm foam (Class 'O')lagging was applied to all pipes, reservoirs and components. In general $1\frac{1}{8}$" wall thickness lagging was used, however in tight access areas, this was sometimes reduced to $\frac{1}{2}$".

Leak Finding

Following completion of the construction, initial leak finding and repairs was conducted using a supply of compressed air at 5 bar. The larger leaks were relatively easy to find as the air escaping produced an audible jet of air. Smaller leaks were discovered using a soapy solution, applied with a paintbrush. This method also worked well for any brazed/flare joints. Following the eradication of all apparent leaks, a vacuum was drawn across the system before all the ball valves were closed. The system was sealed and allowed to stand overnight. Areas where the vacuum had decreased were re-tested using compressed air as described above to find any remaining leaks. When the entire system

could hold a vacuum overnight, the commissioning process could move on to high pressure tests.

Hydrostatic Pressure Tests

Following the period of leak finding and repairs, it was necessary to test the system at high pressures to ensure that the pipe-work was strong enough to cope with the normal operating pressures. The high-pressure generator side of the system is designed to work at a maximum of 32 bar. For safety reasons, it was necessary to ensure that the pipe-work could withstand pressures of up to 150% (safety factor 1.5) of the normal working pressure. The generator sub-system would therefore need to be tested at a pressure of 48 bar. Commercial refrigeration manufacturers use nitrogen to perform these tests, however the equipment required costs several hundred pounds and because nitrogen is compressible, a failure in the pipe-work could result in a dangerous explosion. Water is an incompressible fluid and is therefore safer for high pressure testing. A high-pressure car washer was used to provide the necessary pressure (capable of delivering up to 120 bar). An illustration of the pressure test rig is shown in figure 5.38.

Care was taken when initially filling the system with water to ensure that no pockets of air were left remaining in the system. As air is a compressible gas, this scenario could result in a small explosion. Initially, both taps were left open whilst the system filled water. Once this was complete tap 1 was closed, and then tap 2 was gradually closed. As the flow from exhaust 2 was restricted, a rise in pressure could be observed on the pressure gauge and this represents the pressure exerted on the test line. The high pressure test was left running for 2 hours at 50 bar, to allow time for any small cracks to leak an observable amount of water.

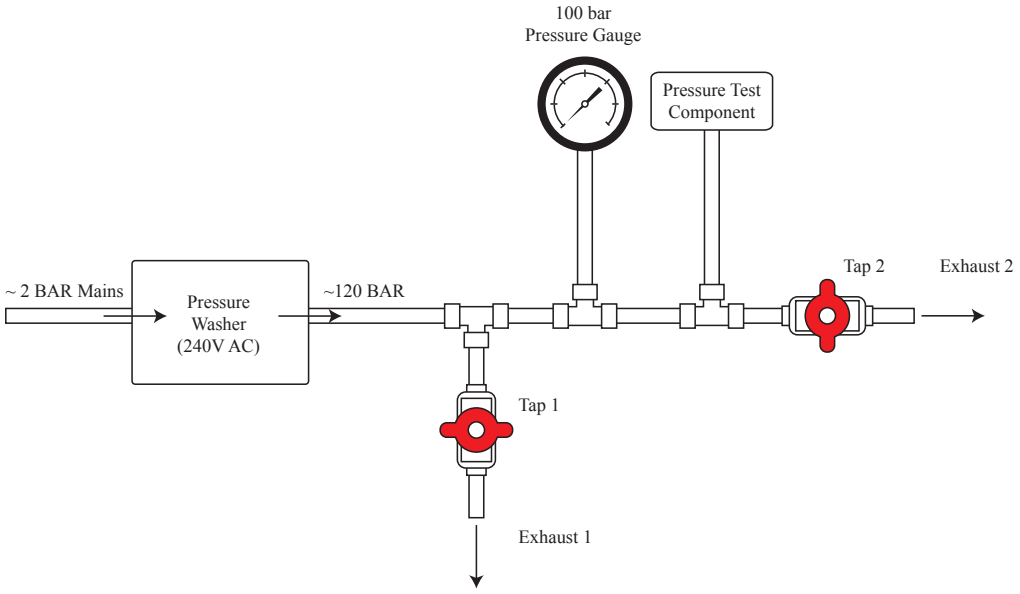

Figure 5.38: Illustration of hydrostatic pressure test rig

Following the testing of the high-pressure circuit, the entire system was tested to 150% of the condenser working pressure (12 bar MWP, hence 18 bar test pressure). Again the test was left to run for 2 hours.

Once the hydrostatic pressure tests had successfully been completed, the system had to be completely drained of water. Compressed air was used to push out the bulk of the water however small puddles remained in certain low points of the system. A vacuum was pulled on the system, and low-points heated using a hot-air gun to vaporise the remaining water and dry out the system. This was time consuming exercise during which the filter-drier had to be replaced several times following saturation. During the draining process it was noted that some of steel pipe-work had began to corrode and small amounts of rust debris could be found in the fluid. Strainers are installed at key locations to prevent these particulates from blocking any of the system seals.

5.8 Chapter Discussion

This chapter has described the experimental method and equipment used during this development study. The prototype construction methods have been presented in detail and the the theoretical performance has been compared to the experimental performance for both the condenser and evaporator sub-systems.

The development work on the first two prototype systems (EP1 and EP2) showed that the jet-pump could operate at the design point conditions set out in chapter 4. The initial prototype system (EP1) provided a test vehicle for each of the individual sub-systems and proved that jet-pump was functional however the lack of an effective generator feed system (delivering refrigerant from the condenser to the generator) made overall system analysis difficult.

EP2 employed a novel, dual reservoir feed system that allowed design point generator operating pressures to be achieved. This allowed for the system to operate effectively for periods of up to 500 seconds and the overall system to be evaluated. This also allowed for the position of the jet-pump nozzle (within the diffuser) to be experimentally optimised. With the nozzle position confirmed, a series of characterisation tests were conducted to validate the theoretical design point operating pressure of both the condenser and the generator.

Despite successful achievement of design point cooling, the performance of EP2 was erratic for several reasons. EP2 is a manually controlled system. This leads to a lack of repeatability in cooling performance. In addition, the charge/discharge ratio of the EP2 operating procedure (1:2) proved to be a limiting factor. Each time the jet-pump primary flow is recommenced, a period of fluctuating performance can be observed. The

effect is audible, and it is thought this poor start up performance is caused by tiny condensate droplets interrupting the entrainment flow.

Given the fact that EP2 was capable of producing design point cooling, if only over short periods, the chosen development focus for EP3 was targeted on achieving continuous jet-pump operation using an enhanced version of the reservoir transfer system already proven on EP2. In addition, the ability to automate control of the system, would allow for test data to be collected over longer test periods and with more accurately controlled test conditions. The next chapter of the thesis , Chapter 6, uses EP2 as a simulation tool, to develop an enhanced reservoir transfer system that is fully automated.

Chapter 6

Automated Experimental Prototype (EP3)

6.1 Introduction

This chapter builds on the prototype development work described in chapter 5. A final version (EP3) of the prototype system is presented and discussed.

The chapter begins with a section that describes the evaluation of various EP3 generator reservoir transfer concepts using simulation data collected from EP2. The final EP3 prototype schematic is then presented following details of the enhancements made to the various sub-systems. Details of the automated control system are then described beginning with a hardware specification. The control logic and implementation is then discussed.

The chapter concludes with an overview evaluation of the system improvements however

the data from experimental testing is presented later, in chapter 7.

6.2 Generator Development Studies (EP2)

One of the key reasons identified for the lack of system stability on EP2 was the intermittent operation of the jet-pump. The EP2 generator sub-system, shown schematically in figure 6.1 for reference, was operated manually during experimental tests. The vapour generator pressure (p_{gen}) was maintained at ∽28 bar by adding more refrigerant liquid, as required, from the generator reservoir via BV6. This pressure (equivalent to $T_g = 85°C$) was selected to maximise the entrainment ratio at average ambient conditions. When the fluid levels in the generator reservoir were exhausted, a refrigerant charge cycle was manually sequenced. During this charge sequence, the generator could not provide high-pressure vapour to the jet-pump.

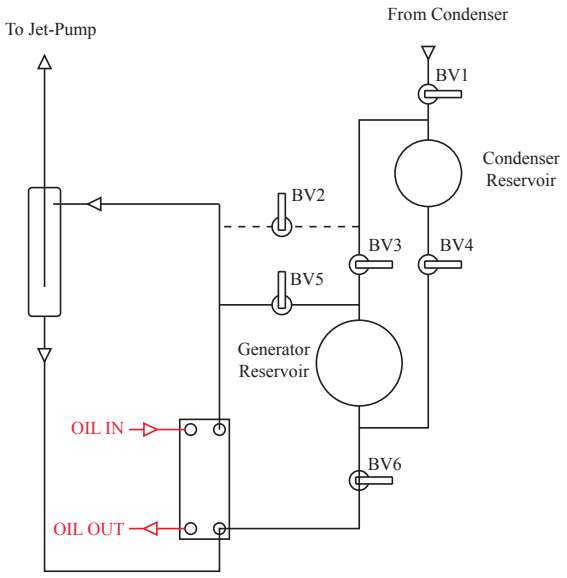

Figure 6.1: Schematic of generator sub-system (EP2)

When the charge cycle was complete and sufficient generator vapour pressure had been achieved, the primary flow inlet to the jet-pump was reopened. The initial performance of the jet-pump was repeatedly observed to exhibit a period of fluctuating performance whilst the flow stabilises. Devising a system that would maximise the the generator discharge duration with respect to refrigerant charge cycle duration, would minimise the disruptive effects observed and allow more consistent suction on the evaporator to be maintained. In an ideal scenario, the generator would be able produce a continuous supply of high pressure vapour to the jet-pump and avoid these issues altogether however the required energy demands of such a system should not be overlooked.

Utilising gravity as a fluid delivery mechanism, was an attractive option as the jet-pump is located at the top of the system, allowing the condenser to feed the generator from above. Gravity feed systems do incur thermal losses (10-20% [39][40]), however in order to evaluate the system as an autonomous thermally-powered unit, sacrificing thermal efficiency to minimise the electromechanical requirement was considered appropriate.

Simulation tests were carried out on EP2 to determine the operating characteristics of the system under various flow scenarios. A series of concepts, that employed combinations of multiple reservoirs, were then devised to decrease the charge / discharge cycle ratio. The data collected from the experimental simulations on EP2 was used to estimate the durations for pressure equalisation and cycle frequency for each concept. These estimates, along with cost information and associated electrical demand, were used to define a final solution for the reservoir fluid transfer system employed in EP3. The final solution, which incorporates 2 primary reservoirs, and 2 secondary reservoirs is presented later in section 6.3

6.2.1 Simulation Tests

Simulations tests were carried out on EP2 to determine the operating characteristics of the system under various conditions. These results could later be used to evaluate the relative merits of the concept generator fluid delivery systems for EP3. For reference, the condenser reservoir on EP2 is sized at 2.8 L and the generator reservoir is sized at 4.6 L

The valving configuration for each of the simulation experiments is described with reference to figure 6.2, by defining which valves are opened. It is therefore implied that all other valves are closed. Unless otherwise stated, the initial pressures should be assumed equal to the design point pressures listed previously in table 4.2.

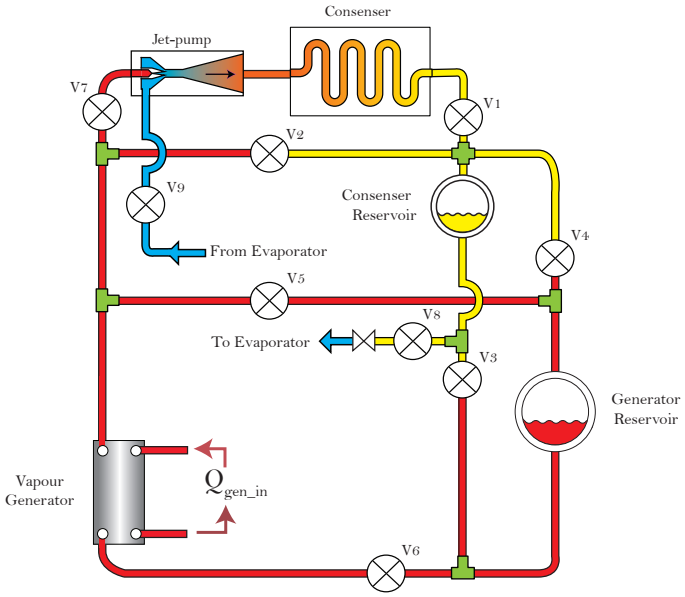

Figure 6.2: Simplified schematic to illustrate simulation valving

Simulation 1 : V3 and V4 open (see figure 6.2)

Simulation experiment was carried out to determine the time taken for a condenser reservoir to exchange all of its fluid with an vapour filled generator reservoir using gravity

This test was carried out under several different pressure scenarios. The first, which is representative of the normal operating procedure, required the generator reservoir to contain R134a vapour at 28 bar and the condenser reservoir to contain R134a fluid at 9 bar. The time to transfer all of the fluid was 101 seconds, with a corresponding equilibrium pressure of 13.5 bar. The test was repeated at a number of different generator pressures pressures, resulting in different equilibrium pressures, however the transfer time remained similar, ranging from 97-105 seconds.

Simulation 2 : V2 and V3 open (see figure 6.2)

Simulation experiment was carried out to determine the time taken for a condenser reservoir to exchange all of its fluid with an vapour filled generator reservoir when assisted with high-pressure vapour, supplied above the liquid head, from the generator.

The generator supplied the vapour at 28 bar, which was piped to the top of the condenser reservoir, pushing the liquid down into the generator reservoir. These tests provided less predictable transfer times ranging from 25-49 seconds for full fluid transfer. The reason for this variation is thought to be linked to the turbulent flow, caused by the rapid equalisation. The equilibrium pressure was slightly higher ($\approx$ 14 bar). Although the transfer time is decreased using this method, the thermal energy losses are increased and an additional load is applied to the condenser once the transfer is complete.

Simulation 3 : V1 and V7 open (see figure 6.2)

Simulation experiment was carried out to determine the rate at which the liquid level, and vapour pressure of an isolated generator will fall.

The generator was brought up to 28bar with a heat exchanger liquid level of approximately 0.3 L (2/3 full) and then isolated from the reservoir. The pump was run at full speed and the both the time and generator pressure were recorded.

The time taken for the pressure to drop from 28 to 20 bar ranged from 30 to 40 seconds. This result showed that the heat-exchanger alone did not have the capacity to supply the jet-pump whilst the reservoirs exchanged fluid.

Simulation 4 : V5,V6 and V7 open (see figure 6.2)

Simulation experiment was carried out to determine the rate at which the condenser pressure rose when the jet-pump was operational and the condenser was isolated from the condenser reservoir.

With the condenser stable at 7 bar, the condenser reservoir was closed off and the time taken for the condenser pressure to rise to 10 bar was measured. The duration for the pressure rise was similar for all the test conducted, ranging from 71-79 seconds. Although this came close to the 110 second target time, this method did not allow the condenser pressure to drop and so subsequent cycles increased the final pressure cumulatively.

Simulation 5 : Isolated condenser reservoir (see figure 6.2)

Simulation experiment was carried out to determine the rate at which the pressure in an isolated condenser reservoir would fall

A static temperature decay experiment confirmed that, in ambient conditions of 22 °C, naturally convective heat loss would decrease the pressure of a condenser reservoir, full of liquid, from 21 bar (70°C) to 9 bar (35°C) in approximately 1800 seconds (30 minutes)

6.2.2 Reservoir Transfer Concepts

Five reservoir transfer concept (RTC) systems were devised that could potentially deliver a continuous supply of high temperature, high-pressure vapour to the primary inlet of the jet-pump.

The flow patterns and valve operations of the various concepts were animated using MS PowerPoint to help in the analysis process. Each concept was evaluated with consideration given to estimated complexity, capital cost, physical volume and electrical power requirements, however the principal evaluation metric used was the estimated refrigerant charge/discharge (CD) ratio. A comparative summary of all five concept systems is presented later in table 6.1

RTC1 : 1 condenser reservoir and 2 generator reservoirs (in parallel)

This concept, shown in figure 6.3 is designed to ensure that a generator reservoir is always connected to the generator. This system is similar to that originally proposed by Huang et al [40] and subsequently Wang et al in 2009 [41].

Strengths: Relatively simple to implement and has the potential to provide favourable charge / discharge ratios as the generator reservoir is never off-line.

Weaknesses: Increased demand on the condenser due to regular discharge of high pressure vapour from two generator reservoirs which increases losses and adds cost to the condenser. The overall size and fluid capacity of the system is also larger.

Estimated charge / discharge ratio: 1:6

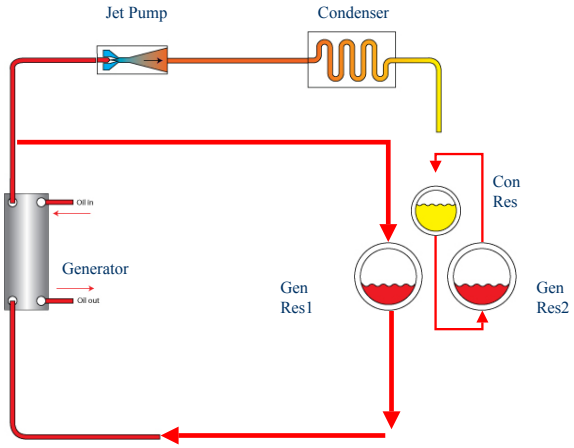

Figure 6.3: Reservoir Transfer Concept 1

RTC2 : 1 condenser reservoir and 2 generator reservoirs (in parallel) with vapour bleed

This concept, shown in figure 6.4, is an enhanced version of RTS1, providing an additional vapour bleed to speed up fluid transfers.

Strengths: Has the potential to allow the speed of fluid transfer from the condenser reservoir to the generator reservoir to be increased. This would then allow (with valving not shown in the schematic) the condenser reservoir to be isolated from the generator reservoir during the remainder of the discharge cycle, thereby reducing the additional load placed on the condenser.

Weaknesses: Significant increase in complexity (and cost) of the system when compared against RTC1 with potentially limited benefit. The additional load placed on the condenser should not be overlooked.

Estimated charge / discharge ratio: 1:8

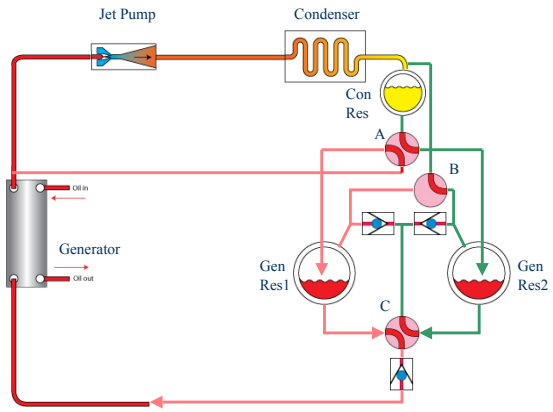

Figure 6.4: Reservoir Transfer Concept 2

RTC3 : 2 condenser reservoirs (in series) and one generator reservoir

This concept, shown in figure 6.5 shows a second condenser reservoir, connected in series. This allows for the primary condenser reservoir (top) and generator reservoir (bottom) to be isolated during charge / discharge cycles.

Strengths: By sizing the reservoirs appropriately, this solution allows the thermal losses, caused by high pressure vapour moving backwards to the condenser, to be minimised. This system also ensures that both the generator and condenser always have at least one reservoir connected at any given time. The system is relatively simple to implement (lower cost).

Weaknesses: As the three reservoirs must be arranged vertically, the height of the system is increased.

Estimated charge / discharge ratio: 1:8

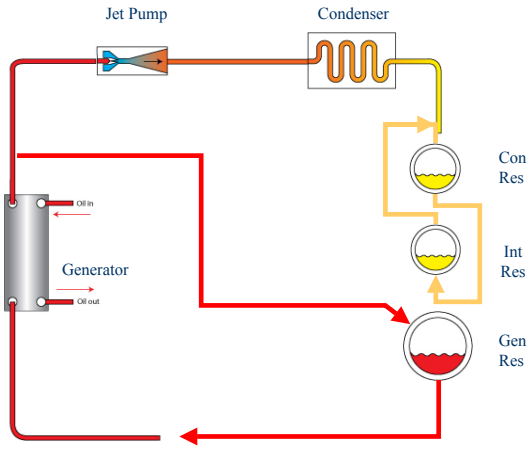

Figure 6.5: Reservoir Transfer Concept 3

RTC4 : 2 condenser reservoirs (in parallel) and one generator reservoir

This concept, shown in figure 6.6, shows the pipe routing for a system that incorporates two condenser reservoirs connected in parallel.

Strengths: As with RTC3, RTC4 minimises the additional load placed on the condenser following charge cycling. The condenser has one of the reservoirs connected at all times.

Weaknesses: The generator reservoir is isolated from the generator during charge cycling. This will limit the effective operation of the jet-pump and reduce the charge/discharge ratio.

Estimated charge / discharge ratio: 1:5

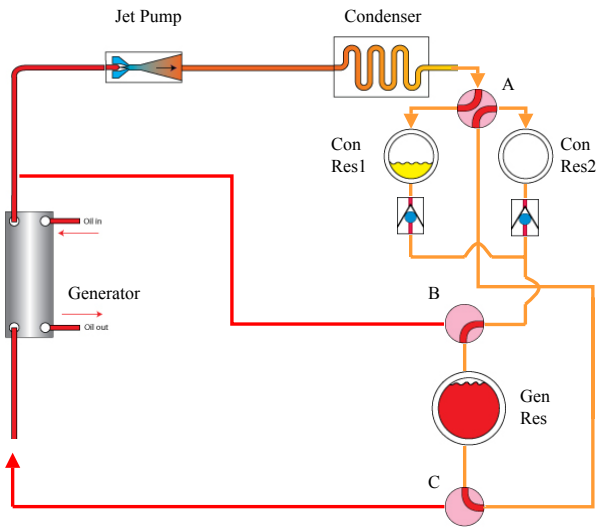

Figure 6.6: Reservoir Transfer Concept 4

RTC5 : 2 condenser reservoirs and 2 generator reservoirs

This concept, shown in figure 6.7, is essentially a twin configuration of the generator sub-system employed on EP2.

Strengths: By *"doubling-up"* on the number of reservoirs, achieving higher charge/discharge ratios would be possible. The additional load, placed on the condenser following a refrigerant charge operation, would also be less as the vapour filled condenser reservoir would have additional time to dissipate heat.

Weaknesses: This concept has more components than any of the other concepts, including 4 fluid reservoirs, 4 check valves and 4 actuated combination valves. The complexity of this system, and associated cost, was considered a significant drawback given the proposed application (low-cost vaccine storage).

Estimated charge / discharge ratio: 1:10

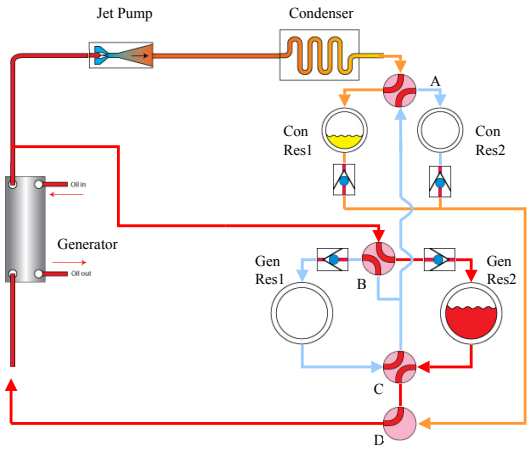

Figure 6.7: Reservoir Transfer Concept 5

6.2.3 Selection and Validation of Concept

The estimated charge/discharge (CD) ratios for each of the reservoir transfer concepts is presented in table 6.1.

Ref	Condenser Reservoirs	Generator Reservoirs	Estimated CD ratio
RTC1	1	2 in parallel	1:6
RTC2	1 with vapour bleed	2 in parallel	1:8
RTC3	2 in series	1	1:8
RTC4	2 in parallel	1	1:5
RTC5	2 in parallel	2 in parallel	1:10

Table 6.1: Summary of reservoir transfer concept details

Although RTC5 (2 condenser reservoirs and 2 generator reservoirs, both operating in parallel) offered the best CD ratio (1:10) the initial capital cost of such a system was estimated to be up to 75% higher than other concepts. When also considering the number of check valves required, it was decided that the vertical arrangement of two condenser reservoirs in series (RTC3) provided the most robust concept solution for further investigation.

Although a secondary condenser reservoir, was not available on EP2, the cycle sequencing could still be implemented and experimentally evaluated. The revised operating procedure for EP2 (Version 2), used to validate the selection of RTC3 is presented in table 6.2.

Simulation 2 had shown that is was possible to transfer all of the charge fluid in under 60 seconds, and simulation 4 had shown that, without the additional capacity of a condenser reservoir, the condenser pressure took up to 80 seconds to increase from 7 bar to 10 bar. These results suggested that it may be possible, with a modified operation sequence to run the jet-pump of EP2 continuously, however as demonstrated later, in Chapter 7, this estimation does not take account of the additional cyclic loading of the condenser.

The new operating procedure (see table 6.2 did provide a significantly improved charge/discharge ratio for the system (approximately 1:6), however the additional load on the condenser affected the system performance after several charge cycles. The experimental results from these tests are illustrated fully in Chapter 7.

Using high pressure vapour from the generator to increase the speed of fluid transfer was explored however this added further to the already increased load on the condenser

6.2.4 Discussion of Generator Development Studies

The experimental characterisation of the system during simulation tests provided a useful evaluation metric for the five reservoir transfer concepts proposed. After selecting RTC3 for further investigation, a new sequence of operation (see table 6.2 was trialled on EP2 and a significantly improved CD ratio was achieved (1:6 versus 1:2 previously)

It was also apparent from evaluation of the reservoir transfer concepts that the physical size of the reservoirs would be the limiting factor in achieving improved CD ratios. In order to achieve continuous jet-pump operation, it would be necessary to provide sufficient reservoir capacity for the system to run uninterrupted whilst the refrigerant fluid charge procedure took place. The estimated volume flow rate of the condenser is

Step	Description	Action	Approximate Time
1	Isolate Generator Reservoir	Close V5 and V6	2
2	Isolate Condenser Reservoir and Evaporator	Close V1 and V8	2
3	Initiate Transfer	Open V3 and V4	$\backsim$ 67
4	Terminate primary flow when P_c >9 bar	Close V7	10-20
5	Terminate Transfer	Close V3 and V4	2
6	Reintroduce condenser reservoir	Open V1 and V8	$\backsim$ 12
7	Reintroduce generator reservoir	Open V5 and V6	2
8	Initiate primary flow when P_g >26 bar	Open V7	$\backsim$ 23
9	Run system until generator reservoir is empty	n/a	$\backsim$ 700

Table 6.2: EP2 Operating Procedure - Version 2
With reference to figure 6.2

approximately 4 ml/s based on a fluid density 1,140 kg/m3 for R134a at 42°C. From simulation 2, we know that the time necessary to transfer fluid between the two reservoirs on EP2 is approximately 100 seconds and therefore the condenser would require an additional capacity of 400 ml to operate normally whilst isolated from the reservoirs.

Similarly, the generator has a design mass flow of 3.76 g/s, or 4.5 ml/s (based on R134a liquid density of 837 kg/m^3 at 90°C) and would therefore require an additional capacity of 450 ml to operate normally whilst isolated from the reservoirs.

6.3 Generator Sub-system EP3

The final solution for the reservoir liquid transfer sub-system, designed to deliver refrigerant fluid from the condenser to the generator, is presented in this section. Based on the concept of using reservoirs connected in series (RTC3) the new system aims to provide continuous operation (or improved CD ratio) and lower thermal losses. This was achieved by the addition of two secondary reservoirs with sufficient capacity to maintain normal operation whilst the majority of the refrigerant liquid was transferred between the two primary reservoirs. Although the additional cost of a fourth reservoir should not be overlooked, the number of required control valves can be limited to five. It is also important to note that the EP3 reservoir transfer system does not make use of any one-way check valves for flow control.

This approach is different in concept to the previous work of others [39][40][41], who proposed systems that would provide continuous operation via two liquid transfer volumes, connected in parallel and operated in alternating sequence. The EP3 reservoir transfer system operates via three sets of liquid transfer volumes reservoirs, connected in

series and operated in series. By maximising the CD ratio, it is hoped that the need for a second transfer system, connected in parallel can be avoided. As discussed in more detail later in this chapter, the EP3 transfer system also makes use of vapour path piping to minimise liquid transfer times and reduce the performance impact of cyclic condenser loading.

As previously discussed in section 5.5.5 the generator reservoirs was sized to provide a 1.2 factor of safety in addition to the required volume allowed for R134a liquid expansion (T_c to T_g). As discussed in section 6.2.4 the secondary reservoirs were sized to provide capacity for the system to run uninterrupted whilst the primary reservoir exchange fluid. A summary of the volumetric sizes of all four reservoirs is provided in table 6.3.

Reservoir Number	Function	Volume (L)
1	Secondary Condenser Reservoir	1.3
2	Primary Condenser Reservoir	2.8
3	Primary Generator Reservoir	4.6
4	Secondary Generator Reservoir	1.3

Table 6.3: EP3 Generator Reservoir Transfer System Specification

The section begins with a presentation of the final solution and fluid transfer procedure. Subsequent sub-sections go on to specify details of the final heat exchanger and phase separation method employed in EP3.

The collector circuit, or oil circuit, was upgraded for the final prototype and details of the new heat transfer fluid and oil pump are presented, followed by a description of the

calibration process. The section concludes with a details of improvements made to the generator outlet pipework to minimise dynamic head losses.

6.3.1 Generator Feed System

After evaluation of the experimental simulation data and with reference to the estimated benefits (i.e. charge/discharge ratio, complexity, cost) of each concept, a decision was reached to use two additional secondary reservoirs; one on the high-pressure generator circuit, and one on condenser side. Based on generator and condenser approximate volumetric flow rates of 4.5 ml/s and 4 ml/s respectively, the secondary reservoirs were sized at 1.3 L to allow the two primary reservoirs to be isolated for periods of up to 290 seconds. Assuming that a fluid charge operation could be completed in less than 290 seconds, these secondary reservoirs would therefore provide the necessary capacity to allow the jet-pump to operate continuously.

A schematic for the EP3 generator sub-system is shown in figure 6.8 The design intent behind the new system is to keep the primary heat exchanger (bottom) flooded at all times, controlling the generator pressure by moderating the speed of the oil pump.

As the cycloidal phase separator installed in EP2 performed poorly under flooded generator conditions, this was replaced with a secondary heat exchanger to remove any liquid from the supply and super-heat the vapour. This modification is described in more detail in section 6.3.2, By ensuring that the primary heat exchanger remains flooded (i.e. full of refrigerant fluid) at all times a continuous vapour supply to the jet pump could theoretically be maintained.

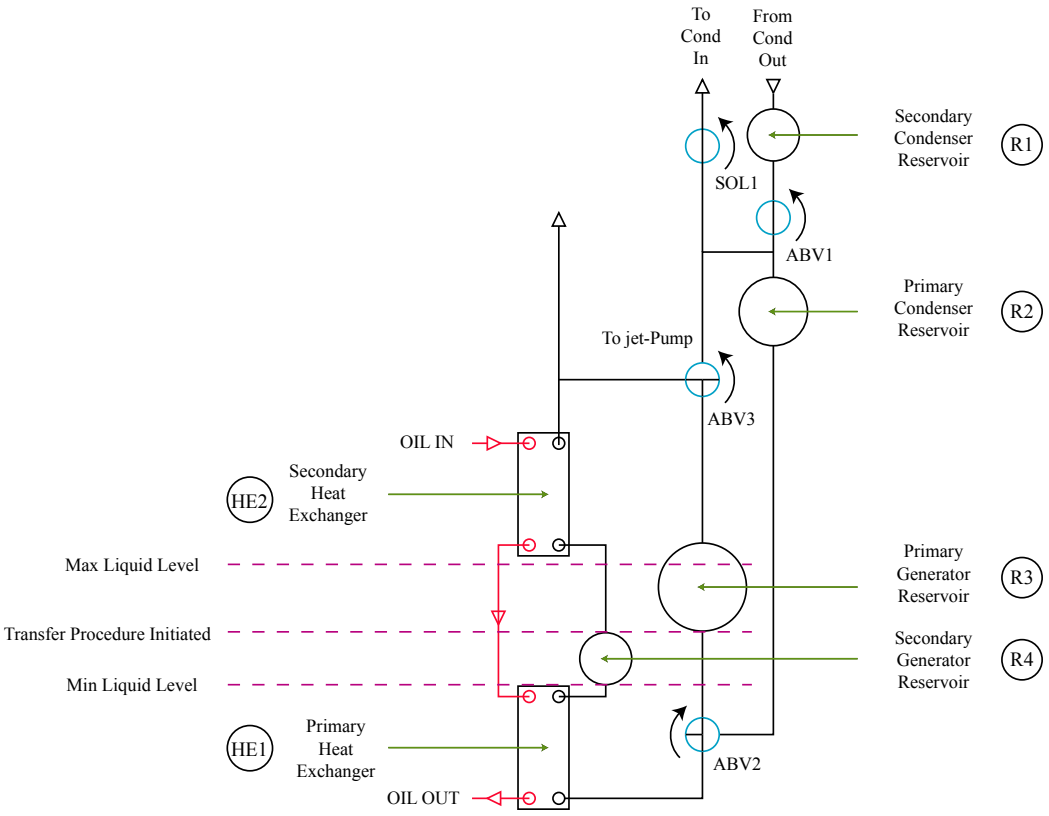

Figure 6.8: Schematic diagram of generator fluid delivery system (EP3)

EP3 Fluid Transfer Procedure

Referring to figure 6.8, the fluid transfer procedure for EP3 can be described. The primary generator reservoir (R3) provides refrigerant fluid to the primary generator heat (HE1). R3 is located below the secondary generator heat exchanger (HE2) and above the secondary secondary generator reservoir (R4) This vertical arrangement helps to maintain a liquid level that ensures the HE1 remains flooded at all times.

When R3 runs dry, it is isolated from the generator circuit by the rotation of two 3-way valves (ABV2 & ABV3). Similarly the primary condenser reservoir (R2), which is now full of recently condensed refrigerant, is isolated from the condenser and secondary condenser reservoir (R1). The two primary reservoirs are now connected in parallel and the condensed liquid refrigerant is transferred from R2 to R3. Meanwhile the two smaller secondary reservoirs (R1 and R4) provide the necessary capacity for the jet-pump to continue to run without the condenser becoming overloaded.

The two, "T" configuration, 3-way valves simplify the system allowing flow paths to be diverted using only one valve. A 2-way valve, (ABV1) is positioned between the two condenser reservoirs to protect the condenser during the fluid transfer procedure.

An electronic liquid level switch has been installed on the bottom of the primary generator reservoir (R3). This opto-electronic device will provide an electrical signal to initiate the fluid transfer procedure. The operation of this sensor is discussed later in section 6.7.

This fluid transfer method forms the basis of the new system, which is illustrated in the full schematic of EP3 in figure 6.18. The sensing and control of the fluid transfer procedure is also descibed in more detail in sub-section 6.8.3

6.3.2 Generator Heat Exchanger and Phase Separator

The cycloidal vapour separator employed in EP1 and EP2 performed poorly under flooded generator conditions and was therefore replaced by a secondary heat exchanger, which superheats the refrigerant ensuring a supply of dry vapour at the jet-pump primary inlet. The refrigerant is delivered to the bottom of the primary heat exchanger and is then vaporized, travelling upwards.

The generator section of EP3 includes two heat exchangers. The primary heat exchanger, the bottom of the pair, is constantly flooded with refrigerant liquid. This liquid is normally supplied by the primary generator reservoir, but an auxiliary volume is also stored in the secondary generator reservoir for supply during the fluid transfer procedure.

The two heat exchangers specified are both brazed plate heat exchangers from SWEP and the OEM part numbers and capacities are listed in table 6.4

Item	OEM Part number	Oil volume	R134a Volume
Primary heat exchanger (HE1)	SWEP 10009-020	0.42 L	0.34 L
Secondary heat exchanger (HE2)	SWEP 10009-016	0.38 L	0.29 L

Table 6.4: EP3 Heat Exchanger Specification

6.3.3 Collector Circuit

Collector Circuit Heat Transfer Fluid

This version of the rig will use a heat transfer (HT) fluid that has been specifically selected for the normal operating temperature of the generator. The fluid is *NoTox HT fluid 32* from Globaltherm. The fluid contains a paraffinic base oil, which helps to provide good thermal stability. It also has excellent thermal conductivity (0.141 W/m·K at 130°C) which helps to provide efficient heat transfer making the oil particularly well suited for use with solar thermal panels. Figure 6.9 shows the specific heat capacity of the oil at various temperatures. At the normal operating temperature for the oil (120°C) the HT fluid has a specific heat capacity of 2.2 kJ/kg·K which is considerably higher than the 1.8 kJ/kg·K heat capacity that was estimated for the vegetable oil used in EP2. Of particular significance to this study is the low viscosity at generator working temperatures, which helps to reduce the electrical power requirement of the oil pump.The kinematic viscosity of *NoTox HT fluid 32* is 5.95 mm^2/s at 100 °C (only 17% of the viscosity of the same fluid at 40°C).

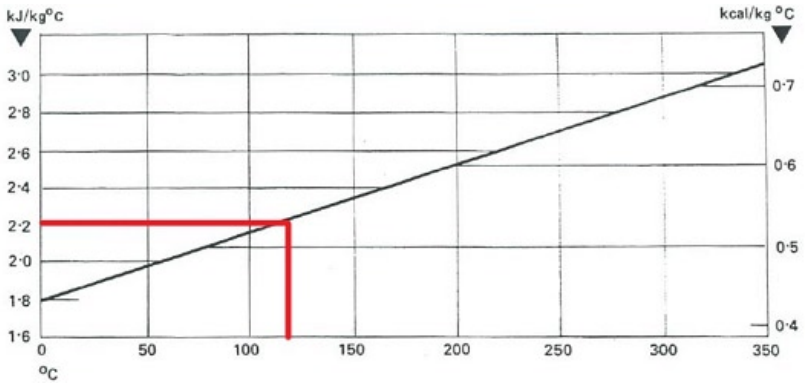

Figure 6.9: Specific heat capacity against temperature for NoTox HT Fluid 32

Collector Circuit Pump

The Mocal oil pump on EP2 had sustained damage following prolonged use at high-temperature. A new, magnetic drive gear pump (Micropump GJ-N27) was specified to allow higher continuous operating temperatures. The Micropump GJ-N27 was also considerably more efficient. The manufacturers pump curves, based on water at 1 Pa·S dynamic viscosity, provide flow rates of 3.95 l/min at 3450 RPM however this assumed a differential pressure of 5.5 bar. In reality, the low differential pressure (0.5-1 bar) required less motor torque and flow rates of over 5 l/min at $T_{g\_oil} = 120$ °C were experimentally achieved. The electrical power consumption of the pump at this speed was 20.4W.

Assuming an 800 W thermal input requirement and an oil ΔT of 5°C, the required volumetric flow rate is 5.46 L/min

Collector Circuit Calibration

Following installation, a series of calibration experiments were conducted to find the oil flow rate at different temperatures. Using the integrated pump tachometer, this would then allow instantaneous heat input to the generator to be calculated through measurement of the temperature difference across the oil inlet/outlet. This heat input was controlled and measured electronically on the EP3 system. The results of these calibration experiments are shown in figure 6.10

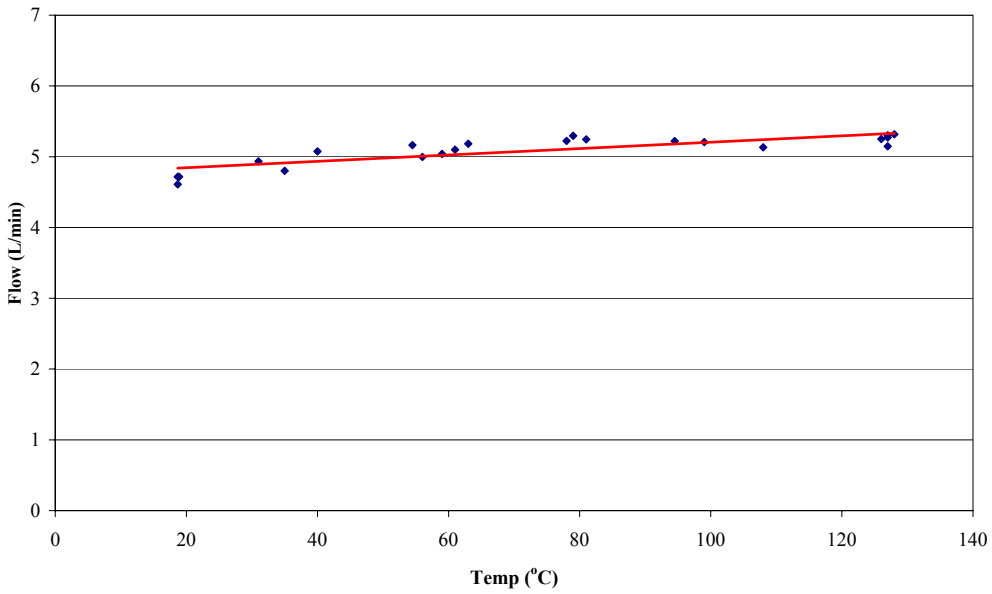

Figure 6.10: Graph showing Micropump (GJ-N27) flow calibration at 3450 RPM

6.3.4 Other Generator Enhancements

Generator Outlet

The NRV installed prior to the jet-pump was removed and replaced with an actuated ball valve. During normal operation, the jet-pump operates continuously and therefore the NRV was no longer required. If the generator pressure falls below the design pressure, the actuated ball valve is closed by the automated control system. The removal of the NRV also meant that the integral strainer was removed and so a 40 mesh bespoke strainer was installed to prevent any debris from clogging the jet-pump nozzle. The design point mass flow, although larger than the evaporator (3.76 g/s) is still relatively small and so turbulence caused by the strainer mesh should not cause a significant pressure drop. The design and specification of this strainer is presented in more detail in

section 6.5.2

Generator Vapour Path

Maintaining the liquid level in the vapour generator heat exchanger of EP2 had proven difficult. One of the identified causes of this issue was the convoluted route and inner diameter of the pipe-work that connected the heat exchanger to the generator reservoir.

The pressure loss (minor loss) caused by bends, junctions and valves can be calculated as shown in equation 6.1. The generator vapour pipe routing of EP2 was sized at 6.35 mm internal diameter and contained seven right angle bends. Assuming a minor loss coefficient (ξ) for each 90°pipe bends of 1.0, equation 6.1 can be used to estimate a dynamic pressure loss of 238.8 Pa

$$\begin{aligned}
\rho_{v_R134A}\ (at\ 32bar) &= 216.45\ kg/m^3 \\
\dot{m} &= 3.76\ g/s \\
\dot{V} &= \frac{\dot{m}}{\rho} \\
&= 17395\ mm^3/s \\
A_{pipe} &= 31.66\ mm^2 \\
v &= \frac{\dot{V}}{A} \\
&= 0.5496\ m/s \\
Dynamic\ pressure\ loss &= \xi \cdot \frac{1}{2} \cdot \rho \cdot v^2 \\
&= 228.8\ Pa
\end{aligned} \tag{6.1}$$

In order to reduce the dynamic head losses on EP3, the pipe diameter was doubled (to 12.7 mm) and the number of right angle bends was reduced to 3. Inspection of equation 6.1 reveals that doubling the pipe diameter increases the cross-sectional area by 400%, which in turn reduces the dynamic pressure loss for a each bend to $1/16^{th}$ that of the previous arrangement

In addition to increasing the pipe diameter, the minor losses were also decreased by reducing the number of right angle bends from seven to three. The EP3 generator vapour path dynamic pressure loss was therefore reduced to 6.13 Pa.

With the respective ball valves in the fully open condition, the reservoir liquid level should now sit less than 10mm higher than that of the heat exchanger (equivalent dynamic head loss = 7.0 mm).

The head level calculated above is based on the dry vapour flow and illustrates the worst case scenario. As the relative density of R134a liquid is approximately four times higher than that of R134a vapour, mixed phase flow would reduce the head difference proportionately.

Functional improvements were also made to the EP3 generator sub-system. Four new sight-glasses were installed in parallel to the generator to aid detection of the liquid level. The new sight-glasses incorporated small plastic float-balls to indicate whether liquid or vapour present.

6.4 Condenser Sub-system EP3

The EP3 condenser had a higher capacity (theoretical maximum is now 2,016 W at design point) than that of EP2. In addition, the vapour return from the condenser reservoir was routed to the inlet of the condenser, rather than the outlet.

6.4.1 Condenser Capacity

Experimental testing of EP2 had highlighted the significance of condenser pressure in overall system performance. With this in mind, the condenser capacity was increased by 40% (i.e. four additional sets of reclaimed condenser pipe-work were added to the condenser bank). The EP3 condenser bank had an approximate volume of 0.8 L (an increase of 230 ml) and a total surface area of approximately 12.5 m^2

Although outside the scope of this research study, the use of forced convection was also explored during the latter stages of experimental analysis. This augmentation, although requiring additional electrical demand, does offer the potential to extend the operational range of the system. Higher ambient temperatures ($\geqslant 32°C$) or lower generator pressures ($\leqslant 28$ bar)are both possible given the flexibility that forced convection provides and the results of this investigation are presented in chapter 7.

6.4.2 Condenser inlet : Vapour Bleed Line

Experimental testing of EP2 had shown that the additional load placed on the condenser following charge cycles was adversely affecting system performance. After the reservoirs had exchanged fluid, the EP2 condenser reservoir discharged high pressure vapour, in

reverse flow, upwards into the condenser outlet. Not only did this impede the normal flow of liquid from top to bottom, but it was also found to have been pushing the desiccant in the filter-drier back up into the condenser, blocking some of the pipes.

For EP3, the high pressure vapour from the condenser reservoir was routed to the inlet of the condenser. In addition, the flow was choked using a length of capillary to prevent large fluctuations in condenser pressure. This arrangement allowed the pressures in the condenser and condenser reservoir to approach equilibrium before the valve (ABV1) on the condenser outlet was reopened. This condenser inlet flow is controlled using a normally open solenoid valve (SOL1). This valve is closed during the transfer procedure, temporarily closing the vapour bleed line.

Condenser Inlet : Capillary Calculations

Capillary pipe was used, as illustrated in the main schematic in figure 6.18, to reduce the flow rate of high pressure vapour to the condenser inlet and prevent large fluctuations in condenser pressure.

Assuming that the primary condenser reservoir (2.8 L) contains vapour only (initially at 27 bar), the total mass of R134a in the reservoir is 0.45 kg. Based on 5K sub-cooling and capillary dimensions of 0.86 mm internal diameter and length 33000 mm, the initial mass flow rate, obtained from extrapolated ASHRAE data table (figure 6.11), was estimated at 9 kg/h (flow correction factor, $\phi = 1.0$). As the condenser reservoir begins to fall, the flow rate also falls. Based on the condenser and reservoir reaching equilibrium pressure, a a mean mass flow of 7.65 kg/h was estimated. At this flow rate, the time taken for the reservoir to reach equilibrium with the condenser would be 212 s.

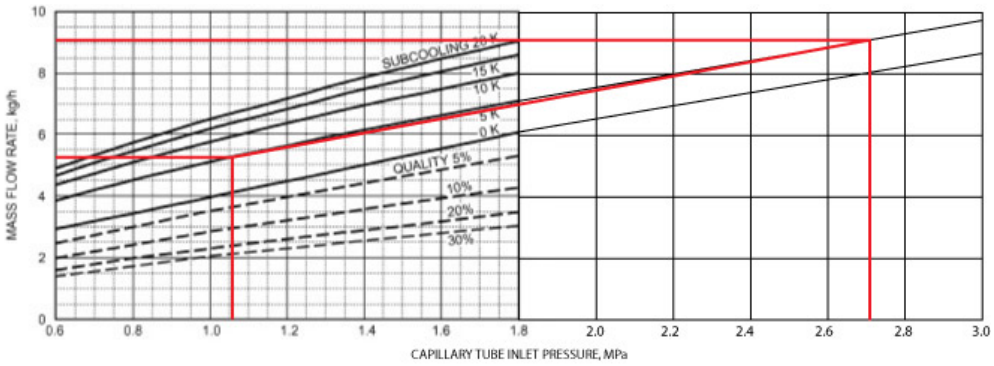

Figure 6.11: Extrapolated capillary data from ASHRAE 2006

A bypass line, with manually actuated ball valve (MCV2), was also installed across the capillary to allow the flow rate to be increased. This allowed verification of the requirement for capillary metered flow.

In the experimental development of the automated control systems for EP3, MCV2 was set at a fixed opening degree and used to reduce this equalisation time to approximately 17 seconds.

Condenser Inlet : Junction Design

It is also important that hot vapour is not sent backwards to the jet-pump and so a directional pipe junction was required to direct the flow towards the condenser.

For the capillary, this was achieved bending the capillary pipe (into an S) and brazing it in place to ensure the flow was directed towards the condenser as illustrated in figure 6.12

The feed from the bypass line required the manufacture of a bespoke directional T junction, shown in figure 6.13. A $\frac{1}{4}$" cap, drilled with a 4mm diameter hole, was brazed

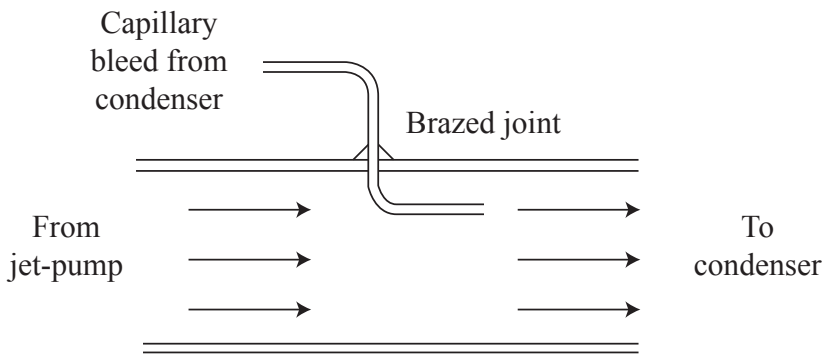

Figure 6.12: Illustration of condenser reservoir capillary bleed line

onto $\frac{1}{4}$" pipe, and inserted, through a $\frac{3}{8}$" reducing socket, into a conventional T junction.

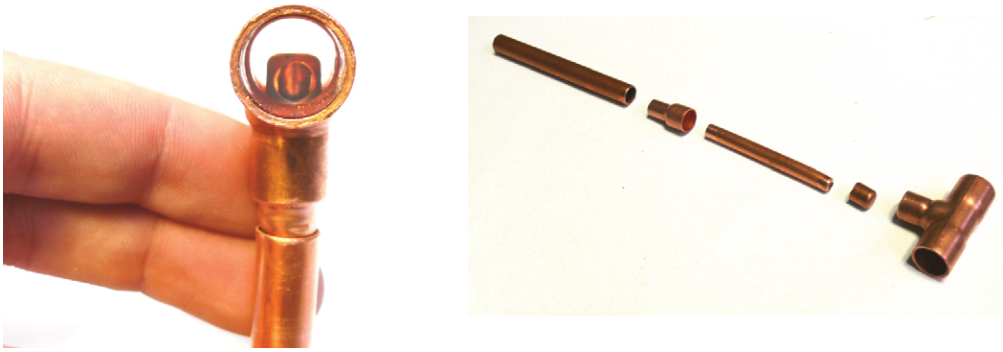

Figure 6.13: Photo - Manufacture of directional T-junction

6.5 Evaporator Sub-system EP3

Several changes implemented on the evaporator for EP3 to improve the flow control and the efficiency. The evaporator liquid level on EP2 was controlled manually however automatic, repeatable control was required for EP3. A thermostatic expansion valve (TEV) rated at 300W was installed. In order to de-rate the TEV to 100W, flow damping

within the evaporator was required and the methods are discussed in section 6.5.1. The EP3 evaporator sub-system also included a suction line heat exchanger to improve evaporator efficiency. Other minor enhancements to the evaporator inlet and outlet piping are also presented in this section.

6.5.1 Evaporator Flow Control

This section describes the specification and installation of a 300W thermostatic expansion valve (TEV). The cooling capacity of this system is only 100W and therefore flow damping within the evaporator (also discussed in this section) was required to prevent large fluctuations in evaporator liquid level.

Thermostatic Expansion Valve

On EP2, the liquid level in the evaporator had been estimated using thermocouples, attached to the evaporator pipe work, and controlled manually using a needle valve. Although this method brought some success, the manual delivery of refrigerant was only a crude intermediate solution.

Commercial refrigeration systems use a passive component called a thermostatic expansion valve (TEV) to control flow to the evaporator. The TEV, positioned at the inlet to the evaporator, is linked, via capillary, to a sensing bulb on the outlet of the evaporator. The TEV throttles the liquid that enters the evaporator to maintain the superheat level at the outlet.

Due to the 100 W design cooling capacity of the system, it proved difficult to find a suitably rated commercial option. The closest available was the *Alco TIS MW /*

TI0-00X. This TEV is externally equalised and rated at 300 W. In order to avoid fluctuating evaporator liquid levels, flow damping was required to provide additional time for changes in superheat to be detected by the TEV.

Capillary Flow Damping

A capillary tube was installed on the outlet of the TEV to reduce the effective flow rate. This allowed the TEV more time to react to changes in evaporator super-heat.

In order to scale down the valve to the 100 W required rating, a length of capillary was installed on the outlet of the TEV, reducing its potential to flood the evaporator. Using the capillary tables from ASHRAE 2006 (see figure 6.14), it was estimated that 5 m of 0.79 mm internal diameter capillary ($\phi = 0.6$) would restrict the peak flow, at 5K sub-cooling, to 3.24 kg/h (0.9 g/s). Knowing from equation 5.3 that $\dot{Q} \propto \dot{m}$ and that

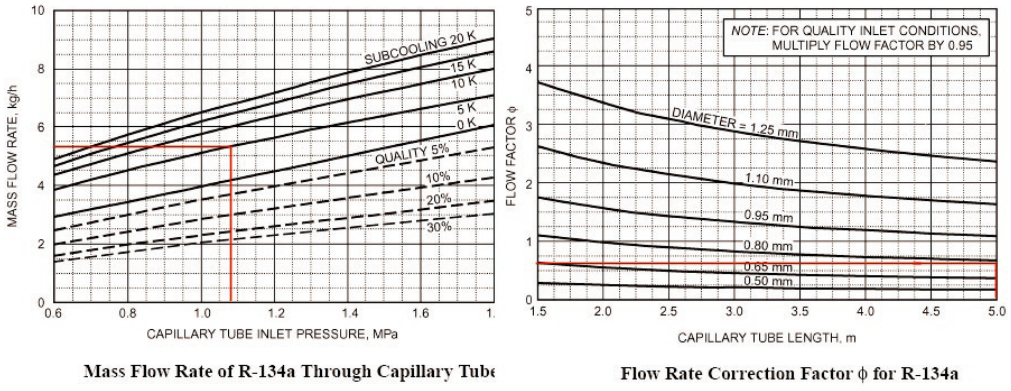

Figure 6.14: ASHRAE 2006 Extract- Capillary tables

design point evaporator mass flow is 0.7 g/s, the capillary flow should reduce the normal working capacity of the TEV to approximately 130 W. This method of metering, although partially effective did not resolve the issue of fluctuating evaporator liquid

levels.

Buffer Zone Flow Damping

Additional pipe-work was installed at the desired refrigerant liquid level to act as a buffer zone.

This buffer zone was fabricated using four loops of $\frac{1}{4}$" pipe and inserted at the desired refrigerant height (75% of total height) as illustrated in figure 6.15 . This buffer zone gave the TEV additional time to react to the changes in superheat level and also provided the evaporator with additional surface area.

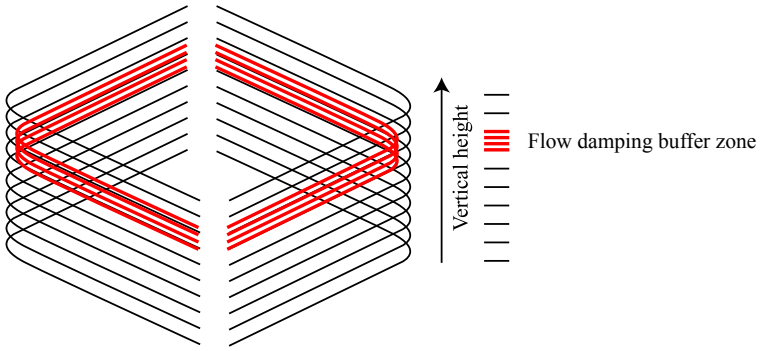

Figure 6.15: Illustration showing implementation of evaporator buffer zone

6.5.2 Other Evaporator Enhancements

Suction Line Heat Exchanger

The previous estimate for evaporator inlet temperature (section 6.5.1) assumed 5 K sub cooling of the liquid entering the TEV. This was achieved with the use of a suction line

heat exchanger. The installation of this new component will have the dual benefit of both superheating the vapour that is leaving and subcooling the liquid about to enter the evaporator. This heat-recovery method has been shown to improve the performance of jet-pump systems. [28][40][44][45]

Evaporator Sub-system Inlet

On EP2, the condenser outlet, flowed down directly into the condenser reservoir. It was only when this reservoir was full, and the connecting pipe above it, that liquid refrigerant would flow horizontally, via a T-junction, to the evaporator inlet. On EP3, this arrangement was reversed, with the vertical flow now prioritised to the evaporator inlet ensuring that there is always "pre-load" liquid available to the TEV.

A branch pipe-line, joining horizontally at 90°, directs the remainder of the flow to the secondary condenser reservoir. The EP3 evaporator inlet arrangement is illustrated in figure 6.16.

Evaporator Sub-system Outlet

A non return valve (Magni-check MS-8)was installed on the EP2 evaporator suction line (the pipe leading from the evaporator to the jet-pump). It had been observed that the NRV had, on occasion, allowed reverse flow to the evaporator, increasing the pressure. During the manufacture of EP3, the faulty NRV was tested and found to be leaking. The NRV was dismantled and found to be damaged. Although the MS-8 valve has an integral strainer, small particulates were getting through the strainer mesh and obstructing the sealing faces. Secondary strainers would be required both downstream

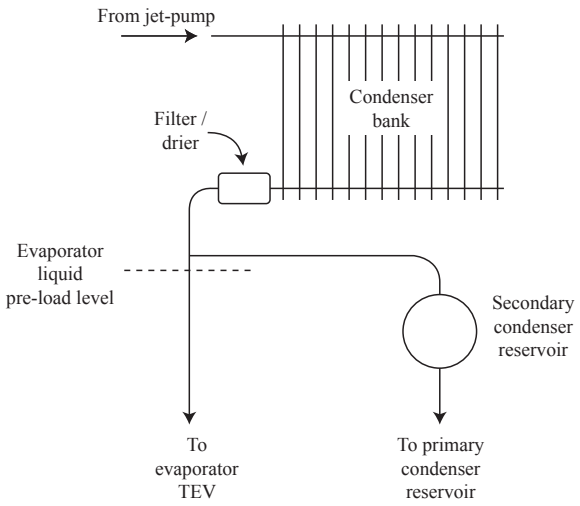

Figure 6.16: Illustration of evaporator feed pipe-work

and upstream of the NRV in order to prevent repeated blocking. Due to the limited space available, it proved difficult to find any products on the market that would meet the requirement. A smaller NRV without a strainer (*Magni-check MTS-8*) was purchased and two small-scale filters were devised and constructed using pipe adapters and wire mesh. The construction of the filters is shown in the photo, figure 6.17.

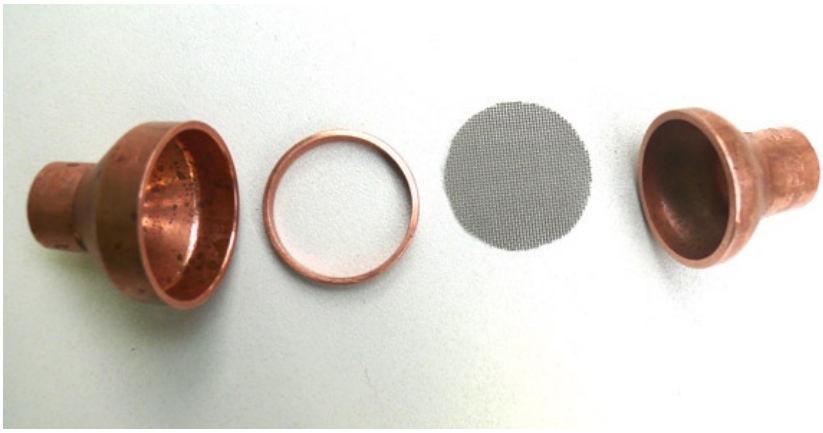

Figure 6.17: Photo - NRV compact strainer solution

The largest, readily available, one-step $\frac{1}{2}$" reducing socket is $1\frac{1}{4}$". The $1\frac{1}{4}$" pipe has a $\approx$ 26 mm inner diameter (ID), or 530.9 mm^2 area. This is the same ID as the *MS8* NRV. The *MS-8* has an integral strainer that uses a 30 mesh woven wire. 30 mesh has an approximate aperture size of 600 microns and a total open area of 45%, or 238.9 mm^2 (for a 26 mm ID). The $\frac{1}{2}$" pipe leading to each strainer has an inner diameter of 10.9 mm, hence 93.3 mm^2 area. This is much smaller than the open area of the mesh however these calculations do not take account of turbulence generated by the mesh. The design mass flow coming from the evaporator is relatively small, (0.7 g/s) and so the turbulence will be minimal. Sizing the strainer before the NRV with a 60 mesh (207 mm^2 open area) and the strainer after the NRV with a 40 mesh (223 mm^2 open area) should not cause a significant pressure drop. Table 6.5 shows the aperture size and open area percentage for the various mesh numbers discussed.

Mesh No	Aperture (Micron)	Open Area (%)	Wire Dia (mm)
30	600	45	0.25
40	400	42	0.22
60	250	39	0.16

Table 6.5: Mesh sizes and open area

6.6 Integrated System Design EP3

A simplified schematic of the full EP3 system is shown in figure 6.18. The schematic is colour coded to aid understanding.

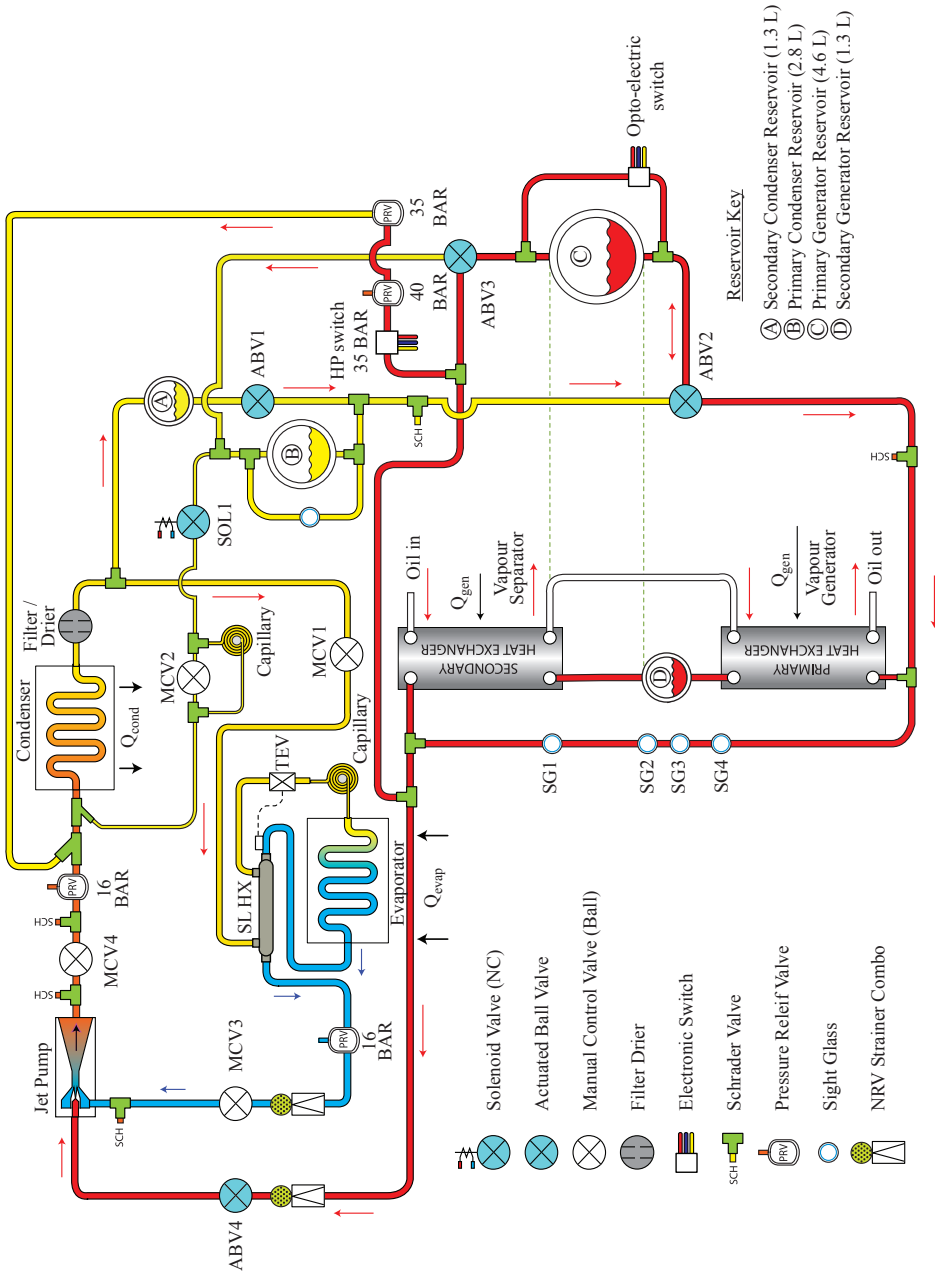

Figure 6.18: 2D Schematic of EP3

The red section of the circuit shows the high-pressure (27-32 bar) generator pipe-work. Refrigerant fluid is supplied to the primary heat exchanger (vapour generator) via two feed reservoirs (C&D). A second heat exchanger is used to super-heat the refrigerant, ensuring a dry vapour is supplied to the primary inlet of the jet pump. An opto-electronic sensor is used to detect when the primary generator reservoir (C) has run dry and actuate a fluid transfer cycle. The secondary generator reservoir (D) is used to extend the operating duration of the jet-pump during charge cycles.

The yellow section of the circuit shows the condenser pipe-work. Two reservoirs (A&B) collect fluid from the outlet of the condenser. The secondary condenser reservoir (A) allows the condenser to continue operating effectively whilst the primary condenser reservoir (B) is being used to replenish the primary generator reservoir (C). This fluid transfer procedure is discussed in more detail in section 6.8.3. A vapour bleed line carries residual high-pressure vapour from the primary condenser reservoir (B) to the inlet of the condenser following completion of the charge cycle. The condenser also supplies liquid to the thermostatic expansion valve (TEV) at the inlet of the evaporator.

The blue section of the circuit shows the low-pressure (around 3.6 bar) evaporator pipe-work. A heat exchanger installed in parallel across the evaporator provides the dual function of both super-heating the outlet vapour and sub-cooling the inlet liquid supply. This heat recovery helps to improve the overall efficiency of the system. Also worthy of mention is the non-return valve (NRV) installed on the suction line that feeds the secondary inlet of the jet-pump. This valve prevents reverse flow from entering the evaporator during charge cycles.

The schematic also shows the location of four manual control valves (MCV's). These ball valves can be used to isolate the subsystems (for maintenance) or re-route the refrigerant

flow through capillary tube (i.e. MCV2). Schrader valves are also installed at various locations throughout the circuit. These provide multiple functions including the ability to re-route flow (using refrigerant charge hoses) or install additional instrumentation.

The position of pressure relief valves are shown in the schematic, however the locations of standard instrumentation (i.e. thermocouples and pressure gauges) are not. The safety control logic is discussed further is section 6.8.1

6.7 Automated Control Hardware Specification

The flow of refrigerant on EP2 was controlled manually using hand-operated ball valves, and based on the information received by the operator from thermocouples, pressure gauges and sight glasses, which were positioned at various key points around the system. Although design point operation was possible, there was limited repeatability. By automating the system it was hoped that more consistent results could be achieved. Pressure transducers, liquid level sensors and temperature sensors would be used as the inputs to a programmable logic controller (PLC) that would monitor the system conditions and control the flow of refrigerant accordingly. Actuated ball valves were chosen to stop or divert the flow due to their low-power requirements and high-pressure ratings. This automated system would provide the repeatability necessary to conduct a detailed analysis of system performance and make incremental changes to the operating procedure.

6.7.1 Electrically Actuated Valves

A number of electrically actuated valve types were considered for EP3 and this subsection details their evaluation and specification.

Solenoid Valves

Solenoid actuated valves are widely available, at a reasonable cost, from OEM suppliers and would therefore be a good candidate for mass manufactured systems. There are however a number of factors that prevent solenoid actuated valves from being the ideal solution.

- **Maximum operating pressure differential (OPD):** The maximum pressure differential between sub-systems of the system under study (22 bar differential between condenser and generator) is on the limits of commercial refrigeration solenoid technology. Above the maximum OPD limit, the valve seat will be pushed open, allowing high pressure refrigerant to bleed back.
- **Multiple-way valves:** Conventionally, solenoid actuated valves are only available in 2-way configuration and the EP3 reservoir transfer concept was based around the use of 3-way valves to provide inherent Boolean logic and reduced part count. One option considered was the use of a 4-way reversing valve (such as those used in hot gas defrost systems) however the maximum OPD of OEM valves in this category was too low.
- **Operating energies:** One of the key drawbacks of solenoid valves is that the coils need to be energized for the duration of time that the valve is closed (for a

normally open (NO) valve). This represents a significant disadvantage over actuated ball valves when the total electricity demand is considered.

- **Bi-directional flow:** Conventional solenoids can only operate in a one-way flow scenario. The seal will only close (for a NO valve) against pressure coming from the inlet side of the valve. If the pressure on the outlet of the valve rises above the inlet pressure, the seat of the valve will lift allowing reverse flow. This is potentially, a serious issue for the reservoir transfer system. Bi-directional solenoid valves are available however the maximum OPDs are too low.

- **Minimum operating pressure differential:** Most solenoid valves also have a minimum OPD. The smallest solenoids are directly actuated, however valves with connections sized 3/8 and above are servo (pilot) assisted and require a small pressure difference (0.05bar) across the valve in order to close (for NO valves).

After review, only one location in the system was identified as suitable for a solenoid valve. A *Danfoss EV6-NO* valve with a 24V DC coil was installed on the vapour bleed line that connects the condenser reservoir to the condenser inlet. The maximum OPD across the valve should not exceed 15 bar and as the valve is only required to be closed during the transfer procedure (approximately one minute in every seven), the electrical requirement of a NO solenoid valve is limited. In addition, the minimum OPD is not an issue because the condenser outlet will always be re-opened to the condenser reservoir before equilibrium is reached. Regarding bi-directional flow limitations, normal operation should only ever see the flow of refrigerant from reservoir to condenser inlet. Any scenario where this is not the case represents a serious malfunction, in which case opening the solenoid to allow reverse flow would help to alleviate the problem.

Actuated Ball Valves

Electrically actuated (motor-driven) ball valves (ABVs) provide several benefits when considered against solenoid valves.

- **Higher working pressures:** ABVs offer higher working pressures ($>$ 50 bar)that are well above the requirements of the study system ((32.5 bar maximum). The pressure ratings for ABVs are governed by the pressure rating of the ball valve, and not the actuator, hence the maximum OPD is the same as the maximum working pressure (MWP) of the valve.
- **Multiple-way valves:** The mechanical arrangement of a ball valve makes the cost of multi-port configurations similar to that of 2-way valves.
- **Operating energies:** ABVs only require electrical power to change the position of the ball valve and could therefore retain their operational state without the need for any additional power input. This provides a distinct advantage for a solar-powered system.
- **Bi-directional flow:** Again, as no direct relationship between pressure and valve operation exists, bi-directional flow is possible.
- **Minimum operating pressure differential:** There is no minimum operating pressure, hence the valve is ideal for performing flow diversion functions.
- **Intermediate Positions:** As with manually operated ball valves, it is possible to to stop the valve at an intermediate point between open and closed, allowing a crude method of flow metering.

Sourcing a suitably sized actuated ball valve was difficult as they are primarily used in the oil and gas industry with high safety factor requirements and therefore tend to have large, heavy actuators and enclosures.

HQ-004 actuators were chosen for their comparatively small size, availability and price. The actuators are compatible with a range of ball valves, including the 3-way "T" port arrangement required. "T"port valves provide flow diverting functionality and prevent any cross-feed between supply lines. Figure 6.19 shows how the valve operates. Port "D" is permanently blocked off and the valve can divert flow travelling from "A" to "C", to travel from "A" to "B" with a 90°turn.

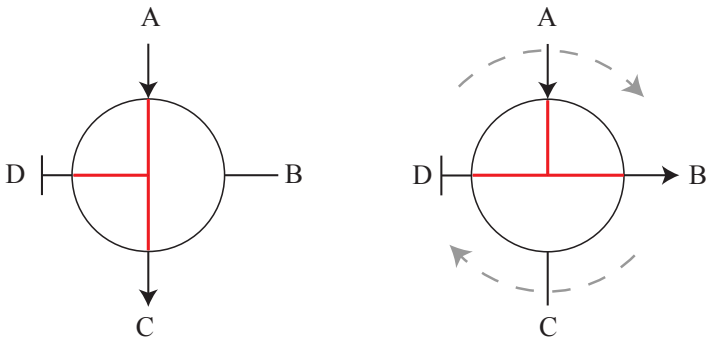

Figure 6.19: Schematic of "T" port valve operation

These actuators provide position feedback via integrated micro-switches, allowing easy implementation of control systems. The actuators also have an integral heater element to prevent condensation on the control PCB. The wiring diagram for the *HQ-004* actuators also shows that suggested wiring to provide two LEDs to indicate when the valves are either fully open or fully closed.

Using ABVs will provide operational characteristics similar to that of the EP2 system that used hand-operated ball valves, however there are several disadvantages to using ABV's (cost,actuation time and physical size).

- **Cost:** The cost of an ABV (*HQ-04* unit ≈ £179) is around twice the cost of a solenoid (*EVR-6-NO* plus 24 V coil ≈ £82) however this can be offset against the fact that two, 2-way solenoid valves would be required to perform the function of one, 3-way ABV.
- **Actuation Time:** Solenoid valves typically have an actuation time of less than 0.5 s, however, due to the gearing of the motor, an actuation time of > 10 seconds is not unusual amongst ABVs. Although this gradual opening/closing does provide a useful damping effect when the valve operation includes pressure equalisation, it also prevents the valve from closing quickly in the event of a critical failure.
- **Physical size:** HQ-004 actuators were chosen for their comparatively small size, however they are still bulky (approx 2,300 cm^3) and heavy (3 kg) and so additional mechanical support is required on EP3 to prevent excess stress on the surrounding pipe work.

6.7.2 Input Transducers

The EP2 system employed conventional pressure gauges and sight glasses to provide visual feedback to the operator. In order to provide feedback of system conditions to the EP3 electronic control system, several new input transducers were added. A diagram showing the wiring for these inputs is shown in figure 6.20. These transducers, described in more detail in the upcoming section, provide input data on pressures, temperatures

and liquid levels.

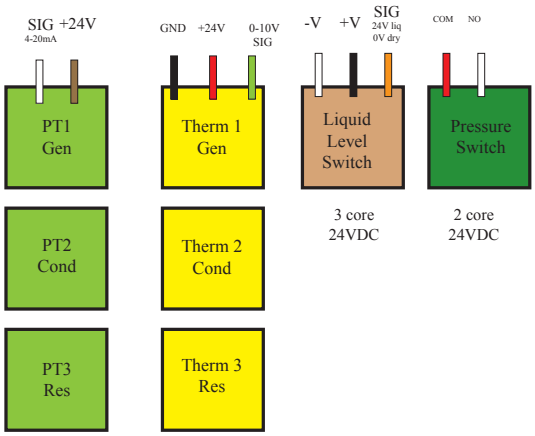

Figure 6.20: PLC Input Wiring Summary

- **Liquid Level Switch:** An *S9400* liquid level switch (*Henry Technologies*) was specified to detect the presence of liquid at the bottom of the primary generator reservoir. This opto-electronic device uses light reflecting from a conical glass prism as a way of detecting the presence of liquid. It was installed horizontally on a pipe that bridges the primary generator reservoir. The contacts on the switch are normally open. When no liquid is present, the light is reflected back off the cone. When liquid is present, the light passes into the liquid and the NO contacts are closed.

- **Temperature Sensors:** *VFG54-TRV4* (*Thermoken*)temperature sensors were specified. These units come complete with a small control box that mounts directly to the pipe and provides a 0-10 V proportional signal over the temperature range 0-160°C.

- **Pressure Transducers:** Two *PT4-50S* and one *PT3-18S* pressure transducers (*Alco Control*) were specified to measure the pressure at three key point on the

system. These transducers provide a 4-20 mA proportional signal across the pressure range. Two 250 Ω shunt resistors were used to convert this signal to a 2-10 V output.

- **Pressure Switch:** A *PSM-50* (*PVL limited*) pressure switch was installed to act as a safety cut out. The switch can be calibrated and adjusted in situ using a flat head screwdriver. The switch was set to close at 33 bar. This will trigger a number of safety cut-outs as discussed in section 6.7.3.
- **Thermostatic Cut-out:** In addition to the inputs discussed above, a thermostatic cut-out was installed inside the control box. This thermostat is in a sealed unit to prevent tampering and provides secondary over-temperature safety control for the generator oil circuit.

6.7.3 Safety Considerations

In addition to the safety logic provided by the PLC (see section 6.8.1, several additional measures were taken to ensure the EP3 system did not exceed maximum safe working conditions.

Two active safety controls, a pressure switch and a thermostat, were installed on EP3. The pressure switch, installed at the generator vapour outlet, is used to cut power to both the oil heater and the oil pump if generator pressure exceeds 33 bar. In addition, power to the oil heater can also be cut if the oil temperature exceeds the thermostat set point. It is important to note that the thermostat does not affect the operation of the oil pump as oil at the maximum temperature can still be delivered to the generator during normal operation. The safety cut out logic can be summarised in using a Boolean table (table 6.6).

Thermostat	Pressure Switch	Oil Heater	Oil Pump
0	0	0	0
0	1	0	1
1	0	0	0
1	1	1	1

Note : ”1” denotes ON and ”0” denotes OFF (safety cut-out condition)

Table 6.6: Boolean logic for relays 1 and 2

In addition to automatic safety controls, an emergency stop button was also installed, enabling the operator to cut electrical power to the system if necessary. The wiring schematic for the safety circuit is shown in figure 6.21. It is important to note that the configuration of relays was arranged to ensure that mains power and DC power do not pass through the same relay. In addition, wiring the switches/relays as illustrated provides fail-safe functionality as the safety control will become active if any wires are dislodged from either of the cut-out devices.

The logic for the safety system can be considered in sequential priority. This begins with the emergency stop button, located on the top of the control box, that cuts both the live and neutral lines of the mains power supply when activated. This component precedes all others to ensure that the electrical supply is cut in an emergency situation regardless of other system conditions. This is followed by the on/off toggle switch for the system, which is coupled with a 240 VAC LED indicator to provide the operator with visual confirmation that the control box is receiving power. Two Type C (slow-blow) fuses have been installed on the live wires that take mains power to the PSU and oil heater. Type C fuses were specified in order to prevent them tripping prematurely when exposed to

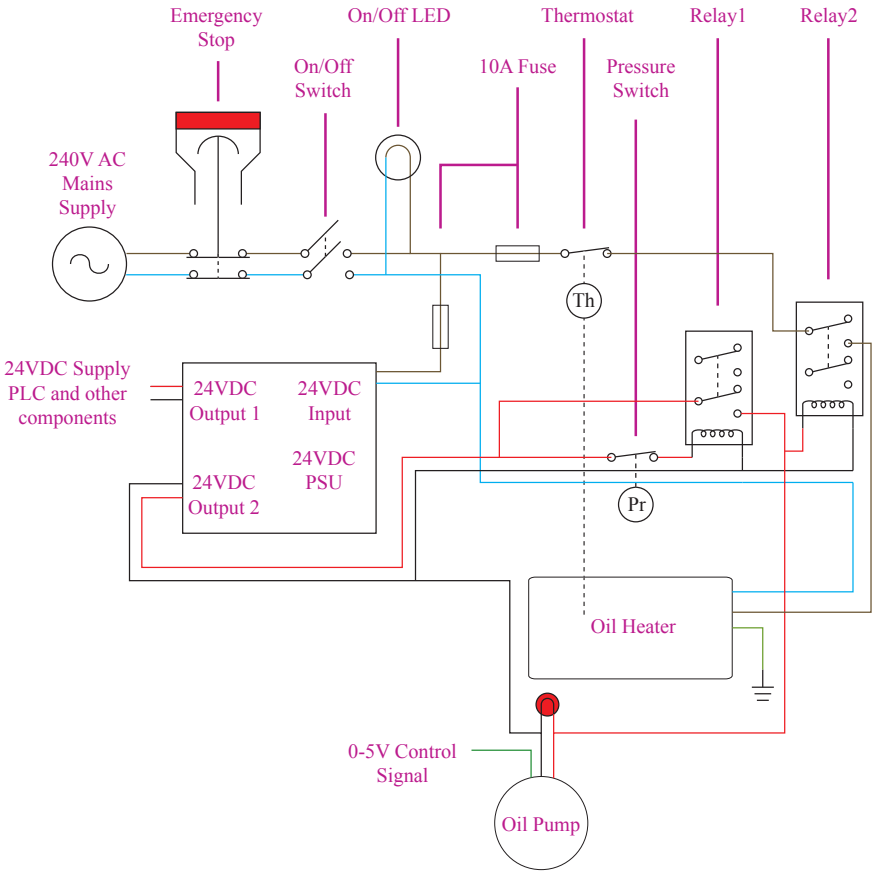

Figure 6.21: Safety circuit schematic

initial spike in voltage during start-up.

In addition to the electrical safety controls described above, pressure relief valves (PRVs) were installed throughout the system to vent off refrigerant in the event of dangerously high-pressure build-ups. The high-pressure side of the system has two PRVs. The first, rated at 35 bar, allows high-pressure vapour to bypass the jet-pump and travel straight to the condenser. If the high-pressure side continues to rise and reaches 40 bar, a second PRV will vent the vapour to atmosphere.

The safety logic described here overrides the safety control provided by the PLC.

6.7.4 Programmable Logic Controller

One of the key development targets for EP3 was autonomous operation. As the system control procedures are non-trivial and under continuous development, a programmable control system was required. A list of all the independent variables (inputs) and dependant variables (outputs) was defined, with analogue signal requirements noted. A total of 16 inputs (including 6 analogue) and 10 outputs (including 1 analogue) were identified and these are listed in table 6.7.

The EP3 control system includes pressure sensors and temperature sensors located at three key points in the system, along with the liquid level switch used as a trigger for reservoir transfer cycling. In addition, the actuated valves came complete with position sensing micro-switches. The control system uses this input data to control both the speed of the oil pump and the operation of the actuated valves.

A review of ten commercially available PLC units (24 V DC) is presented in appendix G. A *Zelio Logic 2* plus *SR3XT43CD* expansion unit (*Telemechanique*) was selected which

Inputs	Analogue	PLC Ref
PSM50 Pressure Switch	N	1
ABV4 CLOSE Microswitch	N	2
ABV4 OPEN Microswitch	N	3
ABV3 CLOSE Microswitch	N	4
ABV3 OPEN Microswitch	N	5
ABV2 CLOSE Microswitch	N	6
ABV2 OPEN Microswitch	N	7
ABV3 CLOSE Microswitch	N	8
ABV3 OPEN Microswitch	N	9
LLS (Liquid Level Switch)	N	A
PT3 Pressure Transducer [GEN] 0-10V	Y	B
PT2 Pressure Transducer [RES] 0-10V	Y	C
PT1 Pressure Transducer [CON] 0-10V	Y	D
TS3 Temp Sensor [GEN] 0-10V	Y	E
TS2 Temp Sensor [RES] 0-10V	Y	F
TS1 Temp Sensor [CON] 0-10V	Y	G
Outputs		
SOL1 CLOSE Signal	N	1
ABV4 CLOSE Signal	N	2
ABV4 OPEN Signal	N	3
ABV3 CLOSE Signal	N	4
ABV3 OPEN Signal	N	5
ABV2 CLOSE Signal	N	6
ABV2 OPEN Signal	N	7
ABV1 CLOSE Signal	N	8
ABV1 OPEN Signal	N	9
PUMP ANALOGUE OUT 0-5V	Y	B

Table 6.7: PLC inputs and outputs

provides 16 inputs (6 analogue)and 10 outputs (one analogue.

6.7.5 Power Supply

All of the system components, including input transducers and electrically actuated valves, were specified to work from a 24 VDC source. Not only was this safer than AC, but it is representative of the electrical power available from a photovoltaic panel in off-grid applications.

A list of all the electrical outputs and their power requirements is shown in table 6.8.

Component	Power (W)	Current (A)
Oil Pump*	20.4	1.2
Solenoid 1	20	0.83
ABV1	19.2	1
ABV2	19.2	1
ABV3	19.2	1
ABV4	19.2	1

Table 6.8: List of electrical outputs and their power requirements

In the scenario where all the outputs required maximum power simultaneously, a total power of 166.8 W (7.73 A) would be needed. With this in mind, a 220 W switch-mode enclosed power supply was sourced (TracoPower TXL 220-24S) that is capable of providing 9.2 A. In addition to the components listed above, the PLC itself will draw a small current however this is negligible compared to the other components.

6.7.6 Control Circuit Design

Once the PLC, input sensors and actuators had been specified, the associated control circuit design could be completed. To allow ongoing empirical development to the control procedures, it was decided that the control system should allow both automatic control, using the PLC, or manual control, using switches and knobs.

The final wiring schematic for the primary circuit, which shows the power and signal connections for PLC automated control is shown in figure 6.22. The secondary circuit which allows switch-over to manual control is shown in figure 6.23.

The secondary circuit uses a 4-pole changeover (4PCO) relay to switch over from manual to automatic control and four 2-pole change-over (2PCO) relays were used to switch the open/close control signals for each of the four ABVs. Separate relays were used for each ABV to prevent cross-feed between two or more actuators. PT-Series (Schrack) miniature plug-in relays were chosen for their simple functionality, ease of wiring and DIN rail mount feature. Diode protection modules were installed on each relay to prevent back-EMF affecting the PLC when the coils are de-energized.

6.7.7 Control Box Hardware

Once the control circuit design was finalised, and the components specified it was possible to design the internal layout of the box, which would contain the power supply unit (PSU), the PLC, the thermostat and all of the switching relays. Following best practice guidelines , control box power inlets were wired with male connectors and outlets with female connectors. This configuration helps to minimise the risk of electric shock. A photo of the completed control-box is shown in figure 6.24.

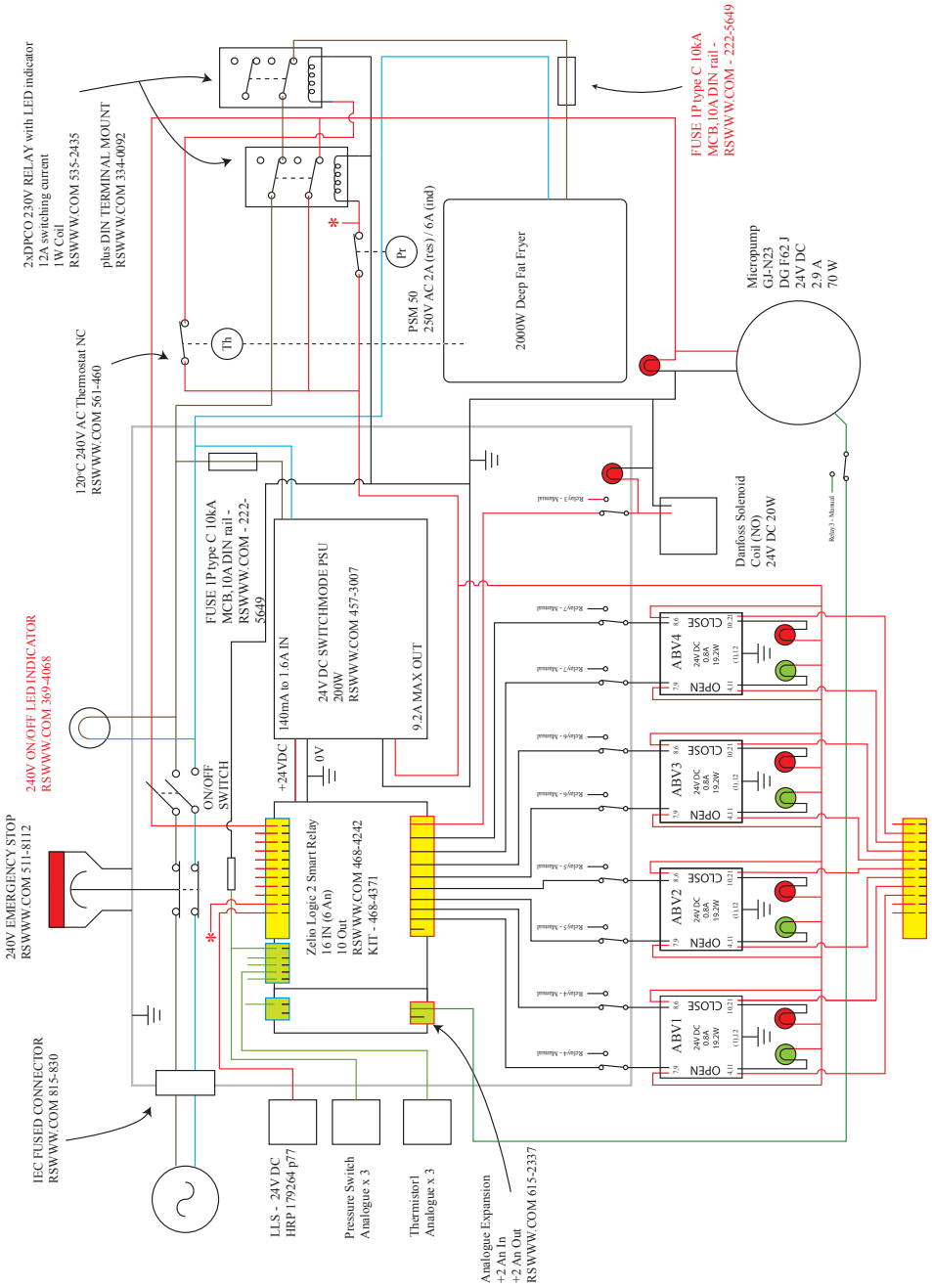

Figure 6.22: Main control box schematic

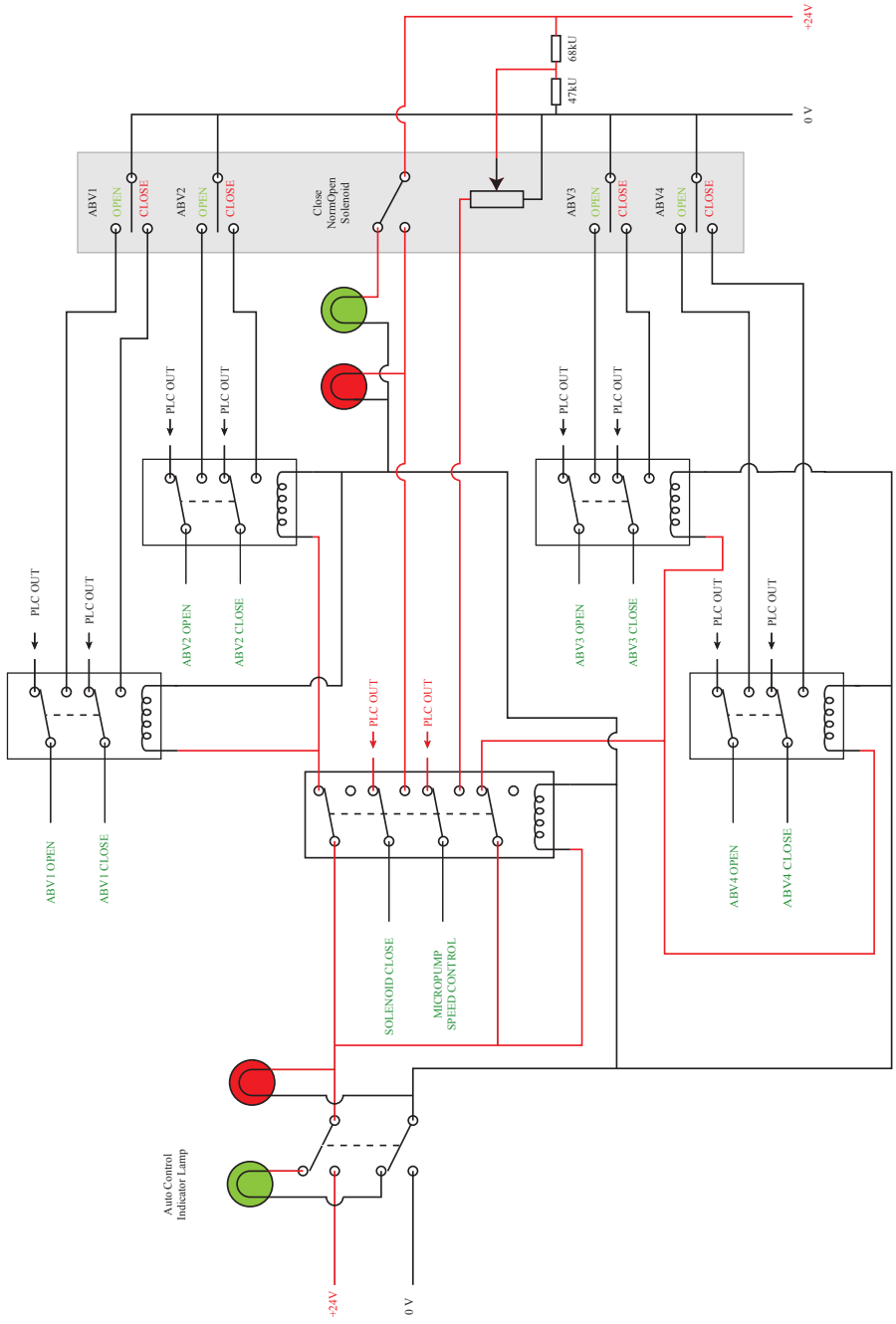

Figure 6.23: Manual / automatic switching circuit

Figure 6.24: Photo of control box

Manual Override Interface

A simplified schematic of the system was drawn up and printed on vinyl for the front of the control box. The various control switches and indicator LEDs are installed on the front panel (at locations corresponding with the printed schematic) to illustrate the current system flow routing. The representative control layout is shown in figure 6.25.

Heavy-duty toggle switches (*Allen Bradley*) were specified to provide manually operated control. 3-way versions of these switches are used to control the ABVs. The three positions enable the operator to either lock the valve to an open/closed position or stop the ball-valve at an intermediate position. LEDs, powered from the ABV feedback circuit (as discussed in section 6.7.1), were installed above each switch to provide the operator with a visual signal that indicates the current position of the valve. Red and green LEDs correspond to the vinyl graphics to illustrate the selected flow path.

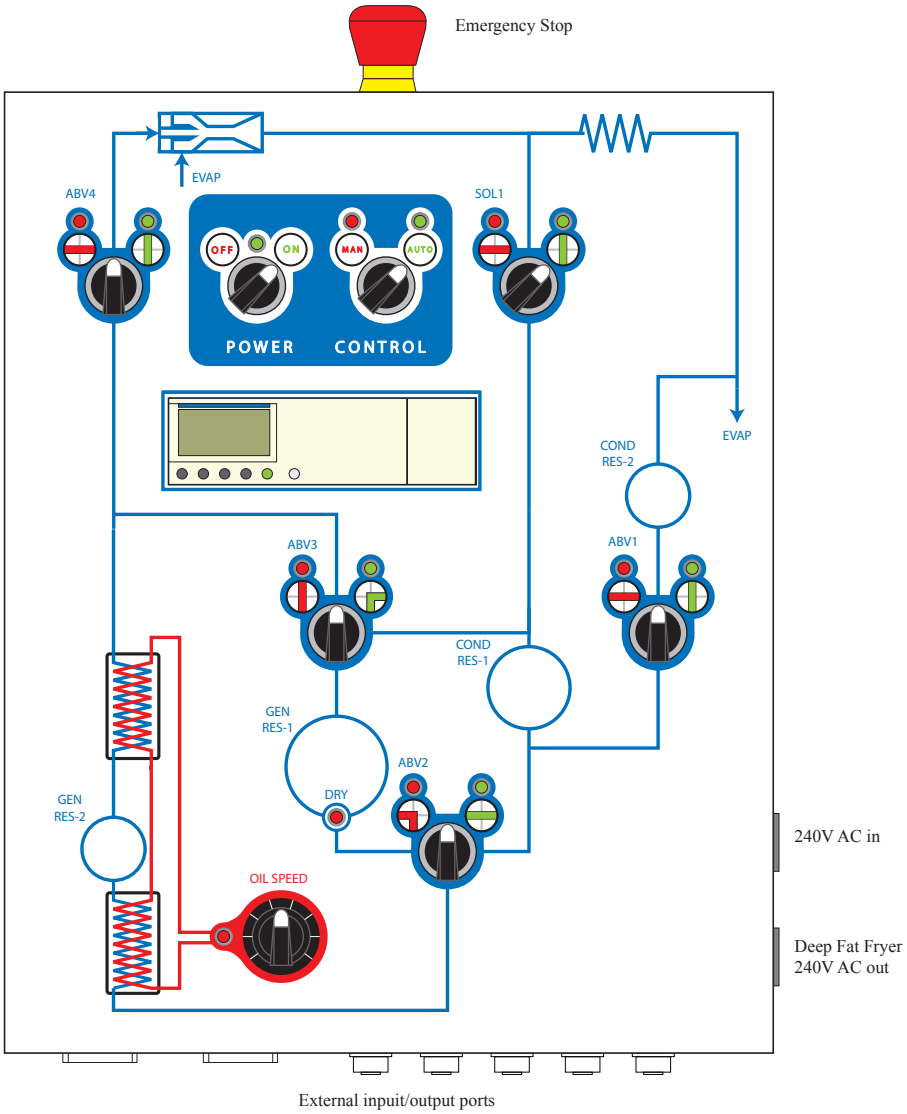

Figure 6.25: Control box layout

6.8 Control Logic

The experimental testing of EP2 provided a good understanding of the required system control logic and, prior to PLC programming, a flow diagram (figure 6.26) was constructed to visualise this logic. Three control branches can be identified at the top of the diagram representing the three key control requirements: safety, generator pressure management and fluid transfer cycling.

6.8.1 High-pressure Safety Logic

Although specific measures to ensure safe operational testing of EP3 had already been implemented (see section 6.7.3), top-tier command functions were programmed into the control software to prevent the generator exceeding the maximum design point pressure. In the event that generator pressures do exceed 33 bar, the PLC will instantly reduce the oil pump speed to zero and ensure ABV4, which controls flow to the jet-pump, is open. This command will override any other PLC operation.

6.8.2 Generator Pressure Management

EP3 generator pressure is controlled by moderating the oil pump speed. This second-tier command process is independent of other second-tier PLC functions and is a closed feedback control loop. If the generator is under design point pressure (< 27 bar), the PLC will increase the pump speed, and if the generator is over pressure (>30 bar), the PLC will reduce the pump speed. Proportional integral derivative (PID) algorithms were not implemented in this study however it is important to note that the oil pump speed is reduced, in 10% increments, at a rate three times faster that of pump speed increase to

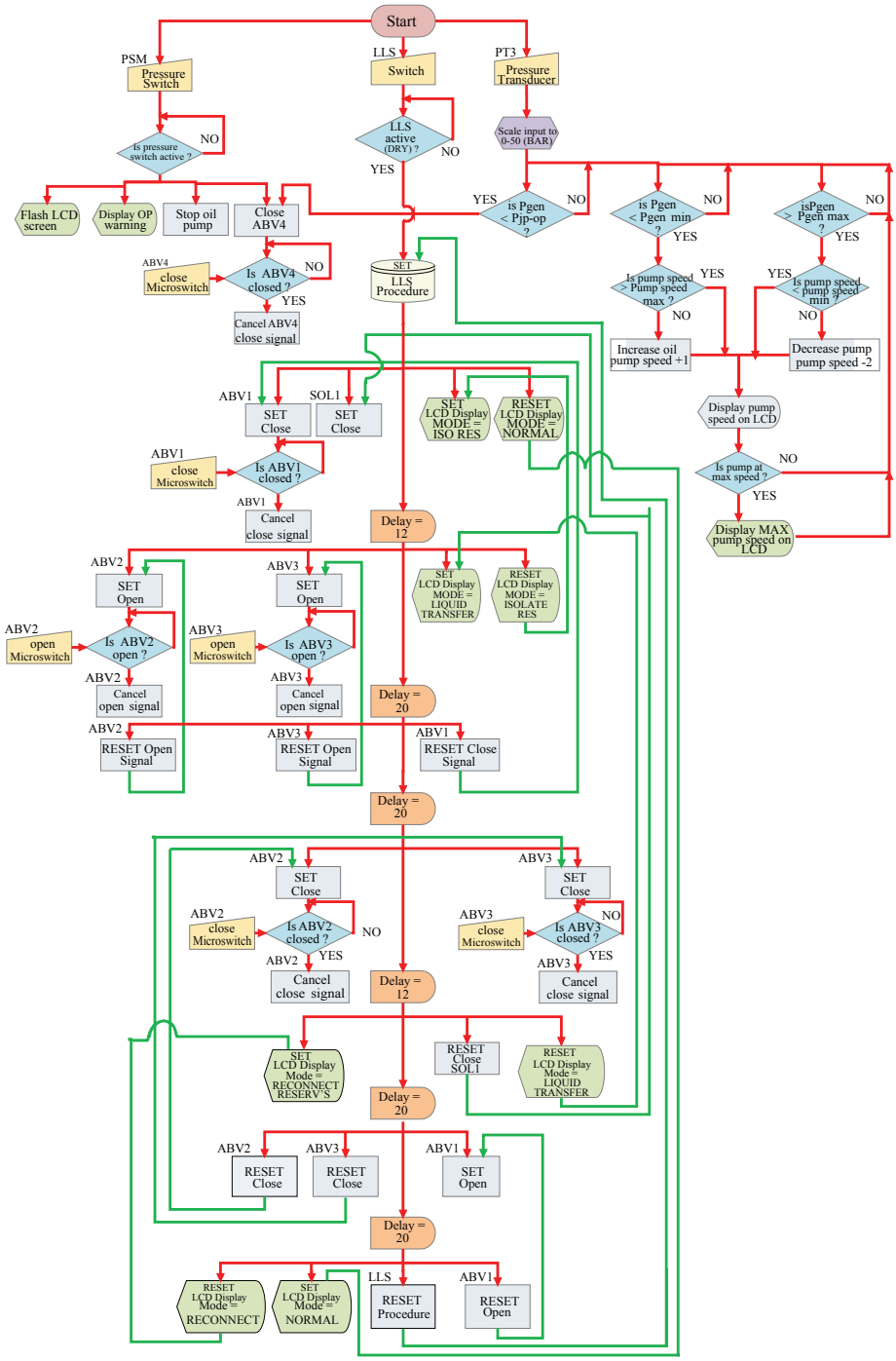

Figure 6.26: Control logic flow diagram

mitigate against the risk of over pressurising the generator.

It is also important to note that if the generator pressure is below the minimum operating pressure of the jet-pump (< 26 bar), the PLC will close ABV4 temporarily to prevent any unnecessarily loading the condenser when suction pressure can no longer be maintained.

6.8.3 Fluid Transfer Cycling

With a future mass-manufacturing solution in mind, the PLC in this system attempts to implement control systems that use a minimal number of input signals. Minimising the number of input sensors helps to reduce the overall cost.

The fluid transfer procedure is initiated when the primary generator runs dry. The liquid level switch, located at the bottom of the primary generator reservoir, is activated and the PLC commences a series of valve operations to transfer the fluid. Each ABV has an actuation time of approximately 12 seconds, which is accounted for in PLC programming.

With reference to figure 6.18 and table 6.9; After the liquid level of the primary generator reservoir (C) is exhausted the refrigerant charge cycle is initiated (step 1). Firstly, ABV1 and SOL1 are closed to prevent high pressure vapour flowing upwards into the condenser during the transfer cycle(step 2). ABV2 and ABV3 are then actuated, isolating the generator and connecting the two primary reservoirs (B& C)(step 3). This allows refrigerant fluid to transfer downwards into the primary generator reservoir (C)(step 4). During this time, the secondary reservoirs (A & D) provide additional volumetric capacity to allow the system to continue functioning however when the generator does drop below 26 bar (≈ 80°C) AB4 is closed as effective jet-pump operation

can no longer be maintained (step 5).

After a period of approximately 100 seconds, the primary generators have exchanged fluid and ABV2 and ABV3 are reverse actuated (step 6), providing the generator with a fresh supply of liquid refrigerant and isolating the primary condenser reservoir (B), which is now full of high pressure vapour. After the generator reservoir has reached 27 bar, AB4 is reopened (step 7) to the jet-pump and flow is entrained from the evaporator.

SOL1 is then opened (step 8), allowing the high-pressure vapour to bleed back to the condenser inlet through a length of capillary. When the pressure of the condenser and primary condenser reservoir (B) approach equilibrium ABV1 is re-opened (step 9) and the charge cycle is complete.

Using valve actuation timing, rather than position sensing will help to reduce the cost of mass-manufactured production systems. The operation sequence and timings of the charge cycle were experimentally refined however the basic procedure is summarised in table6.9.

6.9 Commissioning EP3

The standard commissioning process for all three experimental prototype systems (i.e. pipe-lagging, leak-finding and hydrostatic pressure tests) has already been described in section 5.7.4 however the refrigerant charge volume has not yet been discussed. In addition, commissioning EP3 also included programming of the PLC.

Step	Description	Valve Actuations
1	Liquid level switch detects empty primary generator reservoir	-
2	Condenser sub-systems is isolated	SOL1 & ABV1
3	Connect the two primary rervoirs (B & C) in parallel	ABV2 & ABV 3
4	Fluid transfer occurs ($\backsim$ 100 s)	-
5	Generator outlet closed if pressure falls below 26 bar	ABV4
6	Primary generator reservoir reconnected to generator	ABV2 & ABV 3
7	Generator outlet reopened when pressure reaches 27 bar	ABV4
8	Vapour from condenser reservoir (B) bled back to condenser inlet	SOL1
9	Primary condenser reservoir (B) reopened to condenser	ABV1
10	Repeat cycle	-

Table 6.9: Table showing basic fluid transfer operating procedure (EP3)

6.9.1 Refrigerant Charging

Using the extracted water (following hydrostatic pressure tests) as a reference guide, an approximation on the total system capacity was made. The entire system holds approximately 12.7 L however this is not the volume of refrigerant required. With reference to figure 6.18, it was possible to estimate the required volume of refrigerant, using the fluid transfer initiation command as a datum. Once the generator reservoir(C) has run dry, the secondary generator reservoir (D) and the primary heat exchanger should both be completely full of R134a fluid. In addition, the primary condenser reservoir (B) should be full, ready to transfer fluid to the primary generator reservoir (C). The secondary condenser reservoir (A) should be empty, in preparation to provide the capacity for the condenser to operate normally whilst the two primary reservoirs exchange fluid. In addition, the evaporator should be approximately $\frac{3}{4}$ full, with an amount of liquid sitting above the TEV ready for injection. Finally, a small allowance has to be made for the volume of liquid contained in connecting pipework. A summary of these liquid volumes is contained in table 6.10.

Using the fluid density of R134a at an ambient temperature of 20°C (1225.3 kg/m^3), it was calculated that 6.94 kg of R134a is needed to fill the system to the desired level. With a vacuum drawn across the system, the refrigerant cylinder was put on scales and fed to the system until the required mass of R134a had been transferred to the system.

6.9.2 Programming the PLC

Telemechanique (a division of *Schneider Electric*) provide programming software (Zelio 2) and a USB cable for transferring the program to the PLC. The Zelio 2 environment

Component	Volume (L)	Volume (m^3)
Secondary Generator Reservoir	1.3	0.0013
Primary Condenser Reservoir	2.8	0.0028
Primary Heat Exchanger	0.38	0.00038
TEV supply	0.5	0.0005
3/4 Evaporator	0.18	0.00018
Connecting Pipework	0.5	0.0005
Total	5.66	0.00566

Table 6.10: Table showing liquid volume measurements

allows code to be programmed via a GUI several ways, however FBD was chosen for this application due to the requirement to manage several processes simultaneously. The Zelio 2, windows-based, editing environment uses drag and drop icons to represent a wide range of electronic components. The inputs to the PLC are listed on the right hand side of the page and the outputs on the left. With reference to the logic control flow diagram figure 6.26, various components were added to perform the logic functions required. These include timers, latches, logic gates, numerical comparators and individually defined Boolean operators.

The PLC provides functionality to display key variables and operational states on the PLC LCD screen and was programmed to display the system pressures and the operational mode along with safety warnings. With consideration to a final mass manufactured solution, it was preferable to have a small number of inputs and outputs in order to minimise the overall cost. Pressure transducers are an expensive component and

multiple transducers increase the likelihood of component malfunction. With this in mind, the initial PLC has been programmed to use just three of the seven available sensors. The pressure transducer (PT3), which is located in the generator section will be used to control the oil speed and the liquid level switch (LLS) will be used to trigger the fluid transfer procedure. In addition, the PLC recognises if the pressure safety switch (*PSM50*) is active and overrides all other valve operation commands.

One example of how these three sensors are used to control system process is operation of ABV4. Opening and closing ABV4 controls the flow of vapour from the generator to the primary inlet of the jet pump.

When generator pressures are below 26 bar, ABV4 is used to stop the flow of refrigerant vapour. Table 6.11 shows the control logic for the ABV4 close command signal (ABV4 C-CS). The only time that the AB4 C-CS can be activated is when the following conditions are met;

- ***PSM50:*** The pressure switch is under the high pressure limit,
- **PT3:** The generator is under the minimum operating pressure (26 bar)
- **ABV4 C-MS:** ABV4 micro-switch is indicating that the valve is not closed.

Table 6.12 shows the Boolean control logic for the ABV4 open command signal (ABV4 O-CS). The table is the reverse logic of table 6.11.

PSM50	PT3	ABV4 C-MS	**ABV4 C-CS**
0	0	0	**0**
1	0	0	**0**
0	1	0	**1**
1	1	0	**0**
0	0	1	**0**
1	0	1	**0**
0	1	1	**0**
1	1	1	**0**

Table 6.11: Boolean table for ABV4 close command signal (ABV4 C-CS)

PSM50	PT3	ABV4 O-MS	**ABV4 O-CS**
0	0	0	**1**
1	0	0	**1**
0	1	0	**0**
1	1	0	**1**
0	0	1	**0**
1	0	1	**0**
0	1	1	**0**
1	1	1	**0**

Table 6.12: Boolean table for ABV4 open command signal (ABV4 O-CS)

6.10 Chapter Discussion

EP3 marked a significant achievement. The operational results that follow in chapter 7 demonstrate that autonomous operation allowed more accurate performance data to be obtained over longer test durations. The addition of pressure transducers, necessary for closed loop control, provided an enhancement to the quality of data collected allowing detailed evaluation of the system conditions.

The development an implementation of a reservoir transfer system to deliver refrigerant from the condenser ($\backsim$ 9 bar) to the generator ($\backsim$ 29 bar) was a significant technical achievement. Four electrically actuated valves are used to control the flow of liquid refrigerant between four reservoirs. Three of these valves, actuated ball valves (ABV 1-3), only require electricity to switch position, and the fourth, a normally open solenoid (SOL1), only requires power for one minute in every ten. This provided a low-power (<24 W) solution to the challenge of generator fluid delivery. The remaining electrical requirements comprise an oil circulation pump and the control electronics (<25 W). The total electrical requirement of the system was therefore $<$ 50 W. The low electrical demand of this solution helps to reduce the requirement for expensive photovoltaic panels. Given a photovoltaic (PV) collector efficiency of 20%, the system could therefore be powered using approximately 0.3 m^2 PV collectors. In addition the relative mechanical simplicity of this fluid delivery system provides another compelling argument when considering the system as off-grid equipment. The EP3 system schematic has previously been presented in figure 6.18. A photo of EP3 is shown in figure 6.27

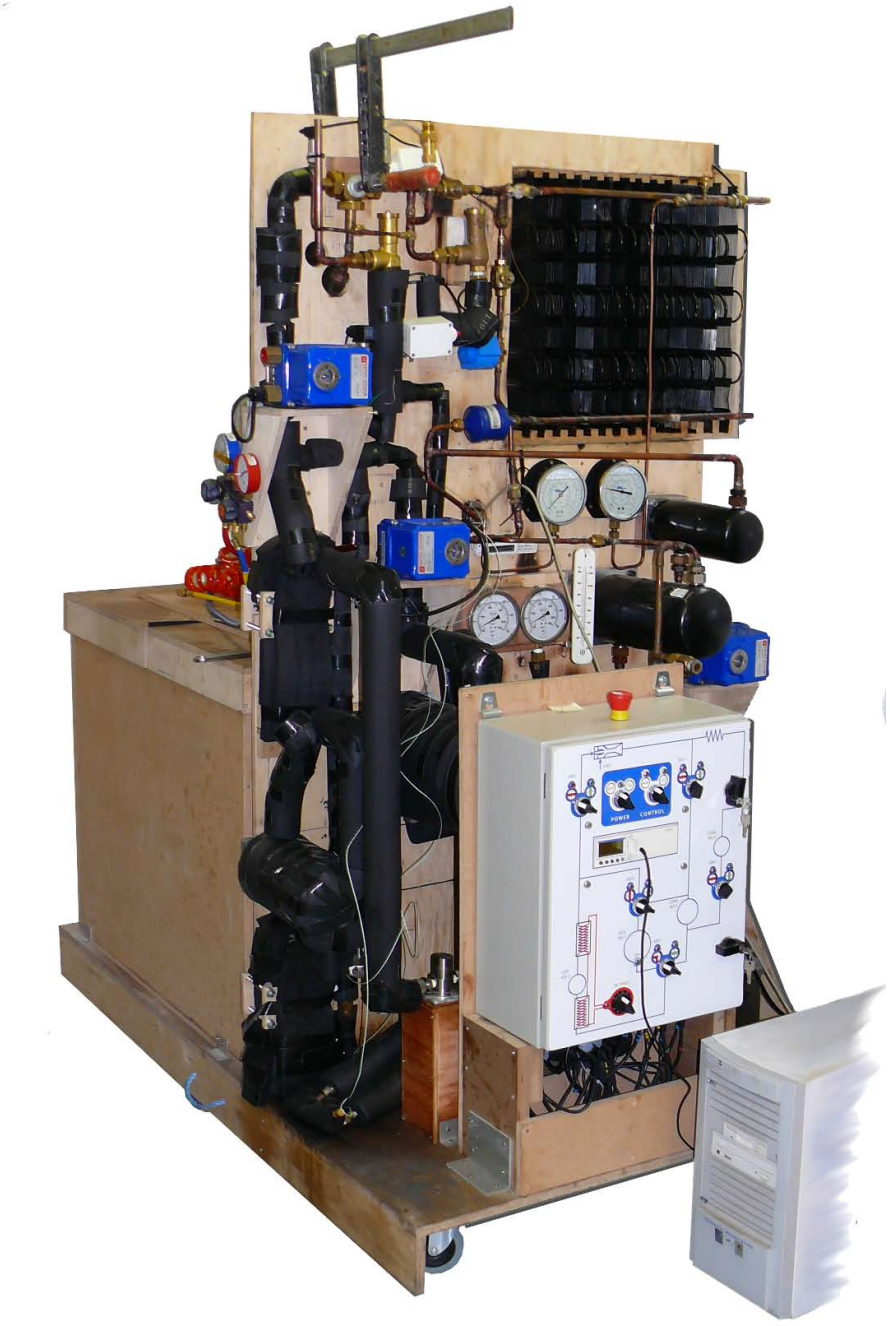

Figure 6.27: Photograph of EP3

Chapter 7

Testing and Analysis of Results

7.1 Introduction

In the previous chapters, the development (Ch5) and automation (Ch6) of the experimental apparatus has been described. This chapter contains operational test results, collected from EP2 and EP3, presented in chronological order.

The chapter weighting is biased towards the results collected from EP3. This reflects the fact that EP2 was primarily used as a development tool, for experimental optimisation of the jet-pump and system performance characterisation. It is also important to note that pressures were logged manually (from calibrated pressure gauges) on EP2, however digital pressure transducers were installed on EP3 to enable the collection of larger and more accurate data-sets.

Various performance related experimental results have already been presented in the body of the thesis, namely;

- Section 5.6.3: The experimental optimisation of the jet pump nozzle (EP2)
- Section 5.7.3: Characterisation of jet-pump entrainment, relative to varying generator and condenser pressures (EP2)
- Section 6.2: Simulation experiments conducted on EP2, used to determine the most effective solution for the generator fluid delivery system employed on EP3.

In total, 124 datasets were collected from all three experimental prototypes, using the data-logging equipment presented in sections 5.2.1 and 6.7.2. Each data-set was assigned a sequential reference number (DLC reference ID) and the information stored in a database (DLC map). The database provided a matrix of all collected data to allow easy cross referencing and characterisation of the results. Table 7.1 provides a summary of the DLC index values for each of the three experimental prototypes.

Apparatus Version	Data-sets
EP1	DLC 1-3
EP2	DLC 4-71
EP3	DLC 72-124

Table 7.1: DLC References for three experimental prototype (EP) versions

7.2 Review of Experimental Procedure

The results presented in this chapter all share the same basic experimental set-up and analysis assumptions as detailed in chapter 4. The apparatus is operated in accordance with the procedures described in chapter 5 for EP2 and chapter 6 for EP3.

The primary evaluation metric for this study is COP. The COP in this context, as defined by equation 2.3, is the quotient of Q_e over Q_g. Q_g and Q_e are both derived experimentally as outlined below.

Q_g, as defined by equation 5.3, is the product of the mass flow rate (m_g) (obtained via the the calibrated volumetric flow rate of the pump and relative density of the heat transfer oil), the specific heat capacity of the oil (C_{p-oil}), and the oil temperature difference across the generator heat exchanger (ΔT_{g-oil}).

Q_e is obtained as a sum of the various cooling duties (air, water, pipework etc) and the known losses (1.41 W/K). Using the mass and specific heat values provided in table 5.8 the cooling duties, when including a 1 L duty load of water, are equivalent to almost 18.35 kJ/K (for a 24 L water load, this figure rises to almost 115 kJ/K). In the performance evaluation of EP2 data, the temperature of the cool box air is assumed to be the same for all of the components within the cool-box, however the evaluation of EP3 data employs more sophisticated modelling thanks to additional thermocouples.

The COP of the system is normally defined over specified time-frames rather than an instantaneous value. This is because the data-noise generated by fluctuations in evaporator pipe temperature and generator flow rate can make instantaneous interpretation difficult.

7.3 Typical Behaviour

7.3.1 Typical Temperature Plot (EP2)

Figure 7.1 shows an extract (at t = 2,000) of the temperature data collected from within the cool-box on EP2. Whilst conducting the experiment, the evaporator liquid level was adjusted manually. By monitoring the evaporator pipe temperature at 5 levels, the superheated vapour level could be detected and more liquid added by opening and closing a bleed valve.

The desired liquid level is between level 3 and level 4. This ensures that the greatest heat transfer occurs in the top half of the chamber. This approach should also provide sufficient capacity to cope with periods of rapid boiling.

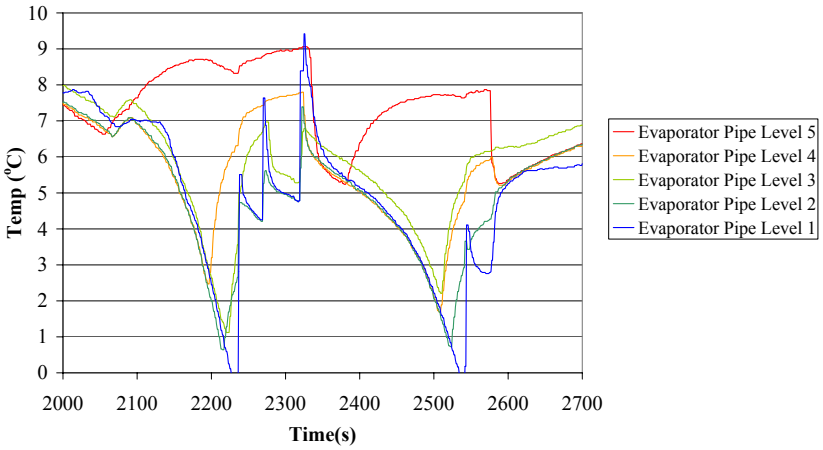

Figure 7.1: Typical evaporator behaviour (DLC 65 extract)

The evaporator pressure gauge generally indicated a saturated liquid temperature 1-3 K below the actual evaporator liquid temperature, indicating level of superheat. As the liquid level within the evaporator pipes drops, the thermocouple data shows the

superheated vapour level falling. Eventually the temperature of level 1 drops below 0 °C and fresh refrigerant is added (t=2,220 and t=2,540). This temporarily causes a sharp rise in temperature. This manual control method, although difficult to accurately measure, did allow for the evaporator performance of EP2 to be validated.

7.3.2 Typical Pressure Plot (EP3)

The pressure transducers (PT) installed on EP3 allowed a detailed picture of the system operating conditions to be recorded. Figure 7.2 shows a typical pressure plot for the charge/discharge (CD) operating cycle of EP3. The red and green lines, showing the pressures of both the generator and generator reservoir respectively peak around 28.5 bar. The pressure then modulates, as the PLC moderates the pump speed to keep the pressure within a tolerance band (27.5 bara ± 1 bar). The thermostatic control of the oil temperature also causes the generator temperature to fluctuate. When the generator reservoir has run dry, the fluid transfer cycle is initiated and both the generator and condenser are isolated before the two primary reservoirs are connected and refrigerant fluid is transferred downwards. This process takes jet-pump suction off-line for periods of ∽50 s for each full cycle. The blue and light blue lines, the condenser and jet-pump suction pressure respectively, can be seen to spike as the condenser reservoir is reintroduced to the condenser system and cooling is paused. Once the generator and generator reservoir reach operating pressure (∽ 25 bar) jet-pump entrainment recommences and the cycle begins again. A charge discharge ratio of 1:6 (50s : 300s) is maintained via the use of the secondary reservoirs which allow the system to continue functioning during a significant portion (69%) of the actual transfer procedure duration (110 s out of 160 s).

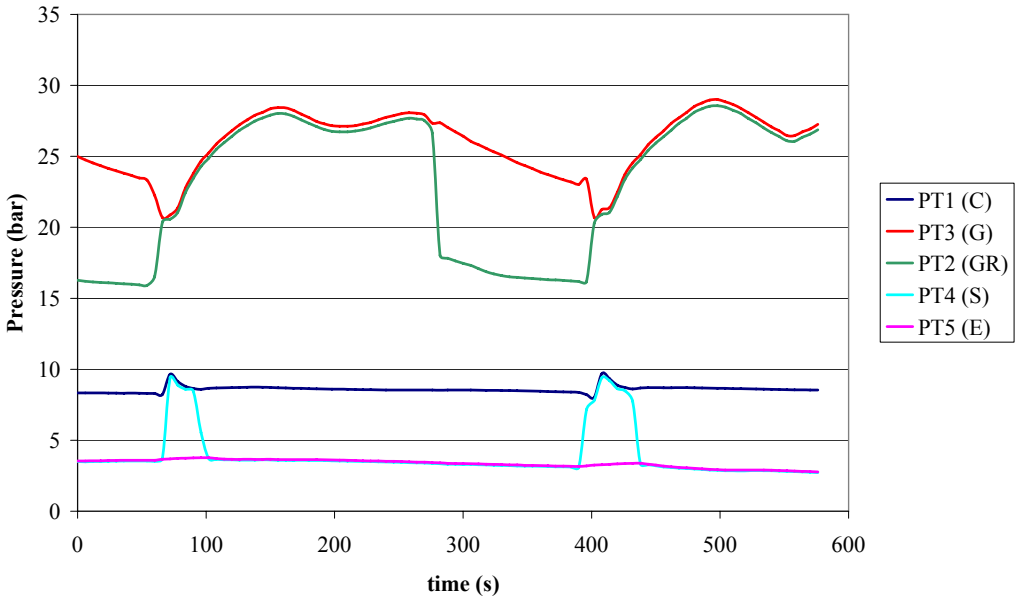

Figure 7.2: Typical systems pressures plot (DLC 119 Extract)

Figure 7.3 is an extract from DLC 103 which illustrates the effect of system pressures on evaporator temperature. The EP3 evaporator system is shown to provide good liquid level management. The superheat levels indicate that the liquid level is being maintained between evaporator levels 3 and 4 (75%). At approximately t = 5500, the superheated vapour reached level 3 of the evaporator (just below the "buffer zone")however the TEV reacts to the change in superheat and delivers more fluid.

What is also apparent is a rise in evaporator temperature during the 50 s each cycle when the jet-pump is not operational.

7.3.3 Typical COP Plot (EP3)

The COP of the system is difficult to measure instantaneously because of the significant effect that changes in evaporator temperatures (principally the temperature of the 24 L

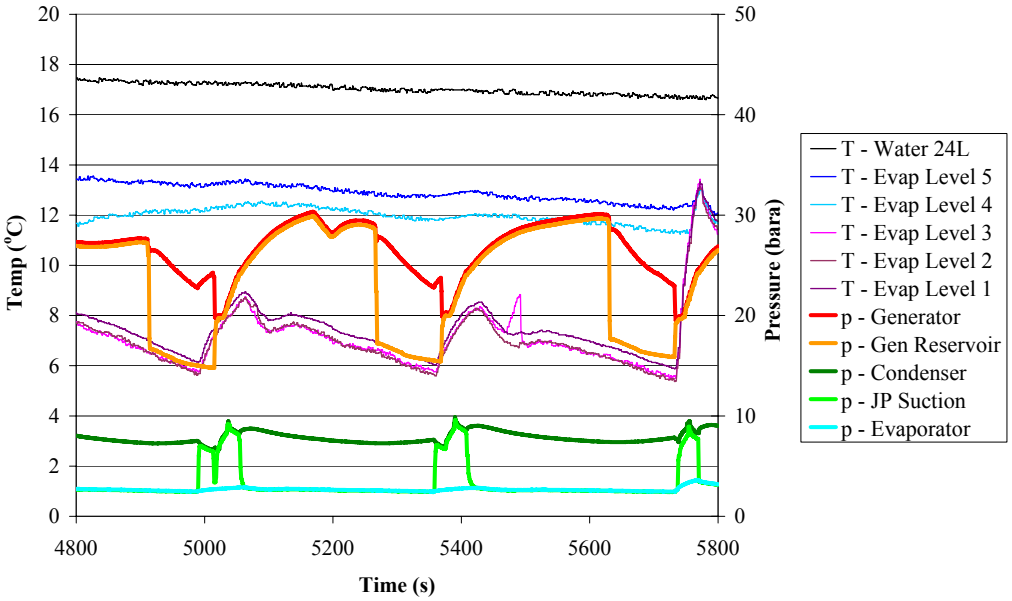

Figure 7.3: Typical systems pressures and temperatures (DLC 103 Extract)

water duty load) have on Q_e and consequentially COP. For this reason, the COP of the system was measured across full cycle intervals. Figure 7.4 shows the relative hysteresis of COP when values are calculated over 1, 5 and 10 cycle intervals. A 5 cycle ($\backsim$ 1900 s) interval period was chosen for evaluation of EP3 data as this provides linear trend characteristics whilst still indicating durations of reduced performance.

7.3.4 Typical Experimental Issues

As described earlier in this thesis, residual water within the system was attributed as the cause of intermittent and temporary failure of several valve seals. As these malfunctions occurred more often, but not always, at lower temperatures, both ice formation and corrosion residue have been identified as potential causes.

The lower temperature (and lower pressure) of the evaporator sub system, made it

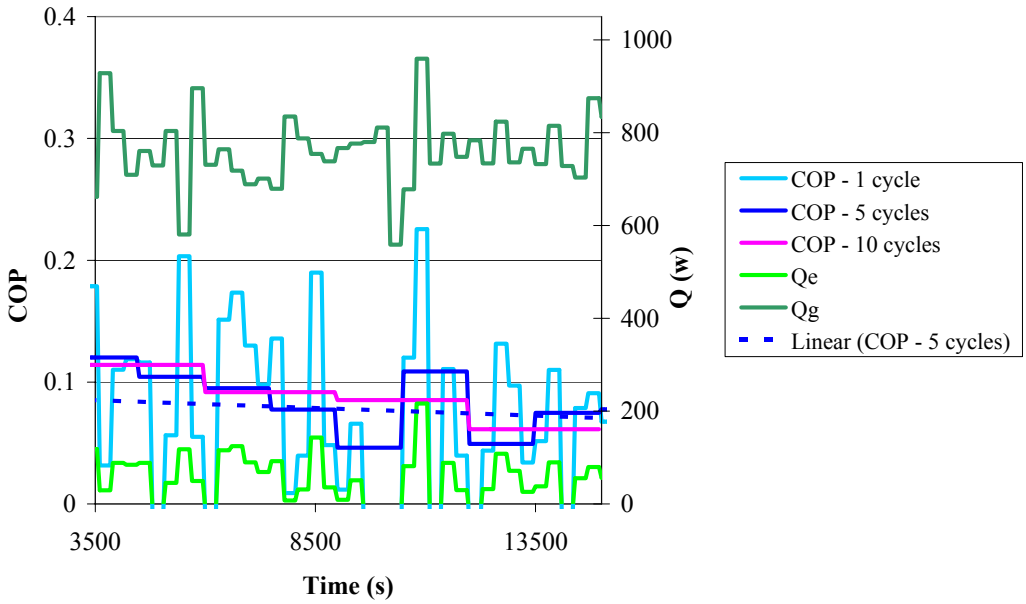

Figure 7.4: Q/COP against time showing various cycle counts (DLC 113 Extract)

particularly sensitive to these seal malfunctions, causing significant effects on overall system performance. Intermittent and temporary seal failures at both the evaporator inlet (TEV) and evaporator outlet (NRV) were observed. The TEV valve jamming in the closed position meant that the the evaporator could be temporarily starved of refrigerant fluid, interrupting effective heat transfer. In the case of the NRV (jet-pump suction line) becoming jammed in the open position, high pressure vapour was allowed to leak into the evaporator during charge cycles. Where relevant, the effect of these issues are highlighted with reference to graph plots of the data.

Experimental difficulties were also encountered with the data-logging software. During the collection of larger data sets, the software was prone to crashing. In most instances, this could be easily remedied by relaunching the application and using the time constant to combine the separate data-sets together. On some occasions however, corruption of individual data-sets created gaps in the experimental results. The data-logging software

was running on a older machine, using Windows 95, and this thought to be the reason for these difficulties.

7.4 EP2: Operational Test Data

As outlined in the introduction to this chapter, EP2 was principally used as a development system, to optimise and characterise the jet-pump performance. EP2 was also used to simulate flow scenarios ahead of the EP3 generator fluid delivery system. A functional, temperature based evaluation of the jet-pump provided all the relevant data required from EP2 and no additional load (i.e. water) was added to the cool-box until EP3 performance testing. It is also important to note that EP2 was manually operated and the generator flow was adjusted to keep the generator pressure within the specified operational range. In addition, the evaporator liquid level was also manually controlled.

7.4.1 EP2: Scope of Collected Data

Although EP2 was primarily used to optimise jet-pump performance and characterise system operating conditions, the data in this section of the thesis has been selected to specifically illustrate the effect of operating cycles on performance. COP is discussed briefly however as no duty load was present the box air temperature is the primary evaluation metric in this instance. Although the thermal input at the generator was recorded for some experiments, the performance evaluation for EP2 is principally considered in terms of temperature rather than COP.

7.4.2 EP2: Selected Operational Test Data

DLC 53 and DLC 65 are presented in this section. These two data-sets show the empirical development of the operating procedure for the test apparatus. DLC 53 shows the results obtained using the initial procedure which had a charge discharge ratio of 1:2. DLC 65 shows a refined procedure, trialled prior to the commissioning of EP3 which achieves a 1:6 ratio.

Test Data: DLC 53

This data-set was collected on EP2 according to the V1 operating procedure (see table 5.12). The graph in figure 7.5 shows the temperature, at various heights, of the evaporator and the temperature of the air within the cool-box. The air temperature has been highlighted with a red plot line.

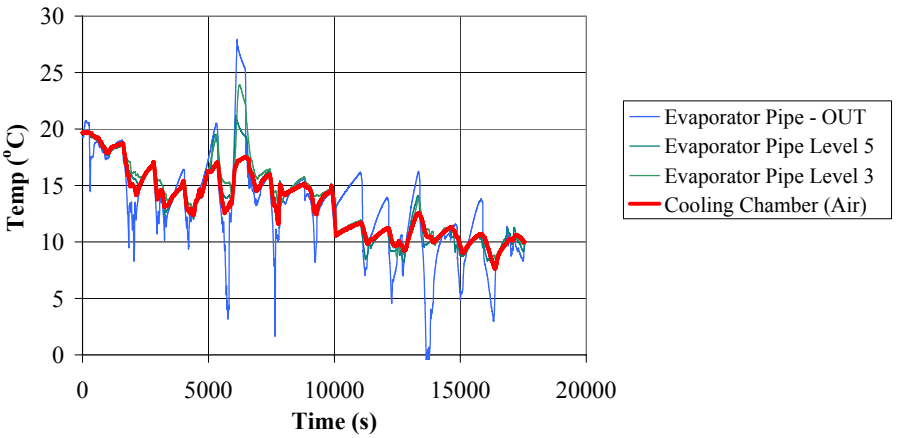

Figure 7.5: Temperature against time plot(DLC 53-54)

Using the relative masses and specific heat capacities of the cool-box contents, the method described in section 7.2 was used to estimate the cooling power (Q_e) of the

system. The cooling power over short intervals, e.g. t=2900-3100 and t=7500-7800, was in line with design point conditions, 160 W and 91 W respectively, however the average performance across the full data range was low (≈ 20W) The primary reason for the poor performance was the significant fluctuations in jet-pump performance caused by the required frequency and duration of charge cycles (CD ratio 1:2). Consequently, the evaporator temperature increases significantly (2-3 K) during each reservoir charging operation. It should also be noted that the cycle durations are irregular due to the manual control method.

Test Data: DLC 65

As discussed in section 6.2, prior to the commissioning of EP3, various simulation tests were carried out on EP2 to assess the benefits of the proposed updates. This led to a revised EP2 operating sequence, with charge cycles initiated before the generator had been allowed to run dry. This sequence allowed more consistent cooling to be achieved and increased the CD ratio to 1:6. This operation sequence is detailed in table 6.2.

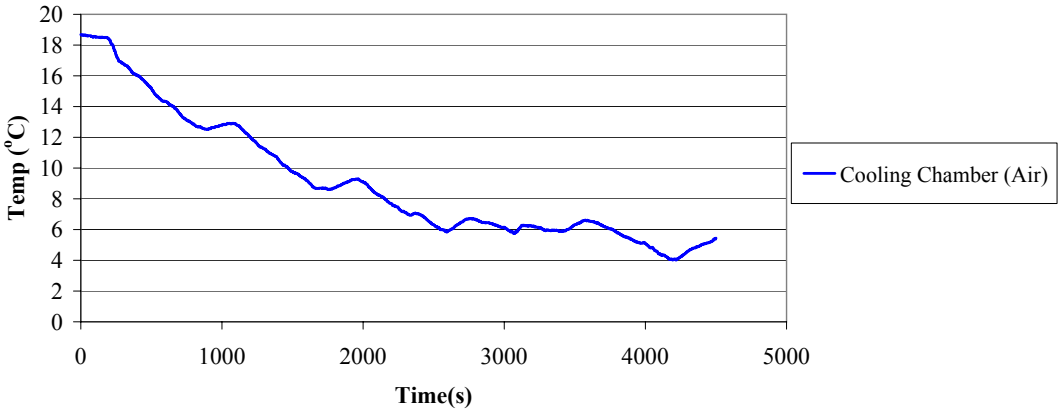

Figure 7.6: Cooling chamber air temperature against time (DLC 65)

The plot in figure 7.6 shows that the air temperature inside the cool-box fell from 19°C to 4°C in just over an hour. Proportionately longer periods of jet-pump operation allowed more effective cooling to be achieved. Based on a theoretical thermal mass of 18.35 kJ/K and a uniform temperature within the evaporator the methods previously discussed in section 7.2 can be used to calculate evaporator cooling rates. This performance is equivalent to an average evaporator cooling capacity (Q_e) of 65.5 W (122 W peak).

These experimental test results coupled with the simulation test data helped analyse the potential benefits of the proposed reservoir transfer solution discussed in sub-section 6.2.2.

7.4.3 EP2: Results Discussion

Despite crude evaporator liquid level control and inherent losses during the charge cycle, EP2 yielded promising results showing that, if only for limited periods, the jet-pump was capable of generating design point cooling. The apparatus also served as a development tool, providing jet-pump characterisation data (see section 5.7.3), and reservoir transfer concept simulations (see section 6.2).

7.5 EP3: Operational Test Data

The section of the chapter contains a selection of results obtained during the final optimisation testing of EP3.

A number of significant changes were made to the experimental prototype from version EP2 to EP3. Most importantly, with the addition of TEV controlled evaporator liquid

levels and PLC control of valving operations, the apparatus was now fully autonomous. This allowed for much longer experiment durations and a larger duty load (24L of water) to be used. In addition, EP3 had pressure transducers installed at key locations in the system. Data on temperature, mass flow rate and system pressures could be logged on equipment that could run autonomously, for periods of 8 hrs or more.

There were several other important changes that were made in the evolution of EP2 to EP3 and these are summarised below;

Generator

The generator subsystem was the primary focus of development attention for EP3, and a new, four reservoir fluid delivery system was manufactured. The pressures within both the new condenser and generator reservoirs are plotted separately to illustrate system operation. Various other improvements were also made to the generator sub-system (as detailed in section 6.3) including the re-specification of the heat transfer oil and and a new oil pump which provided more accurate flow measurement data and reduced energy consumption.

The method of generator vapour separation was also revisited and a second heat exchanger was installed to ensure a source of dry superheated vapour for the jet-pump.

Evaporator

In addition to the installation of a TEV (throttled from 300 W capacity to 130 W using capillary pipe), the final solution also employed a flow damper (buffer zone), located at the desired liquid height within the evaporator chamber. This update was implemented

from DLC 98 onwards and is discussed in more detail in section 6.5.1. It is important to note that the effective thermal mass of the cool box contents are marginally increased due to the increase in copper mass within the evaporator (1.21 kg to 3.11 kg)

Condenser

The condenser capacity was increased and a new piping arrangement routing reverse flow from the condenser reservoir (following charge cycles) to the inlet of the condenser. These improvements are discussed in more detail in section 6.4. During the final experimental tests of EP3, an array of low power fans were installed on the condenser to test the benefits offered by forced convection (see DLC 124).

Although generator pressures are typically lower (28.5 bara) than the design point operating pressures (32.4 bara) this corresponds to a lower critical condenser pressure (8.5 bar versus 10.7 bar design point) at a normal lab ambient temperatures of 21°C.

7.5.1 EP3: Scope of Collected Data

The data collected from the EP3 is used to present the optimised performance of EP3 and, with the exception of forced convection condensing (see DLC 124), include all of the improvements summarised in the introduction to this chapter. Temperature data is collected across the evaporator pipe-work system at various heights, in addition to air and duty load (24 L water) temperatures. The $\frac{\delta T}{\delta t}$ data from each thermocouple is then used to calculate the total cooling load.

7.5.2 EP3: Selected Operational Test Data

A selection of three experimental datasets are provided and discussed, showing examples of the performance of the system in reducing the temperature of a fixed duty load (24 litres of water) The experiments begin with a duty load temperature of approximately 20°C and illustrate the varying performance of the system as the evaporator load temperature decreases. The selected datasets also show the marginal effect of adjusted timings for the control sequence of reservoir valving.

- **DLC 113:** This data set is examined in detail and is used to highlight some of the experimental difficulties encountered. In order to reveal the effects of these difficulties, a time interval resolution of 5 cycles (harmonised with the cycle actuation command) was examined when evaluating system COP.
- **DLC 119:** This dataset provides an example of the experimental results that were obtained when the previously mentioned experimental difficulties caused minimal effect.
- **DLC 124:** A third dataset is also included which shows the effect of forced convection across the condenser. This data helps to illustrate the effect of the enhanced convection offered by a mild breeze in outdoor conditions. The framework of this research does not include an evaluation of the reliability, and associated cost of fans as a system component or the historical, seasonal wind speeds in suggested territories. Dataset DLC 124 is included as a prelude to the suggested areas of research contained in the conclusions chapter of this thesis.

Test Data: DLC 113

Following the construction of EP3 and subsequent, previously discussed, updates (evaporator buffer zone etc) a 10hr operational test was conducted with the oil flow and transfer procedure valving controlled autonomously. Despite the control systems working without fault, the performance of the system was limited by two mechanical issues. In addition, a section of the data was lost due to a fault with the data-logging software. This data-set (DLC 113) has been included here to highlight some of the experimental difficulties that were encountered throughout the development.

The first of the two mechanical issues that caused performance issues was the failure of the NRV on the suction line of the ejector. This valve failed in the open condition, which allowed high pressure vapour to enter the evaporator during charge cycles of the reservoir transfer procedure. This problem was overcome by manual operation of the ball valve on the suction line however performance was still inevitably adversely affected.

Secondly, the TEV became blocked intermittently during the test, preventing effective control of evaporator liquid level. Although this problem only occurred intermittently, the overall cooling performance will be reduced.

It is thought that the reason for these two component malfunctions was metal debris blocking the sealing faces. This entered the system from the reclaimed pipe-work used to construct the evaporator and condenser. It is likely that corrosion had also taken place within each of the reservoirs following the introduction of water for the hydrostatic pressure tests. Residual water can also cause problems if temperatures drop below freezing point and ice formation is another potential cause of the TEV malfunction. In production, the pipe-work would be tested using nitrogen gas and these types of issue

would not be an issue.

In addition, a software crash caused some of the data to become corrupted (time t = 17,200-23,700). The time period for this section of data is known and therefore the full data set still has relevance.

The effects of TEV malfunction are illustrated in figure 7.7. The various temperatures of evaporator pipework and the duty load (24 L water) are plotted against time. When the TEV is jammed closed, refrigerant flow into the evaporator is restricted and the liquid level falls. The effect on the evaporator temperature, across EL1 and EL3, is significant with temperatures reaching sub-zero levels on several occasions. This malfunction was thought to be caused by residual water freezing in the expansion orifice of the TEV. This intermittent malfunction is apparent at t = 16,000 and several more times from from t=27,500 onwards.

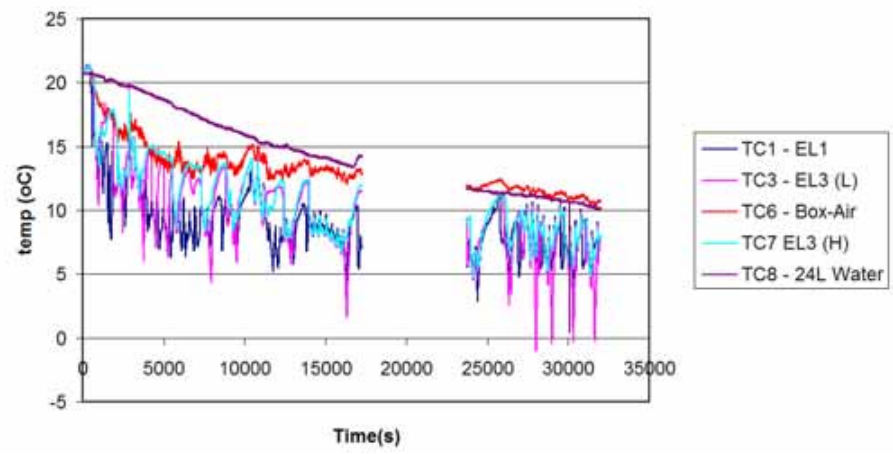

Figure 7.7: Cool box temperatures against time plot (DLC 113)

As discussed previously in section 7.3.3, measuring the COP of the system instantaneously is impractical and therefore Q_g and Q_e are averaged over 5 cycle

intervals to provide system COP values. These intervals were initially plotted over fixed durations, however comparative analysis of results revealed that harmonising the results with PLC command signals (i.e. liquid level switch cycle actuation) provides a closer correlation between system performance and the experimentally observed reasons for fluctuating performance.

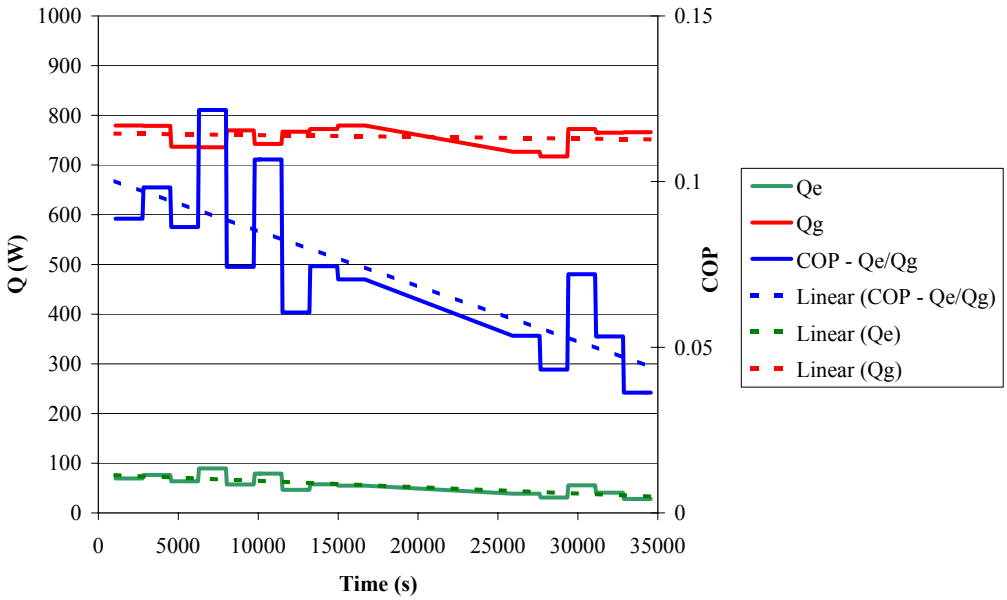

Figure 7.8: Q/COP against time (DLC 113)

Figure 7.8 shows Q_g, Q_e and system cycle COP (secondary Y-axis) against time. As Q_g stays relatively constant, it is apparent that the COP has a proportionate relationship with Q_e.

Referring, in parallel, to figure 7.7 and 7.8, the effect of the suction line NRV jamming open at time t=7,500s clearly has a sharp effect on the evaporator temperature and consequently, the 5 cycle COP for the next period drops by almost 40%.

When the COP is over-layed with temperature data collected from the primary duty

load (as shown in figure 7.9) the correlation between evaporator temperature and overall COP is clear, illustrating the practical limitations of the system. The effects of experimental error (as presented in appendix I should not be overlooked however this error is reduced when evaluating the COP over longer durations. The COP of the system during the first 20 cycles (at $T_e \approx 14.5$°C is 0.095 ± 0.011).

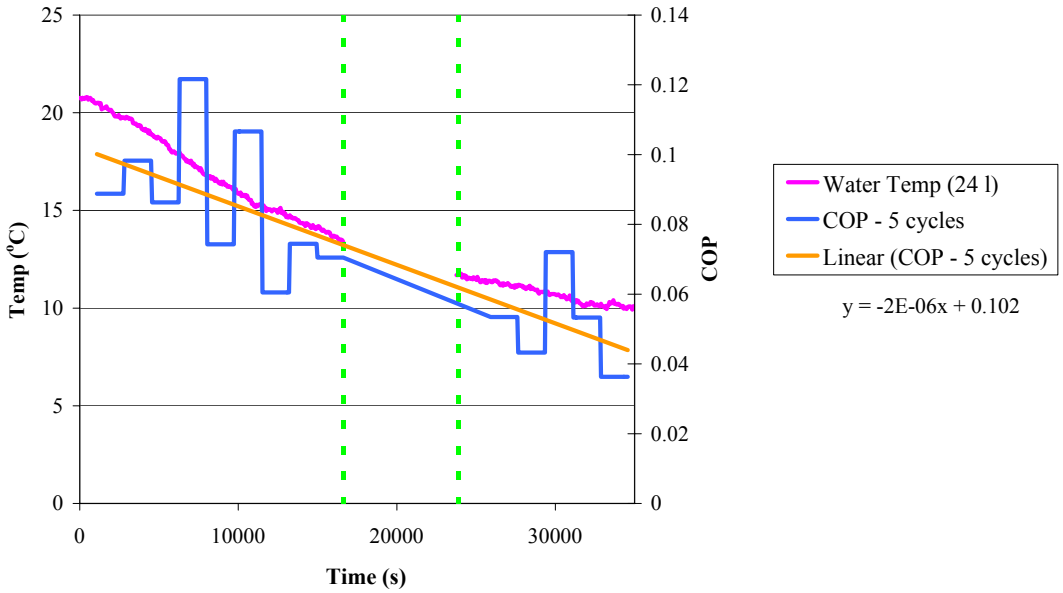

Figure 7.9: Temp 24 l/COP water against time (DLC 113)

Although the system is capable of delivering design point cooling capacity initially, maintaining this performance became increasingly difficult at lower temperatures.

As discussed in subsection 6.5.2, the NRV was replaced and additionally supported by a bespoke filter. The filter of the TEV was also changed and general maintenance of the system (condenser filter/drier replacement) conducted before the system was recommissioned for subsequent testing.

Test Data : DLC 119

With the valve repairs and maintenance completed following DLC 113, DLC 119 is now presented for direct comparison. The performance of the system, particularly at lower temperatures has improved however the apparatus did not operate entirely without fault. Closer inspection of the temperature data revealed that although the problem with the suction line NRV had been solved, accurate control of the evaporator liquid level continued to prove challenging. It is thought that the intermittent performance (variable flow rate) of the TEV was caused by corrosion debris or, as is more apparent at lower temperatures, water ice crystals forming in the TEV expansion orifice.

The DLC control software was programmed with a full cycle duration of approximately 380 s and figure7.10 shows the 5 cycle interval performance of the system across a 7 hr period. As shown in 7.11 the temperature of the the duty load (24 L water) was reduced from 23°C to 12.5°C during the test, and the relationship between evaporator temperature and system COP is clearly illustrated.

At the evaporator temperature falls from 20°C down to 6°C, the 5 cycle COP falls from 0.137 maximum to 0.04 minimum. These values should be interpreted with due consideration to experimental error (as presented in appendix I. Experimental error can be reduced by considering the COP over longer durations. The COP of the system at $T_e \approx 10$°C (across 20 cycles) is 0.094 ± 0.011 and at at $T_e \approx 5$°C (across 20 cycles) the experimental COP is 0.085 ± 0.010.

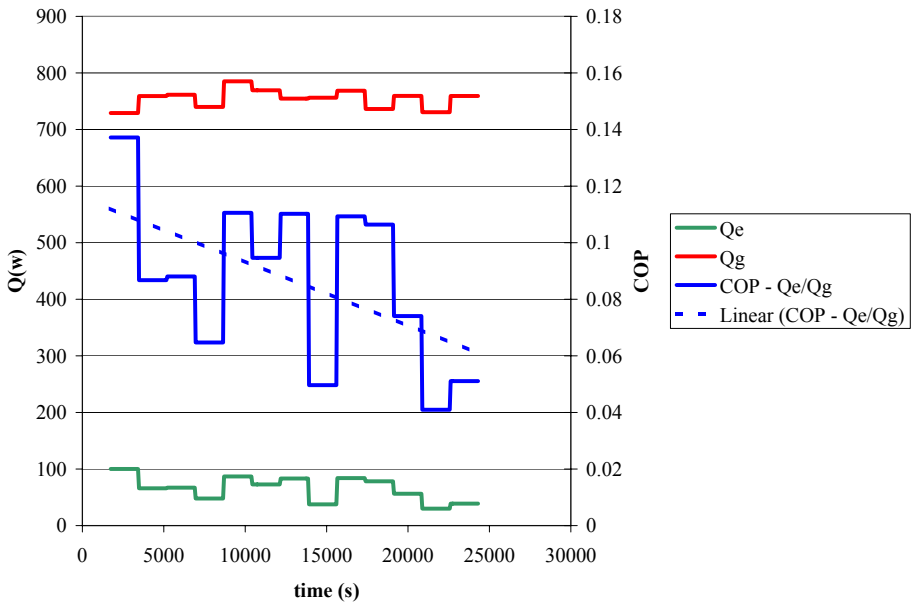

Figure 7.10: Q/COP against time (DLC 119)

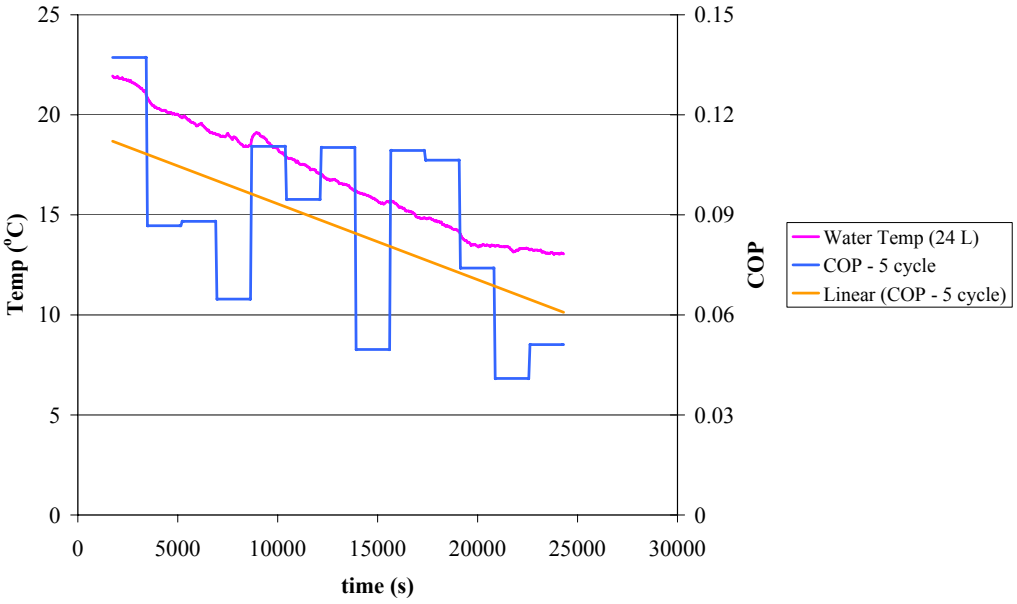

Figure 7.11: T/COP against time (DLC-119)

Test Data: DLC 124

Following completion of the final testing of the system under design point conditions, a supplementary research exercise was conducted to determine the effect of forced convection across the condenser heat exchanger. This exercise helped to illustrate the potential benefits of electric fans (or wind effects) on system performance. An array of low power fans (totalling 6 W electrical demand at continuous maximum speed operation) were installed underneath the condenser heat exchanger. A 3 hr test was conducted and the performance of the system was significantly improved. At evaporator temperatures of 3°C (24 L water duty load = 12.5°C), when supported with forced convection cooling of the condenser, the jet pump cooling circuit could achieve COPs in excess of 0.1 for the entire duration of the experiment (see figure 7.12). The relative effect of these fans was to reduce the working pressure of the condenser from $\backsim$ 9 bar to $\backsim$ 8 bar.

What becomes apparent, when the pressure data for DLC-124 pressure is over-layed with comparable experimental data from the system without forced convection (DLC-119) is that the reduced condenser pressure leads to lower generator mass flow rates (also a higher R_m and lower p_e) and therefore an increase in overall cycle duration. The synchronised pressure data is shown in figure 7.13.

The secondary benefit of lower generator mass flow is that the required refrigerant charge cycle frequency is reduced by $\backsim$ 20% which, in terms of the required electrical input, almost entirely offsets the 6W required for continuous operation of the forced convection fans.

The stabilising effect of forced convection condensing is also apparent when reviewing

figure 7.13. The condenser pressure remains stable at ∽ 8 bar and this allows more consistent cooling to be achieved.

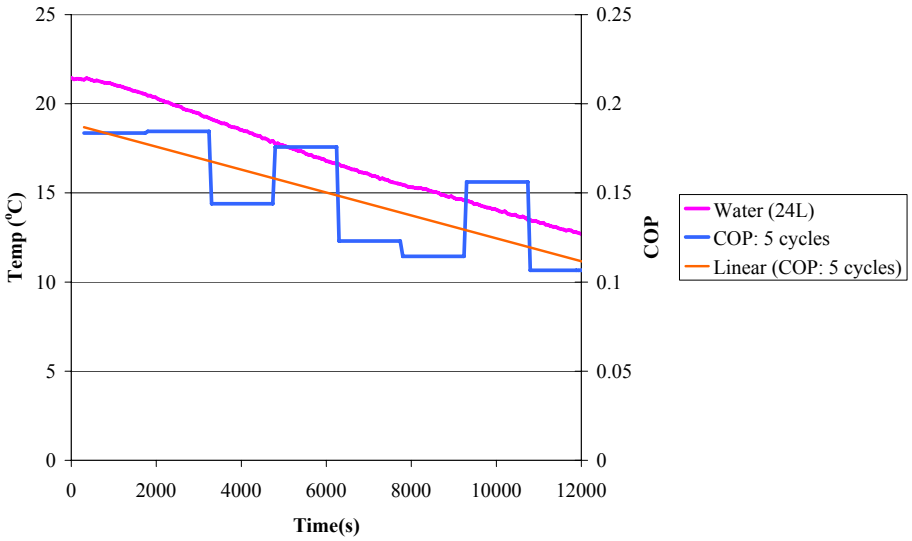

Figure 7.12: Water temperature and COP against time (DLC-124)

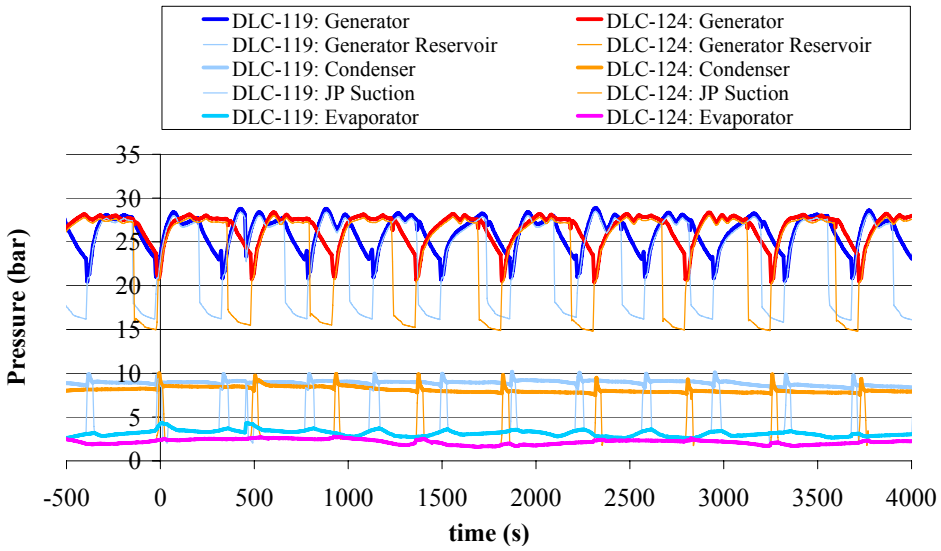

Figure 7.13: Synchronised Pressure Plot : DLC 119 and DLC 124

7.6 Chapter Conclusion

7.6.1 EP3: Results Discussion

The presence of residual water (from hydrostatic testing) continued to cause problems with the operation of both the TEV and the suction line check valve at refrigerant temperatures below 0°C. Nitrogen pressure testing of pipe-work would be recommended for the development of future experimental apparatus to avoid this problem.

Despite these issues, EP3 was able to deliver cooling capacities of 80-175 W. Maintaining performance at the design point conditions was sometimes difficult, however the principles of automated control systems were demonstrated. Considering the dataset DLC 119 specifically, the experimental COP of the system at $T_e \approx 10$°C (across 20 cycles) was 0.094 ± 0.011 and at at $T_e \approx 5$°C (across 20 cycles) 0.085 ± 0.010. These results include the propagated error of 12% as defined in appendix I.

The effect of forced convection condensing (see DLC 124), even at low air flow rates, was significant and illustrates that, at lower evaporator temperatures, the jet-pump performance is more sensitive to higher condenser pressures.

7.6.2 Effects of Thermal Energy Losses Due to RTS

With reference to figure 7.14 the thermal energy requirement of the RTS (originally discussed in section 5.5.6) can be reappraised.

As the charge cycle is operated more frequently (once every 380 s) the mass of recently condensed fluid available for transfer is reduced to 0.985 kg (based on $\dot{m}_{con} = 4.46$ g/s).

The thermal energy is required to operate each CD cycle is therefore reduced to (47.5 kJ). Based on a the new CD cycle duration (380 s) the thermal power required to run the cycle ($\dot{Q}_{RTS}$ is 125 W. The experimental data for DLC-119 provides a mean generator heat rate of 755 W, and therefore the percentage of generator power required to operate the CD cycle is 16.6%. This is in-line with the performance reported by comparable experimental studies (10-20% [39][40]).

If this thermal energy was discounted from the generator thermal input value (to simulate replacement of the RTS with an electrically powered pump) the COP_{cycle} of the system would be increased to from 0.085 to 0.101 at T_e = 5°C (DLC-119).

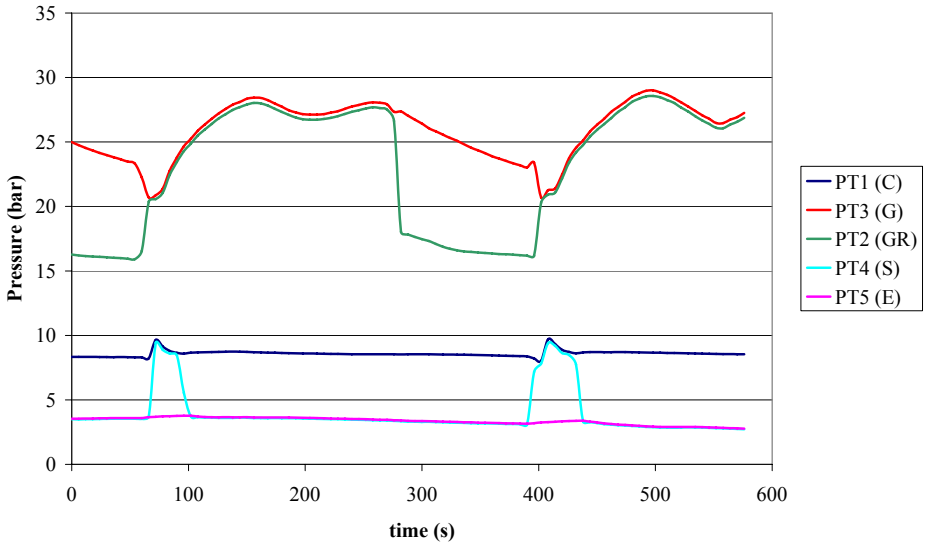

Figure 7.14: DLC 119 Pressure Plot Extract

Chapter 8

Technology Limitations and Applications Research

8.1 Introduction

The practical limitations of the $\approx 100W$ jet-pump system have been experimentally demonstrated and this chapter provides both a review of these limitations and a theoretical/conceptual review of alternate applications of the technology.

An estimate of the initial capital costs of the proposed jet-pump refrigeration system is presented and discussed. Alternate applications for the technology are also presented and conceptually reviewed (e.g. dual-mode heating and cooling). The chapter concludes with a review of the business case for solar powered vaccine refrigerators and discussion of innovative models that could help to subsidise further development.

8.2 Production Design Concept for Solar Powered Jet-Pump Vaccine Refrigerator

A production design for a solar thermal jet-pump vaccine refrigerator was conceived that employs articulated solar panels and canvas cladding to provide convenient transport functionality and quick installation. Manufacturing processes also needed to be considered and low-cost technologies (such as press-forming) are proposed. Where relevant, the production design has also drawn reference from the relevant WHO standards (e.g. control interface and locking system).

The use of an aluminium frame would allow for a lighter construction, facilitating easier transport in less developed regions. Aluminium is also less prone to the effects of corrosion when the painted surface is damaged which could be an important benefit in wet/humid climates. A robust frame is important as the PDS (see section 4.12) defines that the product should be maintenance free.

The use of an vacuum-formed liner (made from durable copolyester), insulated with expanded polyurethane foam is proposed for the internal construction of the cool-box. The cool-box will incorporate two refrigerated compartments. The main, top-loading, compartment houses the bulk store of medicines and vaccines, along with 100 L of phase change material that helps to regulate the temperatures of the cool box. This compartment would only be opened infrequently (maximum of twice daily) to load or unload vaccines. As per the WHO guidelines, this main compartment would be fitted with a lock to prevent unauthorised access or accidental opening. Access to the compartment would be via pin entry on a key pad, mitigating the issues associated with key loss. The key-pad would be located on the main control interface panel and LCD

technology would be used to minimise power consumption. The display would simple to interpret, providing just the current temperatures and estimated hold-over time. The hold-over time is defined as the amount of time (in hours) that the refrigerator can maintain the temperature (+2°C to +8°C) without further solar energy input. The control interface would also incorporate an audio and visual warning signal to alert the user if the temperature fell outside of this specification. An illustration of the proposed control interface is shown in figure 8.1. As the jet-pump system requires thermal energy

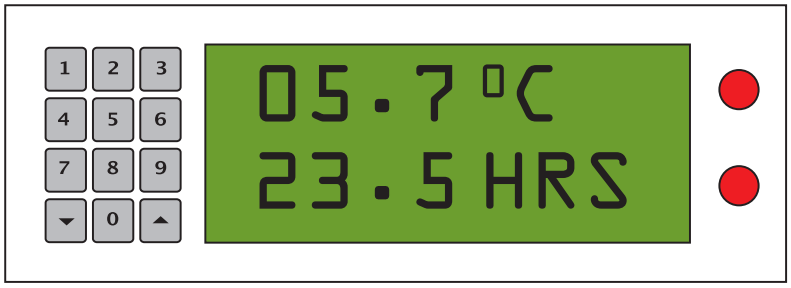

Figure 8.1: Illustration of proposed control interface

to operate, there is very little requirement for electrical energy outside periods of effective solar irradiation, therefore solar direct drive (SDD) technologies could be used and only a small nickel metal hydride battery would be required (0.2 kWh). During normal operation, the main compartment would not be opened when the system was in sleep mode (i.e overnight) as any immediate rise in temperature could not be quickly overcome by the jet-pump cooling cycle. It is important to note however that the PCM tanks also provide a cooling effect (driven by the energy needed for phase change) to maintain the temperature inside the compartment. Achieving effective insulation of the cool-box will greatly effect the achievable hold-over time and careful design and materials selection would be required.

The cool-box would also be fitted with a smaller, secondary compartment which could be

used throughout the day for the storage of vaccines between patient treatments. Figure 8.2 shows the proposed product architecture, illustrating the various mechanical configurations used for shipping, local transport and erected deployment. The vertical arrangement of the system components replicates the layout of the prototype system EP3. The jet-pump is located at the highest point, feeding the condenser which is also located at the top of the system. In this production concept, the condenser is assisted by forced convection fans which draw air up, out of the canvas enclosure and across the condenser array. The reservoir transfer system and generator circuit are housed within the two main support pillars.

Figure 8.2 illustrates the use of four multifunctional beams. During international shipping, these provide fixing points for protective wooden cladding. These beams also provide the ability to secure the product and contents overnight if required. The image in top right shows how these same beams can be used as carrying poles for transporting manually over short distances. The weight of the product would be limited to 100 kg (as specified in PDS : section 4.12) to allow four people to transport the unit safely (one on each end of the two poles). These same poles are then used as props to support the deployed solar array panels and canvas covers.

As discussed previously, a large percentage of the available cool-box volume will be taken by the evaporator pipe work, phase change material (PCM) tanks and surrounding air. The remaining volume will be used to store vaccines. Vaccines are typically supplied in glass vials, however pre-filled syringes are also available. The physical size of these vaccine packages is dependant on the number of doses contained. A 10 dose vial is the most space efficient ($3cm^3$ [72]) however this approach leads to higher vaccine wastage [12] and a higher risk of contamination. Pre-filled, single dose syringes simplifies the logistical elements of vaccine delivery programmes however the physical size of the drug

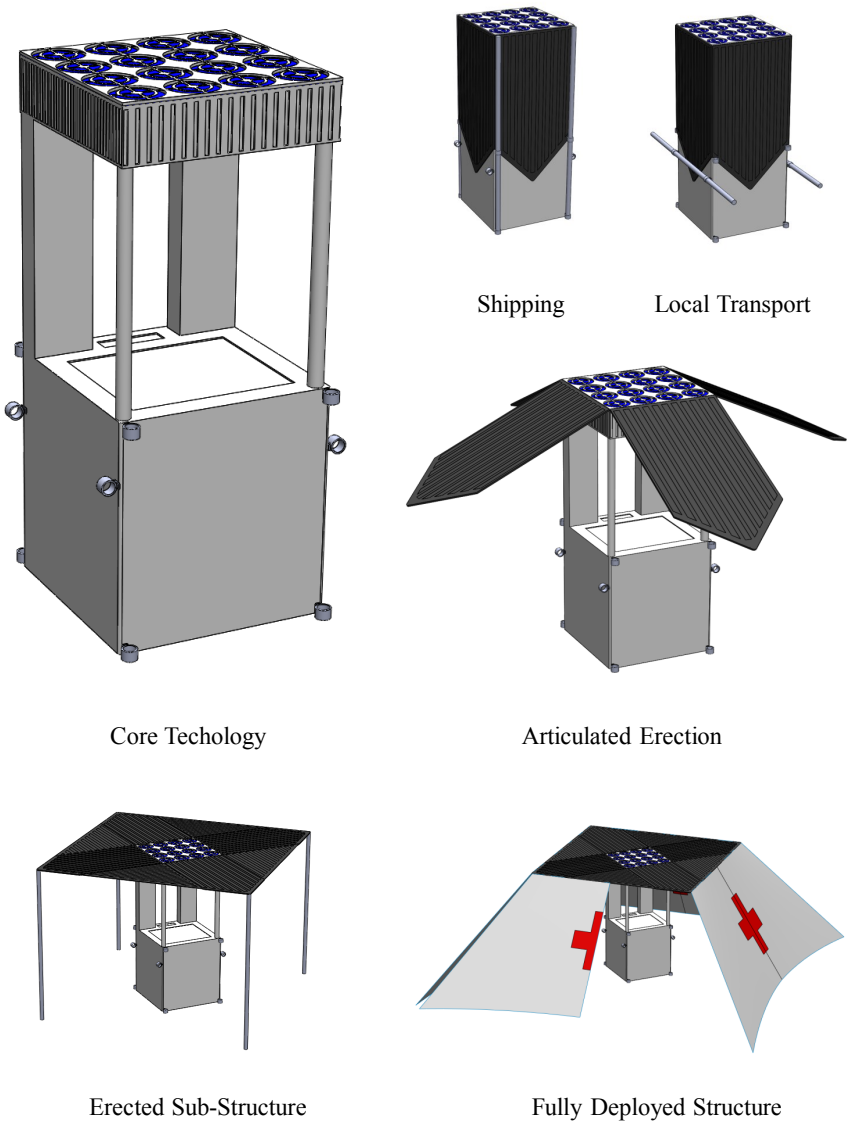

Figure 8.2: Illustration of jet-pump powered vaccination station

packaging should not be overlooked. Based on an available storage volume of 100 L, up to 4,000 pre-filled syringes could be stored in the cool-box.

Although the packaging material will effect the cooling rate of the vials, it is crucial that the vaccines are delivered to the solar-powered refrigerator already at the design point temperature (+2°C to +8°C) they will be maintained at, therefore the effects of the packaging heat transfer rates are negligible.

8.3 Technology Limitations

The results from operational tests of the prototype have shown that the jet-pump theory is robust however the small capacity ($\approx$ 100 W) has proven to be a limiting factor, both in terms of cost and practical implementation. For the purposes of cost evaluation, mass manufacturing quantities have been based around 10,000 p.a. as this represents the approximate volume at which the amortised cost of fixtures and tooling becomes negligible in relation to part cost. The small capacity of the system has proven to be a significant factor when evaluating the cost/kW. This is partly due to the relatively high cost of the electrically actuated valves used to control the reservoir CD cycle. The key practical limitations of working with a low capacity jet-pump system are summarised below;

- The geometry and dimensional tolerances of both the nozzle and diffuser will be difficult to achieve at smaller scales using conventional mass-manufacturing techniques.
- Although the generator fluid delivery system is both novel and electrically efficient (<50 W), the additional cost of the electrically actuated valves and fluid reservoirs

should not be understated (approximately £200-250 at 10,000 units p.a.)

- Control of the liquid level within the flooded evaporator has proven to be challenging and the solutions trialled in this study have provided variable performance. A more reliable, mechanically simple method of liquid level management would need to be achieved for cost-effective operation.

These limitations provide significant technical hurdles which must be overcome in order to provide low-capacity jet-pump cooling systems at a commercially viable cost. The limitations described above are proportionally decreased in significance as the scale and cooling capacity of the system increases. Considering the items in sequence;

- Manufacture of jet-pump : injection moulding or die-casting techniques would be better suited to a jet-pump of larger throat size.
- Transfer of refrigerant between low pressure and high pressure circuits: Specification of a low-power positive displacement pump, rated at generator / condenser pressure differential would be possible given larger flow rates. Alternatively, the cost of the valves and reservoirs used in this study would not increase dramatically as the scale of the system increased, therefore this capital burden would be proportionately much less significant.
- Evaporator liquid level management: A float ball fluid regulator would be possible given larger evaporator capacities.

Larger cooling capacities are typically associated with industrial applications or air conditioning (AC).

Achieving the design point evaporator temperature (6°C) has also proven challenging. At fixed generator temperatures (and fixed Q_g), the COP of the jet-pump is directly proportional to Q_e. As the evaporator temperature decreases, and the secondary inlet pressure falls, so does the COP of the system making it increasingly difficult to reach lower temperatures.

Experimental evaluation of forced convection heat rejection at the condenser has confirmed the importance of working close to the system operating conditions and this should also be considered as a limiting factor for any jet-pump driven cooling system.

8.3.1 Production Cost Estimates

Although the total cost of the prototype (including manufacturing costs at £20 per hour) was in excess of £6,000, the production cost estimate (at volumes of 10,000 units per annum) has been estimated at under £700. Although this falls outside ambitious initial targets (sub £500), the breakdown of costs illustrated in figure 8.3 can act as a tool for future researchers to identify the key areas where cost reduction is specifically needed.

What is particularly relevant to note is that proportional cost for manufacturing the jet-pump (22%) and total system assembly cost (43%) fall considerably at production volumes (6% and 21% respectively. This is in contrast to the marked increase in the proportional cost of the generator sub-system components (20% up to 32%) and collector circuit (5% up to 18%).

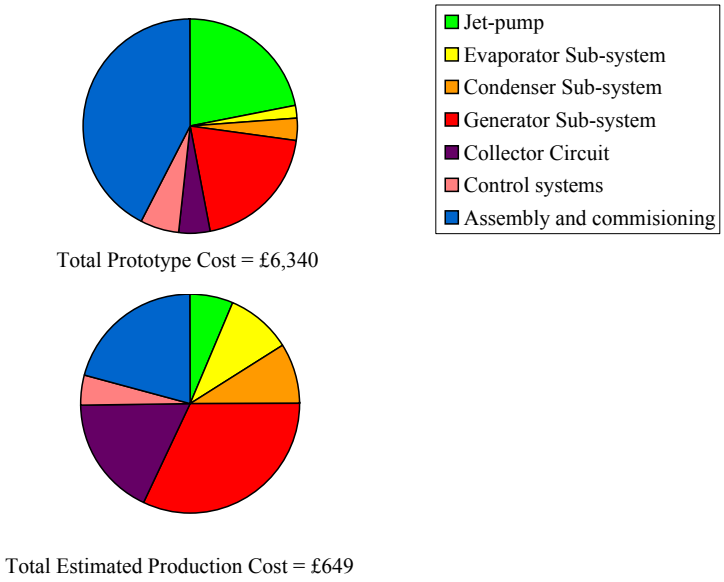

Figure 8.3: Summary of prototype and estimated production costs

8.4 Other Applications for the Jet-Pump Cooling Cycle

As part of this research, a broad review of current solar powered cooling technologies has been undertaken, with specific attention being focussed on the availability of low-cost autonomous solutions for off grid applications. The potential for solar-powered cooling technologies is vast, both in application specific systems and as a vehicle to reduce carbon emissions more generally. As part of the literature review, various low-cost solar powered cooling technologies were identified, however the relative simplicity of jet-pump driven systems continue to represent an attractive alternative. As the jet-pump cooling circuit is almost entirely thermo-mechanical, the manufacturing cost will continue to fall as the manufacturing quantity increases. Applications for low capacity (100 W) jet-pump cooling systems have been identified within several fields including medical (vaccine storage), commercial (vending machines) and consumer (luxury garden fridge) fields.

The use of system as a vaccine storage system to meet WHO requirements for vaccine refrigerators [54] has not been fully demonstrated, however the opportunities for the system in off-grid medical applications are still considered significant. Kukil Hans design concept [73] for a solar-powered mobile hospital could be enhanced using thermally powered jet-pump cooling systems; if not for vaccine storage then to enhance patient comfort via the provision of AC.

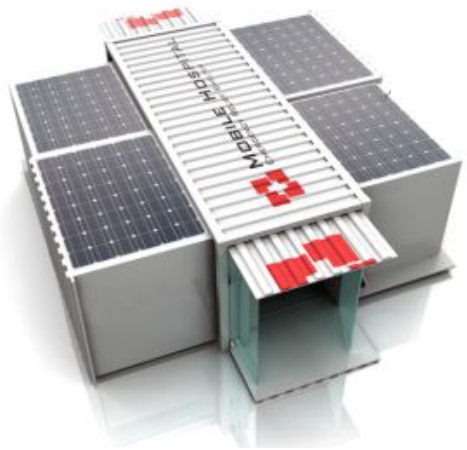

Figure 8.4: Illustration of solar powered mobile hospital - reproduced from [73]

As previously discussed, a number of opportunities to remove or reduce some of the technical challenges of jet-pump cooling are offered when working at higher evaporator temperatures or larger cooling capacities. Air-conditioning meets both of these requirements and has previously been considered as an application for the jet-pump cooling cycle.

8.4.1 Air-conditioning

The higher evaporator temperatures (approximately 10-20°C) and larger capacity (several kW) of air-conditioning units make them a good candidate for thermally

powered jet-pump cooling systems.

Prof I.W. Eames had previously proposed and, in collaboration with IDC Ltd, designed and built a jet-pump driven air conditioning prototype [74]. This system, powered by a 3 kW generator (equivalent to 6 m^2 flat plate collectors) at 110 °C, could experimentally achieve COPs in excess of 0.5. Based on the data collected, the performance characteristics illustrated in figure 8.5 were estimated.

What should not be overlooked when evaluating a system of this nature is the required condenser surface area. Referring to the results mentioned above; the 3 kW of heat added at the generator and 1.5 kW added at the evaporator need to be dissipated as 4.5 kW heat from the condenser. As space for the outdoor mounting of a condenser unit is sometimes limited, it is very likely that forced convection would need to be employed to reduce the overall footprint of the condenser unit. More novel techniques such as evaporative cooling could also be considered to improve the space efficiency of such a unit. As mentioned previously, forced convection would also likely reduce the overall cost of the condenser.

The generator fluid delivery mechanism represented a large percentage of overall cost for the refrigeration system described in this thesis, however this cost will not increase significantly as the system is scaled up therefore the cost/kW would decrease. It is also possible that an electrically powered pump may offer the most efficient and cost effective solution (for generator fluid delivery) for a system of larger capacity. This was not possible on the 100 W system due to the requirement for high pressure differential ($\backsim$20 bar) and low mass flow (4.5 g/s). The cost of the prototype and estimated future production costs (based on 10,000 units per annum) is discussed in more detail in section 8.3.

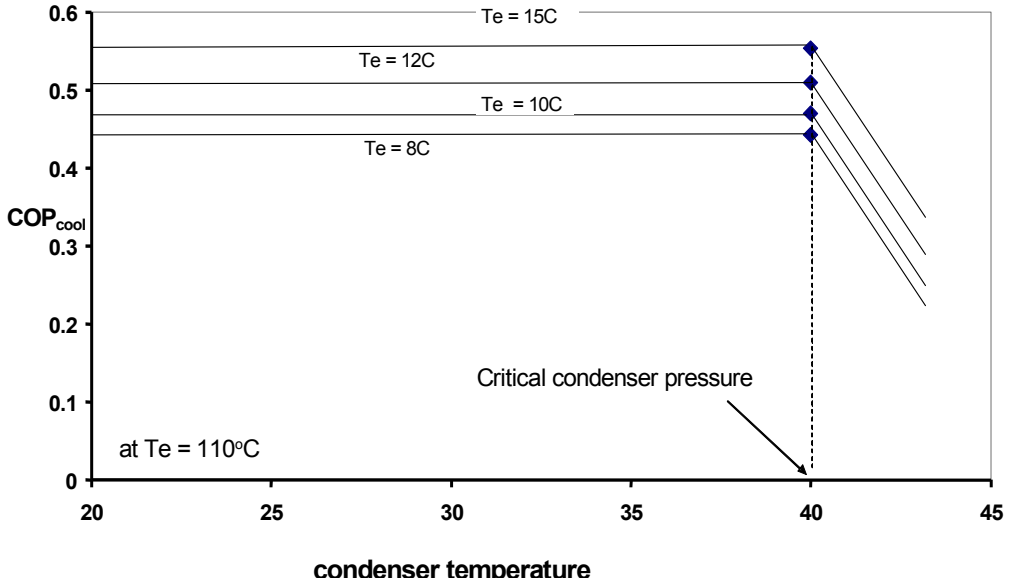

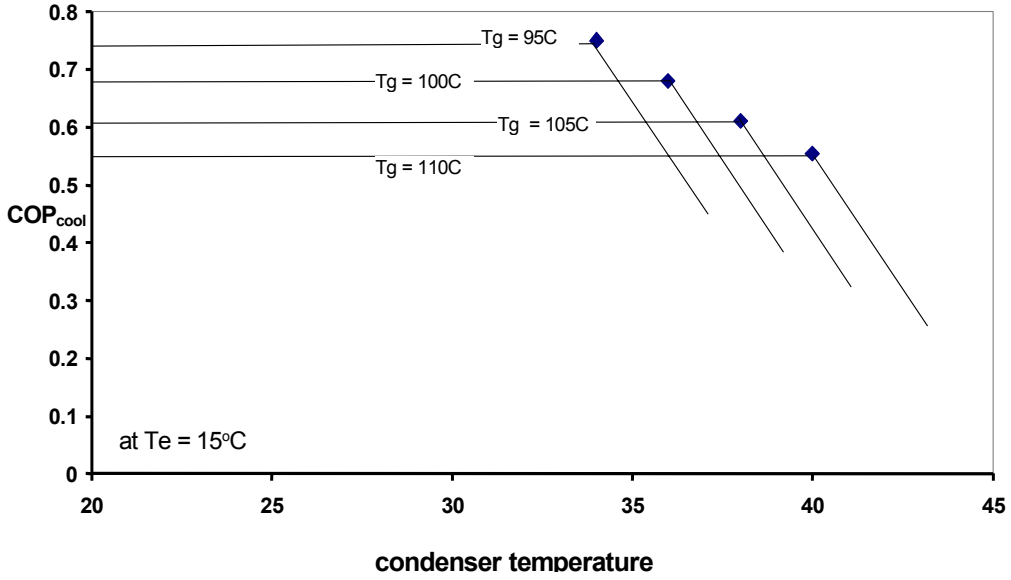

Figure 8.5: Predictions of AC performance

8.4.2 Dual Mode AC and Space Heater System

A paper, co-written by the author of this thesis, titled *'Development of solar thermal heating and cooling systems using the jet-pump cycle'* was presented to delegates at the 1st IIR International Conference on the Cold Chain and Sustainability in Cambridge on 30th March 2010 [74]. This paper described both the research work of this thesis and a summary of prior work conducted at IDC on the development of a jet-pump powered air-conditioning prototype. The paper went on to propose a modular system that would provide AC during hotter periods via the jet-pump cooling circuit and also heating via the same evaporator during colder periods. Theoretical performances of the system, in three seasonal modes, is presented in figure 8.6 showing the working temperatures and heat transfer rates. These estimates are based on the AC prototype experimental results previously described, with a 10% improvement on COP (from 0.55 to 0.6). As outlined, the system would be rated to deliver 4.5 kW cooling during Summer months, and 2-4 kW heating during Autumn/Winter months.

The proposed installation is illustrated in figure 8.7 and simplified schematics of the system in both heating and cooling modes is shown in figure 8.8

Based upon the assumptions laid out in table 8.1, the primary quantitative benefits of the system is an energy saving of approximately 1 tonne CO_2 per annum with significant further savings when space heating loads and hot water system augmentation are taken into account.

Mode	Location	Temperature Refrigerant (^oC)	Temperature Air On (^oC)	Temperature Air Off (^oC)	Power (kW)
Cooling (Summer) Solar input = 500 W/m^2	Evaporator	15	24	21	4.5
	Generator	109	-	-	7.5
	Condenser	37	28	33	12
Heating (Spring/Autumn) Solar input = 300 W/m^2	Evaporator	43	22	30	4
	Generator	45	-	-	4.5
Heating (Winter) Solar Input 150 W/m^2	Evaporator	33	22	26	2
	Generator	35	-	-	2.25

Figure 8.6: Theoretical performance data for combined AC and heating

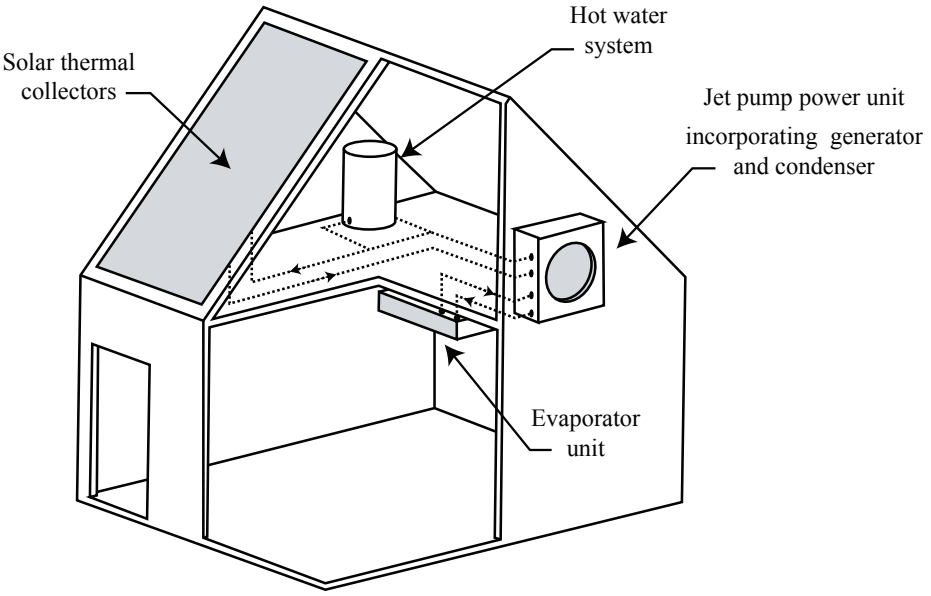

Figure 8.7: Illustration showing dual function system installed in house

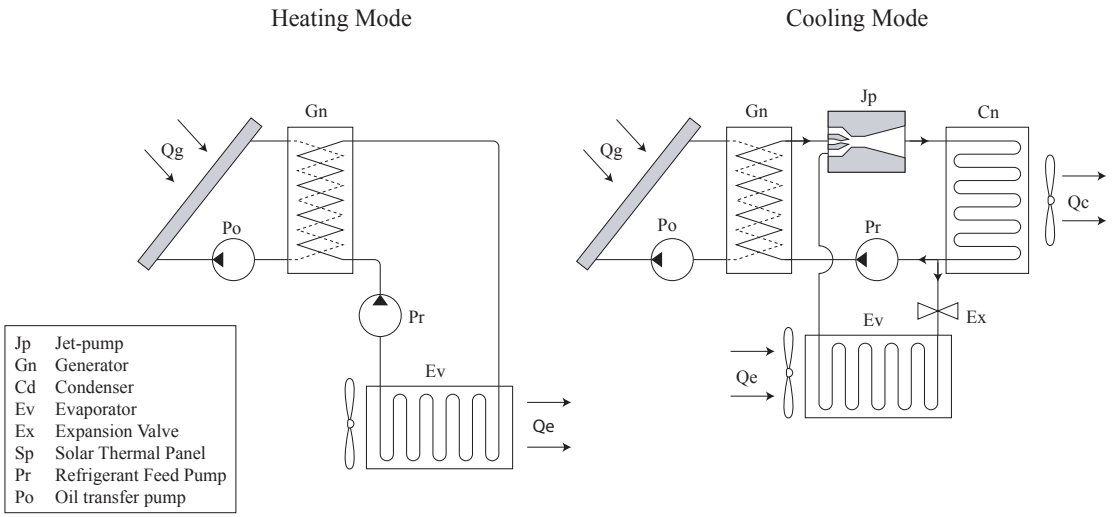

Figure 8.8: Schematic layout of proposed system in heating and cooling mode

Cooling Load	Qe	4.5 kW load
Standard vapour compression AC	COP	2
Thermally powered jet pump AC	COP_{cool}	0.6
CO_2 emissions for UK electricity usage*	W_{CO2}	0.537 kg kWhr-1
Annual Use	t_{ann}	800 hrs

* Carbon Trust 2008 [75]

Table 8.1: Assumptions for energy saving calculation

8.4.3 Industrial Applications

Due to the mechanical simplicity (no moving parts) of the jet-pump it has found numerous applications across a range of industrial applications. Companies like Croll Reynolds design and manufacture jet-pumps for the petro-chemical industry, the pharmaceutical industry and the food processing industry. In these applications, the primary flow is normally steam and rather than a cooling effect and the jet-pump is used to provide motive force (i.e. suction). In these types of industrial applications, it is much easier to control the operating conditions and obtain optimal performance from the jet-pump.

8.4.4 Concept Applications

As part of a knowledge sharing exercise, the physical dimensions of the system, shown in section 8.9 were presented to students at Kingston University as a technology design brief. The jet-pump system mechanics were given only as black box dimensions and the students were invited to conceptualize applications and configurations for the technology. Their concept submissions, a selection of which are shown in figure 8.10, suggested a number of interesting avenues for future development.

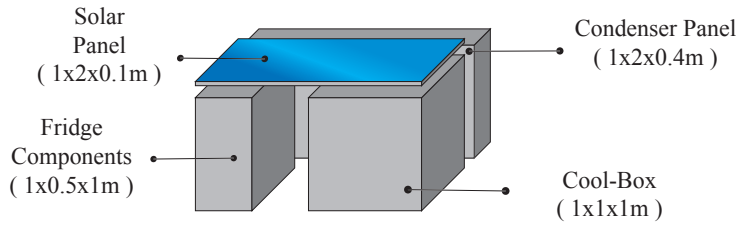

Figure 8.9: Approximate Volume Ratio of System

A : Solar Vaccine Station

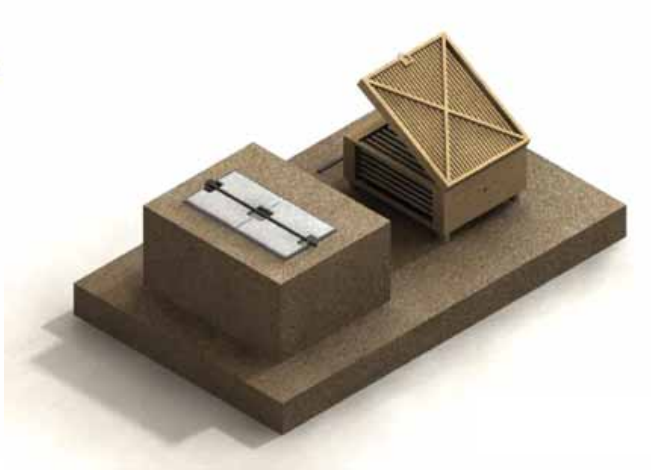

B : Insulation sourced from local materials

C : Mobile Refrigerated Vending

D : Chilled water dispenser

Figure 8.10: Selection of concepts from Kingston University design student project

8.5 Funding Models

The relative cost of a solar powered vaccine refrigerator must be amortised over it's 10 year working life. In order to assess the relative cost of the system in terms of vaccines administered, it is also necessary to approximate the number of patients that can be treated every year per system. Based on an average of 30 patients being vaccinated every day across the lifetime of the product, the total number of vaccinations administered per refrigerator would be 110,000. Assuming a target vaccination program of 100% for every live birth and taking Africa as an example (where over 50% of the population live without access to mains electricity [13]) 17.5M children would have required vaccine administration each year (based on 2014 African birth statistics [76]). These estimates show that 1,600 new solar powered vaccine refrigerators are required every year for the African continent alone. Extending this to the annual global requirement, it is estimated that 2K new products are required annually. As this only represents 20% of the figure used for manufacturing cost estimates (10K p.a.), innovative funding models must be adopted to meet the shortfall.

A number of alternate applications for the system have been identified that could help to subsidise the development and roll-out of small capacity ($\approx$ 100 W) solar powered jet-pump refrigerators.

- **Cold drinks / food vending:** Numerous opportunities exist for the use of solar powered refrigeration in the developed world for (e.g. festivals, golf-courses, beaches etc. These units could be branded to attract corporate sponsorship. If applicable, higher cost component technologies (such as concentrating parabolic collectors) to improve the performance of the system.

- **Transport applications :** including refrigerators for the camping, sailing and road haulage markets.
- **Luxury goods :** Solar powered garden or pool drinks fridges
- **Eco-tourism :** In the provision of refrigeration for eco-resorts and remote travel locations

It may also be possible to license proprietary technologies used in the system for other applications. The low power pumping system (reservoir transfer system) provides one potential opportunity however the potential applications for this technology are limited (i.e. low flow, high pressure differential pumping where $\backsim$ 1 m of vertical height is available)

8.6 Chapter Conclusions

A production design concept for the solar powered jet-pump vaccine refrigerator has been presented and discussed. The limitations of the technology have been outlined and the relative costs estimated. In particular, the challenges associated with small capacity applications has been reviewed. Although the experimental work of this study did not manage to meet the WHO requirements for vaccine refrigerators, the study did demonstrate methods of operation that could be applied to parallel applications. A number of concept applications (e.g. dual mode heating and cooling) have been presented and reviewed as potential areas for future research. The business case for solar powered vaccine refrigerators has been reviewed and innovative funding models presented that may provide subsidised development opportunities.

Chapter 9

Conclusions

9.1 Introduction

Following identification of a gap in existing knowledge, a research proposition was presented to experimentally evaluate the potential of the jet-pump cycle in providing solar-powered, small capacity (≈100 W) refrigeration. In order to evaluate the system as a practical solution for off-grid vaccine storage, the relevant WHO guidelines were used as a specification tool ($T_e = 6°C$). This application also meant that the capital cost per kW cooling load was of particular interest. Due to the relatively high current cost per kW of photovoltaic versus thermal collectors, the electrical demand of auxiliary components was kept to a minimum (< 50 W). In one key instance reducing the electrical input resulted in a 16.6% increase in the thermal energy requirement (i.e. the generator fluid delivery sub-system). A preliminary review of the likely production manufacturing costs (see section 8.3.1) indicates the cost per kW of this system would not be competitive with existing technologies (e.g. photovoltaic power vapour

compression systems) however the opportunity for further cost reduction still exists .

A prototype system was experimentally investigated, optimised and then automated to allow the collection of repeatable datasets. The experimental prototypes made use of appropriate technology (e.g. no cooling water circuits). A summary of the key experimental results is reviewed herewith followed by an evaluation of the research outcomes and original contributions to knowledge. Further guidance and suggested avenues of research are also offered for those wishing to conduct future work in this area.

9.2 Experimental Results

Of particular interest to readers, are the results collected from the experimental prototype systems. COP was used as a key metric in this study. Maintaining performance is increasingly difficult at lower evaporator temperatures and achieving a COP above 0.1 at evaporator liquid temperatures below 10 °C proved difficult.

This section of the chapter provides a summary of the experimental difficulties that were encountered, the key performance data and the limitations of the system.

9.2.1 Experimental Difficulties

As described earlier in this thesis, residual water within the system (following hydrostatic pressure testing) was attributed as the cause of intermittent and temporary failure of several valve seals.

The evaporator sub system was particularly vulnerable to the effects of these component malfunctions and numerous attempts were made to eradicate the problem (component

replacement, vacuum pump evacuation etc) however this continued to hamper system performance, particularly at lower temperatures. These seal failures were likely caused by either corrosion debris or ice formation.

9.2.2 Key Performance Data

10 hr data-sets were collected using automated control systems and despite the experimental difficulties mentioned above, repeatable cooling performance was achieved. Although COPs in excess of 0.15 were measured, maintaining this efficiency at lower evaporator temperatures was not possible.

A total of 124 data-sets were collected, spanning the three iterations of the prototype (EP1, EP2 and EP3). 52 of these data-sets were specific to the final, automated system (EP3) which could repeatedly cool a duty load of 24 litres of water from 21 °C to 10 °C in around 9 hrs. During this period, the linear trend COP of the system decreases from approximately 0.12 initially ($Q_e \approx 100W$) to 0.06 $Q_e \approx 50W$) at lower temperatures. Considering the dataset DLC 119 specifically, the experimental COP of the system at $T_e \approx 5$°C (across 20 cycles) was 0.085 $\pm$ 0.01.

As the evaporator temperature decreases, so does the critical condenser pressure causing the mixed flow to become choked within the mixing section of the diffuser. Assuming the thermal energy available from the generator is fixed, the lowest evaporator temperature is dependent on the ambient conditions.

Forced convection condensing experiments, carried out late in the testing phase of this research, verify that the system is sensitive to small changes in condenser temperatures. One option, to avoid the requirement for electrical fans to be added would be to increase

the surface area of the condenser allowing natural convection to have a greater effect. It is important to consider however that the condenser, array used in EP3 is of considerable surface area (12.5 m^2), and would cost in excess of £50 even at bulk ordering volumes, therefore the relative merits of fan assisted convection should be further assessed.

9.3 Evaluation of Prototype Against PDS

A product design specification for solar powered vaccine refrigerators (table 4.3), based on WHO guidelines, was previously presented in section 4.12.

- **Refrigerator Temperature :** Achieved the PDS requirement of 6°C
- **Ambient Temperature :** Tested in ambient temperatures of 25°C however testing at PDS of 32°C was not possible as no environmental test chamber was available
- **Cooling Capacity :** Achieved the PDS requirement of 100 W
- **Holdover Period :** The holdover period, is defined as the time in hours that the vaccine compartment will remain between +2°C and +10°C at the maximum ambient temperature (32°C) after the system is turned off [14]. Given experimentally known losses (U·A) of 1.41 W/K, an estimated cool-box thermal mass (m·C_p) of 113 kJ and assuming a uniform start and end temperature of 6°C and +10°C respectively, it is possible to calculate a holdover time of 3.7 hours via equation 5.1. This exceeds the PDS requirement of 1.5 hours. It is important to note that achieving this holdover time relies heavily on the thermal mass of the 24 L water duty load.

- **User Requirements :** Achieved the PDS requirement of fully autonomous operation however ISO 20282-1: 2006 not evaluated as part of this study
- **Electrical Requirements :** Achieved the PDS requirement by employing 24V DC electrical components suited to photovoltaic source
- **Product Lifecycle (MTBF) :** Not evaluated as part of this study.
- **Size :** 1,600 x 1,000 x 1,850 mm. This did not meet the PDS requirement of 710 x 710 x 1700 mm however the prototype was intentionally made larger to facilitate data-collection and ease of development modifications.
- **Weight :** Did not meet the PDS requirement of 100 kg (approximate weight was 120 kg) however this could be significantly reduced (≈50%) by using aluminium frame construction rather than MDF.
- **Corrosion Resistance :** Not evaluated as part of this study.
- **Electrical Safety :** Control box designed in line with IEC 60335-1.
- **Refrigerant :** R134a is compliant with the Montreal Protocol, meeting the PDS requirement.
- **Ingress Protection :** Not evaluated as part of this study.
- **Estimated manufacturing cost :** As decribed in section 8.3.1 the PDS target production cost of £500 was not met. The estimated cost of the system, based on production quantities of 10,000 units per annum, was £700.

The implementation of design requirements, specific to a thermally powered jet-pump driven vaccine refrigerator system (i.e. generator phase separation, minimal reliance on electrical energy, natural convection heat transfer, the use of a flooded evaporator and

adjustable position of the jet-pump nozzle) are all described in more detail elsewhere in this chapter. The use of existing production technologies has been employed (or simulated) where possible to approximate the performance characteristics of a mass-manufactured product and practical consideration has also been given to the final use scenario (i.e. no secondary heat sinks).

9.4 Research Outcomes

Following review of the current technologies and identification of a gap in existing knowledge, an experimental study was devised to investigate the potential of jet-pump technology in providing autonomous cooling at small scales. The investigation has overcome significant technical challenges to highlight both the strengths and limitations of the system. Knowledge has been gained throughout the investigation which will help to inform future studies, including the development of a novel, low-power fluid delivery sub-system. The experimental study has met the original research aims and a summary of the outcomes is listed below;

- Assessed competing technologies and identified gap in existing knowledge
- Provided a theoretical system specification for a 100 W jet-pump refrigerator (derived from WHO standards for solar powered vaccine refrigerators)
- Provided manufacturing design data for adjustable geometry jet-pump based on prior work (both experimental and theoretical), first principles calculations and CFD analysis [55]. This design is specific to the system operating conditions and the use of R134a as a refrigerant however could be easily scaled for larger cooling capacities.

- Experimentally optimised jet-pump geometry and validated CFD predictions [55].
- Experimentally characterised the effects of both generator pressure and condenser pressure on jet-pump performance
- Theoretically calculated and experimentally evaluated ;
  - evaporator cool-box losses.
  - evaporator cool-box thermal mass.
  - thermal energy balance of reservoir transfer system.
- Developed and refined experimental jet-pump driven apparatus through three iterations (EP1, EP2 and EP3) with the use of appropriate technologies, parts and materials to assess practical and economic benefits of system (including avoidance of reliance on cold water circuits).
  - Manufactured and experimentally evaluated a low power method of transporting refrigerant fluid from the condenser to the generator ($\Delta p \approx 20$ bar): i.e. the EP2 generator feed system.
  - Utilised the EP2 test apparatus for simulation experiments to inform the development of a novel generator feed system (EP3) that reduced charge cycle durations and condenser loading.
  - Minimised the electrical energy requirements of the system (< 50 W).
  - Experimentally evaluated condenser and evaporator heat exchangers manufactured from reclaimed pipework.
  - Experimentally evaluated the use of natural convection, for the transfer of heat at the evaporator and condenser, as an alternative to electrically powered (fan-driven) forced convection.

  - Experimentally evaluated the benefits of a forced convection condenser.
  - Experimentally evaluated methods of controlling the liquid height in a flooded evaporator without the use of a float valve including development of an evaporator "buffer zone"
  - Experimentally tested two methods of generator vapour phase separation.
  - Experimentally tested the implementation of a suction line heat recovery circuit.

- Specified and experimentally verified automated control systems including
  - Specification of system feedback and control methods.
  - Definition an automated control system operating procedure.
  - Collection of experimental data over extended test durations (10 hrs).
  - Definition of typical performance behaviour for automated system.

- Provided method for evaluation of the system including;
  - Defined time interval for COP evaluation of system.
  - Assessed error and experimental uncertainty and applied to results.

- Reported experimental results
  - Achieved experimental cooling power of 100 W (175 W max) (though not at design point evaporator temperature)
  - Achieved experimental COP in excess of 0.1 (though not at design point evaporator temperature)

- Evaluated practical limitations of system including

  - Provided estimated manufacturing costs for both the experimental prototype and a production volume equivalent
  - Identified other applications for the technology, supported by theoretical calculations

9.5 Contributions to Knowledge

The literature review and research proposition identified specific research opportunities and this experimental study has resulted in several original contributions to knowledge. Although the system did not achieve design point cooling, the experimental results show that a small scale ($\approx$ 100 W) jet-pump cooling system, constructed with the use of *appropriate* technologies, can achieve COPs in excess of 0.1 at evaporator temperatures above 10°C. Appropriate technologies, in this context, refers to a focus on the electrical energy requirements of the system and the absence of cooling water circuits.

- Reported on the experimental results collected from a small capacity ($\approx$100 W) jet pump refrigeration system operating with R134a and compared results against theoretical performance.
- Experimentally investigated the practical implementation of jet-pump refrigerator, as an entire system, with the use of appropriate technologies, including;
  - Avoidance of cooling water circuits.
  - Minimal reliance on electricity and moving parts (e.g. natural convection heat transfer employed at evaporator and condenser).
  - Use of a flooded evaporator to mitigate against the effects of charge/discharge cycling.

  - Use of a novel generator feed system that utilises fluid reservoirs and automated valve sequencing to achieve electrically efficient transfer of refrigerant.
  - Adaptive, automated control systems to provide effective jet-pump operation outside of design point conditions

- Used experimental results (COP) to assess the practical limitations of the system including evaluation of the likely manufacturing costs.

9.6 Future Work

This section of the concluding chapter provides some useful advice for those wishing to continue the research into low capacity jet-pump refrigeration systems. It begins with review of the experimental issues that were encountered with a view to providing future readers with a road map to avoiding the same difficulties. A discussion of the commercial development opportunities is then provided including a conceptual specification for EP4, the next planned iteration of the experimental system. Finally, a review of the opportunities for further research is presented, including some ambitious ideas to improve system efficiency.

9.6.1 Recommendations for Future Experimental Studies

A number of lessons for future researchers have been identified.

- **Pressure Testing :** Testing the pressure integrity of the pipework should be completed using nitrogen at an accredited facility. Eradicating residual water from

hydrostatic pressure tests was a time-consuming and expensive activity. The water also caused corrosion and damage to many of the small moving parts within the prototype apparatus.

- **Data-logging:** The use of a 16 channel, or 32 channel temperature data logger would be recommended to achieve a more detailed picture of system operating conditions.
- **Data management:** Decide on and implement a clear variable naming convention when logging data. Do this as early as possible to prevent any confusion in the future.
- **Leak finding:** Do not underestimate the effectiveness of washing-up liquid solution applied with a paintbrush.

9.6.2 Commercial Development Opportunities

A draft specification for EP4 was created and initial planning for manufacture was made, however funding for this research was subsequently withdrawn.

Several companies including *Manor Concepts, Pitkin & Ruddock, and Energy Technique* all appraised the project and could offer significant development and manufacturing expertise however one company, *Polestar*, provided the most compelling proposition. With previous experience in developing solar powered refrigerators, and a range of in-house manufacturing facilities (including acrylic vacuum forming and expanded polyurethane foaming) they are a suitably qualified development partner. These manufacturing technologies would reduce the cool-box conductive losses and more closely simulate a mass manufactured solution. *Polestar* also provided a competitive quote

(£8,000-12,000 for an EP4 prototype and £900 per system (plus material costs) for subsequent small batch production runs).

The specification of the system would have remained largely unchanged, however the following items would have been updated;

- All pipe-work re-manufactured and pressure tested using nitrogen to prevent the previous problems with internal corrosion and residual water
- Component specification reduced where possible to minimise cost
- Thermostatic control of oil circuit enhanced with proportional integral derivative (PID) loops to smooth out fluctuations in generator pressure
- Fans added to both condenser and evaporator heat exchangers to asses the benefits of forced convection heat transfer
- Cool-box re-manufactured using production techniques to minimise conductive losses
- 32 channel data-logger installed to provide a more detailed picture of system conditions

9.6.3 Scope for Further Research

Given the benefit of more time and resources, the author believes that significant gains can be achieved to address the issues of performance and cost per kW cooling. A selection of some of the ideas that could help to meet this challenge are provided in the list below.

- A secondary jet-pump, located in parallel to the primary jet-pump could provide the system with the flexibility to work over a wider range of operating conditions (e.g lower generator pressures or higher condenser temperatures). Flow could be diverted to the chosen jet-pump using a three-way ABV. A smaller diameter nozzle throat area could provide lower evaporator temperatures, however the critical condenser pressure would also fall.

- A variable geometry jet-pump could offer similar benefits to multiple jet-pumps. Implementation methods that could be considered include variable nozzle position (NXP), possibly achieved with servo drive, and variable throat diameters, possibly achieved with inflatable membranes. The performance benefit would have to be evaluated against capital cost.

- Not discussed in any detail within this thesis is the fact that the prototype system is only capable of delivering useful cooling during the hours of effective solar irradiance. The use of phase change materials (PCMs) could help to extend this operational range to 24 hrs however the capacity of the system would have to be significantly larger to ensure sufficient "ice" was formed during peak irradiance hours. Some photovoltaic powered VC systems (e.g. Dulas VC200SDD) employ a similar system that uses a water chamber, surrounding the refrigerated compartment, to achieve the same result.

- Development of a low-cost float ball valve to replace the TEV ensuring accurate control over evaporator liquid level management. This would ensure that the evaporator was performing optimally in a charge discharge cycle scenario

- Development of a reservoir transfer system that provides continuous operation of the jet-pump. This development would prove advantageous for several reasons, not least of which are the benefits associated with continuous refrigerant flow through

the evaporator. Rather than rely on electrically actuated valves, the new system could employ a bi-stable, thermally activated transfer mechanism. The system could also be designed to transfer refrigerant with the use of a piston pump, employing pressure differentials and mechanical advantage.

- The potential to maximises heat gain from the panels, whilst still delivering on-demand flow to the generator could be exploited with the use of a secondary oil pump or flow diversion valve. As with all potential enhancements, the benefit must be assessed in relation to initial capital expenditure.

- With the appropriate design and materials selection, it may be possible to remove the need for an oil circuit entirely and route the refrigerant directly through the solar thermal collectors. The engineering challenges of this idea are considerable however worthy of further investigation.

- The implementation of jet-pump technology in a dual mode (heating and cooling) system could be further considered (as previously described in section 8.4.2. As this system is dependant on solar irradiation, augmenting the system with a bivalent heat pump could be considered during winter months.

- The use of new refrigerants (e.g. HFO's) to evaluate the performance of the jet-pump system operating with working fluids that exceed the current F-gas regulations for ODP and GWP[77].

- Developments in the field of solar thermal collectors (e.g. selective surfaces) and heat exchangers (e.g. metal foams) could provide routes to improving the practical application of the jet-pump refrigerator.

- A study of a multi-function generator that could also be powered from stove heat (fire)

- Transient/dynamic mathematical modelling of the system
- Development of a theoretical model for country specific climates

9.7 Conclusion

When evaluating jet-pump technology as a simple solution to the challenges of vaccine storage in off-grid locations, the practical development of prototype apparatus has elucidated some of the key difficulties in achieving an economical solution when working at low cooling capacities (≈100 W).

In particular, the difficulties in transporting refrigerant, at low flow rates, from the condenser to the evaporator and from the condenser to the generator were highlighted.

Control of the liquid level within a small capacity flooded evaporator is an area where further research and development is required to achieve a simple but reliable mechanism at low cost. Although this study did not achieve precise control of the evaporator liquid level, elements of the design did prove effective in mitigating the effects of intermittent suction (i.e. evaporator buffer zone).

The other major challenge of operating with low flow rates is the transfer of refrigerant fluid from the condenser to the high pressure generator. Significant progress was achieved in this respect and benefits of a two stage reservoir transfer mechanism have been reported and evaluated.

The experimental testing of EP3 has shown that 100 W cooling at a COP of 0.1 is achievable, however, sustaining this performance at lower evaporator temperatures (6°C) was not possible. The author strongly believes that with sufficient development effort,

and innovative design approaches, a portable incarnation of this technology for vaccine storage could be possible. Ensuring that the system makes use of mechanically simple components with minimal moving parts, requiring little or no maintenance, could one day provide a cost effective solution to the challenge of low-cost, low-capacity refrigeration in off-grid locations.

References

[1] Abdulateef J.W., Sopian K., Alghoul M.A., and Sulaiman M.Y. Review on solar-driven ejector refrigeration technologies. *Renewable and Sustainable Energy Reviews*, 13:1338–1349, 2009.

[2] MIT Technology Review. A billlion people in the dark, 2012 [Online]Available from. `www.technologyreview.com/featuredstory/429529/how-solar-based-microgrids-could-bring-power-to-millions/`. [Accessed 28 August 2013].

[3] World Health Organisation. Immunisation service delivery: Projected vaccine wastage [Online] Available from. `apps.who.int/immunisation_delivery/systems_policy/logistics_projected_wastage/en/index.html`. [Accessed 25 October 2014].

[4] Plotkin S.L. and Plotkin S.A. *Vaccines*, chapter 1 - A Short History of Vaccination, pages 1–15. Elsevier Saunders, Philadelphia, 4th edition, 2004.

[5] World Health Organisation. Global and regional immunization profile : Global region [Online] Available from. `www.who.int/immunization/monitoring_surveillance/data/gs_gloprofile.pdf?ua=1`. [Accessed 25 August 2015].

[6] Ehreth J. The global value of vaccination. *Vaccine*, (21):596–600, 2003.

[7] World Health Organisation. Immunisation coverage: Fact sheet number 378 [Online] Available from. `www.who.int/mediacentre/factsheets/fs378/en`. [Accessed 25 October 2014].

[8] Barnighausen T., Bloom D.E, Canning D., Friedman A., Levine O., O'Brien J., Privor-Dumm L., and Walker D. The economic case for expanding vaccination coverage of children. Program on the Global Demography of Aging - Working Paper Series, 2009.

[9] Otten M., Kezaala R., Fall A., Masresha B., Martin R, Cairns L., Eggers R., Biellik R., Grabowsky M., Strebel P., Okwo-Bele J.M., and Nshimirimana D. Public-health impact of accelerated measles control in the who african region 200003. *The Lancet*, 366(9488):832–839, 2005.

[10] Miller M.A. and Sentz J.T. *Disease and Mortality in Sub-Saharan Africa*, chapter 12 Vaccine-Preventable Diseases. World Bank, Washington (DC), 2nd edition, 2006.

[11] World Health Organisation. Antimicrobial resistance : Draft global action plan on antimicrobial resistance [Online] Available from. `http://apps.who.int/gb/ebwha/pdf_files/WHA68/A68_20-en.pdf?ua=1`, March 2015. [Accessed 25 August 2015].

[12] Brenzel L., Fox-Rushby J., Wolfson L.J., Miller M., and Halsey N.A. *Disease Control Priorities in Developing Countries - 2nd Edition*, chapter Chap 20 - Vaccine-Preventable diseases. World Bank, 2006.

[13] The Organisation for Economic Co-operation and Development (OECD)/International Energy Agency (IEA). World Energy Outlook 2012 [Online]

Available from.
http://www.worldenergyoutlook.org/media/weowebsite/energydevelopment/2012updates/Measuringprogresstowardsenergyforall.WEO2012.pdf. [Accessed 8 May 2014].

[14] Refrigerator or combined refrigerator and water-pack freezer: absorption cycle (PQS E003/RF02.2)[Online] Available from. http://www.who.int/immunization_standards/vaccine_quality/pqs_e03_rf2.2.pdf, July 2010. [Accessed September 2014].

[15] Marchio D. High efficiency and low environmental impact air-conditioning systems. Centre Énergtique et Procédés de l'Ecole des mines de Paris. [Online] Available from. www-cep.ensmp.fr/english/themes/syst/index.html, June 2005. [Accessed 20 July 2008].

[16] Jakob U. Solar cooling in europe [Online] Available from. www.solarnext.eu/pdf/ger/publications_presentations/jakob/09ausSCIG_conference_2009_Solar_Cooling_Europe, 2009. [Accessed 3rd November 2013].

[17] Seyboth K., Beurskens L., Langniss O., and Sims R.E.H. Recognising the potential for renewable energy heating and cooling. *Energy Policy*, 36(7):2460–2463, 2008.

[18] Cogeneration Technologies. Solar HVAC systems, 2008 [Online] Available from. www.cogeneration.net/solar_hvac_systems.htm. [Accessed 11 July 2008].

[19] Kim D.S. and Infante Ferreira C.A. Solar refrigeration options : A state-of-the-art review. *Int J Refrig*, 31:3–15, 2008.

[20] Beedie M. Solar argument heats up. Power Technology, 2008 [Online]Available from. www.power-technology.com/feature1480/. [Accessed 11 July 2008].

[21] Pridasaws W. *Solar-Driven Refrigeration Systems with Focus on the Ejector Cycle.* PhD thesis, School of Industrial Engineering and Management, Royal Institute of Technology, KTH, 2006.

[22] Reysa G. Solar water heating. build it solar: The renewable energy site for do-it-yourselfers. [Online] Available from. `www.builditsolar.com/Projects/WaterHeating/water_heating.htm`. [Accessed 20 July 2008].

[23] Eames I.W. Absorption refrigeration and jet pumps. In *Inst of Refrig*, volume 103, London, July 2007. Inst of Refrig.

[24] SunFrost. Sun Frost RFVB-134a Solar Powered Vaccine Storage DC Refrigerator Freezer. [Online] Available from. `www.sunfrost.com/vaccine_refrigerators.html`. [Accessed 22 July 2008].

[25] Feldman D., Barbose G., Margolis R., James T., Weaver S., Darghouth N., Fu R., Davidson C., Booth S, and Wiser R. Photovoltaic system pricing trends - historical, recent and near-term projections. Technical report, U.S. Dept of Energy, 2014.

[26] Pedersen P.H., Poulsen S., and Katic I. Solarchill a solar PV refrigerator without a battery. Danish Technologies Institute, Denmark. [Online] Available from. `www.solarchill.org/wp-content/uploads/2014/02/EuroSun2004_paper_254.pdf`. [Accessed 8 May 2012].

[27] Abdul-Wahab S.A., Elkamel A., Al-Damkhi A.M., Al-Habsi I.A., Al-Rubai'ey H.S., Al-Battashi A.K., Al-Tamimi A.R., Al-Mamari K.H., and Chutani M.U. Design and experimental investigation of portable solar thermoelectric refrigerator. *Renewable Energy*, 34(1):1–5, 2008.

[28] Chunnanond K. and Aphornratana S. Ejectors: applications in refrigeration technology. *Renewable and Sustainable Energy Reviews*, 8:129–155, 2004.

[29] Balaras C.A., Grossman G., Henning H., Infante Ferreira C.A., Podesser E., Wang L., and Wiemken E. Solar air conditioning in Europe: an overview. *Renewable and Sustainable Energy Reviews*, 11:299–314, 2007.

[30] Strickland L Kneass. *Practise and Theory of the Injector*. John Wiley and Son, 3rd edition, 1910.

[31] Eames I.W., Aphornratana S., and Haider H. A theoretical and experimental study of a small-scale steam jet refrigerator. *Int J Refrig*, 18(6):378–386, 1995.

[32] Selvaraju A. and Mani A. Experimental investigation on R134a vapour ejector refrigeration system. *Int J Refrig*, 29:1160–1166, 2006.

[33] Ablwaifa A. *A Theoretical and Experimental Investigation of a Jet-Pump Refrigeration System*. PhD thesis, University of Nottingham, May 2006.

[34] Grazzini G. and Mariani A. A simple program to design a multi-stage jet pump for refrigeration cycles. *Energy Conversion and Management*, 39(16):1827–1834, 1998.

[35] Aphornratana S. and Eames I.W. Experimental investigation of a combined ejector-absorption refrigerator. *Int J Refrig*, 22:195–207, 1998.

[36] Sun D. Solar powered combined ejector-vapour compression cycle for air conditioning and refrigeration. *Energy Conversion and Management*, 38(5):479–491, 1997.

[37] Hendricks T.J., Johnson V.H, and Keyser M.A. Heat generated cooling opportunities. Center for Transportation Technologies and Systems. National Renewable Energy Laboratory, Golden, Colorado. [Online] Available from.

http://www.nrel.gov.transportation/pdfs/heat_cooling.pdf. [Accessed 17 March 2011].

[38] Webster P. Toyota introduces new Denso A/C technology. *Automotive Engineering International*, pages 41–42, February 2008.

[39] Srisastra P., Aphornratana S., and Sriveerakul T. Development of a circulating system for a jet refrigeration cycle. *Int J Refrig*, 31(5):921–929, 2008.

[40] Huang B.J., Hu S.S, and Lee S.H. Development of an ejector cooling system with thermal pumping effect. *Int J Refrig*, 29(3):476–484, 2006.

[41] Wang J.H., Wu J.H., Hu S.S., and Huang B.J. Performance of ejector cooling system with thermal pumping effect using R141b and R365mfc. *Applied Thermal Engineering*, (29):1904–1912, 2009.

[42] Petrenko V.O., Huang B.J., and Shestopalov K.O. Innovative solar and waste heat driven ejector air conditioners and chillers. In *IPCBEE*, volume 6. IACSIT Press, 2011. 2nd International Conference on Environmental Science and Technology, Singapore.

[43] Nguyen V.M., Riffat S.B., and Doherty P.S. Development of a solar-powered passive ejector cooling system. *Applied Thermal Engineering*, (21):157–168, 2001.

[44] Sun D. Variable geometry ejectors and their applications in ejector refrigeration systems. *Energy*, 21(10):919–929, 1996.

[45] Sun D. Comparative study of the performance of an ejector refrigeration cycle operating with various refrigerants. *Energy Conversion and Management*, 40(8):873–884, 1999.

[46] Keenan J.H., Neumann E.P, and Lustwerk F. An investigation of ejector design by analysis and experiment. *ASME J Appl Mech Trans*, 72:299–309, 1950.

[47] Alexis G.K. and Karayiannis E.K. A solar ejector cooling system using refrigerant R134a in the athens area. *Renewable Energy*, 30:1457–1469, 2005.

[48] Pridasawas W. and Lundqvist P. A year-round dynamic simulation of a solar-driven ejector refrigeration system with iso-butane as a refrigerant. *International Journal of Refrigeration*, 30:840–850, 2006.

[49] Selvaraju A. and Mani A. Analysis of a vapour ejector refrigeration system with environment friendly refrigerants. *International Journal of Thermal Sciences*, 43:915–921, 2004.

[50] Anand S., Gupta A., and Tyagi S.K. Simulation studies of refrigeration cycles: A review. *Renewable and Sustainable Energy Reviews*, 17:260–277, 2013.

[51] Chen X., Ommer S., Worall M., and Riffat S. Recent developments in ejector refrigeration technologies. *Renewable and Sustainable Energy Reviews*, 19:629–651, 2013.

[52] Srinivasa Murthy S., Balasubramanian R., and Krishna Murthy M. Experiments on vapour jet refrigeration system suitable for solar energy aplications. *Renewable Energy*, 1(5/6):757–768, 1991.

[53] Yu J., Chen H., Ren Y., and Li Y. A new ejector refrigeration system with an additional jet pump. *Applied Thermal Engineering*, 26:312–319, 2006.

[54] World Health Organisation. E03 refrigerators and freezers for storing vaccines and freezing water-packs. [Online] Available from. `www.who.int/immunisation_`

standards/vaccine_quality/pqs_e03_fridges_freezers/en/. [Accessed September 2013].

[55] Ablwaifa A. R134a jet-pump design. Technical report, University of Nottigham, 2007.

[56] Mokheimer E.M.A. Performance of annular fins with different profiles subject to variable heat transfer coefficient. *International Journal of Heat and Mass Transfer*, 45:3631–3642, 2002.

[57] Nahdi E., Champoussin J.C., Hostache G., and Cheron J. Optimal geometric parameters of a cooling ejector-compressor. *Int J Refrig*, 16(1):67–72, 1993.

[58] Yapici R. and Ersoy H. Performance characteristics of the ejector refrigeration system based on the constant area ejector ow model. *Energy Conversion and Management*, 46:3117–3135, 2005.

[59] British Standards. BS EN 378, 1994 [Online]Available from. www.bsol.bsigroup.com. [Accessed 16 May 2009].

[60] Chen Y. and Sun C. Experimental study of the performance characteristics of a stem-ejector refrigeration system. *Experimental Fluid and Thermal Science*, 15:384–394, 1997.

[61] Refrigerator or combined refrigerator and water-pack freezer: compression cycle. solar direct drive without battery storage(PQS E003/RF05.2)[Online] Available from. http://www.who.int/immunization_standards/vaccine_quality/pqs_e05_rf2.2.pdf, July 2010. [Accessed September 2014].

[62] Rogers G.F.C and Mayhew Y.R. Thermodynamic and transport properties of fluids. Blackwell Publishing, 1995. 5th Edition.

[63] Eames I.W., Wu S., Worall M., and Aphornratana S. An experimental investigation of steam ejectors for applications in jet-pump refrigerators powered by low grade heat. *Power and Energy*, pages 351–361, 1999. Proceedings of Inst of Mech Engineers - Part A.

[64] Huang B.J., Chang J.M., Petrenko V.A., and Samofatove I.Y. A joint research on ejector cooling technologies. *2nd International workshop on non-compression refrigeration and cooling*, Odessa, Ukraine, 2001.

[65] Jia Y. and Wenjian C. Area ratio effects to the performance of air-cooled ejector refrigeration cycle with R134a refrigerant. *Energy Conversion and Management*, 53(1):240–246, 2012.

[66] *ASHRAE Thermodynamic Properties of Refrigerants*. Atlanta, Georgia, 1984.

[67] U.S. Environmental Protection Agency. Comparing light bulbs. [Online] Available from. `www1.eere.energy.gov/eductation/pdfs/efficiency_comparinglightbulbs.pdf`. [Accessed 15 December 2013].

[68] Keefe T.J. The nature of light[Online] Available from. `http://archive.is/me55`, September 2010. [Accessed 15 December 2013].

[69] Roy K. *Illuminating Engineering*. Laxmi Publications, 2nd edition, 2006.

[70] Chalko T. A fridge that takes only 0.1 kWh a day [Online]Available from. `www.builditsolar.com/projects/Conservation/chest_fridge.pdf`. [Accessed 25 August 2015].

[71] Dunn D.J. Engineering science - thin walled vessels [Online] Available from. `http://www.freestudy.co.uk/c103/t5.pdf`. [Accessed 27 May 2013].

[72] Drain P.K., Nelson C.M., and Lloyd J.S. Single-dose versus multi-dose vaccine vials for immunisation programmes in developing countries [Online] Available from. http://www.who.int/bulletin/volumes/81/10/Drain1003.pdf, 2003. [Accessed 25 August 2015].

[73] Han K. Anytime, anywhere deliverable hospital. www.yankodesign.com/2011/07/25/anytime-anywhere-deliverable-hospital. [Accessed 01 May 2015].

[74] Fenton R.L., Knowles S., Eames I.W., and Maidment G. Development of solar thermal heating and cooling systems using the jet-pump cycle. In *1st IIR Conference on Cold Chain and Sustainability*, 2010.

[75] Carbon Trust. Resources-conversion factors, 2008 [Online]Available from. www.carbontrust.co.uk/resources/conversion_factors/. [Accessed 29 November 2008].

[76] World Health Organisation. Global and regional immunization profile : Africa region [Online] Available from. www.who.int/immunization/monitoring_surveillance/data/gs_afrprofile.pdf?ua=1. [Accessed 25 August 2015].

[77] The European Parliament and the Council of the European Uniion. Regulation (eu) no 517/2014 on fluorinated greenhouse gases and repealing regulation (ec) no 842/2006. *Official Journal of the European union*, 2014.

[78] Whitelaw J.H. Convective Heat Transfer [Online] Available from. http://www.thermopedia.com/content/660/, 2011. [Accessed 15 January 2014].

[79] Bergman T.H., Lavine A.S., Incropera F.P., and Dewitt D.P. *Fundamentals of Heat and Mass Transfer*. John Wiley and Sons, 7th edition, 2007.

[80] Robinson W. and Dickson J. *Applied Thermodynamics*. Sir Isaac Pitman and Sons, 2nd edition, 1940.

[81] Launder B.E. and Spalding D.B. The numerical computation of turbulent flows. *Computer Methods in Applied Mechanics and Engineering*, 3:269–289, 1974.

[82] Harrison D.M. Error analysis in experimental science [Online] Available from. `http://www.upscale.utoronto.ca/PVB/Harrison/ErrorAnalysis/All.pdf`, September 2011. [Accessed 23 February 2015].

Appendices

Appendix A

R134a Refrigerant Data

Saturation Values							Superheat ($T - T_s$)			
							10 K		20 K	
T [°C]	p_s [bar]	v_g [m³/kg]	h_f [kJ/kg]	h_g [kJ/kg]	s_f [kJ/kg K]	s_g [kJ/kg K]	h [kJ/kg]	s [kJ/kg K]	h [kJ/kg]	s [kJ/kg K]
−103.30	0.0041	34.032	77.69	335.24	0.4453	1.9616	341.16	1.9955	347.29	2.0287
−100	0.0058	24.341	80.89	337.15	0.4640	1.9439	343.14	1.9776	349.35	2.0106
− 90	0.0155	9.5984	90.97	343.05	0.5205	1.8969	349.27	1.9300	355.70	1.9624
− 80	0.0370	4.2333	101.60	349.09	0.5770	1.8584	355.55	1.8910	362.20	1.9229
− 70	0.0800	2.0522	112.70	355.25	0.6330	1.8270	361.95	1.8592	368.84	1.8907
− 60	0.1591	1.07785	124.23	361.48	0.6884	1.8015	368.44	1.8334	375.57	1.8646
− 50	0.2944	0.60592	136.14	367.76	0.7430	1.7809	374.99	1.8126	382.38	1.8436
− 40	0.5188	0.36089	148.37	374.03	0.7965	1.7644	381.56	1.7960	389.22	1.8269
− 30	0.8435	0.22577	160.89	380.27	0.8490	1.7512	388.12	1.7828	396.07	1.8137
− 25	1.0637	0.18146	167.25	383.37	0.8748	1.7457	391.38	1.7774	399.49	1.8082
− 20	1.3272	0.14725	173.67	386.44	0.9003	1.7408	394.63	1.7726	402.90	1.8034
− 15	1.6393	0.12055	180.16	389.49	0.9256	1.7365	397.86	1.7683	406.29	1.7992
− 10	2.0060	0.09949	186.71	392.51	0.9506	1.7327	401.07	1.7647	409.67	1.7956
− 5	2.4335	0.08273	193.32	395.49	0.9754	1.7294	404.25	1.7614	413.02	1.7924
0†	2.9281	0.06925	200.00†	398.43	1.0000†	1.7264	407.40	1.7587	416.35	1.7897
5	3.4966	0.05834	206.75	401.33	1.0243	1.7238	410.50	1.7562	419.65	1.7874
10	4.1459	0.04942	213.57	404.16	1.0484	1.7215	413.56	1.7542	422.90	1.7855
15	4.8833	0.04208	220.46	406.93	1.0723	1.7194	416.57	1.7524	426.12	1.7838
20	5.7162	0.03599	227.45	409.62	1.0961	1.7176	419.52	1.7508	429.29	1.7825
25	6.6525	0.03092	234.52	412.23	1.1198	1.7158	422.41	1.7494	432.40	1.7813
30	7.7000	0.02665	241.69	414.74	1.1434	1.7142	425.21	1.7482	435.44	1.7803
35	8.8672	0.02304	248.98	417.14	1.1669	1.7126	427.93	1.7470	438.42	1.7795
40	10.163	0.01998	256.38	419.41	1.1903	1.7109	430.55	1.7460	441.32	1.7788
45	11.595	0.01735	263.92	421.53	1.2138	1.7092	433.06	1.7449	444.13	1.7781
50	13.174	0.01510	271.61	423.47	1.2374	1.7073	435.44	1.7438	446.84	1.7775
55	14.910	0.01315	279.46	425.20	1.2610	1.7051	437.69	1.7426	449.45	1.7769
60	16.812	0.01145	287.51	426.69	1.2848	1.7026	439.77	1.7412	451.93	1.7762
65	18.892	0.00997	295.77	427.89	1.3088	1.6995	441.67	1.7397	454.29	1.7754
70	21.161	0.00866	304.29	428.72	1.3332	1.6958	443.36	1.7378	456.50	1.7745
75	23.633	0.00750	313.13	429.09	1.3580	1.6911	444.82	1.7356	458.54	1.7734
80	26.323	0.00645	322.36	428.85	1.3835	1.6851	446.01	1.7330	460.42	1.7721
85	29.249	0.00550	332.16	427.77	1.4101	1.6771	446.88	1.7298	462.09	1.7706
90	32.433	0.00462	342.79	425.40	1.4386	1.6661	447.40	1.7259	463.55	1.7687
95	35.906	0.00375	355.05	420.64	1.4709	1.6491	447.49	1.7212	464.76	1.7663
100	39.728	0.00266	373.53	406.93	1.5193	1.6088	447.04	1.7153	465.65	1.7633
101.00	40.550	0.00196	389.67	389.67	1.5621	1.5621	446.84	1.7139	465.77	1.7626

Figure A.1: R134a (CH_2F-CF_3)- Highlighted extract from Rogers and Mayhew [62]

Appendix B

Estimation of Natural Convection Surface Heat Transfer Coefficient

A natural convention heat transfer coefficient of 7.5 W / $m^2 \cdot K$ is applied throughout the thesis. This value was initially estimated based on approximations from web resources ([78]) however this approximation was subsequently verified using the a theoretical method of evaluating natural convection heat exchange from a horizontal pipe, extracted from the book, Fundamentals of Heat and Mass Transfer [79].

The convective heat transfer coefficient is derived from the thermodynamic properties of the transfer fluid/gas (in this case air), the temperature difference (Δ T) and the pipe diameter. Various pipe diameters were evaluated, however both the evaporator and the condenser systems in this study were constructed with pipes of 4.2 mm. At Δ T = 2 K, the natural convection heat transfer coefficient (NCHTC) of a 4.2mm pipe is 7.48 W/ $m^2 \cdot K$. Note : At Δ T = 1 K, H = 6.77 W/ $m^2 \cdot K$ and at Δ T = 3 K, H = 7.96 W/ $m^2 \cdot K$.

Grahof (Gr);

$$Gr = \frac{D^3 \cdot \rho^2 \cdot g \cdot \Delta T \cdot \beta}{\mu^2}$$

$$= 16.0$$

Prandtl number (Pr);

$$Pr = \frac{\mu \cdot C_p}{k}$$

$$Pr = 0.69$$

Nusselt number (Nu);

$$Nu = \frac{H \cdot D}{k}$$

When Ra $\leq 10^{12}$, the relationship Ra = Gr· Pr can be applied and equation (B.1) used to find the natural convection heat transfer coefficient of a 4.2 mm diameter pipe at Δ T = 2 K (H = 7.48 W/m^2· K)

$$Nu = 0.60 + \left(\frac{0.387 \cdot Ra^{\frac{1}{6}}}{\left(1 + \left(\frac{0.559}{Pr}\right)^{\frac{9}{16}}\right)^{\frac{8}{27}}} \right)^2 \tag{B.1}$$

Appendix C

Transient Cooling Model

The transient cooling model can be used to determine either of the unknowns U·A or m·Cp in static temperature decay experiments.

$$
\begin{aligned}
&\textit{Given...} && Q = U \cdot A \cdot \left(T_o - T_i\right) \\
&\textit{and...} && Q = m \cdot C_p \cdot \frac{dT_i}{dt} \\
&\textit{Energy balance yields...} && m \cdot C_p \cdot \frac{dT_i}{dt} = U \cdot A \cdot \left(T_o - T_i\right) \\
&\textit{Let...} && \Delta T = T_o - T_i \\
&\therefore && \frac{d\Delta T}{dt} = -\frac{dT_i}{dt} \\
&\textit{Substitution gives...} && m \cdot C_p \cdot \frac{d\Delta T}{dt} = -U \cdot A \cdot \Delta T \\
&\therefore && \frac{d\Delta T}{\Delta T} = -\frac{U \cdot A}{m \cdot C_p} dt \\
&\textit{Integration yields} && \frac{\Delta T}{\Delta T_{init}} = e^{\left(-\frac{U \cdot A}{m \cdot C_p} \cdot t\right)} \\
&\therefore && ln\frac{\Delta T}{\Delta T_{init}} = -\frac{U \cdot A}{m \cdot C_p} \cdot t
\end{aligned}
\tag{C.1}
$$

Appendix D

Jet-pump Throat Area Calculation Proof

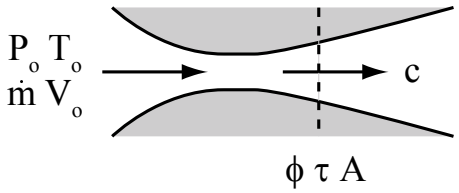

Figure D.1: Schematic diagram of jet-pump

Based on a proof published by Robinson in 1927 [80], the relationship between nozzle mass flow rate and throat orifice area can be theoretically described in terms of specific heat capacity ratio, specific volume (at stagnation) and total pressure.

For isentropic (frictionless and adiabatic) flow the steady flow energy equation (SFEE)

for the nozzle shown in figure D.1 can be written as...

$$C_p \cdot T_o = C_p \cdot \tau + \frac{1}{2} \cdot c^2$$

$\div C_p \cdot \tau$ gives

$$\left(\frac{T_o}{\tau}\right) = 1 + \frac{c^2}{2 \cdot C_p \cdot \tau} \tag{D.1}$$

Sonic velocity (a)

$$a = \sqrt{\gamma \cdot R \cdot \tau} \tag{D.2}$$

Mach number (M)

$$M = \frac{c}{a} \tag{D.3}$$

Rearranging (D.2) and (D.3) yields

$$c = M\sqrt{\gamma \cdot R \cdot \tau} \tag{D.4}$$

Applying the thermodynamic identities...

$$R = C_p - C_v$$

and...

$$\gamma = \frac{C_p}{Cv}$$

then the individual gas constant (R) can also be described as...

$$R = C_p \left(\frac{\gamma - 1}{\gamma}\right) \tag{D.5}$$

Rearranging equation (D.5) provides

$$C_p = \left(\frac{\gamma \cdot R}{\gamma - 1}\right) \tag{D.6}$$

Substituting (D.6) into (D.1) gives

$$\left(\frac{T_o}{\tau}\right) = 1 + \left(\frac{\gamma - 1}{2}\right) \frac{c^2}{\gamma \cdot R \cdot \tau}$$

Sub-identity (D.2) gives

$$\left(\frac{T_o}{\tau}\right) = 1 + \left(\frac{\gamma - 1}{2}\right) \frac{c^2}{a^2}$$

Sub-identity (D.3) gives

$$\left(\frac{T_o}{\tau}\right) = 1 + \left(\frac{\gamma - 1}{2}\right) M^2 \tag{D.7}$$

Also, for isentropic flow,

$$\frac{P_o}{\phi} = \left(\frac{T_o}{\tau}\right)^{\frac{\gamma}{\gamma-1}}$$

Therefore equation (D.7) can be rewritten as...

$$\frac{P_o}{\phi} = \left(1 + \left(\frac{\gamma - 1}{2}\right) M^2\right)^{\frac{\gamma}{\gamma-1}} \tag{D.8}$$

Generally, for 1D flow, mass flow ($\dot{m}$) can be expressed as...

$$\dot{m} = \rho \cdot A \cdot c$$

for compressible flow (large changes in density with velocity)

$$\dot{m} = \frac{\phi}{R \cdot t} \cdot A \cdot c$$

Applying sub-identity (D.4) gives

$$\dot{m} = \frac{\phi}{R \cdot \tau} \cdot A \cdot M \sqrt{\gamma \cdot R \cdot \tau}$$

$$\dot{m} = \frac{\phi \cdot \sqrt{\gamma} \cdot A \cdot M}{\sqrt{R \cdot \tau}} \tag{D.9}$$

Rearranging equation (D.7) provides the static temperature (t);

$$\tau = \frac{T_o}{\left(1 + \left(\frac{\gamma-1}{2}\right) M^2\right)} \tag{D.10}$$

Rearranging equation (D.8) provides the static pressure (ϕ);

$$\phi = \frac{P_o}{\left(1 + \left(\frac{\gamma-1}{2}\right) M^2\right)^{\frac{\gamma}{\gamma-1}}} \tag{D.11}$$

Substituting (D.10) and (D.11) into (D.9) gives

$$\dot{m} = \frac{P_o}{\left(1+\left(\frac{\gamma-1}{2}\right)M^2\right)^{\frac{\gamma}{\gamma-1}}} \cdot \frac{\left(1+\left(\frac{\gamma-1}{2}\right)M^2\right)^{\frac{1}{2}}}{\sqrt{R\cdot T_o}} \cdot \sqrt{\gamma}\cdot A\cdot M$$

$$\therefore \dot{m} = \frac{P_o}{\sqrt{R\cdot T_o}} \cdot \sqrt{\gamma}\cdot A\cdot M\cdot\left(1+\left(\frac{\gamma-1}{2}\right)M^2\right)^{\left(\left(\frac{1}{2}\right)-\left(\frac{\gamma}{\gamma-1}\right)\right)}$$

$$\therefore \frac{\dot{m}}{A} = \frac{P_o}{\sqrt{R\cdot T_o}} \cdot \sqrt{\gamma}\cdot M\cdot\left(1+\left(\frac{\gamma-1}{2}\right)M^2\right)^{-\frac{1}{2}\left(\frac{\gamma+1}{\gamma-1}\right)} \tag{D.12}$$

Equation (D.12) offers the general solution. At the nozzle throat the flow velocity is always sonic, i.e. c=a and therefore M=1. Substituting this condition into equation (D.12) gives...

$$\frac{\dot{m}}{A_{throat}} = \frac{P_o}{\sqrt{R\cdot T_o}} \cdot \sqrt{\gamma}\cdot\sqrt{\left(\frac{1+\gamma}{2}\right)^{-\left(\frac{\gamma+1}{\gamma-1}\right)}} \tag{D.13}$$

Given

$$\frac{P_o}{V_o} = \frac{{P_o}^2}{R\cdot T_o}$$

Equation (D.13) can be further simplified to give

$$\frac{\dot{m}}{A_{throat}} = \underline{\underline{\sqrt{\gamma\cdot\left(\frac{2}{1+\gamma}\right)^{\frac{\gamma+1}{\gamma-1}}\cdot\left(\frac{P_o}{V_o}\right)}}} \tag{D.14}$$

Appendix E

Computational Fluid Dynamics: Method and Assumptions

Guided by Prof I.W. Eames, University of Nottingham researcher, Dr Ali Ablwaifa modelled a jet-pump in ANSYS Fluent software, suited to operate using R134a at the approximate operating conditions of the system [55]. The contents of the appendix introduce and summarise the technical input provided by Dr. Ablwaifa.

The CFD model used in this study (compressible flow) was validated against prior experimental work [33],[63],[64]). This allowed the model to be used to simulate the performance of the jet-pump at various operating conditions. It also allowed different nozzle outlet positions to be simulated, a variable that has previously been shown to have a dramatic effect on system COP (up to 100% [33]). Adjusting the system conditions and geometry of the model provided simulation data that helped to characterise the performance of the jet-pump. The predicted performance, including COP and critical condenser pressures, was experimentally validated as discussed in section 5.6.3.

E.1 CFD Simulation Criteria

E.1.1 Turbulence Model and Boundary Conditions

The standard $K-\varepsilon$ turbulence model was used in the simulation as prior research [33] had shown that this was suitable for working fluids with lower molecular mass. The $K-\varepsilon$ model also provides a computationally economic simulation route.

The walls of the jet-pump are considered adiabatic in this simulation, however the boundary layer turbulence must be considered. Standard wall functions, originally proposed by Launder and Spalding [81] and included within ANSYS Fluent software, are used to compute the turbulence close to the jet-pump walls.

E.1.2 Grid Size and Type

The accuracy of the simulation is dependent on the quality and size of the mesh cells used. Finer meshes (higher resolution simulations) are preferred due to the increased accuracy of the result however solving models with a large number of cells requires considerable computing power and time.

One approach to reducing the required computational requirements is adaptive meshing (also known as gradient mesh). In order to maintain resolution and accuracy, whilst reducing the overall number of cells, the cell size can be reduced in areas of increased simulation complexity An example of adaptive meshing, focussed on the convergent-divergent tip of the jet-pump nozzle is shown in figure E.1[33].

When referring to the optimum cell size in this study, this relates to the standard cell

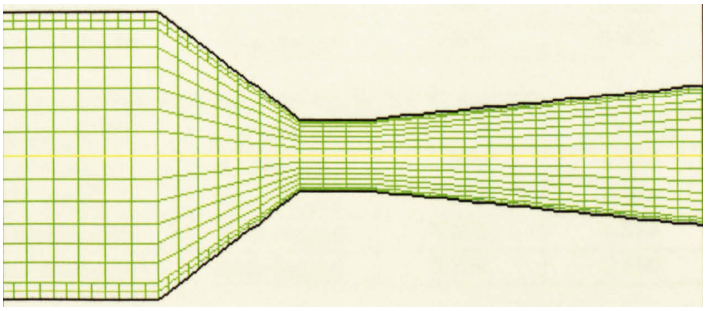

Figure E.1: Example of mesh grid adaptation[33]

size used across the majority of the mesh and does not include the smaller cells in the adaptive mesh zones. A quadrilateral mesh was used in this study created using *Gambit* software. An iterative convergence study was completed to determine the cell size at which asymptotic behaviour could be observed and an optimised equivalent cell size of 0.05 mm^2 was defined. Residual errors (convergence criteria) were reduced to 10^{-6}.

E.2 CFD Assumptions

In order to compute the jet-pump behaviour at various conditions, several assumptions needed to be made.

- **Adiabatic walls**. The walls of the jet-pump assembly are considered adiabatic.
- **Ideal gas** Although running the simulation as a real gas model would have been more accurate, it would also take considerably more time to compute. In this instance, the accuracy offered from ideal gas modelling was considered satisfactory.
- **Choked flow at nozzle throat** The simulation assumes that the primary flow is choked within the jet-pump nozzle throat, achieving sonic velocity (M=1)

Appendix F

Jet-pump Dimensioned Drawings

The following three pages contain manufacturing drawings for the jet-pump body F.1, the jet-pump diffuser F.2 and the jet-pump nozzle F.3.

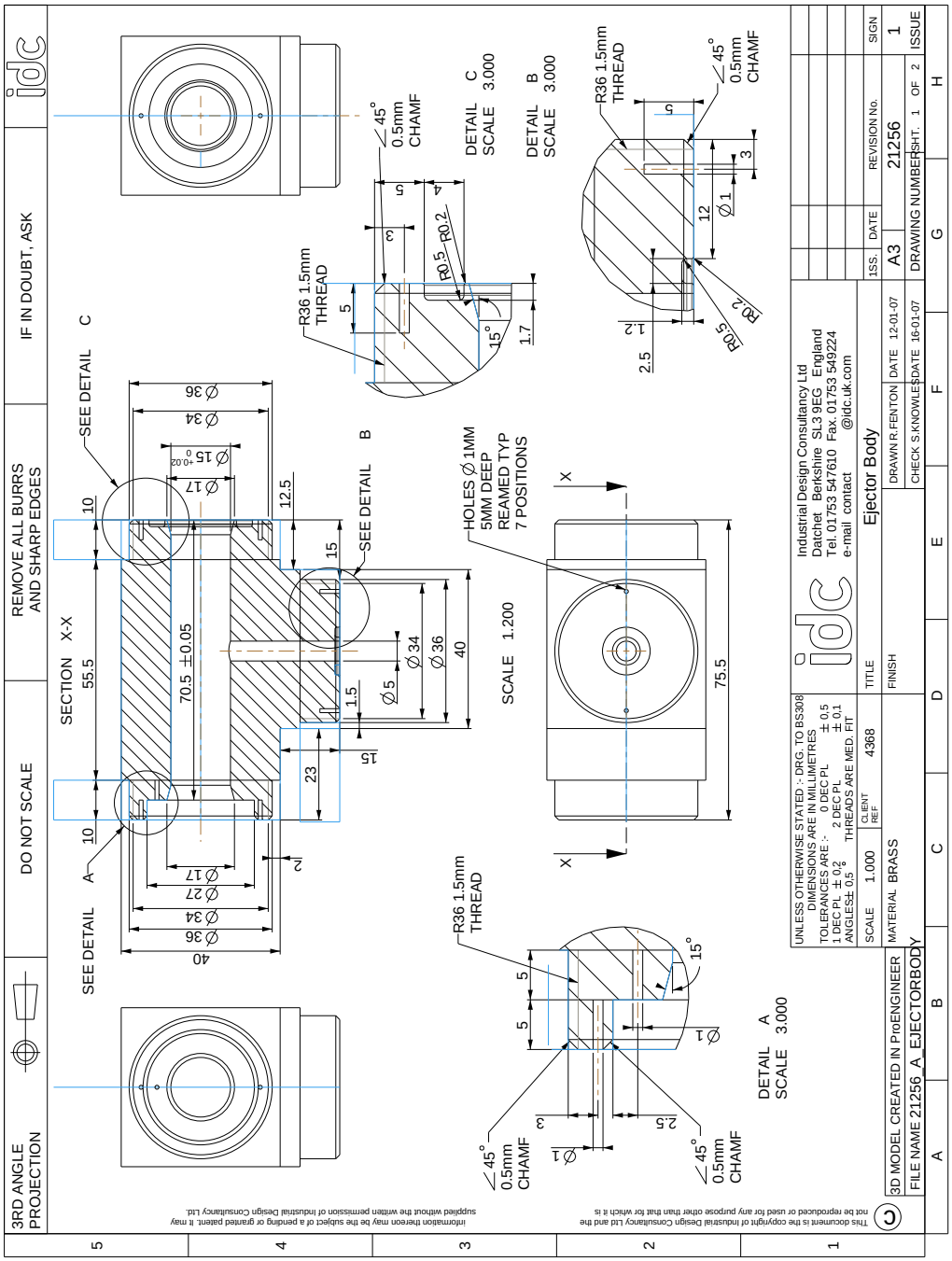

Figure F.1: Dimensioned drawing of the jet-pump body

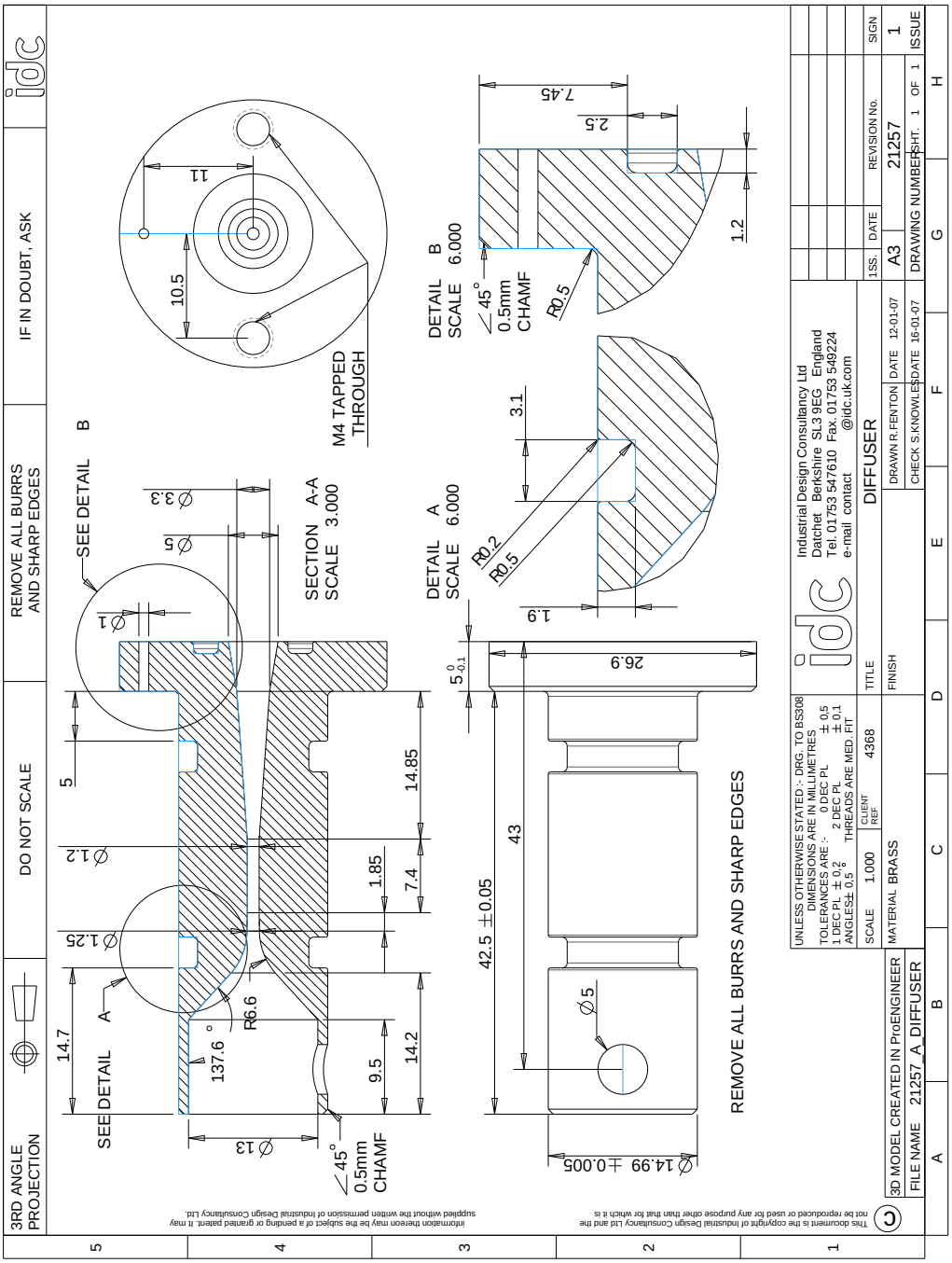

Figure F.2: Dimensioned drawing of the jet-pump diffuser

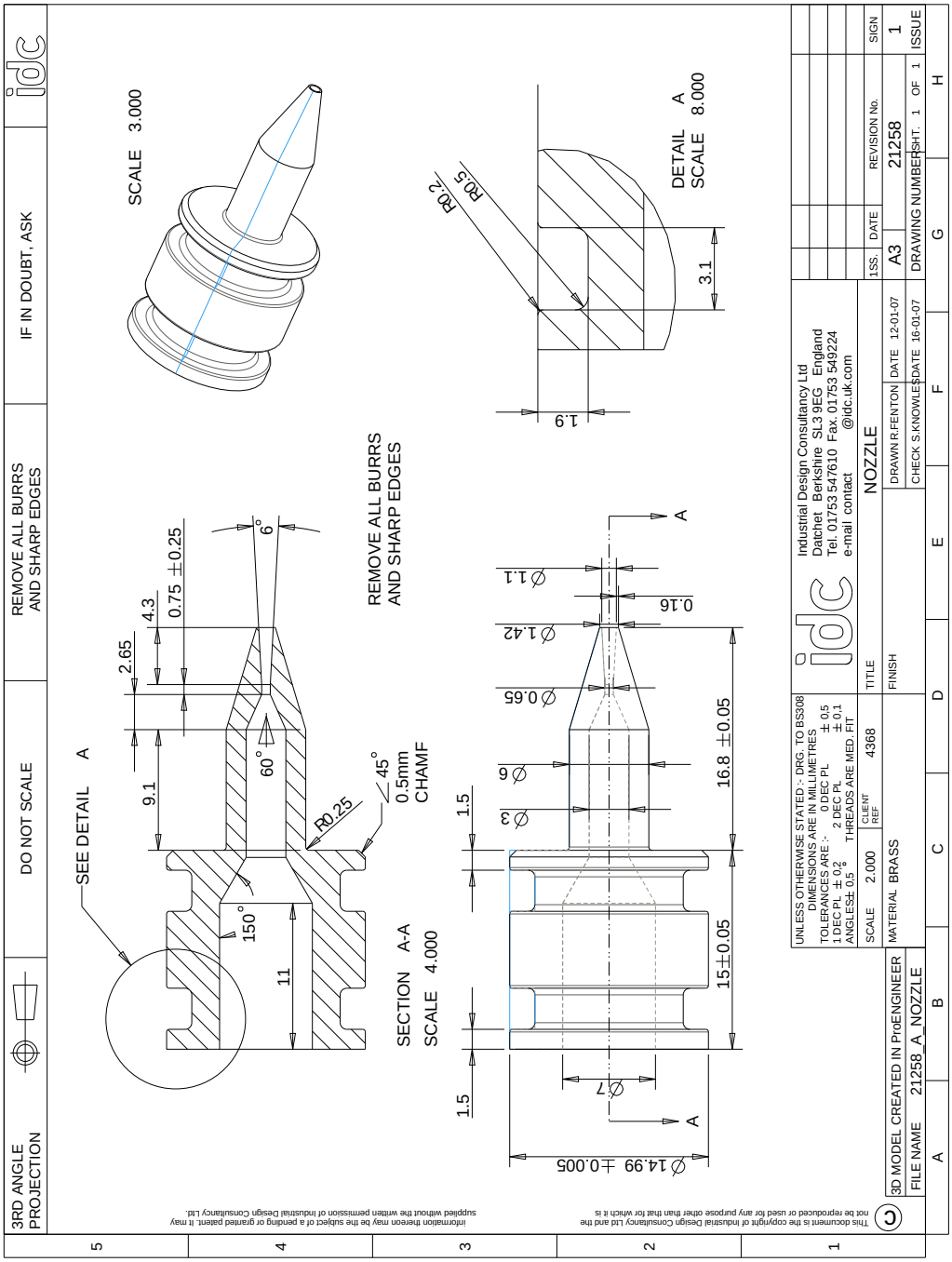

Figure F.3: Dimensioned drawing of the jet-pump nozzle

Appendix G

PLC Specification

A review of the PLC market was initiated, with units assessed on price, complexity, functionality and technical suitability. A summary of this research is shown in figure G.1. Most mid-range PLC do not offer analogue output signals as standard but some provide expansion modules to meet this functional requirement. The bracketed numbers in the input and output column show the number of connections available with an expansion unit.

RS Stock No	Name	Inputs	Outputs	Analogue In	Analogue Out	Expandable	Price
443-3820	Mitsubushi Alpha 2	8 (12)	6(10)	Y(8)	-	Y	£ 169.00
492-4275	Siemens LOGO! (6G)	8 (16)	4(8)	Y(2)	Y	Y	£ 140.06
468-4371	Telemech Zelio Logic 2	16 (18)	10(12)	Y(6)	Y(2)	Y	£ 160.00
488-9510	Moeller Easy721	12(24)	8	Y(4)	-	Y	£ 190.00
478-9965	Moeller Titan	12(24)	4(12)	Y(4)	Y	Y	£ 310.00
413-4078	Crouzet Millennium 2 Plus	12(24)	8(16)	Y(8)	-	Y	£ 158.62
536-9045	Crouzet Millennium 3	16(24)	10(16)	Y(6)	-	Y	£ 155.00
333-8718	Allen Bradley Micrologix 1000	10	6	Exp Y	Y	-	£ 238.00
539-0162	Siemens S700	8	6	-	Y	Y	£ 349.00
613-0141	Telemech Twido	12	8	Exp Y	Exp Y	Y	£ 279.00

Figure G.1: PLC market research table

The PLC systems listed in figure G.1 are a selection of the most suitable 24 VDC systems

offered by leading UK electronics distributor, RS components. Web based research, not included in the table, also provided information on ease-of-use and product support.

The decision to use a Zelio Logic 2 unit from Telemechanique was taken as this meets all of the requirements at a reasonable cost and also receives favourable reviews in terms of usability. The Zelio Logic 2 provides 16 inputs (6 of which could be configured as analogue) and 10 outputs. An SR3XT43BD analogue expansion unit was added to provide the analogue output required. The 24 VDC PLC can be programmed using Zelio 2 software on a PC and the program transferred via USB connection.

Appendix H

Control electronics : Supporting calculations

This appendix provides details of the supporting calculations used in the control electronics (used on EP3), including the mathematical operations that were used to convert transducer signals to applicable unit data.

H.1 Input Transducers

This study makes the distinction of defining thermocouples and temperature transducers separately. Thermocouples are used for data acquisition only whereas the information contained here on temperature transducers relates to the thermal sensing and and associated circuity used for monitoring and control purposes. Calibration of all the input transducers was conducted experimentally and error approximation defined.

H.1.1 Temperature Transducers

The temperature sensors provide a linear 0-10V signal based on the temperature of the pipe across a 0-160°C range. To convert the voltage to temperature required the following mathematical operation:

$$\begin{aligned} T &= (V * \frac{T_{MAX} - T_{MIN}}{V_{MAX} - V_{MIN}}) + T_{MIN} \\ &= \underline{\underline{(16 * V) + T_{MIN}}} \end{aligned} \tag{H.1}$$

H.1.2 Pressure Transducers

PT4 pressure sensors provide a 4-20mA signal based on the pressure across a 0-50 bar range. Two 250Ω shunt resistors were used to convert this into a 0-10V signal. Converting from the voltage to pressure therefore required the following mathematical operation:

$$\begin{aligned} P &= (V - 2) * \frac{P_{MAX}}{V_{MAX} - V_{MIN}} \\ &= \underline{\underline{6.25 * (V - 2)}} \end{aligned} \tag{H.2}$$

A similar mathematical operation was required for the PT3 pressure transducer, on the condenser, that operates over a 0-18 BAR range.

H.2 Analogue to Digital Conversion

An *ADC-11* was sourced from Pico Technologies Ltd to record the voltages of the input transducers. The *ADC-11* has a 10-bit resolution, providing a 1% accuracy on the voltages recorded. The voltage range for *ADC-11* inputs is 0-2.5 V and therefore some additional circuitry was required to convert the 0-10 V transducer signals. A potential divider board was constructed to perform this function. The circuit diagram for one of the PT4 pressure transducer inputs is shown in figure H.1.

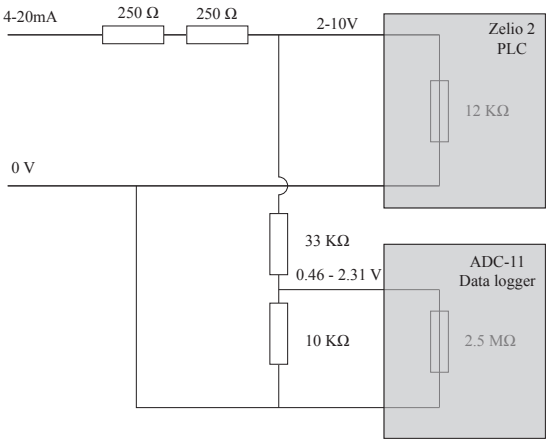

Figure H.1: Pressure transducer to PLC potential divider circuit

Rearranging Ohms law provided a form that helped select the values for the *ADC-11* potential divider circuit. The resistors were sized at 10 KΩ and 33 KΩ to scale the pressure transducer output voltage (V_{PT} = 2-10 V) down to the required ADC-11 input voltage ($V_{ADC} \leq$ 2.5V). Where R_A is sized at 33KΩ and R_B at 10KΩ, Ohms law shows

that V_{ADC} will have a range from 0.47 V to 2.33 V.

$$\begin{aligned} V_{ADC} &= I * R_B \\ I &= \frac{V_{PT}}{R_A + R_B} \\ \Rightarrow V_{ADC} &= \frac{V_{PT} * R_B}{R_A + R_B} \end{aligned} \tag{H.3}$$

Converting this voltage to a pressure was a mathematical operation required the voltage to first be re-scaled to a 0-10V signal and then entered into equation H.2. Working backwards from equation H.3

$$\begin{aligned} V_{PT} &= V_{ADC} * \frac{R_A + R_B}{R_B} \\ V_{PT} &= V_{ADC} * 4.33 \end{aligned} \tag{H.4}$$

Initial tests showed that the figures were slightly under those predicted. The cause of this was discovered to be in the internal circuitry of the data-logger. The ADC-11 has an impedance of 2.5MΩ, which has a small effect on the voltage across the potential divider circuit. The following equation takes account of this discrepancy:

$$R_{B\_IMP} = \frac{R_B * R_{ADC}}{R_B + R_{ADC}} \tag{H.5}$$

R_{B_IMP}(9.96 KΩ) was substituted for R_B (10 KΩ) in the conversion mathematics and a more accurate figure was obtained.

H.3 Oil Pump Speed Control

The circuit in figure H.2 was constructed to provide a 0-5 V speed control signal for the oil pump. The circuit is based on a standard 7805 regulating circuit.

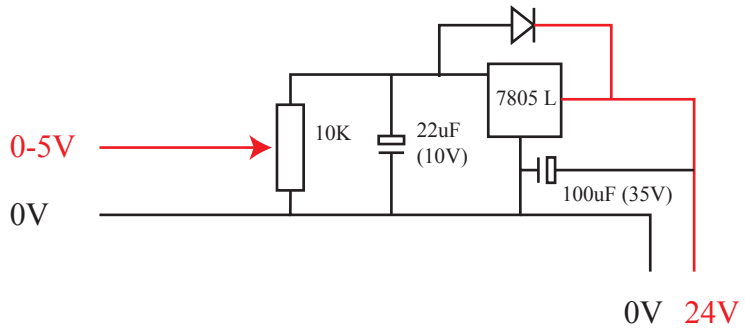

Figure H.2: 0-5V Speed control signal circuit

Appendix I

Experimental Uncertainty and Error Analysis

In order to properly evaluate the validity of any experimental result it is important to understand the relative effect of associated error. This section of the thesis describes the various error approximations for this study and their combined effect on the reported results.

The results presented throughout this thesis make use of significant figures in order to omit the need for continuous reference to the effects of error. For example, if a systematic accuracy error of ± 0.3 % was defined for a set of weighing scales, and the measured mass (digital scale to omit bias errors) was 148.06 g, then the reported measurement will be 148 g. With zero decimal places, 148 g implies that the true value lies somewhere between 147.5 g and 148.5 g, equivalent to ± 0.5 g or 0.3 % accuracy error.

I.1 Error Approximation Method

Error can broadly be considered in one of two categories; systematic error(limitations of the measurement equipment) and random, or bias error (the skill of the experimenter in reading the measurement equipment).

When considering error, it is also important to understand the difference between the terms *precision* and *accuracy*. The precision of a value, is a measure of the reproducibility or repeatability of a result (reducing the standard deviation from the mean measured value.) Precision accounts for the repeatability of a measurement, however the deviation from the true value determines the accuracy of a measurement.

In most cases, the required result is dependant on two or more variables, each with an associated errors to consider. In these instances, quadrature is used to provide the propagated error ([82]). Considering two measured quantities, X and Y, with errors ΔX and ΔY respectively.

Where $Z = X + Y$ or $Z = X + Y$ then

$$\Delta Z = \sqrt{\Delta X^2 + \Delta Y^2} \tag{I.1}$$

Where $Z = X \cdot Y$ or $Z = \frac{X}{Y}$ then

$$\Delta Z = Z \cdot \sqrt{\left(\frac{\Delta X}{X}\right)^2 + \left(\frac{\Delta Y}{Y}\right)^2} \tag{I.2}$$

The propagated error for simple relations can be defined by equations (I.1) and (I.2) however the more general form, where $Z = f(X_1, X_2...)$ is defined by equation (I.3)

$$\Delta Z = \sqrt{\left(\frac{\delta f(X_1, X_2...)}{\delta X_1} \cdot \Delta X_1\right)^2 + \left(\frac{\delta f(X_1, X_2...)}{\delta X_2} \cdot \Delta X_2\right)^2 + ...} \tag{I.3}$$

This propagated error analysis is applied to the thermal power equation, (I.4), used in the evaluation of system COP.

$$Q = \dot{m} \cdot C_p \Delta T \tag{I.4}$$

I.2 Experimental Error Evaluation

As EP2 and EP3 both employed data-logging equipment the effects of the random bias errors associated with the skill of the experimenter in reading gauges etc was not relevant to this error analysis.

The various errors that must be considered are presented below.

I.2.1 Systematic Errors

The precision of the measurement equipment was experimentally validated. In the absence of the relevant certification, equipment accuracy was assessed using calibration methods.

It is also important to consider the potential error in values obtained from data tables. Using the thermophysical properties for a given material from data-tables assumes that

the material used in the experiment is identical. In most instances, experimentally validating the data-table values is impractical and a systematic errors must be estimated. Where a higher level of confidence exists (e.g. water) a 2% error is included. Where data must be interpreted from graphs (e.g heat transfer oil), a user bias error of 5% error is included.

The primary evaluation metric in this study is COP which is defined (see equation (I.4)) as the quotient of the evaporator power (Q_e)and generator power (Q_g). We must consider these two thermal power values separately in order to determine the overall error in COP. As COP values were primarily calculated from experimental test data collected from the automated prototype (EP3), the error analysis described here is specific to EP3. In order to determine the error limits, the upper design point operating points were selected (Q_g = 950 W, Q_e = 95 W, COP = 0.1).

In order to assess the systematic error of temperature measurements, the specifications of the TC-08 data-logger were reviewed. The manufacturer (PicoLog) provided an accuracy of ± 0.5°C however as alternative sources suggested lower accuracies (± 1.1°C) for type-K thermocouples, this error was experimentally validated.

24 (3 sets of 8) type-K thermocouples were tested. The thermocouples were bound together and submerged into water at 60°C, 20°C and 1°C to assess the precision and response time. A graph of one set of experimental results is shown in figure I.1. The accuracy of the measurements was verified using a NEMA certified thermometer

The variance of temperatures at t = 230 s and t = 350 s was due to experimental error. The water was cooling at different rates across different levels in the container. When the water was stirred and the thermocouple re-submerged, the variance disappears as illustrated at t = 420 s. The signal from channel TC2 showed the largest deviation in

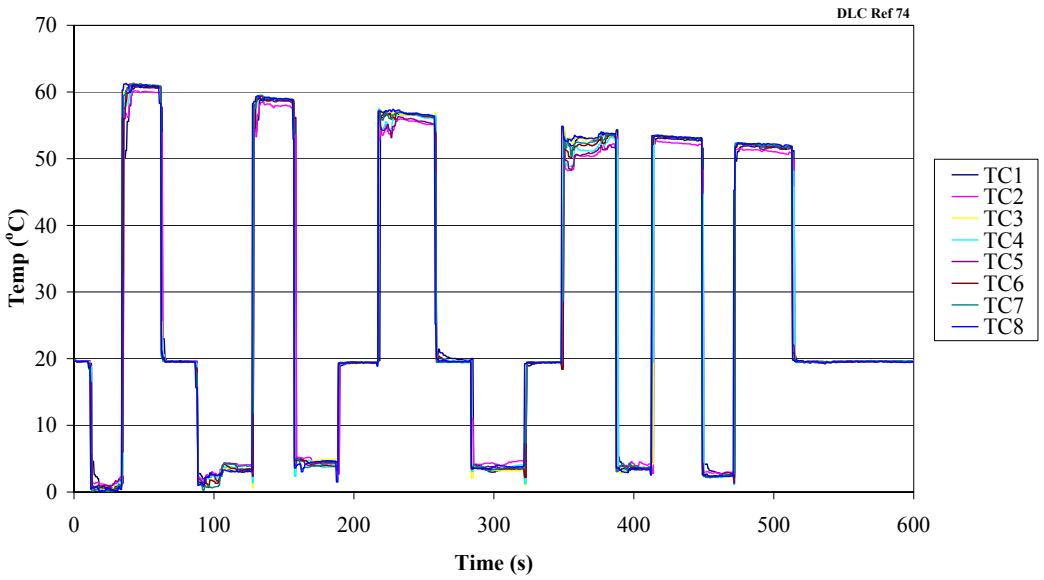

Figure I.1: TC-08 Thermocouple calibration test

these experimental results ± 0.43°C.This result was supported by several further tests and an accuracy tolerance of ± 0.5°C has been used in the calculation of propagated error.

Generator input (Q_g): As previously discussed the generator thermal power is estimated using equation (I.4).

Section 6.3.3 describes the experimental validation of the EP3 generator oil mass flow and an accuracy of 1% is defined.

Considering the specific heat capacity (C_{p-oil}) of the heat transfer fluid an accuracy of 5% is estimated. This estimate takes account of both material conformity error (to graphed values) and user bias error (in interpreting the graph). As discussed above, the accuracy of temperature component of the Q_g calculation has been experimentally validated as ± 0.5 °C.

Using the error propagation theory, previously described in equations (I.1),(I.2) and (I.3) a 9% accuracy can be calculated for Q_g

Evaporator Output (Q_e): The evaporator thermal power is also estimated using equation (I.4).

Section 5.4.5 describes the experimental method in detail for calculating Q_e. Although losses and numerous materials (and their associated temperature changes) affect the calculated value of Q_e, figure 5.16 shows that 65% of Q_e is dependant on the 24 litre duty load of water. With this in mind, the rate of change for water is used to assess the accuracy of Q_e.

As the mass of the water load could be measured using calibrated scales, and the time constant error of the data-logger was negligible, a systematic accuracy error of 1% could be applied.

Considering the specific heat capacity ($C_{p-water}$) of the water an accuracy of 2% is estimated.

As previously discussed, the accuracy of temperature component of the Q_e calculation has been experimentally validated as $\pm$ 0.5 °C.

Using error propagation theory, a 28% accuracy can be calculated for Q_e.

Further implementation of error propagation theory yields an accuracy error of 29% in the COP. It is important to note that this error relates to a 5 cycle analysis interval. If this interval is extended to 20 cycles, the accuracy error is reduced to 12% of the COP value.

A summary of the component accuracies, relative percentages and propagated accuracies

is presented in table I.1

I.3 Other Errors

Geometry : Due to the relatively small size of the jet-pump (nozzle throat diameter = 0.65 mm) manufacturing tolerances ± 0.05 mm (and inspection equipment limitations ± 0.005 mm) had a significant effect on the final part geometry (± 7%). The effects of this manufacturing error and it's relevance to the CFD comparison, are not evaluated as part of this study.

Variable : In some instances, the accuracy of measurement equipment can vary over time, caused by changes in experimental set-up (e.g. thermocouple positions or working fluid mass changes). To mitigate against these errors, calibration tests were repeated at regular intervals.

Pressure Sensors Although not directly relevant to the experimental evaluation of system COP, the readings obtained from five pressure transducers are presented in chapter 7 to illustrate the system operation. The transducers themselves (Alco PT4 30S and PT4-50S) have a manufacturer specified accuracy of ± 2% full-scale (33 bar and 50 bar respectively. In addition, the accuracy of the analogue to digital converter data-logger (Pico-log ADC-11) must be considered ± 0.2%. Given these accuracy values, a propogated systematic error of ± 0.1 bar can safely be assumed.

Symbol	Units	Mean Value	Accuracy	Error evaluation method	Error (± W)	Percentage
$\dot{m}_g$	kg/s	0.068	0.001	Systematic error experimentally validated	13.86	1
C_{p-oil}	J/kg K	2200	100	5% bias error in approximating from data table	47.12	5
ΔT_g	K	6.3	0.5	Systematic error experimentally validated	74.80	8
Q_g	**W**	**942.5**	**87.3**	**Propagated error from 3 values above**		**9**
$\dot{m}_e$	kg/s	0.0126	0.0001	Calibrated scales	0.75	1
$C_{p-water}$	J/kg K	4186	84	2% error on data table value	1.90	2
ΔT_e	K	1.8	0.5	Experimentally validated (5 cycle basis)	26.44	28
Q_e	**W**	**95.2**	**26.5**	**Propagated error from 3 values above**		**28**
COP	**-**	**0.10**	**0.03**	**Propagated error : Q_e / Q_g (5 cycle)**	**n/a**	**29**
ΔT_e	K	7.2	0.5	Experimentally validated (20 cycle basis)	6.61	7
COP	**-**	**0.10**	**0.03**	**Propagated error : Q_e / Q_g (20 cycle)**	**n/a**	**12**

Table I.1: Summary of propagated errors (EP3 - 5 cycle)